CANADIAN THESES

THÈSES CANADIENNES

INVESTIGATION OF STEEL MESH REINFORCEMENT FOR EARTH STRUCTURES

by

Humberto Manuel Morgado

A thesis
presented to the University of Ottawa
in partial fulfillment of the
requirements for the degree of
Master of Applied Science
in
Civil Engineering

OTTAWA, Ontario, 1983

The University of Ottawa requires the signatures of all persons using or photocopying this thesis. Please sign below, and give address and date.

ABSTRACT

The use of ribbed metal strips to reinforce soil structures was devised in France in the late 60's and marketed by the Reinforced Earth Company as a patented system of construction. The economic advantages of the system are that it eliminates the need for massive lateral support at the face of the backfill, reduces fill material requirements and land use.

This study analyses the behaviour of earth structures using steel wire mesh as an alternative mode of reinforcement.

Using large-scale pullout tests, triaxial tests and three dimensional large-scale models of reinforced embankments and reinforced walls, the behaviour of the wire mesh reinforced system under strip footing loads for a cohesionless backfill is studied.

For an identical working stress and weight, the wire mesh system exhibits a pullout resistance that is more than five times that of the Reinforced Earth ribbed strips. The introduction of wire mesh reinforcement in triaxial tests increases the load capacity and reduces the volume change in test samples while increasing the apparent angle of friction. Reinforcing mesh in embankment models increases

the ultimate bearing capacity of strip footings and reduces the settlement of the footings. When the embedment length is sufficient to provide anchorage of the mesh layers in reinforced wall models, the critical failure path assumes a logarithmic spiral shape.

The results of the experimental measurements are compared to analytical predictions (at failure conditions). Conclusions have been drawn as to the capability of the analytical approaches to predict the behaviour of reinforced soil structures.

ACKNOWLEDGEMENTS

The author wishes to express his gratitude to Dr. N.J. Gardner for his guidance and advice throughout the duration of this study.

The helpfull suggestions made by Dr. B. Trak of the University of Ottawa and Dr. G.E.A. Bauer of Carleton University are greatly appreciated.

The help received from the technical personnel of the Civil Engineering Department, especially Mr. William Watson, Mr. Claude Lavigne, Mr. Mike Burns, Mr. Greg Duchesne and Mr. Dick Moore, made the experimental work possible and is gratefully acknowledged.

Assistance during the triaxial test phase of the study was given by Messrs. J. Plavka, L. Rice and R. Ellis of the technical staff of the Engineering Faculty of Carleton University.

Special thanks go to Messrs. R. Paquette, N. Wasson, H.C. Fu and T.M. Lam for their help during the experimental work.

The author would also like to thank NSERC for its support, in part, of this research under Grant no. A1021.

Last but not least the author wishes to express his gratitude to his family and friends for their support and understanding.

CONTENTS

LIST OF FIGURES

LIST OF TABLES

NOMENCLATURE

a	Spacing of the crossbars
$(a)_s$	Cross-sectional area of longitudinal bars per reinforcing panel
A, A_s	Cross-sectional area of reinforcing ties
A_c	Anchorage factor
b	Perimeter of a reinforcing tie
b'	Breadth of a slice
b	Width of the reinforcing mesh
B	Width of the surcharge footing
c	Apparent cohesion of the soil
c'	Cohesive strength with regard to effective stresses
C_c	Coefficient of concavity
C_u, CU,	Coefficient of uniformity
d	Diameter of the reinforcing bars
d, h, h_i, y, z	Depth below surface of reinforcing layer
D	Width of the active zone in the earth structure
Dr	Relative density
D_{10}	Grain size, or effective diameter of the soil particles with 10% of particles finer by weight
D_{60}	Grain size, or effective diameter of the soil particles with 60% of particles finer by weight

e	Void ratio
e', x, y	Lever arms about centre of gravity
E_c	Coefficient of angularity
E_t	Tangent modulus of elasticity
$f, f^*, \delta, \mu, \psi$	Coefficient of friction between soil and reinforcing strip
$f_{all}, F_y, R_t, \sigma_y$	Yield or failure stress of the tie material
$f_o{}^*$	Coefficient of friction at the surface of the fill
F, F_r	Skin friction (resisting) force
F_e	Total earth pressure force acting on the wall over the area that is supported by one tie
F_t	Ultimate tensile stress of the reinforcing ties
$F_{sp}, F_{s\phi}$	Factor of safety against pullout of reinforcing tie
FS	Factor of safety
g	Acceleration due to gravity
G_s, ρ	Specific gravity
H	Height of wall
H_c	Critical height of the reinforced wall
i	Strip-bed number
I_d	Density index
Ka	Coefficient of active earth pressure
Ko	Coefficient of earth pressure @ rest
L_1	Length of net which is laid behind the sliding surcharge and bears the surcharge load
L_2	Residual length of net behind the sliding

	surcharge which does not bear the surcharge load
L	Length of the slip plane
L	Total length of the reinforcing strip
L_a, L'	Effective length of tie, length of adherence
L_b	Length over which bearing is considered
M_r	Reinforcement resistance moment
n	Total number of strip-beds (layers)
n	Porosity
N, σ_v	Vertical normal stress
N	Number of ties or crossbars
N_{2s}	Resultant normal force on the soil in the reinforced earth mass
p	Maximum bearing resistance developed against the mesh crossbars
P	Total sliding force
P_o	Uniformly distributed surcharge loads
P_{max}	Maximum pullout load
q	Surcharge pressure
r_u	Pore water pressure ratio
R	Reduction factor
R	Radius of slip circle
R_n	Resistance of the reinforcing net against sliding
R_s	Resistance of soil block against earth pressure
R_t	Earth reaction acting on a plane
S, τ	Shear stress
S_r	Resistance capacity of the soil
S_{th}	Theoretical specific surface assuming that all

	grains are of spherical shape
S_w	Actual measured specific surface
t	Thickness of reinforcing strip
T, T_d, T_{max}	Force required to break a strip, maximum tension force
T	Tensile force supplied by reinforcing grids, kN/m per metre width of reinforcement
T, T_1	Actual tension in the grid layer or strip
T_e	Total effective frictional force along the reinforcing tie
T_s	Force exerted on the wall facing
T_x	Strip capacity per unit width of soil
w	Width of reinforcing strip
W, W_s	Weight of earth mass
W_L	Surcharge load
X	Horizontal spacing of reinforcing strip
Y	Vertical spacing of reinforcing strip
α	Inclination of the slope
β	Angle between the wall facing and the failure plane
β	Angle of visibility
γ	Unit weight of overburden soil mass
ΔH	Spacing between two strip beds
ε	Lateral strain of soil mass
θ	Angle between critical failure path and horizontal
ρ	Density of soil

σ	Principal stress difference, $\sigma_1 - \sigma_3$
σ_h	Horizontal normal stress
σ_v	Vertical normal stress
σ_1	Major principal stress, vertical stress
σ_3	Minor principal stress, confining pressure
ΣT	Summation of tension in reinforcing ties
ΣT^*	Maximum possible total force exerted by the strips
τ, S	Shear strength of the soil
τ_f	Shear stress between the tie and the surrounding soil at failure
τ_m	Maximum frictional stress along the tie
ϕ	Internal angle of friction
ϕ_{cv}	Critical or constant volume friction angle
ϕ_μ	Angle of frictional sliding resistance between the soil and the tie

Chapter I

INTRODUCTION

In 1966, French engineer Henri Vidal introduced a theoretical concept of soil reinforcement utilizing metal strips to carry induced tensile forces in earth structures which he termed Reinforced Earth[1] (Terre Armée).

It has been repeatedly stated that this is not a new concept, but merely a modern approach, applying modern materials to an old and well established building practice.

The same practice has been observed in birds and animals who utilize the same principles in constructing their shelters.

Ancient Romans used a material of interwoven twigs and branches called "Fascines" when building on peat. The use of "Fascines" prevented contamination of the surcharge area by peat and to a lesser extent the tensile properties of the inclusions allowed some stress distribution to occur.

Other examples include corduroy roads and the use of mud and sticks in low ditches as described by Lee et al. (1973).

However, one cannot deny Vidal's contribution to the present day state of knowledge and the tremendous achievements accomplished by the reinforced soil system of

---

[1] Registered trademark of the Reinforced Earth Company.

construction.

1.1 BASIC CONCEPT OF REINFORCED EARTH SYSTEM

The Reinforced Earth system utilizes the inclusion of horizontal strips of metal reinforcement in an earth structure in order to improve the poor mechanical properties of the earth backfill.

Soils, in particular granular soils, exhibit very low tensile strengths. However, by placing linear elements within the structure which are able to withstand important tensile forces, a composite material is obtained which combines the compressive and shear strength of the soil mass, with the tensile strength of the reinforcing strips.

The behaviour of a reinforced soil structure is similar to a reinforced concrete system in which the mechanical properties of the basic material: plain concrete, which possesses high compressive strength but little tensile strength are supplemented by reinforcing steel rods embedded in the concrete providing the needed strength in tension (maximum strain direction). However, the stress transfer from earth mass to the tensile reinforcement is accomplished by friction between the reinforcing elements and the backfill soil, while the bond between steel and concrete is accomplished by mechanical interlock.

In analysing an earth structure, two. design criteria must be kept in mind (Smith 1978):

1. the internal stability of the composite earth/ reinforcement material
2. the external stability of the structure.

The internal stability analysis includes the tensile resistance of the reinforcing strip and the bond resistance between the reinforcement and the soil backfill. These analyses are undertaken in order to prevent two types of failures: failure of the strip reinforcement in tension and/or pullout of the reinforcement from the earth structure.

The external stability analysis of the structure is undertaken in order to investigate and prevent failure of the structure as a rigid body by: rotation, sliding or bearing failure of the supporting soil.

The Reinforced Earth system is now in use around the world and has been applied to a wide variety of structures and climates. However, the vertical wall is still the most common application of the system and a schematic presentation of a typical wall structure is shown on figure 1.1.1.

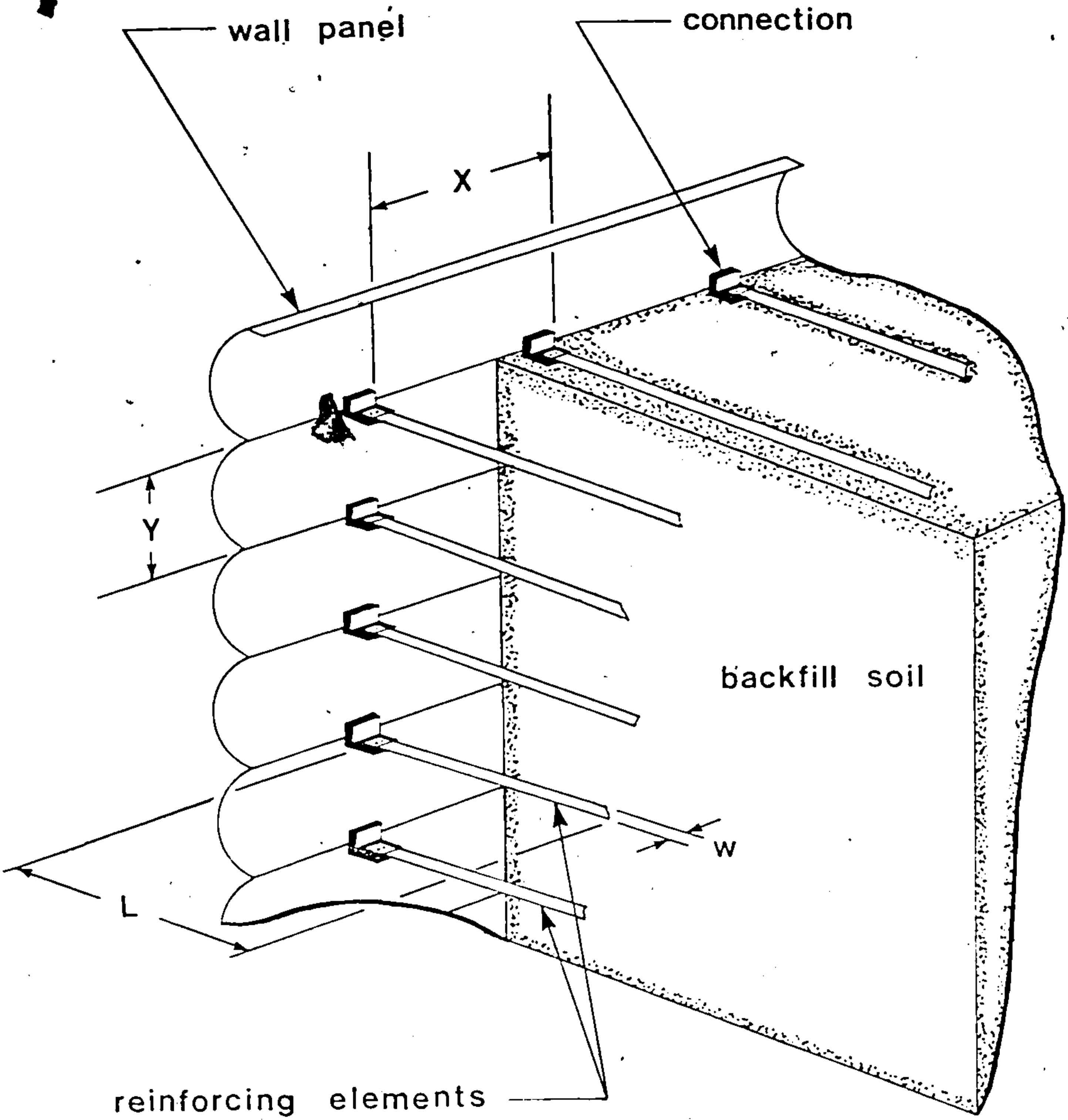

FIG. 1.1.1- SCHEMATIC VIEW OF A REINFORCED EARTH WALL

1.2 ELEMENTS OF A REINFORCED SOIL STRUCTURE

The basic components of the wall structure are:

1. wall facing, or skin
2. reinforcing elements
3. backfill material

The wall panels have the primary purpose of preventing the backfill material from flowing out of the structure. Theoretically, they have no structural purpose and can be designed with a very small thickness (few millimetres). Initially the skin elements were cylindrical semi-elliptic metal panels, but for aesthetic purposes, precast concrete panels are now more usual.

The reinforcing elements or strips are connected to the wall panels at predetermined vertical and horizontal spacings. Initially, smooth stainless or galvanized steel strips were utilized, but today many shapes are in use depending on the desired soil/reinforcement friction coefficient: smooth strips, ribbed strips, wires, wire meshes or mats etc.. Also, the constituent materials can be as different as metals, fiber glass, polymer nets and polymer fabrics.

The backfill material is generally granular to allow an adequate frictional bond to develop between the soil and the reinforcement material. Cohesive soils are not recommended in order to avoid problems of 'creep'. A granular soil also permits better drainage and is usually less corrosive. The soil should be well graded with a maximum particle size of 125 mm with no more than 10 percent fines (Smith 1978).

As enunciated by McKittrick (1979) soils used in Reinforced Earth structures are:

1. granular
2. subjected to low strain levels
3. normally stressed in plain strain (except under point loads), and
4. compacted to relatively high densities

Some of the advantages of the Reinforced Earth system are the relatively simple method of construction which necessitates no special equipment, the large deformations which can be tolerated without risk of collapse and the lower cost of a Reinforced Earth structure compared to a retaining wall structure.

1.3 OBJECTIVES OF RESEARCH

Since the Reinforced Earth system is a patented method of construction, it is of interest to study the behaviour of an alternative reinforcing material compared to the patented reinforcing members.

The alternative reinforcement chosen for this study is a wire mesh system of reinforcement similar to the mesh utilized for temperature reinforcement in reinforced concrete floor slabs (figure 1.3.1).

The different reinforcing members were compared experimentally using a large-scale pullout device to determine the friction coefficient of the different materials. Large-scale triaxial tests were then used to analyse the change in internal angle of friction that the introduction of wire mesh members produces. Finally, large-scale three dimensional models of reinforced embankments and walls were tested to determine the behaviour of the wire mesh reinforced system under strip footing loads.

These different tests permitted the analysis of the alternative system of reinforcement under different load conditions and design parameters.

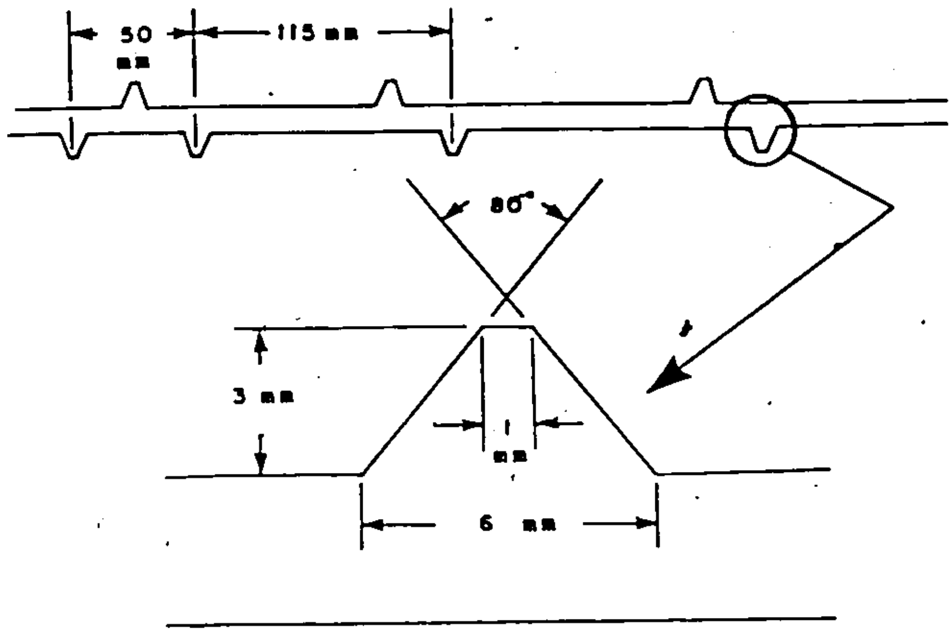

(a)

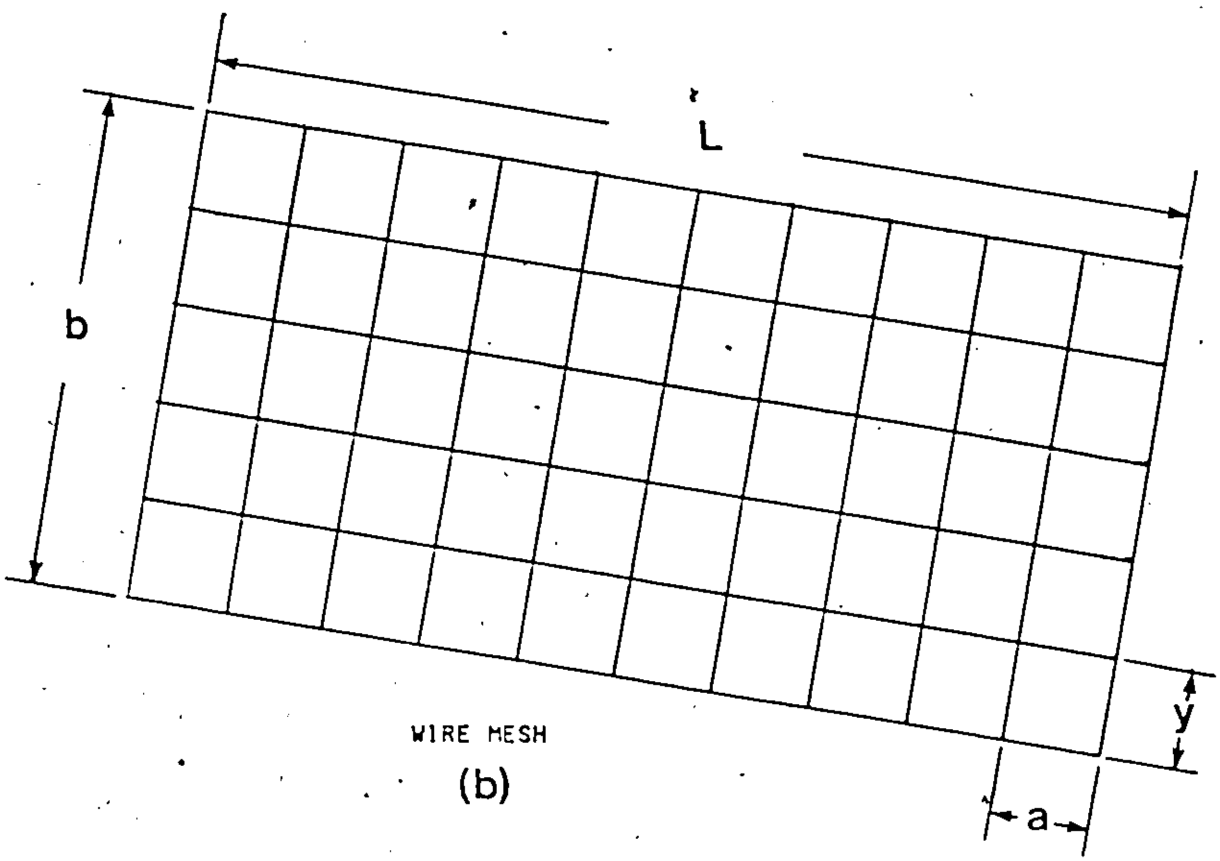

(b)

FIG. 1.3.1- SCHEMATIC REPRESENTATION OF RIBBED AND WIRE MESH SYSTEMS OF REINFORCEMENT

Chapter II

THEORETICAL DEVELOPMENTS

Since Vidal introduced the Reinforced Earth concept, a significant amount of research has been devoted to the investigation and analysis of the behaviour and characteristics of the Reinforced Earth system and of alternative concepts.

In 1963, Vidal published a book on the theoretical and practical aspects of combining granular materials (sand) with flexible reinforcements (Vidal 1978). The new material being of a cohesive nature, was called 'Reinforced Earth'. However, this new construction concept became known only in 1966 with the construction of the first Reinforced Earth wall in the Pyrenees Mountains in France and with the presentation of the system by Vidal to the French Soil Mechanics Committee.

The following chapter presents an overview of some of the significant theoretical developments that have been presented by researchers around the world on the concept of Reinforced Earth and on alternative systems.

2.1 SCHLOSSER AND VIDAL (1969)

In 1969, F. Schlosser (head of the Soil Mechanics Section of the Laboratoire Central des Ponts et Chaussées of France) and H. Vidal presented a paper on the theory and design methods associated with Reinforced Earth.

In describing the basic concepts of Reinforced Earth, Schlosser and Vidal (1969) assumed horizontal sets of reinforcements embedded within an earth mass to represent a Reinforced Earth structure. If the structure is failed by lateral stretching it was stated that:

> Any soil layer located between two adjacent reinforcement sets is restrained along its upper and lower boundaries and the only lateral strain that can take place is the strain of the reinforcements, providing that friction between soil and reinforcements be large enough and reinforcements be close enough to each other. Thus a traction force develops in the reinforcements, and in the most common cases where their constituent material is such as its Young's modulus is by several magnitudes higher than the deformation modulus of the soil, the lateral strains of the reinforced mass are negligible and have no influence at all on stresses within the soil.

Therefore, the principal stresses acting within the reinforced soil mass at any depth h, if the lateral strain, ϵ, of the soil mass is zero and as long as the reinforcements do not rupture are (figure 2.1.1):

$\sigma_{vertical} = \gamma \cdot h$ and

$\sigma_{horizontal} = Ko \cdot \gamma \cdot h$

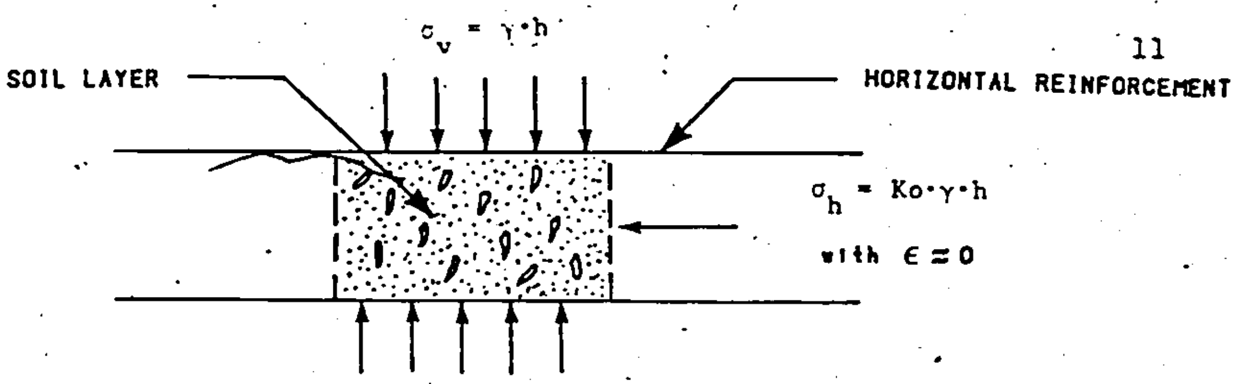

FIG. 2.1.1- PRINCIPAL STRESSES ACTING WITHIN THE REINFORCED SOIL MASS AT ANY DEPTH h (SCHLOSSER AND VIDAL, 1969)

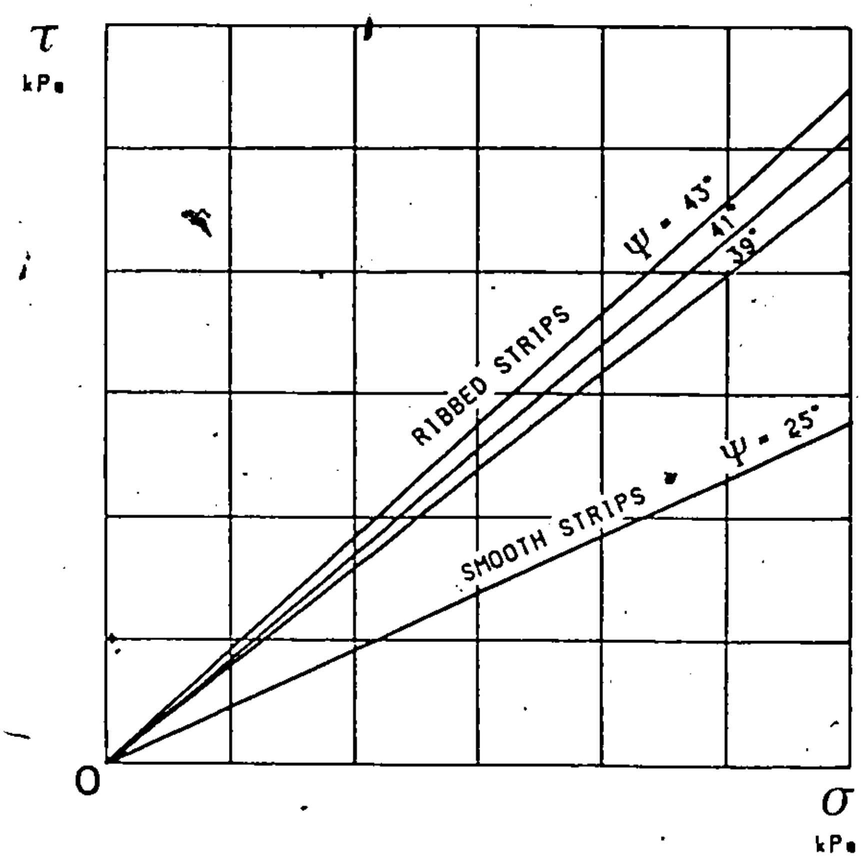

FIG. 2.1.2- COEFFICIENT OF EARTH-STRIP FRICTION ($f = tg\,\Psi'$) FOR LEUCATE SAND (SCHLOSSER AND VIDAL, 1969)

with $\sigma_{vertical}$ = principal vertical stress

$\sigma_{horizontal}$ = principal horizontal stress

γ= unit weight of soil overburden

h= depth

Ko= coefficient of earth pressure at rest

The composite earth mass is said to have gained cohesion along the direction of the reinforcements which is proportional to the tensile strength of the reinforcing inclusions.

Schlosser and Vidal (1969) concluded that if reinforcements are properly placed and designed, any shearing and sliding within the earth can be prevented, so that the whole mass behaves like a solid having cohesion and able to support its own weight as well as important external forces.

The design and construction of reinforced soil structures are governed by three basic requirements:

1. friction (adherence) between earth and reinforcements without any sliding, allowing a transfer of forces between the soil grains and the reinforcing strip
2. support of tensile forces by the reinforcements and support of the compression and shearing stresses by the earth mass

3. presence of a skin element to prevent the soil close to the boundaries from flowing out.

The coefficient of earth-strip friction f, was defined by plotting on (τ; σ) axes the points corresponding to the peaks of various shear stress-strain curves obtained from direct shear tests between the granular material (Leucate sand) and reinforcing strips.

These points fall onto a straight line through the origin for specific reinforcing strips and granular material at different values of the normal stress (σ). The slope of this line corresponds to the friction coefficient ($f = \tan \Psi$) between the strip and the sand (figure 2.1.2).

2.1.1 <u>Design of a reinforced soil wall</u>

For an elementary reinforced soil wall composed of horizontal strips and retaining an horizontal backfill, Schlosser and Vidal (1969) state that the stability of such a wall depends on both the internal and external stability of the wall.

The external stability is governed by the soil mechanics analyses which are usually performed for any retaining wall, such as punching, overturning, sliding on its base, general sliding, etc., if the structure is considered as a rigid body.

Failure of the wall structure can occur due to its internal instability either by lack of adherence of the strips or by insufficient width of the wall (length of reinforcing strips), or by failure of strips under tensile forces.

The analysis and design of a reinforced soil wall was performed by Schlosser and Vidal (1969), first, by a transposition of Coulomb's method for the computation of active or passive thrust acting on a wall and, then, by a derivation from Rankine's method.

Coulomb's method is illustrated in figure 2.1.3 and yields a tensile resistance for each reinforcing strip of:

$$T_i = i \frac{n}{n+1} Ka\, \gamma\, \{\Delta H\}^2 \simeq i\, Ka\, \gamma\, \{\Delta H\}^2$$

The internal stability of the wall is insured by checking that each strip tensile force is smaller than the frictional resistance of the corresponding strip-bed:

$$T_i < (R_t)_i$$

where: T_i = tensile resistance at each reinforcing strip

i = strip-bed number

n = total number of strip-beds

Ka= coefficient of active earth pressure which is a function of the internal friction angle (ϕ)

Ka= $\tan^2 (45^\circ - \phi/2)$

γ = unit weight of overburden soil mass

ΔH= spacing between two strip-beds

R_t= earth reaction acting on the plane AC

Rankine's method is illustrated in figure 2.1.4 , and yields a tensile resistance in the strip-bed number i which is approximately identical to Coulomb's method:

$$T_i = (i-\tfrac{1}{2})\ Ka\ \gamma\ \{\Delta H\}^2$$

Schlosser and Vidal (1969) concede that the two design methods are based on simplified assumptions and that the design of a reinforced soil wall must be checked on model tests or by observations on actual structures. Also, the exact sufficient length of the reinforcing strips still remains undetermined.

In practice, to prevent internal failure, rectangular distributions of the strips in the case of very high walls are recommended (L= 0.8 H). For lower walls, strip lengths larger than the height of the wall are suggested.

Finally, Schlosser and Vidal (1969) indicate that the backfill must be granular in nature, or only slightly cohesive (less than 15% of grain size distribution passing sieve no. 200), in order to provide the required adhesion between reinforcing strip and soil grains.

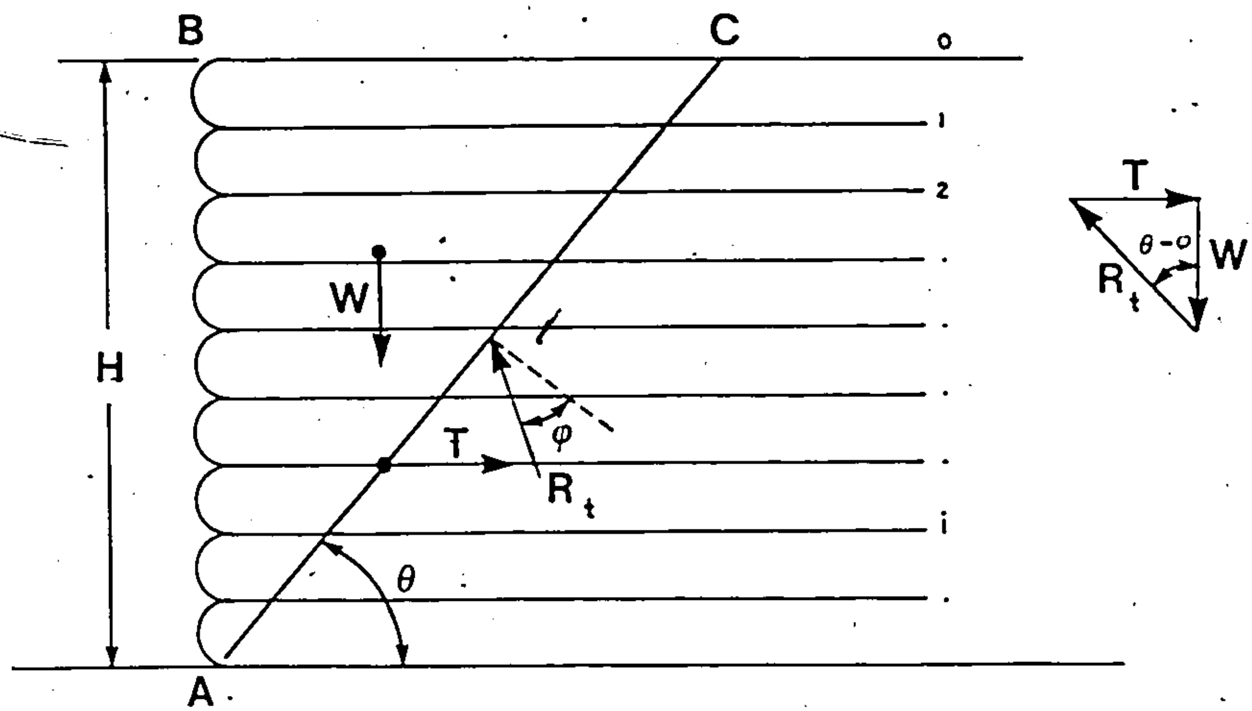

FIG. 2.1.3- ANALYSIS OF A REINFORCED EARTH WALL USING COULOMB PRESSURE (SCHLOSSER AND VIDAL, 1969)

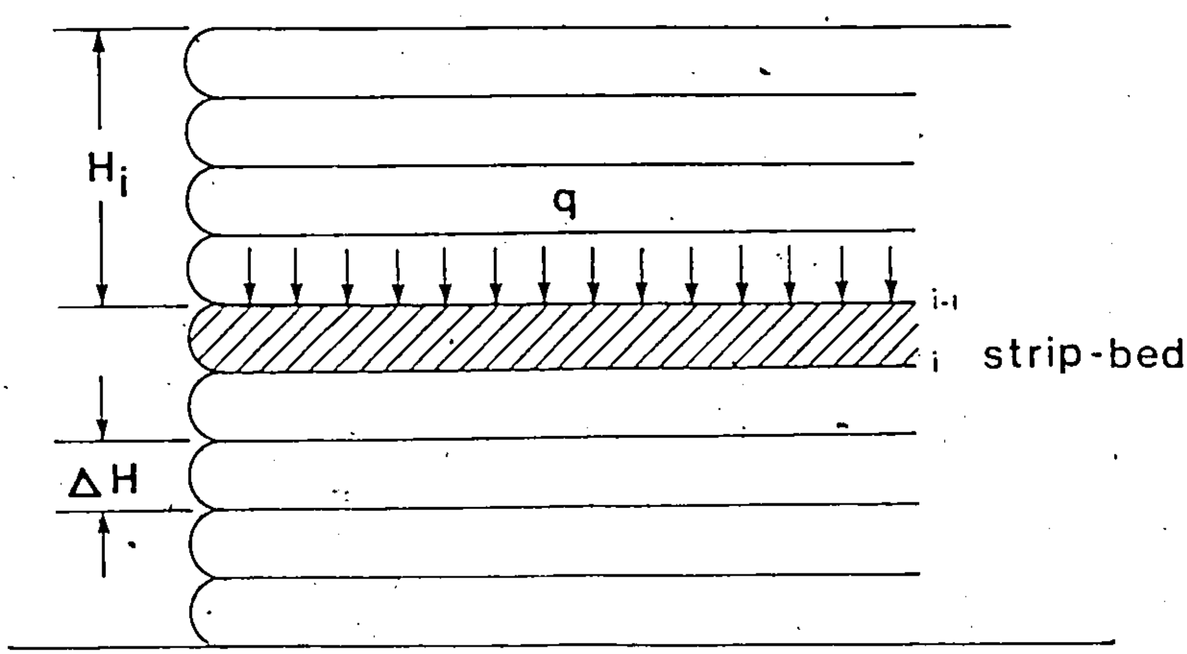

FIG. 2.1.4- ANALYSIS OF A REINFORCED EARTH WALL USING RANKINE PRESSURE (SCHLOSSER AND VIDAL, 1969)

2.2 LEE, ADAMS, VAGNERON (1973)

Lee and his co-workers published in 1973 an analysis of Reinforced Earth walls (Lee et al., 1973). In analysing the stresses and designing the reinforcing elements, it was assumed that the lateral earth pressure against the wall increased linearly with depth (figure 2.2.1), and at any depth, d, below the surface it is equal to $\sigma_h = Ka\,\gamma d$, in which $Ka = \tan^2(45° - \phi/2)$.

As was stated previously, the reinforcing strips or ties must be strong enough to prevent failure by breaking in tension and they must also be wide, long, and have sufficient friction to prevent failure by pulling out.

Lee et al. (1973) followed classical retaining wall design methods for their analysis of Reinforcing Earth structures. In order to calculate the maximum stress developed in the ties, three approaches were used:

1. Rankine method- which considers the equilibrium of a single representative critical element of soil at any depth
2. Coulomb method- which considers the overall stability of the entire wall

   a) Coulomb force method- the total force due to the active earth pressure over the entire wall is equated to the sum of the forces developed in each of the n ties just at failure

b) Coulomb moment method- the sum of moments about the toe are equated.

2.2.1 Tie failure by rupture in tension :

Lee et al. (1973) assumed that the tensile force developed in any tie increases from zero at the free end to a maximum at the face of the wall, with the maximum force increasing with depth.

Therefore, by the Rankine method, the maximum tension force, T_d for any tie is:

$$T_d = Ka\ \gamma\ d\ X\ Y \qquad \text{and,}$$

$$T_{max} = Ka \cdot \gamma\ H\ X\ Y$$

where X and Y are the horizontal and vertical spacing of the ties and H is the total height of the wall.

The calculated value of T_d is used to determine the required cross-sectional area of the tie at that depth after allowing for a factor of safety and for corrosion.

The Coulomb force method gives a maximum force which occurs on the lowest tie and is equal to:

$$T_{max} = \frac{n}{n+1}\ Ka\ \gamma\ H\ X\ Y$$

Finally, the Coulomb moment method gives a maximum force T_{max} equal to:

$$T_{max} = \frac{n^2}{n^2-1} \quad Ka \; \gamma \; H \; X \; Y$$

For a large number of layers (n), all three approaches yield approximately the same maximum force. Therefore, the factor of safety against yielding or failure of the tie is:

$$F_{sy} = \frac{\sigma_y \; w \; t}{Ka \; \gamma \; H \; X \; Y}$$

where σ_y = yield or failure stress of the tie material
$w*t$= cross-sectional area of the tie (width*thickness)

2.2.2 Tie failure by pulling out

Lee et al. (1973) assumed that the effective length,L', of the tie which resists the pullout force equals the portion of the total length extending beyond the zone of active Rankine failure bounded by plane BC as in figure 2.2.1.

The total frictional resistance of a tie at depth d is given by:

$$F_r = 2\ L'\ w\ \gamma\ d\ \tan\phi_\mu$$

in which w= width of the tie and ϕ_μ = the angle of frictional sliding resistance between the soil and the tie.

Therefore, the Rankine method yields the total earth pressure force acting on the wall over the area that is supported by one tie as:

$$F_e = X\ Y\ \gamma\ d\ Ka$$

giving a factor of safety with respect to pulling out at depth d of:

$$F_{s\phi} = \frac{2\ L'\ w\ \tan\phi_\mu}{X\ Y\ Ka}$$

Assuming ties of constant length, the most critical condition occurs at the top where the length L', behind the failure plane is a minimum. This assumption allows the determination of the required total length of the tie which would be:

$$L = \frac{H}{\tan\theta} + \frac{X\ Y\ Ka\ F_{s\phi}}{2\ L'\ w\ \tan\phi_\mu}$$

On the other hand, the Coulomb methods yield a maximum frictional resisting force, for ties of constant length L of:

$$F_r = 2 \gamma Y w \tan \phi_\mu \sum_{i=N}^{n} i[L- (n-i) Y \tan (45° - \phi/2)]$$

where i= summation index counting the number of ties beginning from i=1 at the top to i=n at the bottom

and N= value of i for the first tie from the top to extend beyond the plane BC.

The Coulomb force method gives a factor of safety against pullout of:

$$F_{s\phi} = \frac{4 Y w \tan \phi_\mu}{Ka H^2 X} \sum_{i=N}^{n} i[L-(n-i) Y \tan (45° - \phi/2)]$$

and the Coulomb moment method gives:

$$F_{s\phi} = \frac{12 w Y^2 \tan \phi_\mu}{Ka H^3 X} \sum_{i=N}^{n} (n-i) i [L-(n-i) Y \tan (45° - \phi/2)]$$

In comparing the three approaches for tie pullout, Lee et al. (1973) find that the Coulomb force method computes the shortest length of tie, whereas the Rankine method leads to the longest tie, and is therefore the more conservative (figure 2.2.2).

From this analysis, it can be concluded that the first step in the design procedure of a reinforced soil wall is to assume a set of dimensions, and then calculate the maximum tensile forces in the ties. The next step is to compare these forces with the tensile strength of the ties to ensure adequate safety against breaking. Finally, the length of the ties must be checked to ensure adequate safety against the possibility of failure by the ties pulling out of the backfill.

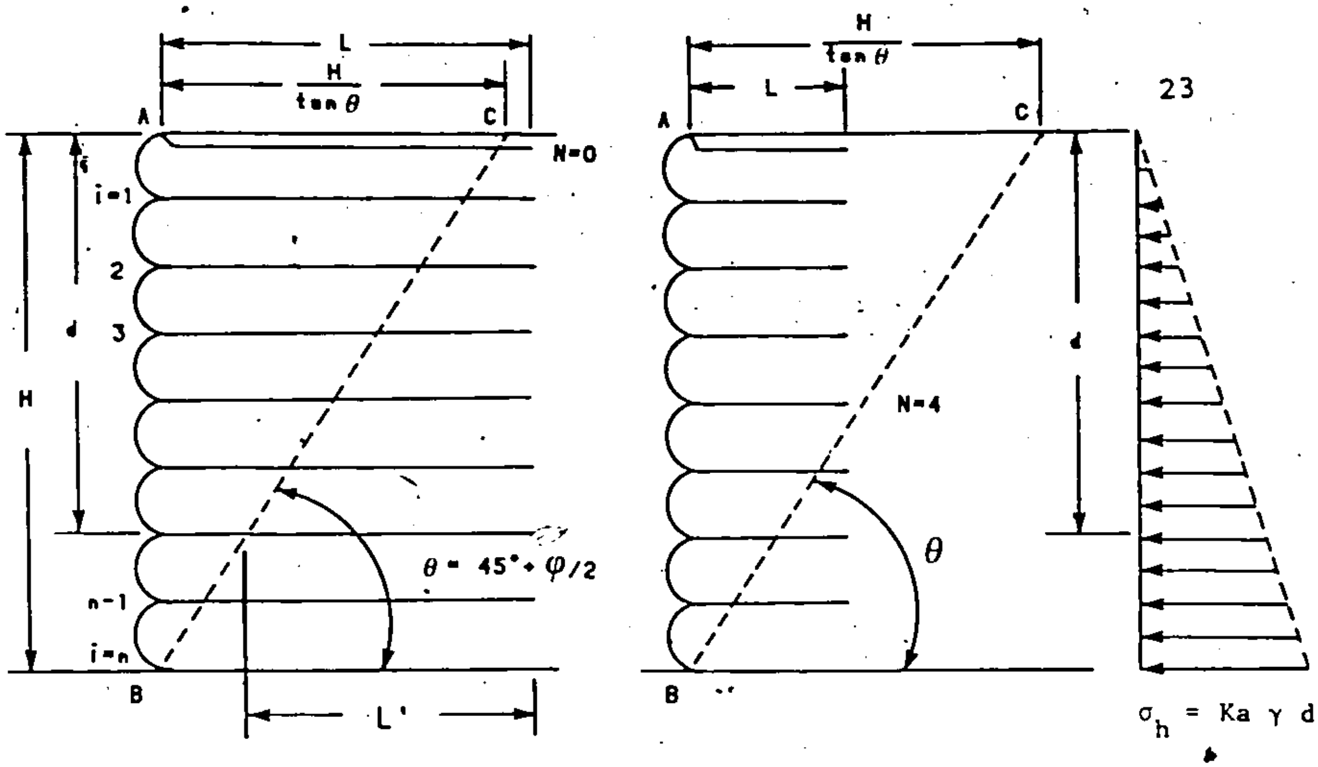

FIG. 2.2.1- KEY FACTORS USED IN DESIGN OF A REINFORCED EARTH WALL
(LEE et al., 1973)

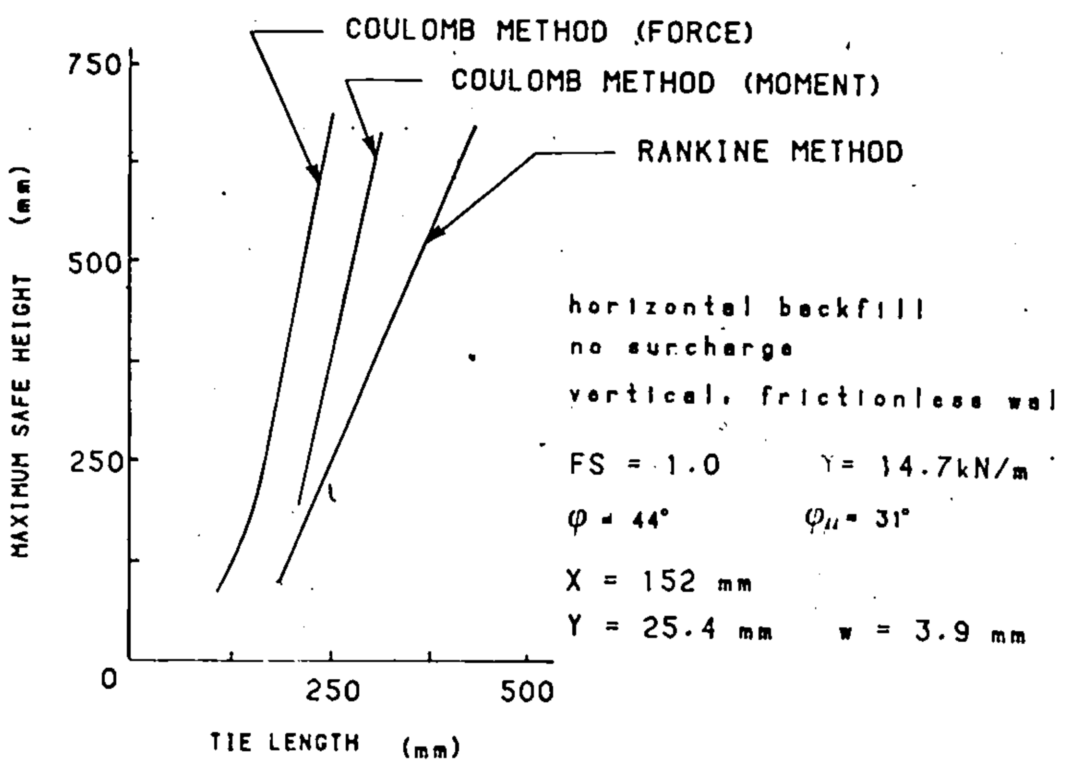

FIG. 2.2.2- COMPARISON OF RESULTS FROM THREE METHODS OF ANALYSIS FOR PULLOUT FAILURE
(LEE et al., 1973)

2.3 BANERJEE (1975)

Banerjee (1975), demonstrated that the sum of tensions in the horizontal reinforcing strips, which is produced by friction, opposes the pressure from the earth mass, thus maintaining equilibrium.

Using Coulomb's wedge analysis, Banerjee (1975) proposed that bond failure of the reinforcing strips can be measured by the following expression:

$$\Sigma T = N\ A_s\ F_t \qquad \text{or,}$$

$$\Sigma T = \psi\ N\ L\ b\ [\ c + (\gamma H + P_o)\ \tan\phi\ ]$$

where ΣT is the summation of tension in the reinforcing ties

N, the number of ties

A_s, the cross-sectional area of the ties

F_t, the ultimate tensile stress of the ties

ψ, the coefficient of friction between the soil and the tie

L, the length of the ties

b, the perimeter of a tie

c, the apparent cohesion of the soil

and P_o is the uniformly distributed surcharge load.

Subsequent analysis by Banerjee showed that the total sliding force P is a function of P_o, the surcharge load and β, the angle between the wall facing and the failure surface, and can be evaluated by:

$$P = (1/2 \ \gamma H^2 + P_o H) \sin \beta$$

and the total resisting force F can be expressed as:

$$F = (1/2 \ \gamma H^2 + P_o H) \sin \beta \tan \beta \tan \phi + (\cos \beta \tan \phi + \sin \beta) \Sigma T$$

$$+ c H \sec \beta$$

Hence, the factor of safety is determined by dividing the resisting force by the sliding force.

$$FS = \frac{F}{P}$$

2.4 AL-HUSSAINI AND PERRY (1978)

Al-Hussaini and Perry developed a design procedure in 1978 for reinforced soil walls, based on large-scale models in the field. Assuming Rankine failure in the soil mass, the pressure distribution along the face of the wall is linear with depth and can be expressed as:

$$\sigma_h = Ka\ (q + \gamma d)$$

in which q is the surcharge pressure.

As previously stated, to ensure the internal stability of a reinforced soil wall, the reinforcing ties should not fail in tension or pullout due to lack of frictional resistance under applied loads.

The design criteria for ties breaking in tension was the one proposed by Lee et al. (1973) which was presented in section 2.1.1.

In the case of failure by tie pullout, Al-Hussaini and Perry (1978) differed from Lee et al.(1973) by using only the portion of the tie beyond the point of maximum tensile stress as the effective anchorage.

The shear stress distribution at the initial active failure is determined from the slope of the tensile stress distribution curve as shown in figure 2.4.1, and the total effective frictional force along the reinforcing tie, T_e, is:

$$T_e = 2\,w\,(2/3\,\tau_m\,L') = 4/3\,\tau_m\,L'\,w$$

where τ_m is the maximum frictional stress along the tie, L' is the effective length of the tie, and w is the width of the tie.

The factor of safety against pullout failure, F_{sp} is defined by Al-Hussaini and Perry (1978) as:

$$F_{sp} = \frac{\tau_f}{\tau_m}$$

where τ_f is the shear stress between the tie and the surrounding soil at failure.

Therefore the resisting force due to friction, T_e, is expressed as:

$$T_e = 4/3\;w\,L'\,(q + \gamma d)\;\frac{\tan\phi_\mu}{F_{sp}}$$

with ϕ_μ being the angle of friction between the reinforcing tie and the surrounding soil as obtained by direct shear tests.

By combining the maximum tensile force equation, T_d, which was developed by Lee et al.(1973) (section 2.2.1) with the above equation for the resisting force due to friction, T_e, and assuming that Rankine active earth pressure exists, Al-Hussaini and Perry (1978) obtained the following equation for factor of safety, F_{sp}, with respect to tie pullout:

$$F_{sp} = \frac{4\ L'w \tan \phi_\mu}{3\ Ka\ X\ Y}$$

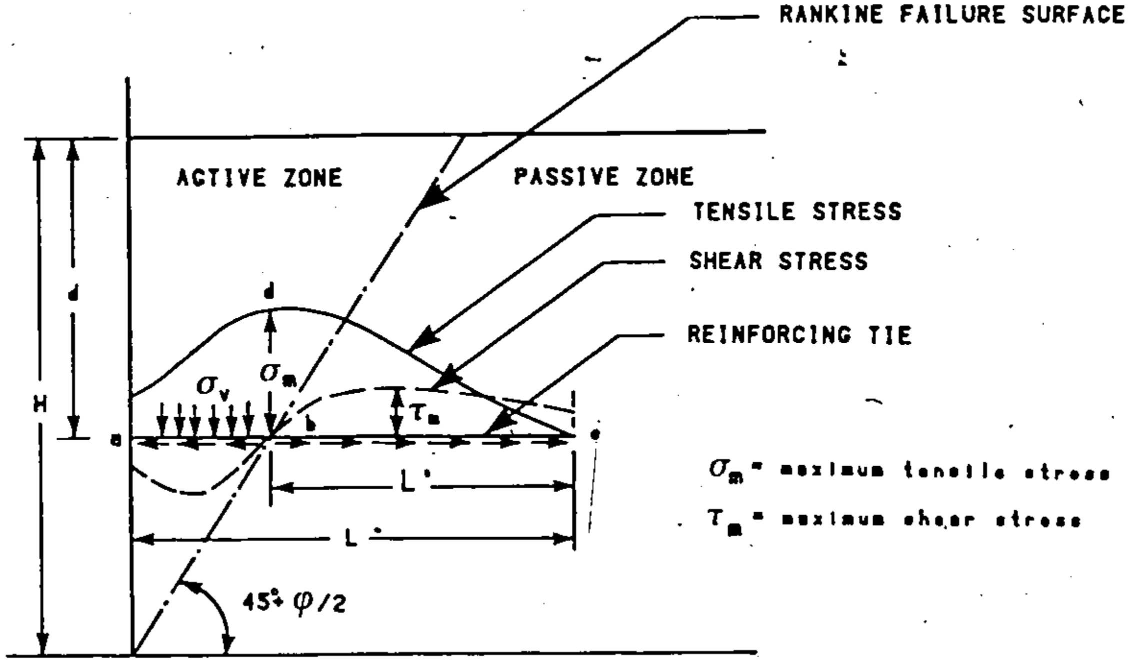

FIG. 2.4.1- HYPOTHETICAL STRESS DISTRIBUTION ON THE FACE OF THE WALL
(AL-HUSSAINI AND PERRY, 1978)

2.5 IWASAKI AND WATANABE (1978)

In Japan, Iwasaki and Watanabe (1978) analysed railway embankments reinforced with nets of synthetic resin. Figure 2.5.1 illustrates the stability analysis of an embankment with and without reinforcing nets.

Assuming planar sliding, the earth pressure P acting on plane OB in an unreinforced embankment can be expressed as follows:

$$P = (W_L + W_s) \tan (\beta - \phi)$$

where W_L denotes the surcharge load, W_s is the weight of the triangular soil block AOB, β is the inclination of the surface AB, and ϕ is the angle of internal friction.

The resistance R_s of soil block OBC against the earth pressure P is expressed as:

$$R_s = (\gamma/2)\, H^2 \cot \alpha \tan \phi$$

with α being the inclination of the slope.

Therefore, the safety factor for the slope is expressed as:

$$FS = R_s/P$$

In the case of the net reinforced embankment, the resistance R_n of the net against sliding may be given by:

$$R_n = 2\, f\, ((W_L/B) + \tfrac{1}{2}\,\gamma\, H)\, L_1 + \tfrac{1}{2}\,\gamma\, H\, L_2$$

where f denotes the coefficient of friction between the soil and net, B is the width of the surcharge footing, L_1 is the length of net which is laid behind the sliding surcharge and bears the surcharge load, and L_2 is the residual length of net behind the sliding surface which does not bear the surcharge load.

Hence, the safety factor for the net reinforced embankment becomes:

$$FS = \frac{R_s + R_n}{P}$$

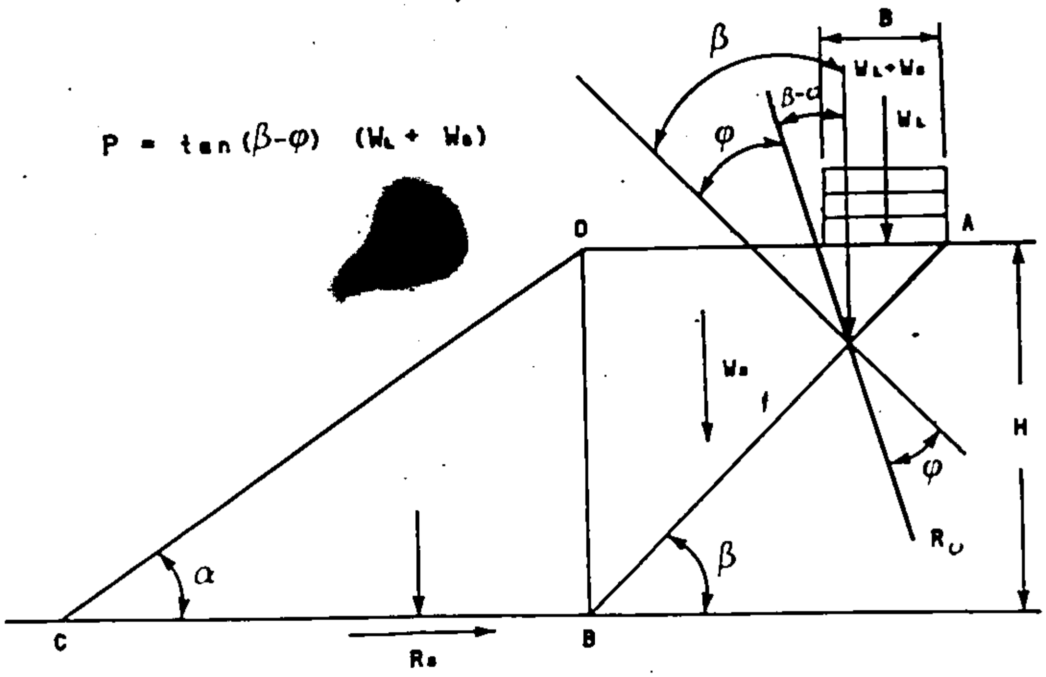

(A) STABILITY ANALYSIS OF SLOPE WITHOUT NET

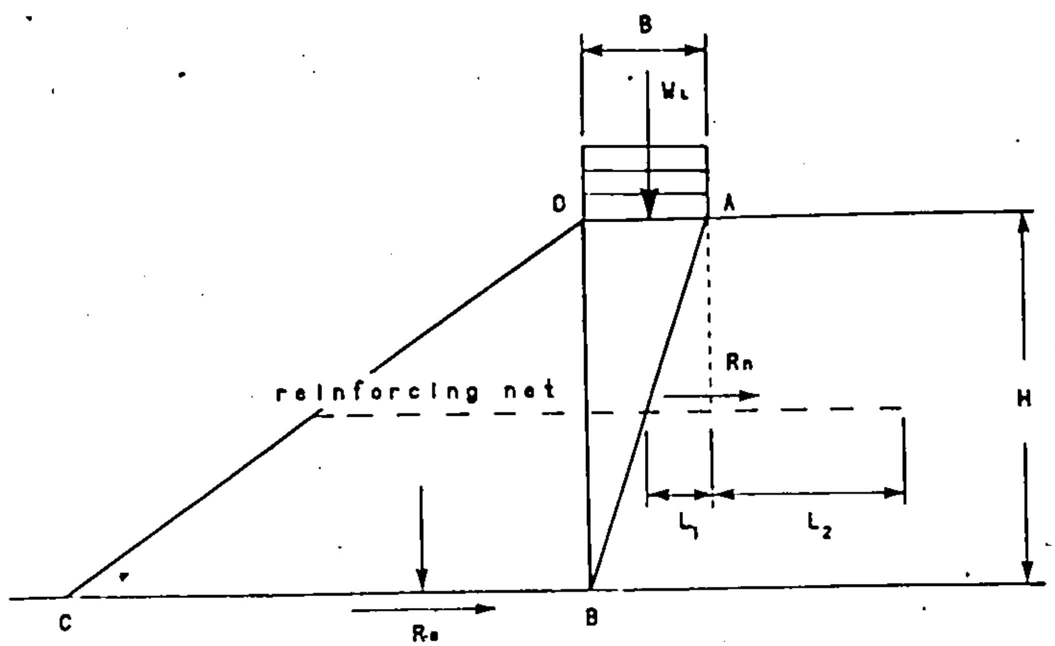

(B) STABILITY ANALYSIS OF SLOPE WITH NETS

FIG. 2.5.1- STABILITY ANALYSIS OF SLOPE WITH AND WITHOUT NETS
(IWASAKI AND WATANABE, 1978)

2.6 ROMSTAD ET AL. (1978)

Romstad and his co-workers developed a finite element failure model for reinforced soil structures which allows the determination of failure surfaces and critical heights for field prototype conditions.

The equation used in the determination of the factor for cohesionless material at specific locations is given by:

$$FS = \frac{2\,\sigma_3 \,\sin\phi}{(\sigma_1 - \sigma_3)_m\,(1 - \sin\phi)}$$

The idealized failure surface derived from the finite element studies is illustrated in figure 2.6.1, along with the maximum resultant normal and shear forces at collapse due to failure along the selected surface. This surface can be divided into three components, a rectangle and two triangles.

Analysing the induced forces on the failure surface Romstad et al. (1978) determined the resistance capacity, S_r, of the soil. This capacity to resist the applied shear forces is a function of the frictional capacity of the soil, the resistance of the reinforcing strips and cohesion of the soil material, and may be written as follows:

$$S_r = C_1L_2 + C_2L_3 + N_{2s}\tan\phi_1 + N_3\tan\phi_2$$

C_1 and C_2 represent the cohesion of the reinforced soil and backfill material respectively, ϕ_1 and ϕ_2, the associated friction angles and N_{2s}, the resultant normal force on the soil in the reinforced soil mass.

The strip capacity per unit width of soil, T_x, assuming the failure surface passes through the end of the strip at level n, is determined by the equation:

$$T_x \leq \frac{A_s f_y}{XY}$$

A_s is the cross-sectional area of the strips, F_y is the yield stress of the strips and X and Y are the horizontal and vertical spacing of the reinforcing strips respectively. The above equation is obtained if the strip reinforcement capacity is not treated at discrete points but averaged over the vertical height through which the failure plane passes.

After some mathematical manipulations a nondimensional parameter X_y/X_n may be obtained which incorporates all the design values required in a Reinforced Earth wall.

$$\frac{X_y}{X_n} = \frac{1 + \dfrac{H/L}{\tan\theta_1} - \sqrt{\left(1 + \dfrac{H/L}{\tan\theta_1}\right)^2 - \dfrac{4\,H/L}{\tan\theta_1}\left[1 - \dfrac{C_2}{H/L}\right]}}{2}$$

X_y/X_n is a ratio of the height of the reinforcing strip being examined over the height at which a change in slope is encountered in the failure surfaces H_2 .

Therefore, if significant yielding of the reinforcement at failure is desired, the design criteria becomes:

$$H < \frac{A_s f_y L}{2 w f \gamma L^2}$$

where f is the coefficient of friction between the soil mass and the reinforcement.

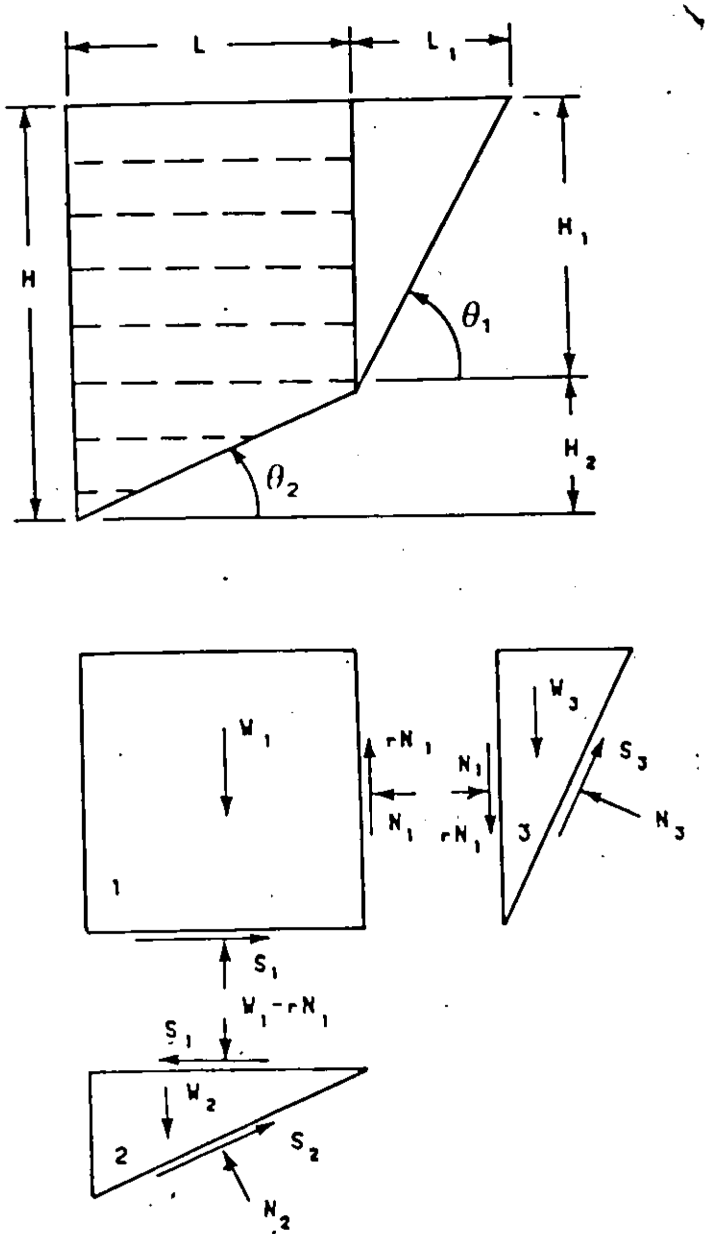

FIG. 2.6.1- MODEL FOR PREDICTING WALL HEIGHT
(ROMSTAD et al., 1978)

2.7 SMITH AND WROTH (1978)

Stating that current methods are based on either empirical rules, or unsupported theories, Smith and Wroth (1978) conducted an experimental study of model reinforced soil retaining walls to develop a more rational method of design.

The model walls were tested in a 200 mm wide glass-walled tank and the structures were built up until collapse occurred. Radiographs were taken to illustrate rupture surfaces after failure and to monitor displacements and strains during construction. In a narrow tank, it is possible that the frictional force exerted by the side walls may be significant, therefore adversely affecting the experimental results. Dense sand was used as backfill material and all model structures were tested at very low stress levels.

2.7.1 Failure as a rigid block

For a wall with densely packed reinforcements, Smith and Wroth idealized the reinforced zone as a rigid block. Extending the work of Smith and Bransby (1976), Smith and Wroth (1978) analyzed the structure by considering a Coulomb wedge acting behind the reinforced block. Figure 2.7.1 shows an exploded section through a reinforced soil wall.

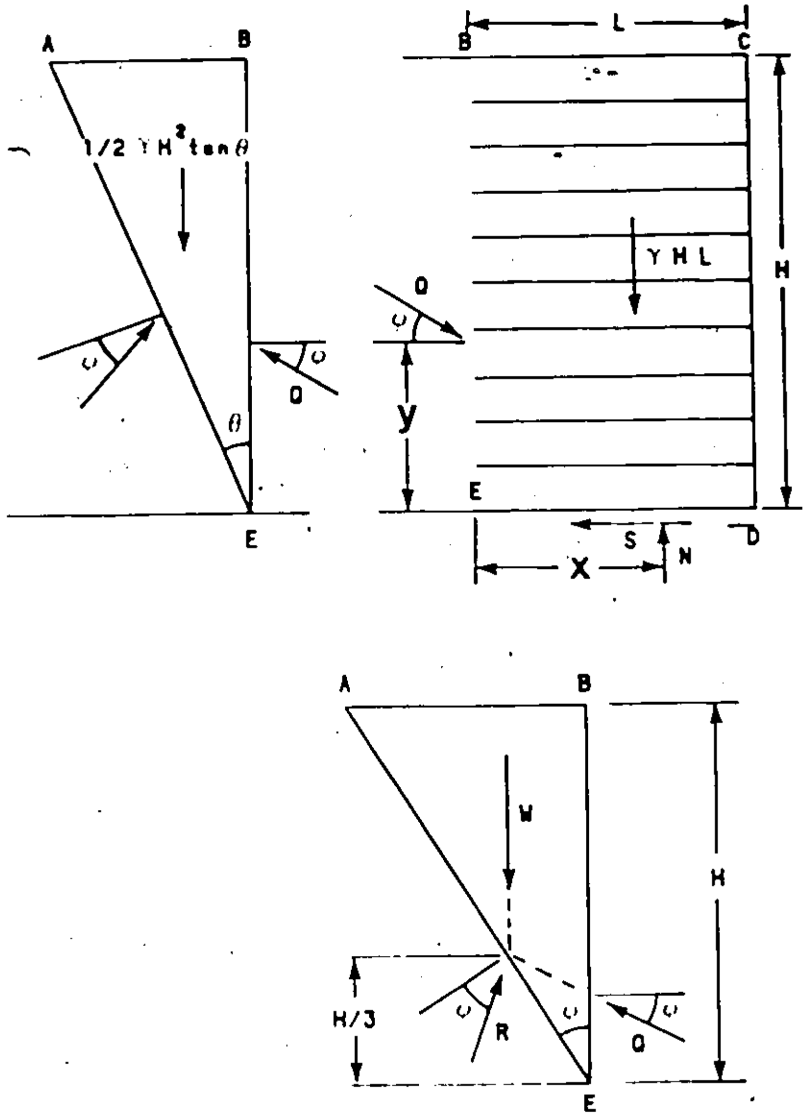

FIG. 2.7.1- FORCES ACTING ON WEDGE AND REINFORCED ZONE AT FAILURE
(SMITH AND WROTH, 1978)

The reaction Q, between the wedge and the reinforced zone is found by resolving forces horizontally and vertically for the wedge ABE. Q can be expressed as:

$$Q = \frac{1/2\ \gamma\ H^2 \tan\theta}{\cos\phi'\ \tan(\theta + \phi') + \sin\phi'}$$

All parameters in the equation are illustrated in figure 2.7.1 and have been defined previously.

With the base DE of the reinforced zone exerting a normal force N, acting a distance x from E, and a shear force S on DE, two possible failure mechanisms may occur. Firstly, failure may occur by sliding of the reinforced block along the plane DE, when

$$S = N \tan\phi$$

Secondly, failure may occur by overturning of the block BCDE. In investigating the possibility of failure by overturning, assumptions concerning the points of action of the forces on the base DE and the back BE of the reinforced zone must be made.

Using load cells, Smith and Wroth (1978) determined that the point of action of the force on the base when the wall fails is at the mid-point of DE, and that the force Q acts at a height of H/3.

Furthermore, Smith and Wroth (1978) assume that the force R acts at a height of H/3, and the lines of action of the forces R, W, and Q pass through the same point on AE in order to satisfy equilibrium conditions.

Hence, the height of action, y, above point E of force Q is given by:

$$y = 1/3\ H\ (1 - \tan\theta \tan\phi')$$

Thus, by substituting the estimated values of θ and ϕ in the above equation, the height of action, y, can be evaluated as a function of the height of the wall.

Finally, by taking moments about point E and substituting for forces N and Q, an expression which relates the failure height of the wall to the length of the reinforcements is found:

$$\frac{H}{L} = \frac{0.5\ \gamma \tan\theta \sin\phi}{0.16\ \gamma \tan\theta \cos\phi} \qquad \text{or,}$$

$$H = 3.125\ \tan\phi\ L$$

2.7.2 Failure analysis by block movement

According to Smith and Wroth (1978), the reinforced zone cannot be treated as a single block for wall structures with reinforcements that are short and wide or long and thin. An alternative analysis, which is an adaptation of Lee et al. (1973) and Bolton et al. (1978) was suggested for the determination of the height of failure. The factor of safety of a reinforced wall structure is given by:

$$FS = \frac{w\ L\ \mu}{Ka\ Y\ X\ \ (1 + (Ka\ z^2/L^2))}$$

where w and L are the width and length of the reinforcing strip, μ is the coefficient of friction and z is the depth of the reinforcement. Ka, X and Y have already been defined.

The above expression permits the calculation of the factor of safety at different heights of wall for failure by the tie pullout mode. If failure occurs with ties breaking, the maximum possible force in a strip is now its breaking strength and the above equation becomes:

$$FS = \frac{T}{Ka\ Y\ z\ X\ Y\ \ (1 + (Ka\ z^2/L^2))}$$

where T is the force required to break a strip.

Unlike Lee et al. (1973), Smith and Wroth (1978) find that the maximum tension in the ties occurs in the lower levels of reinforcement.

Smith and Wroth (1978) observed a change in direction of the main rupture surface at the back of the reinforcement zone and greater vertical displacements behind the reinforced zone for walls with short wide reinforcement. Hence, Smith and Wroth undertook to examine the overall equilibrium of a reinforced earth structure by the simple Coulomb method of considering block movement. Overall equilibrium methods are thought to be more realistic than local equilibrium methods for pullout failure.

As shown in figure 2.7.2, the area of sand that moves is divided into two blocks, with the boundary surface BE situated at the back of the reinforced zone.

Using the velocity diagram in figure 2.7.2, the forces acting on the reinforced block BCDE are its weight W, the reaction Q from block ABE, the reaction R acting on the plane ED, and the total tension in the reinforcing strips extending beyond ED, ΣT.

Solving for vertical and horizontal forces:

$$W + Q \sin \phi' = R \sin (\theta + \phi') \qquad \text{and,}$$

$$\Sigma T = R \cos(\theta + \phi') + Q \cos \phi'$$

The maximum possible total force exerted by the strips, ΣT^* is the product of the total surface area extending past DE, the normal stress, and the coefficient of friction between the soil and the reinforcement. Hence, the factor of safety becomes:

$$FS = \frac{\Sigma T^*}{\Sigma T}$$

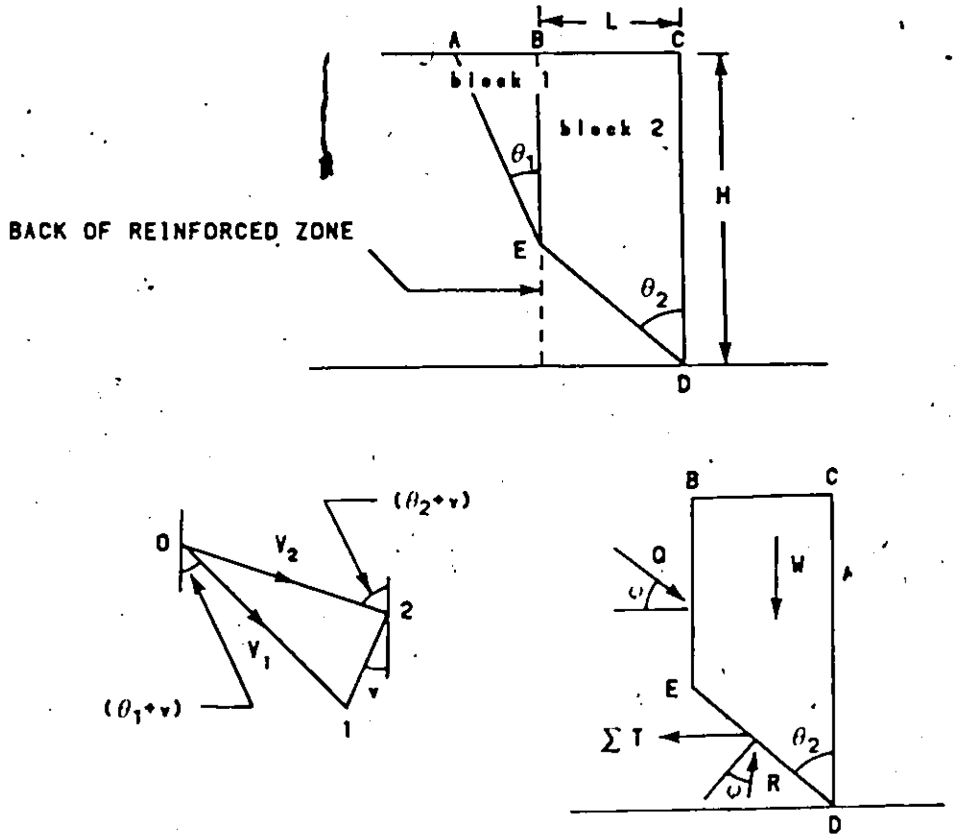

FIG. 2.7.2- FORCES AND VELOCITY DIAGRAM FOR WEDGE AND REINFORCED ZONE AT FAILURE (SMITH AND WROTH, 1978)

2.8 SCHLOSSER ET AL. (1978-79)

In a series of articles and papers, Schlosser et al. investigated the behaviour of reinforced soil structures using models and full scale experiments.

The reinforced structure is divided into two zones, an active zone, where the friction between the reinforcement and the soil tends to pull the reinforced mass towards the wall panels and a passive zone, where friction permits the anchorage (adherence) of the reinforcing element (figure 2.8.1). The tensile resistance developed in the reinforcing strips varies along the length of the strip, with a maximum value being reached at the junction of the two zones.

Failure of the structure by lack of adherence between the reinforcing element and the earth backfill (pullout) is prevented by ensuring that T_{max}, the maximum pullout force respects the following expression:

$$T_{max} \leq 2\,w \int_{L-L_a}^{L_i} f^* \,\sigma_v \,dL$$

With the apparent coefficient of friction, f^*, between the element and the earth backfill being defined as:

$$f^* = \frac{T}{2\,w\,L\,\gamma\,h}$$

where w is the width of the reinforcing element, L is the length of the element, L_a is the length of adherence, and h is the depth of embedment.

For the ribbed Reinforced Earth strips, the apparent coefficient of friction varies with depth of embedment, y, and internal angle of friction, ϕ, according to the formulae:

$$f^* = f_o^* (1 - y/y_o) + \tan\phi \ y/y_o \qquad \text{for } y \leq y_o = 6 \text{ m, or}$$

$$f^* = \tan \phi \qquad \text{for } y > y_o = 6 \text{ m}$$

f_o^* being the coefficient of friction at the surface of the fill which depends on the coefficient of uniformity of the backfill, $CU = D_{60} / D_{10}$.

$$f_o^* = 1.2 + \log CU$$

if CU is unknown, f_o^* is assumed to equal 1.5.

Juran and Schlosser (1979) presented a new design method which consists of studying the equilibrium conditions of the active zone, limited by a potential slip surface (circular or logarithmic spiral) which develops within the soil along the locus of the maximum tensile forces in the reinforcements.

The design method allows the determination of the locus and the determination of the maximum tensile forces in the reinforcing elements. This determination is essentially different from the classical limit analysis design methods which are derived from theories of plasticity and assume straight line slip surfaces (Coulomb).

Experimental observations of full scale structures and models lead Juran and Schlosser (1979) to adopt a logarithmic spiral shape to link the maximum tensile points on the reinforcing elements.This spiral is orthogonal to the surface and passes through the toe of the wall panels (figure 2.8.1).

Thus, the analysis yields an expression for the maximum pullout force, T_{max} :

$$T_{max} = Ka \, \gamma \, H \, X \, Y$$

Furthermore, the critical height, H_c, of the reinforced wall can be evaluated, first, for failure by tension of the reinforcing strips:

$$H_c = (R_t) / Ka \, \gamma \, X \, Y$$

R_T is the resistance of the reinforcing element to tension, secondly, for failure by lack of adherence:

$$\tan \beta < 2 \, f^* \, \frac{w}{y} \, \frac{L_a}{X}$$

The width of the active zone, D, in the earth structure can also be determined by the proposed design method:

$$D = \left[\frac{66 - \phi}{100} \right] H$$

Schlosser and Segrestin (1979) applied the design method to reinforced soil walls subjected to concentrated surcharges (strip footings), using superposition principles, that is, calculating separatly the maximum tensile forces in the reinforcing elements due to the self-weight of the structure and the concentrated surcharge.

The design method yields satisfactory results if the vertical stress resulting from the surcharge is assumed to disperse uniformly on an area bounded by 1:1 dispersion lines instead of the usual 2:1 dispersion.

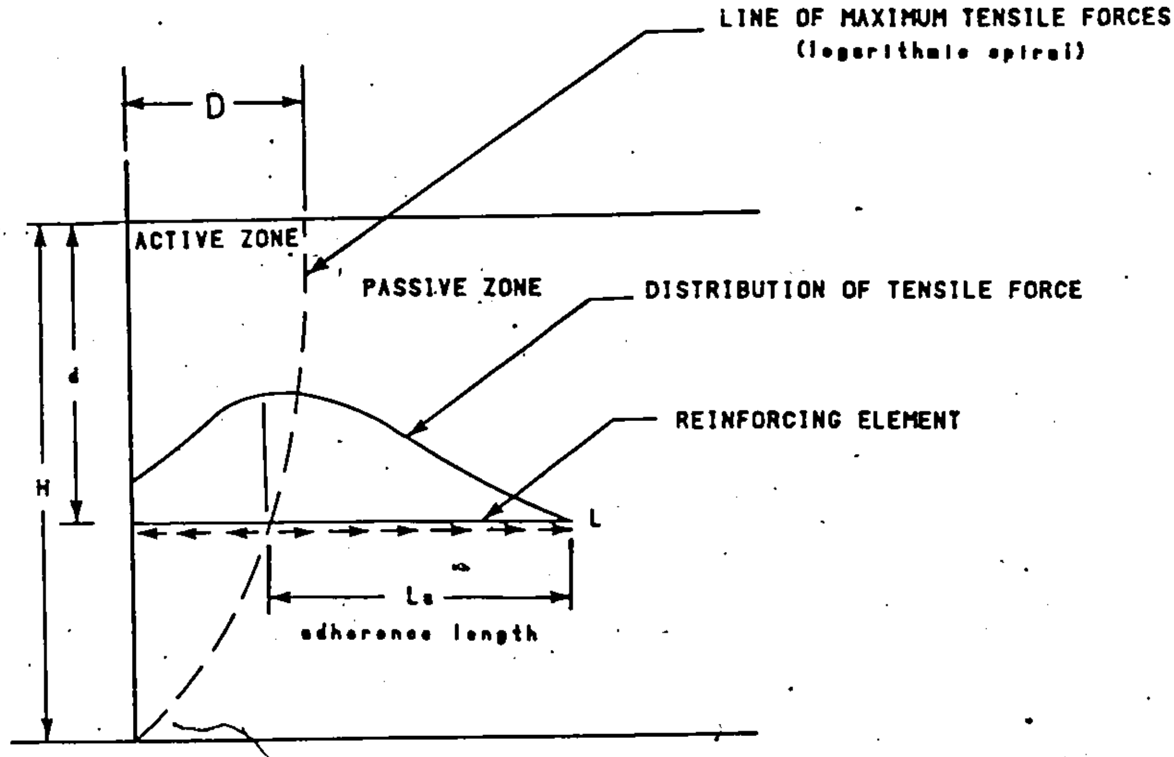

FIG. 2.8.1- LOGARITHMIC DISTRIBUTION OF TENSILE FORCES (JURAN AND SCHLOSSER, 1979)

2.9 OSMAN, FINLAY AND SUTHERLAND (1979)

In 1979, Osman et al. proposed a method of analysis which has been designated as the Energy Method. It is based on a consideration of the equilibrium of the external work due to earth pressure and the internal strain energy stored in the reinforcing ties, and can take into account:

1. the effect of tie length on the magnitude of tension
2. the variation of tension along a particular tie and the distribution of tension in the ties with depth
3. the deflected shape of the wall facing

Assuming that the external work done is stored in the ties as an elastic strain energy ,which can be calculated if the tie tension distribution is known, the following expressions were obtained which permit the direct calculation of various parameters in a rapid and convenient manner. All variables have been previously defined.

Maximum tension in tie at depth h,

$$T = \sqrt{\frac{6 \quad Ka^{2.5}}{L}} \cdot \gamma \, h \, X \, Y \sqrt{H - h}$$

Maximum tie tension in wall,

$$T_{max} = \sqrt{\frac{8 \quad Ka^{2.5}}{9L}} \quad \gamma \, X \, Y \, H^{1.5}$$

Critical wall height, H_c,

$$H_c = \left(\frac{R_t}{\gamma \; X \; Y} \sqrt{\frac{9L}{8 \; Ka^{2.5}}} \right)^{0.67}$$

and the safety factor against tie pullout is:

$$FS = \frac{2 \; w \; f \; L^{1.5}}{X \; Y \sqrt{6 \; Ka^{2.5} \; (H - h)}}$$

2.10 <u>KENNEDY</u>, <u>LABA</u>, <u>MOSSAAD</u> (<u>1980</u>)

Kennedy et al. (1980) presented an analytical method to estimate the force distribution along the reinforcing elements and the forces transmitted to the facing of a reinforced earth wall subjected to a surcharge strip load.

Working from the basis that the case of a reinforced soil wall lies between that of a semi-infinite solid with a horizontal surface and the case of a conventional rigid retaining wall (figure 2.10.1 a&b); the horizontal pressure on a reinforced soil wall is defined as:

$$\sigma_h = \frac{(2 - R) \; q \; (\beta - \sin \beta \cos 2\alpha)}{\pi}$$

in which q is the surcharge strip load, β is the angle of visibility from a specific point on the wall facing, α is the angle between the vertical and the bisector of angle β, and R is a reduction factor, dependent upon the stiffness characteristics of the backfill and the reinforcing elements.

$$R = \frac{(AE_t)\ \text{backfill}}{(AE_t)\ \text{backfill} + (AE_t)\ \text{reinforcing element}}$$

where A is the cross-sectional area and E_t is the tangent modulus of elasticity (Kennedy et al. 1980).

From this analysis, a maximum tensile force, T_{max}, resulting from the surcharge strip load is applied to each reinforcing element and can be determined by the following equation:

$$T_{max} = \sigma_h\ X\ Y$$

in which Y and X are the vertical and horizontal spacings of the reinforcing elements.

Furthermore, Kennedy and his co-workers divided the soil mass into two major zones, the resisting and active zones (as in figure 2.4.1). The frictional forces exerted by the soil on the reinforcing strip are mobilized away from the facing in the resisting zone and towards the facing in the active zone. Therefore, the force exerted on the facing (figure 2.10.2), T_s, is estimated by the following equation:

$$T_s = T_{max} - (\Delta T/\Delta L)\ (ab)$$

where ab is the length of the reinforcing element and $\Delta T / \Delta L$ is the rate of change of the tensile force T with respect to the length of the reinforcing element L and is equal to:

$$\Delta T/\Delta L = 2\ w\ \mu\ \sigma_v$$

in which w is the width of the reinforcing element, μ is the actual mobilized coefficient of friction between the reinforcing element and the soil backfill and σ_v is the uniform vertical stress.

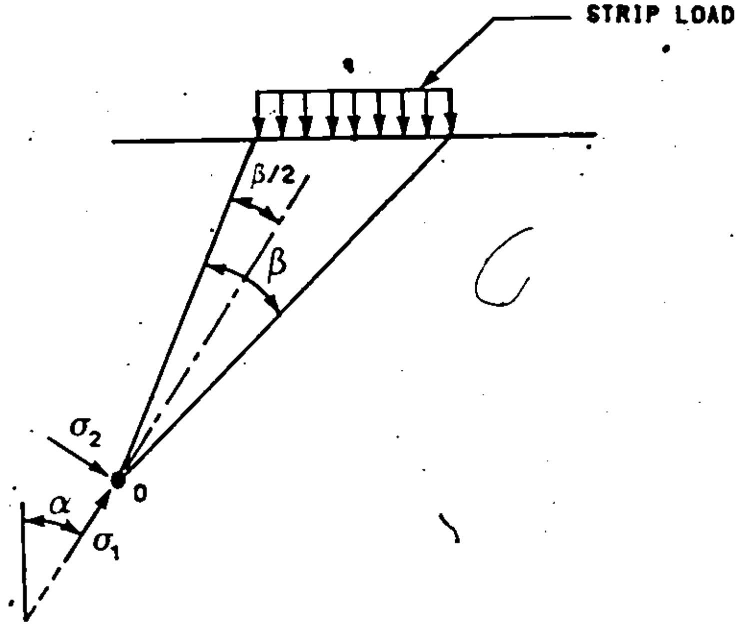

FIG. 2.10.1 (a) - PRINCIPAL STRESSES IN A SEMI-INFINITE SOLID DUE TO SURCHARGE LOAD (KENNEDY et al., 1980)

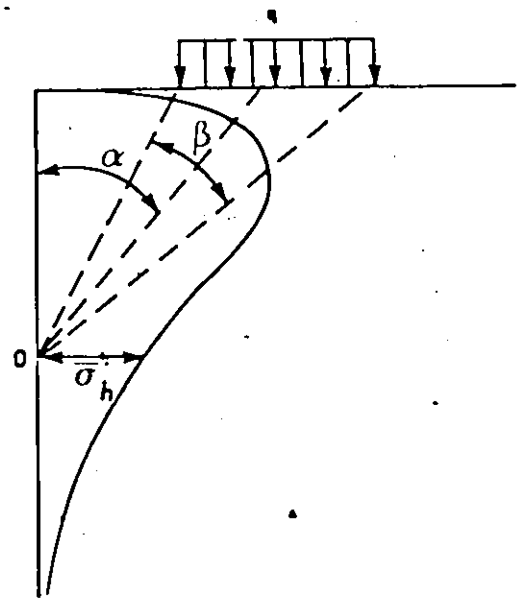

FIG. 2.10.1 (b) - LATERAL EARTH PRESSURE ON A RIGID RETAINING WALL DUE TO SURCHARGE LOAD (KENNEDY et al., 1980)

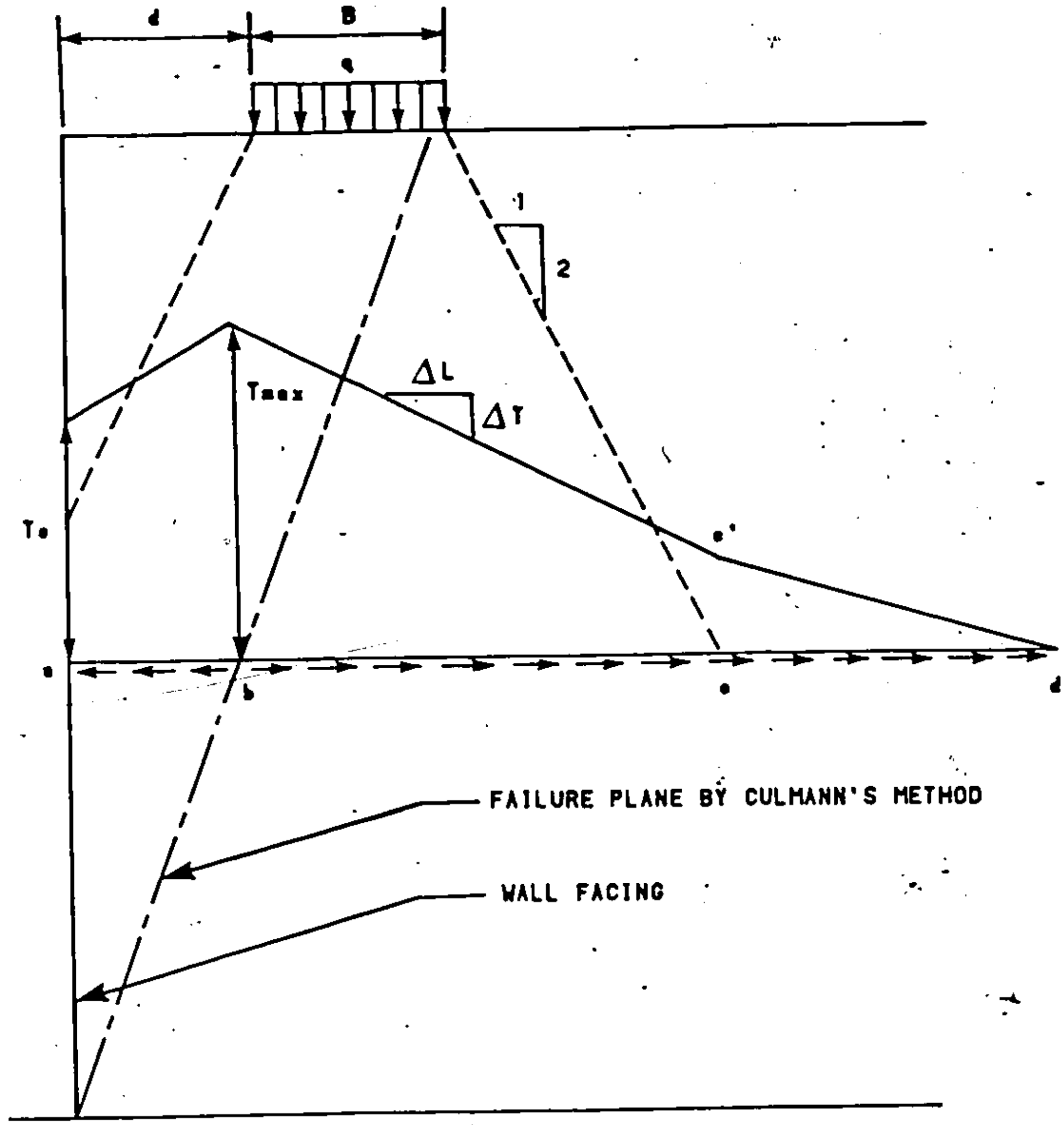

FIG. 2.10.2- IDEALIZED DISTRIBUTION OF TENSILE FORCE IN A REINFORCING ELEMENT
(KENNEDY et al., 1980)

2.11 TOBUTT (1981)

D.C. Tobutt adapted the Bishop slip circle method to analyse reinforced embankments. Tobutt (1981) contends that the resistance moment of the reinforcement about the circle centre, M_r, can be added, by superposition, to the existing resistance moment of the unreinforced embankment (figure 2.11.1).

Thus, the Bishop expression for the factor of safety of a reinforced embankment becomes:

$$FS = \frac{R\sum\left(\dfrac{c'b + W(1 - r_u)\ \tan\phi'}{\cos\alpha + \dfrac{\tan\phi'\ \sin\alpha}{FS}}\right) + M_r}{R\sum W\sin\alpha}$$

where W is the weight of a slice, R, the radius of slip circle, c', the cohesive strength with regard to effective stresses, α, the slope of the base of the slice, r_u, the porewater pressure ratio and b, the breadth of a slice.

The reinforcement resistance moment M_r is calculated by finding the allowable tensile force for a given layer of reinforcement (lesser of the actual ultimate tensile force and pullout force) and multiplying it by the vertical lever-arm to the centre of the circle, similarly for all reinforcement layers for which the individual resistance moments are summed.

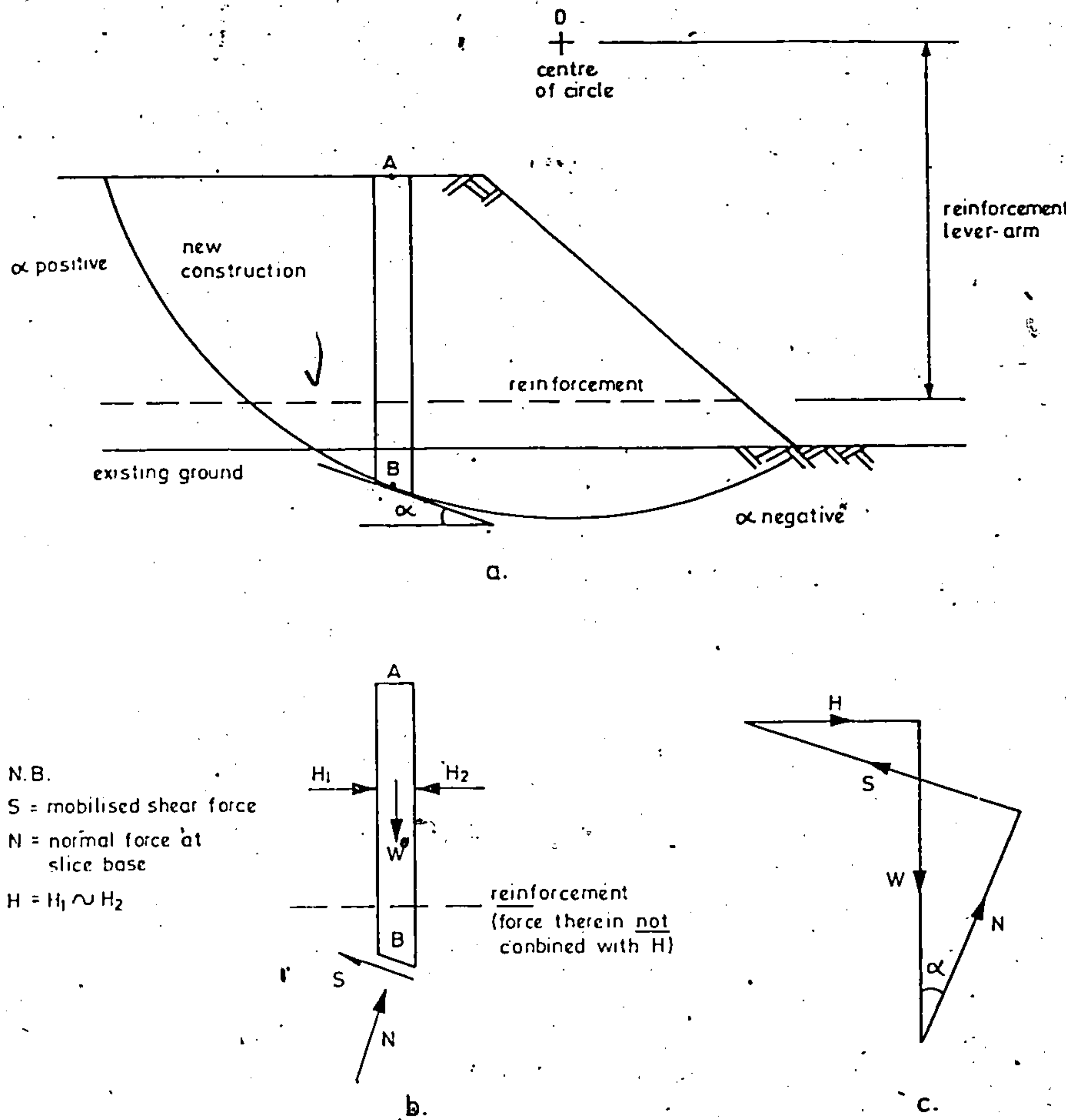

a = Embankment with reinforcement layer slip-circle analysis.
b = Isolated slice.
c = Force Diagram.

FIG. 2.11.1- ANALYSIS OF REINFORCED EMBANKMENT BY
MODIFIED BISHOP SLIP CIRCLE METHOD
(TOBUTT, 1981)

2.12 VSL RETAINED EARTH (1981)

The VSL Corporation[2] has developed an alternative soil reinforcement system based on bearing rather than friction. The reinforcing element is a galvanized welded wire mesh (figure 1.3.1 b) which uses the bearing pressure developed along the projected area of the crossbars and transfers it from the soil mass to the longitudinal bars, thus developing tensile forces in these bars.

The electrically welded wire mesh has an ultimate tensile strength of 75 ksi (517 MPa) with a bar diameter which varies from 3/8" to 5/8" (9.5 to 16 mm) and with grids of 6"x24" (.15m x .61m).

The backfill material used in the reinforcing system should not contain more than 15% of soil particles passing sieve no. 200. The angle of internal friction should approximate 35 degrees and the plasticity index of the soil should be less than 6 (Al-Yassin 1980).

The stability analysis of a Retained Earth structure is two-fold as in the Reinforced Earth system. First, the external stability of the structure must be investigated for:

1. sliding at the base of the structure
2. punching of the foundation soil

---

[2] VSL Retained Earth is a registered trademark of the VSL Corporation.

3. settlement
4. general slope failure

Factors of safety are kept above 1.5, with the factor of safety for sliding at the base of the structure being determined by the equation:

$$FS = \frac{\gamma\ H \tan \phi_{\mu}\ L}{\frac{1}{2}\ Ka\ \gamma\ H^{2}} \geq 1.5$$

ϕ_{μ} being the angle of interface friction at the base and L, the length of the reinforcing elements.

Second, the internal stability of the structure is investigated for:

1. pullout failure
2. tensile failure of the reinforcing elements

The factor of safety against pullout is determined by dividing the pullout resistance generated by the reinforcing element by the maximum force developed in these elements, T_{max} (figure 2.12.1).

$$FS = \frac{p\ d\ b\ (L_b/a + 1)}{T_{max}}$$

where $p = \gamma\ h_i A_c$

with A_c being the anchorage factor,

$$A_c = \frac{P_{max}}{\sigma_v \, d \, b \, N}$$

Thus, giving a factor of safety against pullout of:

$$FS = \frac{d \, b \, \gamma \, h_i \, A_c((L_b/a) + 1)}{T_{max}}$$

with

p = maximum bearing resistance developed against the crossbars

A_c = anchorage factor

d = diameter of the reinforcing bars

b = width of the reinforcing mesh

L_b = length over which bearing is considered

a = spacing of the crossbars

γ = unit weight of soil backfill

h_i = depth of reinforcing layer

P_{max} = maximum pullout load

σ_v = normal pressure

N = number of crossbars

The factor of safety against failure by tension of the reinforcing members is calculated by the following expression:

$$FS = \frac{F_{all}\,(a)_s}{T_{max}}$$

where F_{all} = maximum allowable steel stress (42% of yield, based on corrosion studies)

$(a)_s$ = cross sectional area of longitudinal bars per reinforcing panel

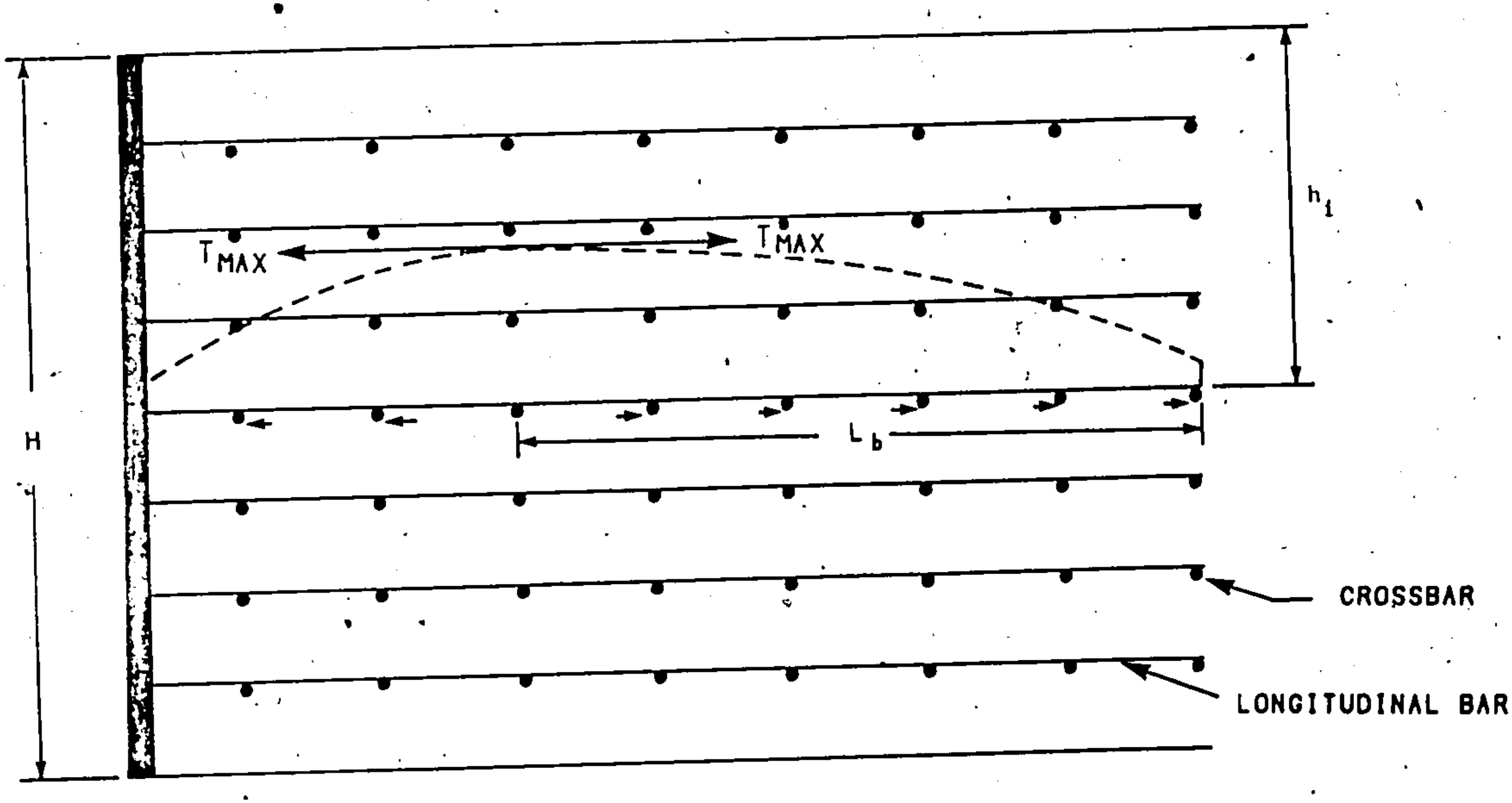

FIG. 2.12.1- DISTRIBUTION OF TENSILE FORCE ALONG WIRE MESH REINFORCEMENT
(VSL Corp., 1981)

2.13 TENSAR GRIDS (1982)

Tensar[3] high tensile strength grid reinforcing elements are produced from polymers which are resistant to chemical substances normally found in soils. The Tensar grid, which is a product of Netlon Limited, is an alternative to the reinforcing strips used by the Reinforced Earth Company.

The technique can be applied to the construction of reinforced embankments, reinforced soil retaining walls and many other earth structures.

2.13.1 Reinforced embankments

The factor of safety of an embankment can be evaluated, assuming shear failure in the form of a circular slip, by dividing the resisting moment developed in the embankment by the disturbing moment caused by its self-weight and any surcharge load.

Whenever the calculated factor of safety is below the required value, the resisting moment can be supplemented by the inclusion of reinforcement in the form of Geogrids, laid in horizontal layers in the zone of weakness, to intercept the shear plane (figure 2.13.1).

[3] Tensar is a registered trademark of Netlon Limited.

Hence, the factor of safety becomes:

$$FS = \frac{(S\ L\ R) + Ty}{Wx + qe'}$$

where S = shear strength of the soil

L = length of the slip plane

R = radius of the slip circle

W = weight of earth mass

x,e' = horizontal lever arms about centre of rotation

q = surcharge

T = tensile force supplied by reinforcing grids kN/m per metre width of reinforcement

y = vertical lever arm about centre of rotation from the centre of gravity of the tension zone

The tensile forces in the reinforcement are effectively transferred to the soil by mechanical interlock as in reinforced concrete. Mechanical anchorage on both sides of the grid has been indicated by pullout tests and direct shear box experiments, hence the grip length, L, is defined by the following expression:

$$L = \frac{T_1}{2\ \mu\ S}\ FS$$

where T_i is the actual tension in the grid layer and μ is the coefficient of friction between reinforcement and soil, varying between 0.5 and 1.0 depending on soil type and grid type.

2.13.2 Reinforced earth walls

Utilizing horizontal grid reinforcing layers in wall structures as illustrated in figure 2.13.2, the horizontal pressure P_a applied to the wall facings at any depth h, ignoring the effects of friction between the soil and the wall is:

$$P_a = Ka\ (\gamma h + q)$$

where $$Ka = \frac{1-\sin\phi}{1+\sin\phi}$$

Therefore, the tension T, to be resisted by reinforcement at depth h with a vertical spacing d between reinforcing layers is:

$$T = Ka\ (\gamma h + q)\ d$$

Assuming a granular fill of known density and shear resistance angle, the factor of safety against pullout for each reinforcing layer is determined by the following equation:

$$FS = \frac{T_i}{Ka\ (\gamma h + q)\ d}$$

T_i being the permissible tensile strength of the polymer grid. Futhermore, the grid lengths, L, can be evaluated:

$$L = \frac{(FS)\ T_i}{2\ (\gamma h + q)\ \mu \tan \phi}$$

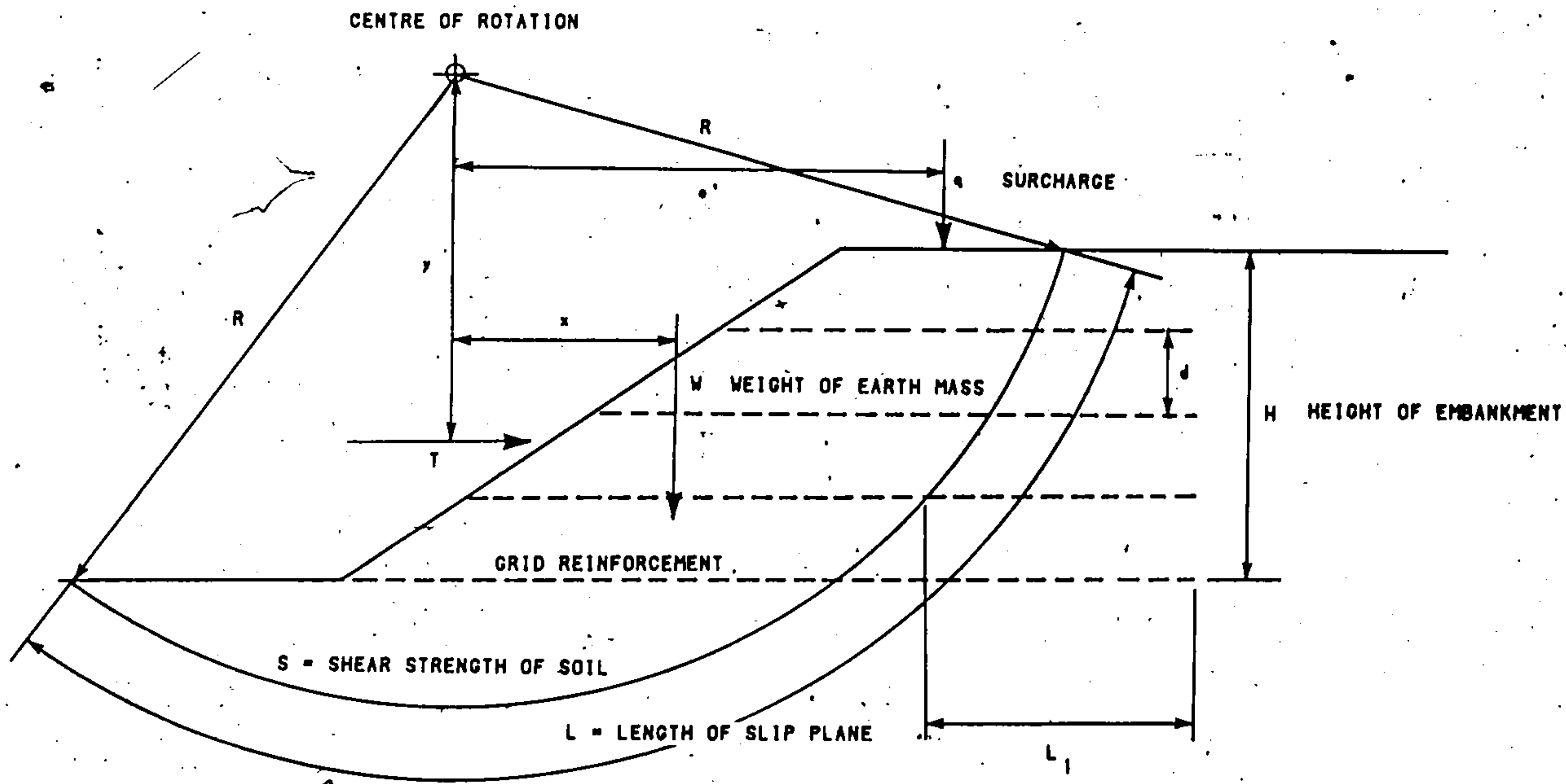

FIG. 2.13.1- STABILITY ANALYSIS OF A GRID REINFORCED EMBANKMENT BY BISHOP'S CIRCULAR SLIP SURFACE METHOD (TENSAR, 1982)

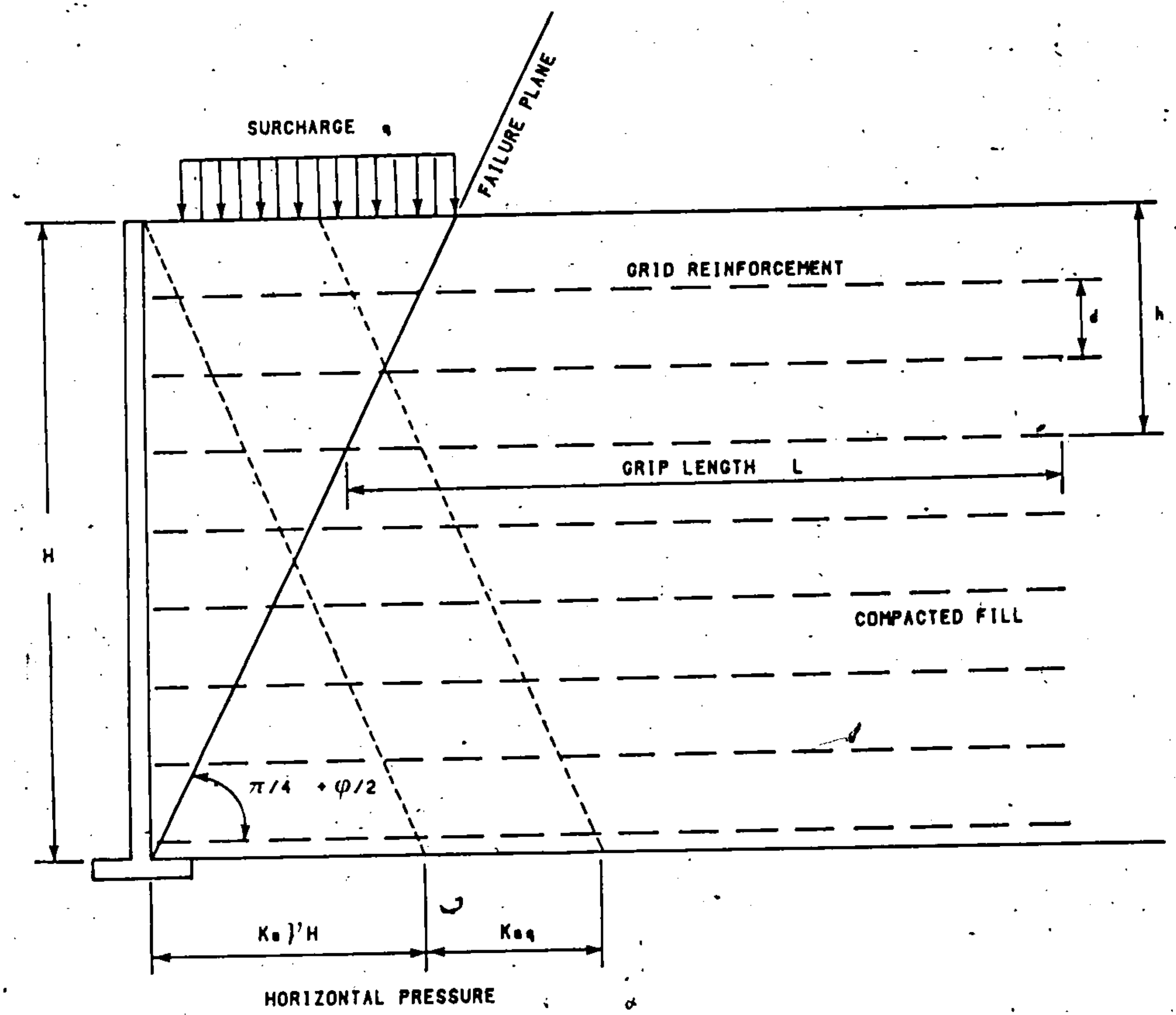

FIG. 2.13.2- STABILITY ANALYSIS OF A GRID REINFORCED WALL
(TENSAR, 1982)

Chapter III

DESIGN PARAMETERS

An experimental program of model testing was undertaken in the years 1981 and 1982 in order to investigate the behaviour of reinforced soil structures utilizing steel wire mesh reinforcement.

The program included:

1. pullout tests of different reinforcing elements
2. triaxial compression tests of wire mesh reinforced samples
3. large-scale models of wire mesh reinforced embankments
4. large-scale models of wire mesh reinforced walls

The following chapter describes and analyses the design parameters used for each specific test.

3.1 SOIL CHARACTERISTICS

As the backfill soil is the most crucial parameter in such a testing program a single soil type was selected for all the different tests. Due to its availability in large quantities, a specially selected crushed silica sand was chosen for this investigation. The silica sand was factory crushed quartz, designated as Silica-24.

Figure 3.1.1 presents a typical grain-size distribution of the silica sand employed in the laboratory testing. A grain-size analysis (ASTM D1140-54) is an attempt to determine the relative proportions of the different grain sizes which make up a grain soil mass. The curve gives a coefficient of uniformity, C_u, of 2.0 and a coefficient of concavity, C_c, of 0.98. These coefficients permit us to classify the soil as a relatively poorly graded sand (uniform).

A value of specific gravity is necessary to compute the void ratio of a soil, and is useful in determining the unit weight of a soil (this term is called "relative density", D_r, in the SI-System). Using Bowles (1970) definition of specific gravity as the unit weight of a material divided by the unit weight of distilled water at 4 degrees Celcius, the specific gravity of the crushed silica sand sample was determined to be 2.66.

Hasnain (1974) and Moore (1978) performed additional tests in order to describe the material more fully, and determined the average coefficient of angularity of the crushed silica sand to be 1.52, classifying the material once again as angular. The coefficient of angularity being defined as follows:

$$E_c = \frac{S_w}{S_{th}}$$

where E_c =coefficient of angularity

S_w =actual measured specific surface in m²/kg

S_{th} =theoretical specific surface assuming that all grains are of spherical shape in m²/kg

Perfectly spherical grains would have an E_c value of 1.0.

Hasnain (1974) also determined the mean sphericity of the crushed silica sand to be 0.68 and the roundness of the grain particles to be 0.17.

The last characteristic of the silica sand to be studied was its density index, I_d, (ASTM D2049-69, Bowles 1970), which permitted the determination of the unit weight of the soil. A maximum value of 1.66 gm/cm³ (16.28 kN/m³) and a minimum value of 1.25 gm/cm³ (12.26 kN/m³) were recorded for the unit weight of the soil. Upon further analysis the maximum and minimum void ratios were calculated to be 1.13 and 0.61, with maximum and minimum porosities set at 0.53 and 0.38.

The internal angle of friction of the crushed silica sand was determined later on as part of the experimental testing program. The characteristics of the silica sand are listed in table 1 .

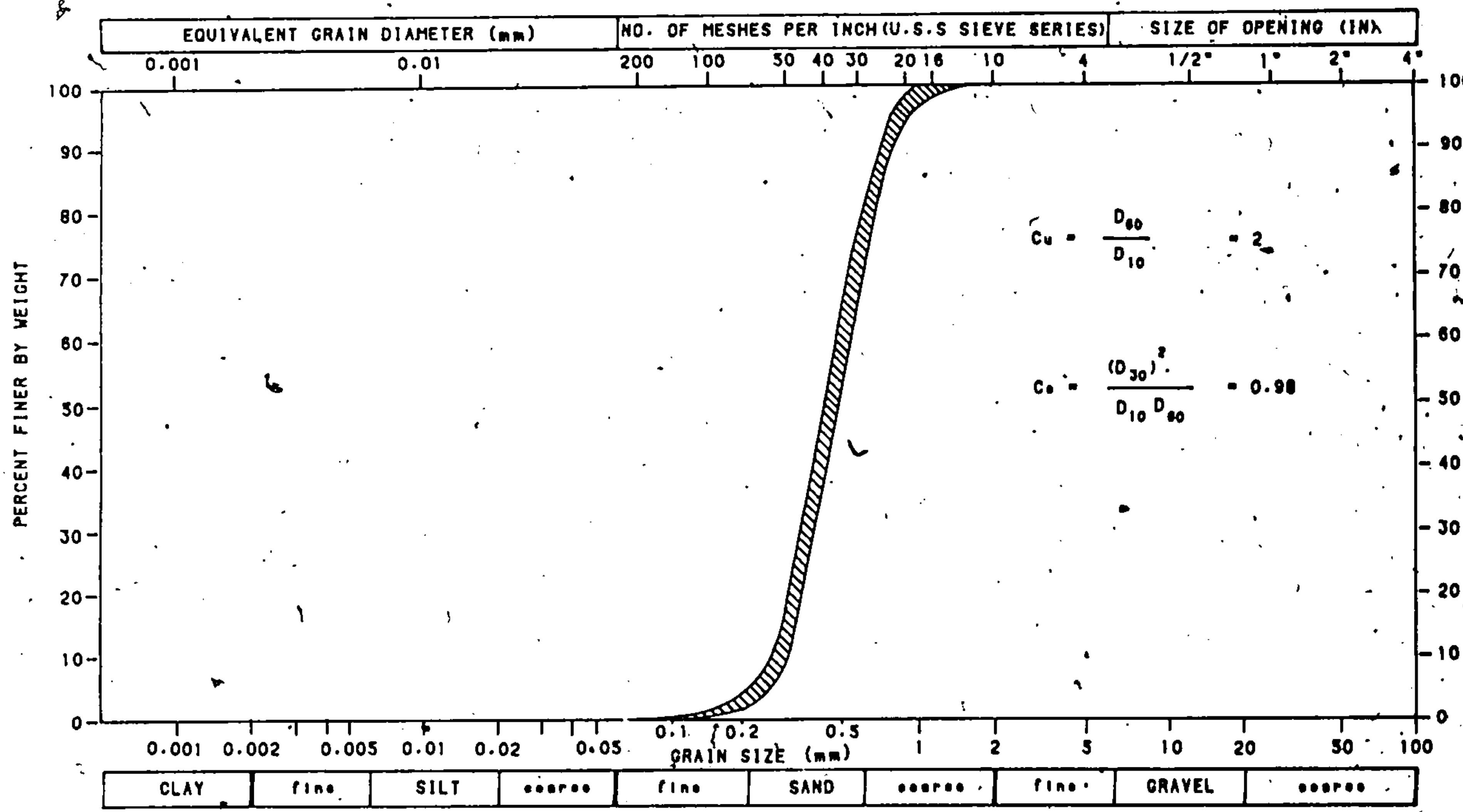

FIG. 3.1.1- GRAIN SIZE DISTRIBUTION OF CRUSHED SILICA SAND

TABLE 1

Characteristics of crushed silica sand

		crushed silica sand (Silica-24)
% crushed		100
coefficient of uniformity, C_u		2.00
coefficient of concavity, C_c		0.98
classification		uniformly graded sand
specific gravity, G_s		2.66
coefficient of angularity		1.52
coefficient of mean sphericity		0.68
coefficient of mean roundness		0.17
max. unit weight (kN/m³)		16.28
min. unit weight (kN/m³)		12.26
void ratio, e		
	maximum	1.13
	minimum	0.61
porosity, n		
	maximum	0.53
	minimum	0.38

3.2 TEST FACILITIES

Excluding the triaxial tests, all of the experimental testing was performed in the University of Ottawa 'Sandbox'. The 'Sandbox' is a metal structure measuring 15 metres in length, 2.13 metres in height and 1.84 metres in width. The height for testing purposes is restricted to 1.84 metres and the length of the box can be adjusted by introducing temporary walls made of 4x4 (in.) wood sections. The box contains more than 50 tonnes of the previously described crushed silica sand.

The sand mass can be displaced and deposited at any selected density by a rotating drum spreader covering the entire width of the box. This drum spreader, operated back and forth on rail guides, deposits the sand particles in air dry conditions. The spreader can be compared to a raining device with sand densities being calibrated by the drum speed, the height of fall of the sand grains, the velocity of the spreader along the guide rails and the gap or opening between the drum and the hopper regulating the flow of sand.

A bucket excavator loads the hopper on the spreader with sand and removes the sand after testing is performed to the storage end of the 'Sandbox'. Figure 3.2.1 illustrates the 'Sandbox' and the spreading mechanism.

3.2.1 Spreading of sand mass

Once the area required for testing purposes is selected, a temporary wall made of 4x4 sections is installed at the rear of the test section to segregate the area from the remaining 'Sandbox'. The wall is covered with polyethelene sheets to prevent sand leaks through the wall.

The opposite end of the wall is the actual testing area and its configuration varies depending on the type of test performed. This is discussed further in subsequent sections.

With the sand base of the box levelled, the spreading operation can proceed. Depending on the requirements of the specific test, four to seven days are required for completion of the operation.

The density of the sand being deposited is verified by calibrated density pots. These pots, with known volumes, are introduced within the sand spreading area at predetermined height levels. Once filled they are weighted and the measured unit weight allows the determination of the density index of the sand deposit at specific heights.

All tests were performed with the sand deposited in a dense state (I_d = 95%) in order to simulate the high compaction of soils in reinforced soil structures.

The location of local planes of weakness was determined by pushing a 3 mm diameter probe (steel rod) vertically into the backfill soil at a number of points upon completion of the test. The location of the slip planes was noted by a marked decrease in penetration resistance followed by a substantial increase in resistance.

Once the test is performed, the equipment is dismantled and the sand mass removed. This operation may take from one to two weeks to be executed. Depending on the type of test and whether or not strain gauges are utilized, the turnaround time between tests may vary from three to eight weeks.

FIG. 3.2.1- PHOTOGRAPHIC VIEW OF SAND SPREADING OPERATION

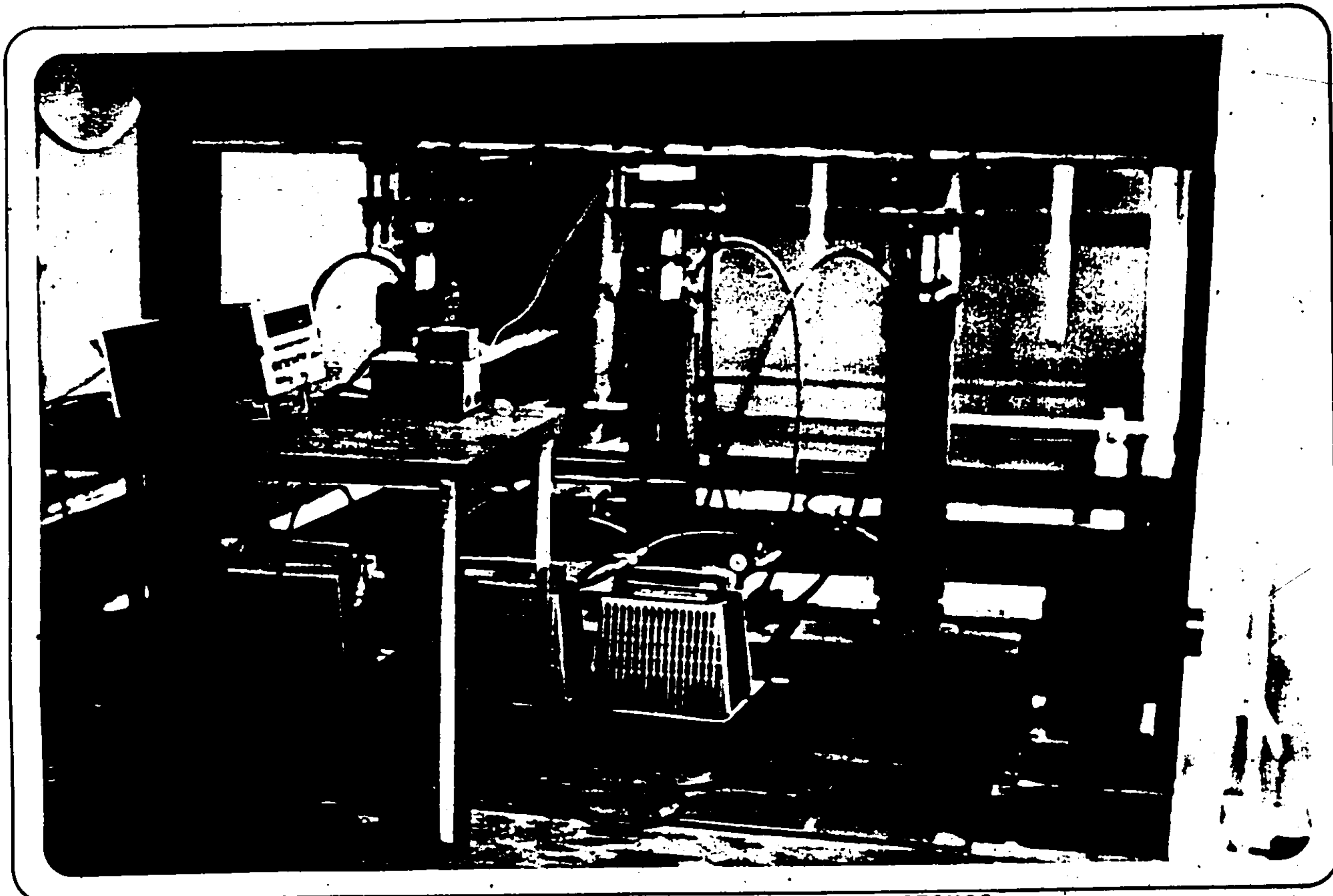

FIG. 3.2.2- LOAD FRAME AND TEST FOOTINGS

3.2.2 Load frame and test footings

In the reinforced embankment and wall tests, hydraulic jacks were utilized to simulate the load application of strip footings on an earth structure.

After completion of the sand spreading operation, a load frame is installed over the test footing location to provide a reaction for the hydraulic jacks. Each jack has a maximum working capacity of 30 tonnes and the load system is illustrated on figure 3.2.2.

The footings span the width of the 'Sandbox' to create a two-dimensional loading case or a plain strain condition in order to eliminate friction effects from the sides of the box on the outer segments of the footings. Therefore, while the three footings were identical, readings were taken only on the central segment. Rotation of the footing segments was prevented by rigidly attaching the segments to the loading jacks.

Each footing was loaded independently using electric hydraulic pumps with a constant rated delivery of 196.6 cm^3/min, independent of the applied pressure. This arrangement permitted all sections to be displaced into the sand at an equal rate, regardless of the load required for each segment.

Measurements taken on the central footing, included the applied load, which is read by a calibrated compression load cell rated at 222 kN, but with an ultimate working capacity of 444 kN and the settlement of the footing, read on a dial gauge with a travel length of 130 millimetres.

3.2.3 Strain gauging of reinforcing elements

Whenever axial loads in reinforcing elements were required, strain gauges were installed on the elements at predetermined positions.

The installation of these strain gauges was found to be an extremely slow process that required careful manipulation. Once installed, the gauges were calibrated individually or as group before each load test. Calibration was accomplished by static load whenever possible or by using a tensile load machine and a gauged sample material representing the elements being tested.

To minimize bending effects in the recording of the axial strain, a two gauge quarter bridge set-up was used for the installation of the strain gauges. Each selected strain location has a double gauge set-up with each gauge being carefully positioned opposite the other (figure 3.2.3) in order to obtain reliable results.

For temperature compensation, a 'dummy' gauge was installed on material identical to the one being tested using a half-bridge connection.

The strain reading equipment was for the most part B.L.H. Electronics model 1200 digital strain indicators and model 1225 Switching and Balancing units.

The gauges and terminals were covered by gaugecoat #8 waterproofing to minimize damage caused by the displacement of the reinforcing elements and the overburden pressures.

To reduce pullout resistance from the gauge wiring, the connecting wires were coiled and inserted into a rigid pipe (200 mm long) allowing the wires to be pulled out of the pipe without offering any resistance whenever the reinforcing strips were displaced.

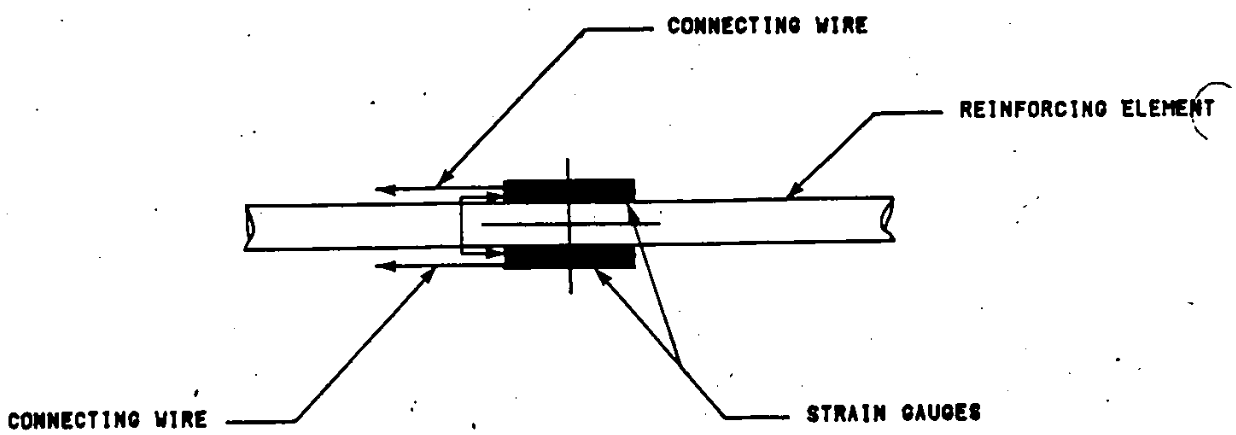

FIG. 3.2.3- TWO GAUGE QUARTER BRIDGE SET-UP

3.3 DESIGN PARAMETERS OF PULLOUT TESTS

In order to examine the friction behaviour of different reinforcing elements a series of pullout tests were conducted on three types of reinforcements. From these pullout tests, load-displacement curves and stress distributions along the reinforcing elements were acquired.

The three types of reinforcement were:

1. cold rolled flat strips (original Reinforced Earth strips)
2. Reinforced Earth Company ribbed strips
3. wire mesh system

A complete description of each type of reinforcement is supplied in chapter IV.

The maximum length of reinforcement having been restricted to 3.05 metres, the experimental section of the 'Sandbox' was reduced in length to 3.65 metres. The width and height of the box were kept constant at 1.84 metres.

By using this arrangement it was possible to perform up to nine pullout tests on reinforcing elements. The vertical and horizontal spacings between elements were identical and set at 0.46 metre. This distance avoided any undue interference between neighbouring elements.

Schematic presentations of typical pullout tests are shown on figures 3.3.1 and 3.3.2. Photographic views of a test set-up are presented in figure 3.3.3.

The pullout tests were performed at a constant rate of displacement requiring a special test arrangement. The test set-up was composed of five main components:

1. the reinforcing element being pulled out
2. the connection between the reinforcing element and the pulling jack
3. the pulling jack
4. the triaxial system of compression to maintain a constant pullout rate, and
5. the strain measuring system (strain gauges)

Components one and five having been reviewed previously, are excluded from the following analysis.

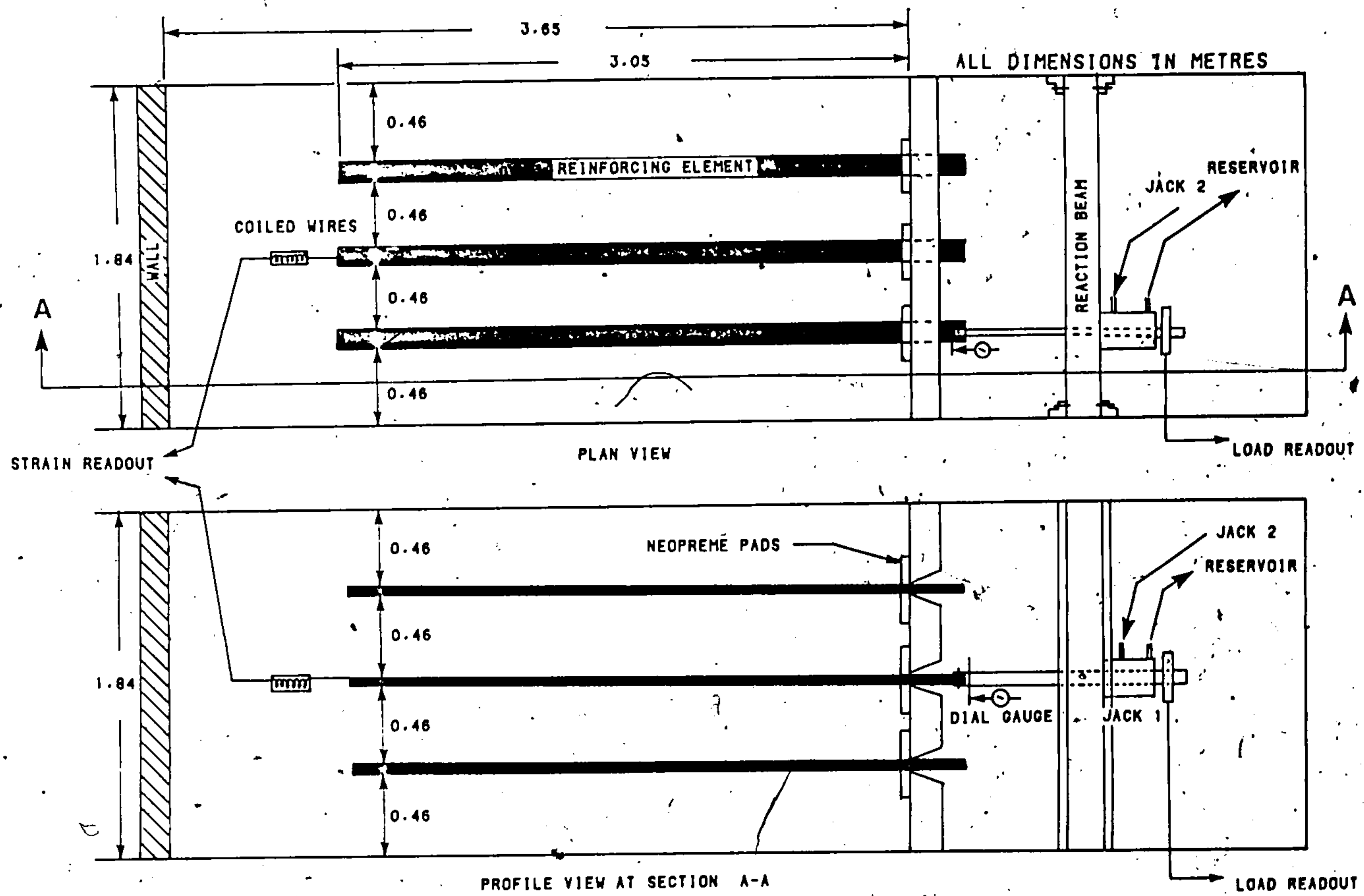

FIG. 3.3.1- SCHEMATIC VIEW OF PULLOUT TEST

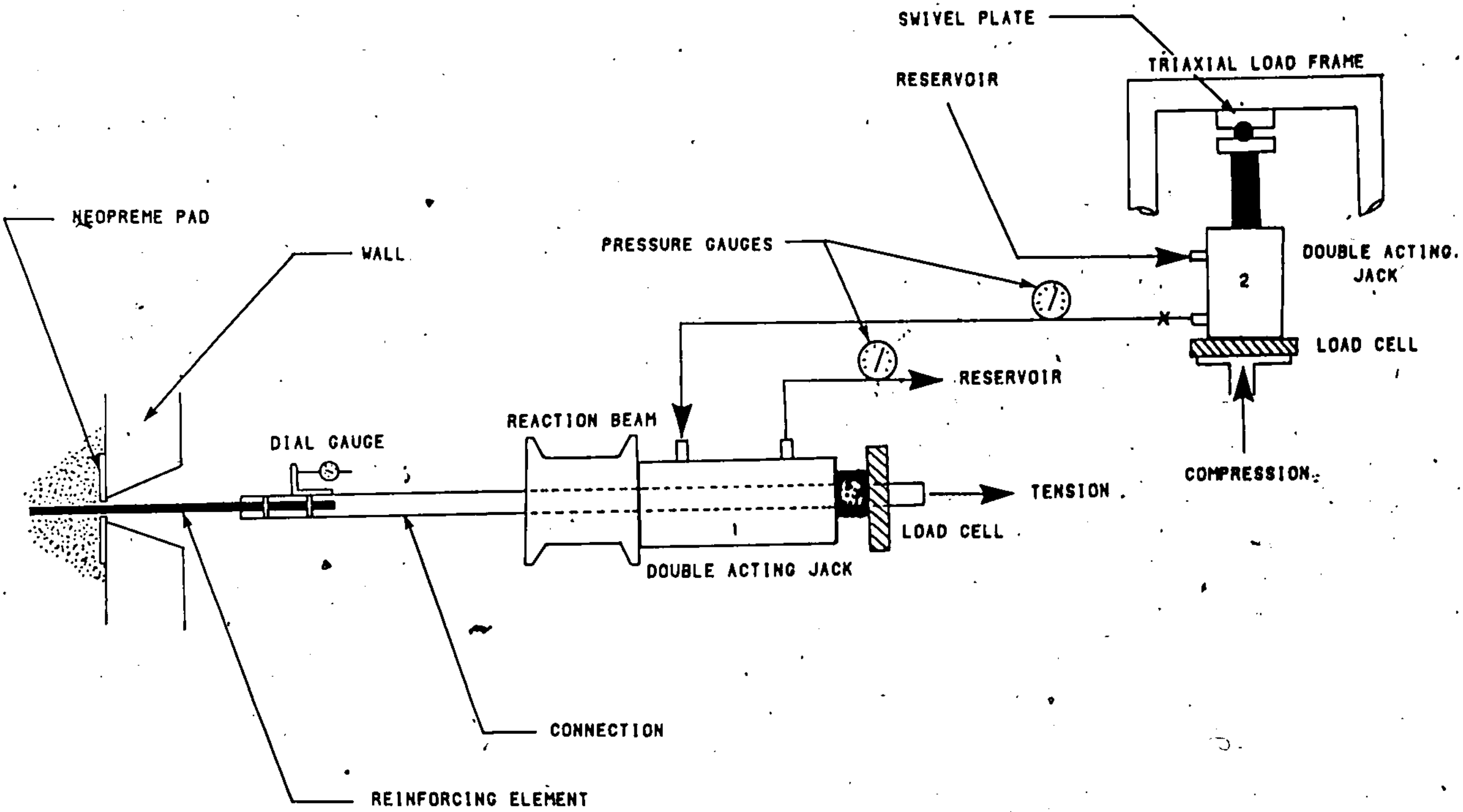

FIG. 3.3.2- SCHEMATIC VIEW OF PULLOUT APPARATUS

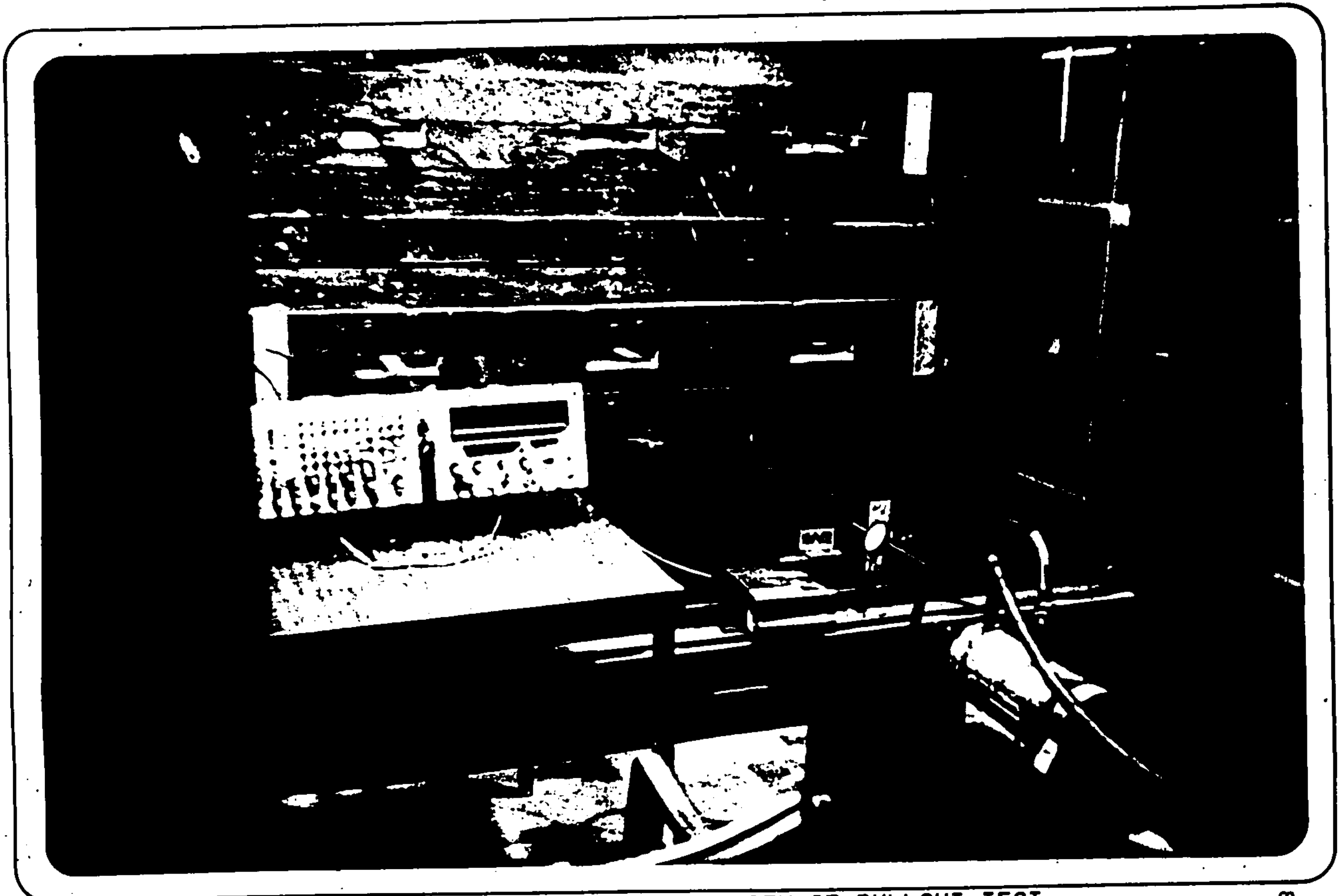

FIG. 3.3.3- PHOTOGRAPHIC VIEW OF PULLOUT TEST

3.3.1 Pullout connection

Connections had to be devised that permitted the linkage between the reinforcing elements and the pulling jack. These connections had to be rigid in order to prevent slippage from occurring and had to transfer the applied load without losses or discrepancies.

The selected connections were a single bolted connector for the flat and ribbed strips and a pinned connection for the mesh elements, which locked the mesh between two steel bars. These connections are shown on figure 3.3.4 and performed adequately throughout the testing program.

3.3.2 The pullout system

Components three and four can be combined to form the pullout system. The system comprises two hydraulic jacks (30 tonnes, double acting, 152 mm stroke), a connecting rod, a reaction beam, two load cells, two pressure gauges, dial gauges, a triaxial loading frame and a swivel plate.

The reaction beam was a hollow box section bolted to the sides of the 'Sandbox' with openings permitting the passage of the connecting rod. A support frame bolted to the reaction beam permitted the placement and support of the pulling jack at zero load. The connecting rod passed through the reaction beam and the pulling jack, with the piston of the jack applying pressure on a load cell which was screwed in place on the connecting rod. The load cell was calibrated on a Tinius-Olsen tensile load machine.

The pullout jack was connected at the pushing end hydraulically to the second hydraulic jack which was loaded on a triaxial frame and at the pulling end to a reservoir to ensure free hydraulic flow. A pressure gauge permitted the monitoring of damaging back pressure buildup.

The triaxial load frame was a 5 tonnes Wykeham-Farrance triaxial machine on which the second hydraulic jack was placed, piston extended. The jack was compressed at a constant rate and the hydraulic oil flowed towards the pullout jack, pulling out the reinforced element. A second load cell permitted the recording of the load in the triaxial apparatus and a pressure gauge measured the back pressure caused by any oil flow resistance between the two jacks. A swivel plate insured axial loading of the triaxial jack.

The measurements recorded were the pullout load and the displacement of the reinforcing element. The loads were recorded by the load cell acting on the pullout jack. The cell was a Universal flat load cell with a working capacity of 111 kN and a hole diameter of 26 mm permitting the connecting rod to be screwed into the load cell.

Displacements were read on dial gauges which measured the movement of a perplex plate attached to the connection between the reinforcing element and the pulling rod. The gauge had a 100 mm travel distance and was mounted on fixed supports.

3.3.3 Surcharge application

In some cases, the overburden pressure on the reinforcing elements had to be supplemented to achieve a required pressure. When surcharge was required, concrete blocks were placed as needed on the levelled sand surface. Figure 4.1.2 illustrates a pullout test with surcharge blocks.

The concrete blocks were 1.83 metres long, 0.61 metre wide and 0.31 metre high. Each level of surcharge represented an equivalent height of soil of 0.42 metre.

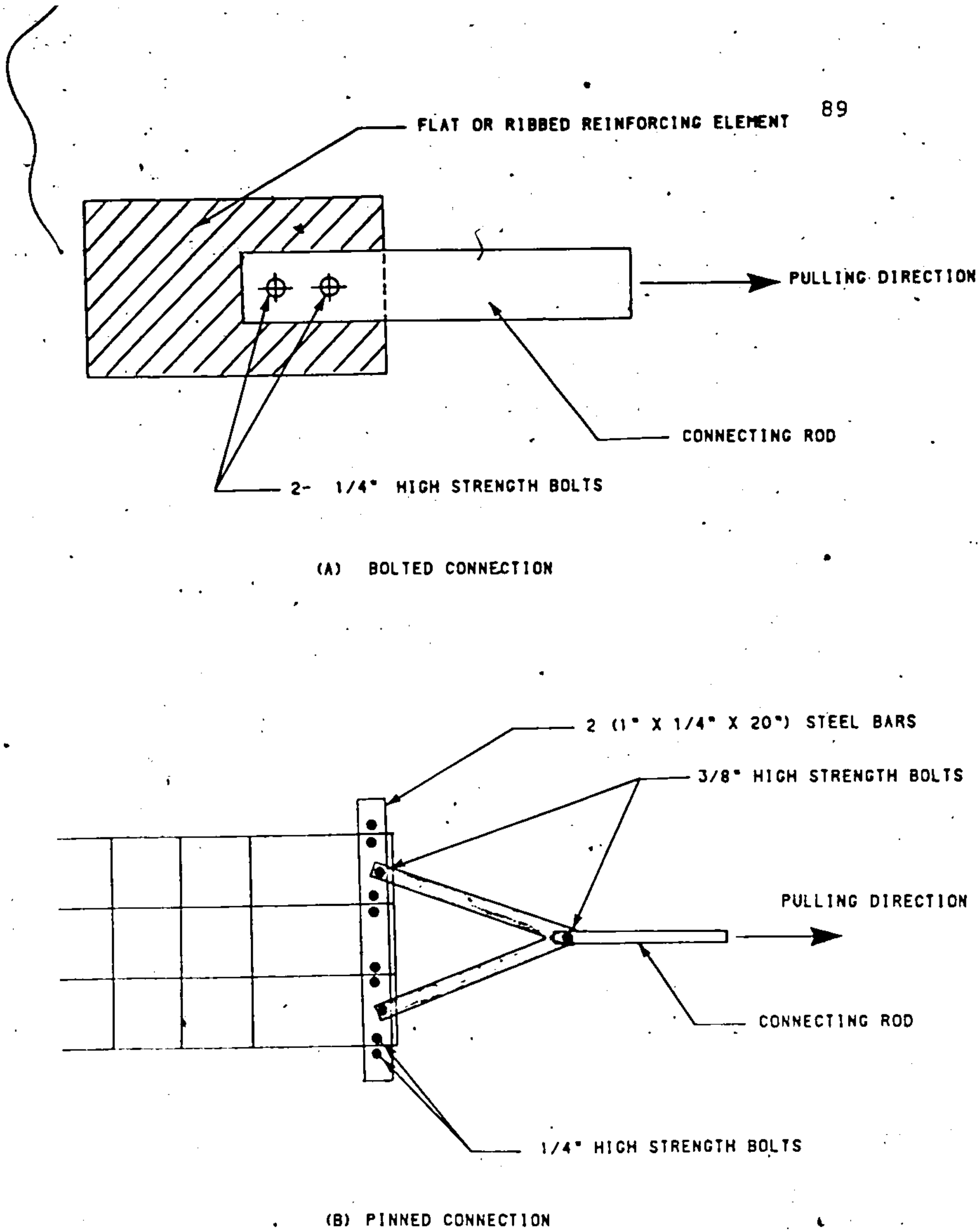

FIG. 3.3.4- SCHEMATIC VIEW OF CONNECTIONS BETWEEN REINFORCING ELEMENTS AND PULLING JACK

3.4 PARAMETERS FOR TRIAXIAL TESTS

A series of triaxial tests were performed in order to investigate the internal angle of friction of the crushed silica sand and of mesh reinforced samples. All tests were conducted on a specially constructed large-scale triaxial cell which was modelled on a 230 mm Wykeham and Farrance cell.

Credit for the manufacture and assembly of the cell goes to the technical staff of the Civil Engineering department at the University of Ottawa.

Details of the cell are given on figure 3.4.1. For a complete description of the cell components, the reader is directed to an unpublished report by R.J. Moore (1978) titled 'Large scale triaxial testing of granular "A" material'.

In addition to the triaxial cell, a monitoring panel was constructed specifically for use with the large triaxial cell. Details of the panels are shown on figure 3.4.2. The main functions of the panel were the following:

1. to supply and monitor a confining pressure, σ_3
2. to measure the volume change of the sample
3. to measure sample suction

The membranes used for sealing the samples were either bought commercially or made in the laboratory from self-vulcanizing latex. Stress corrections for this specific type of membrane were determined to be in the order of one to two kiloPascals.

In order to simulate the sand spreading operation in the 'Sandbox', a miniature sand spreader was constructed. This raining device was used to deposit the uniform quartz sand in the sample molds. This method of deposition ensured that the test samples had the same structure and density as the sand in the large-scale models of embankments and walls. Figures 3.4.3, 3.4.4 and 3.4.5 illustrate the raining device and the sand spreading operation. The optimum height of fall of the sand particles was found experimentally to be one metre.

An induced vacuum within the test samples permitted the testing in a dry state. The vacuum was released only when a confining pressure was exerted on the sample. Axial stresses (σ_1) were applied to the sample by a Tinius-Olsen compression machine. Complete sampling operations as described by Moore (1978) were used.

Test procedures were identical to any drained triaxial test in which a sample confined by a constant pressure (σ_3), is slowly loaded to failure under a controlled rate of strain. Measurements of load, strain and volume changes were noted.

The geometry and configuration of the wire mesh selected for the reinforced samples is presented in chapter IV.

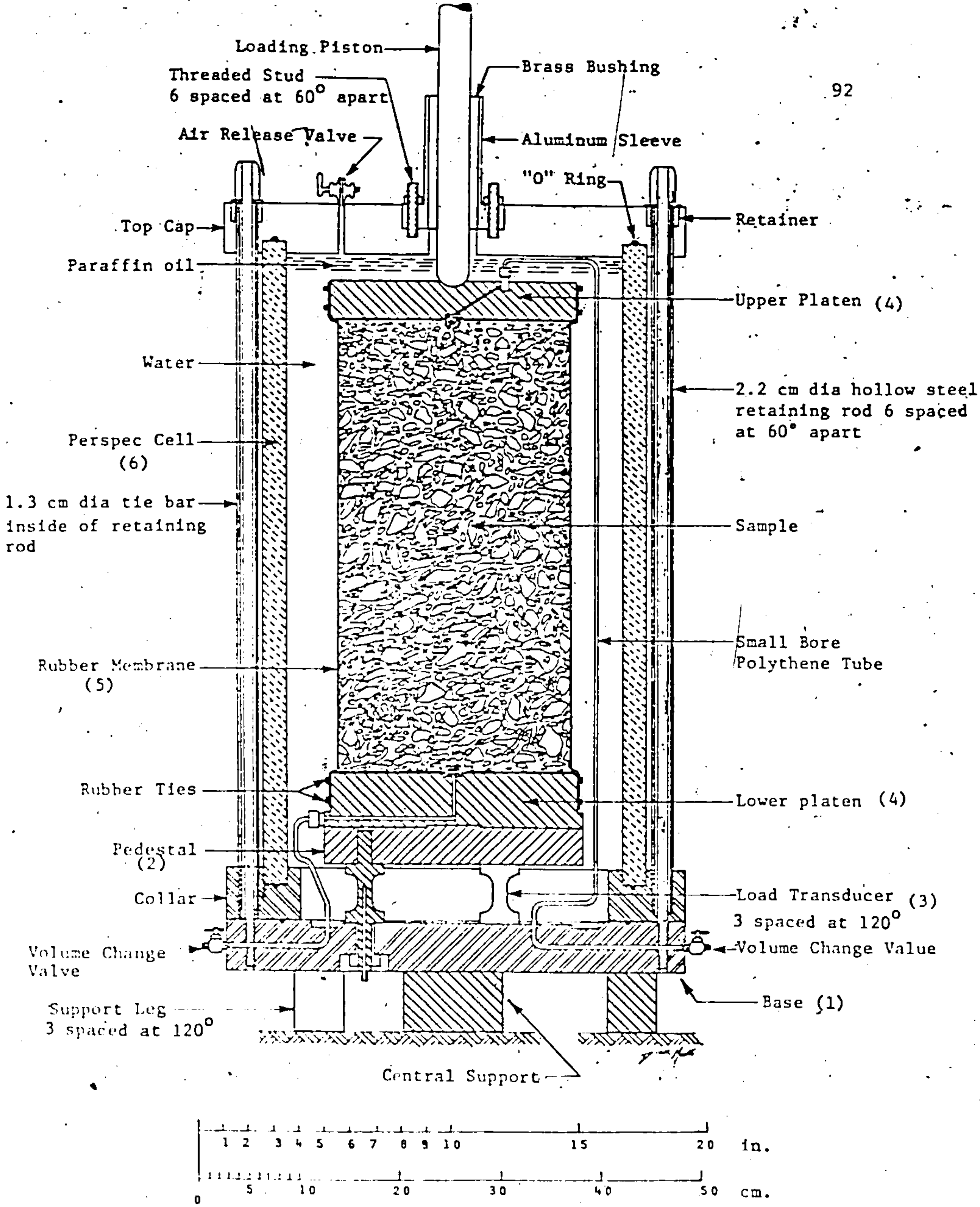

FIG. 3.4.1 - TRIAXIAL CELL
(MOORE, 1978)

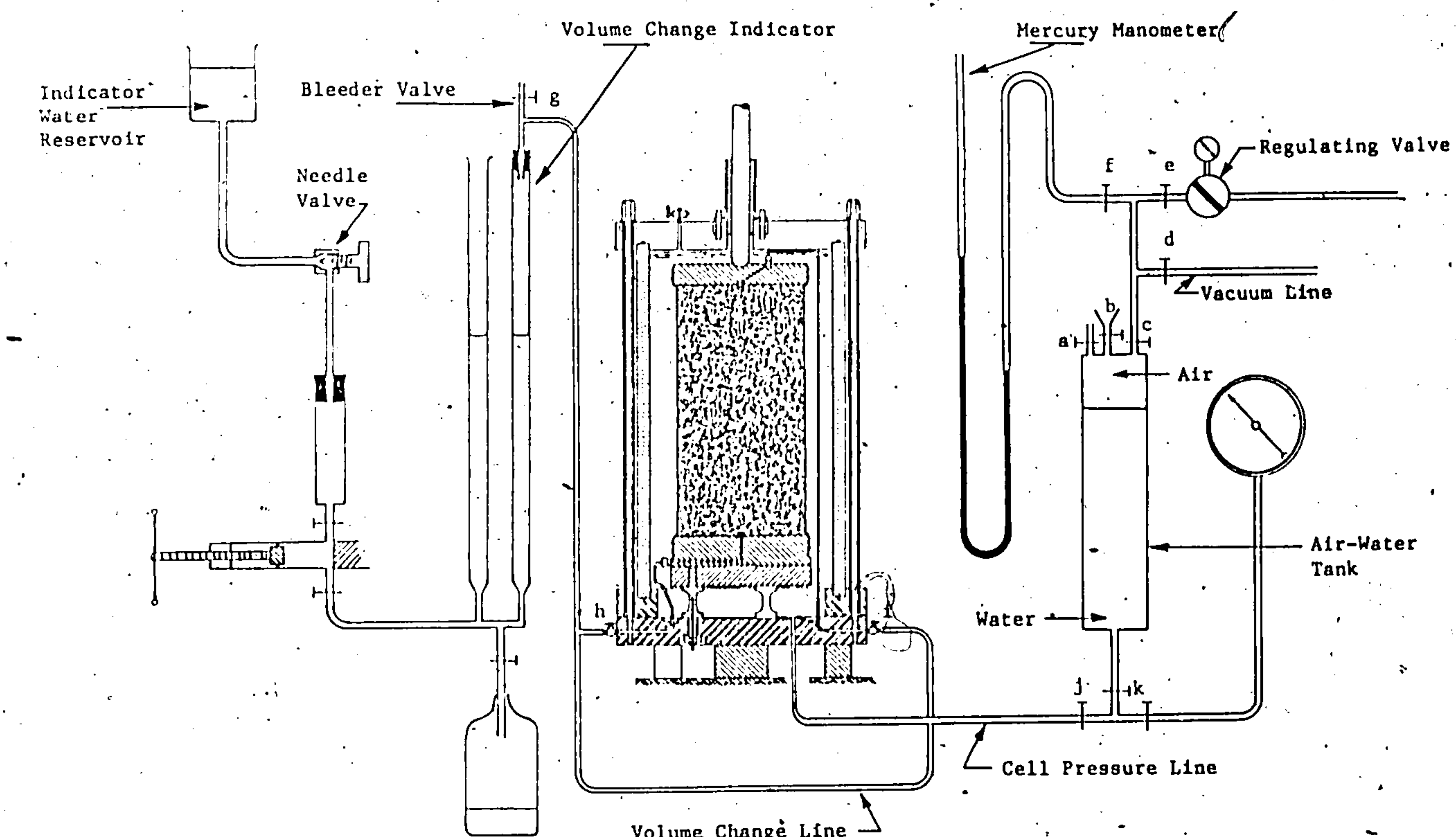

FIG. 3.4.2- SCHEMATIC VIEW OF PRESSURE AND VOLUME CHANGE MEASURING DEVICES (MOORE, 1978)

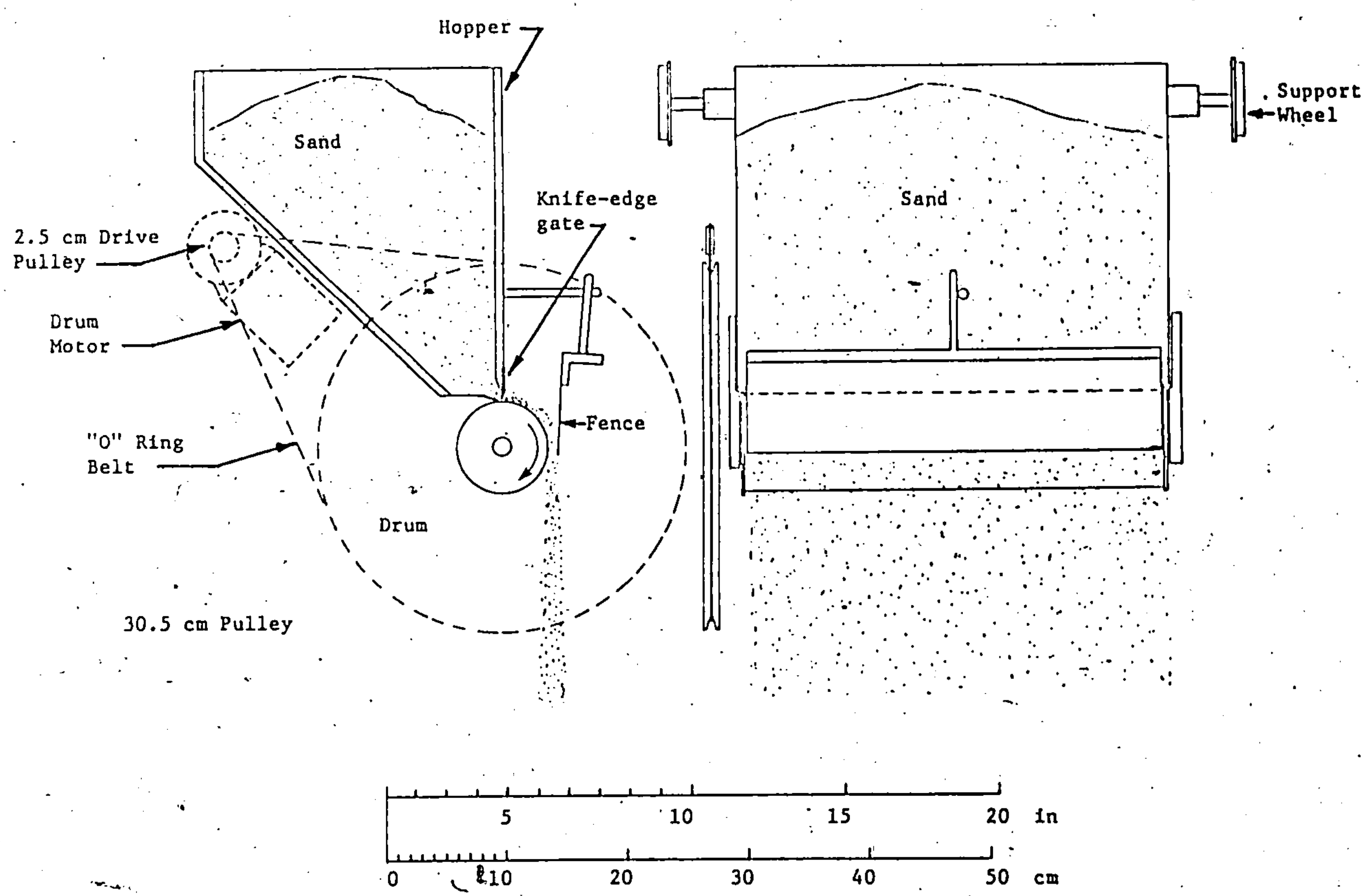

FIG. 3.4.3- SAND SPREADER
(MOORE, 1978)

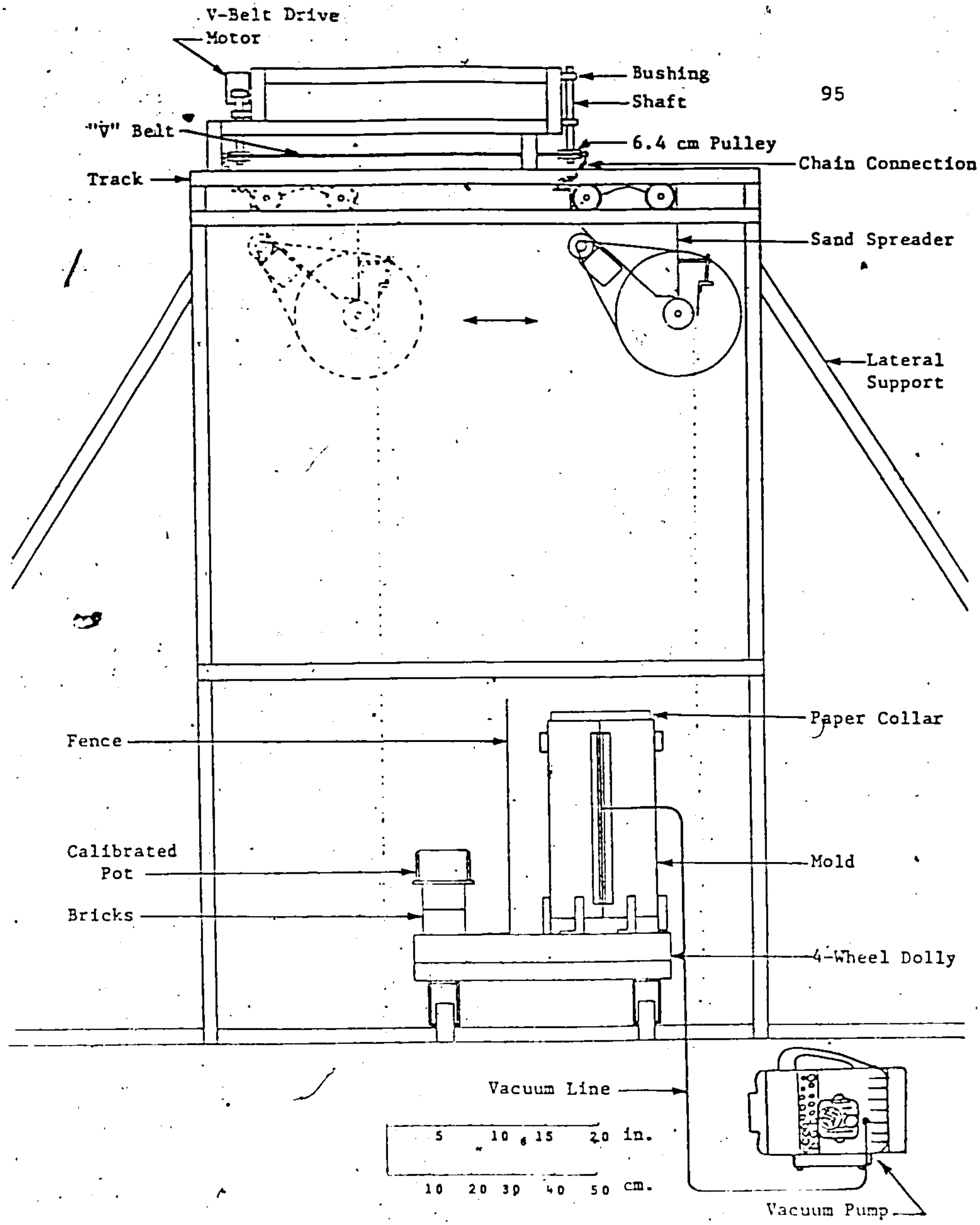

FIG. 3.4.4- SAND SPREADER ASSEMBLY
(MOORE, 1978)

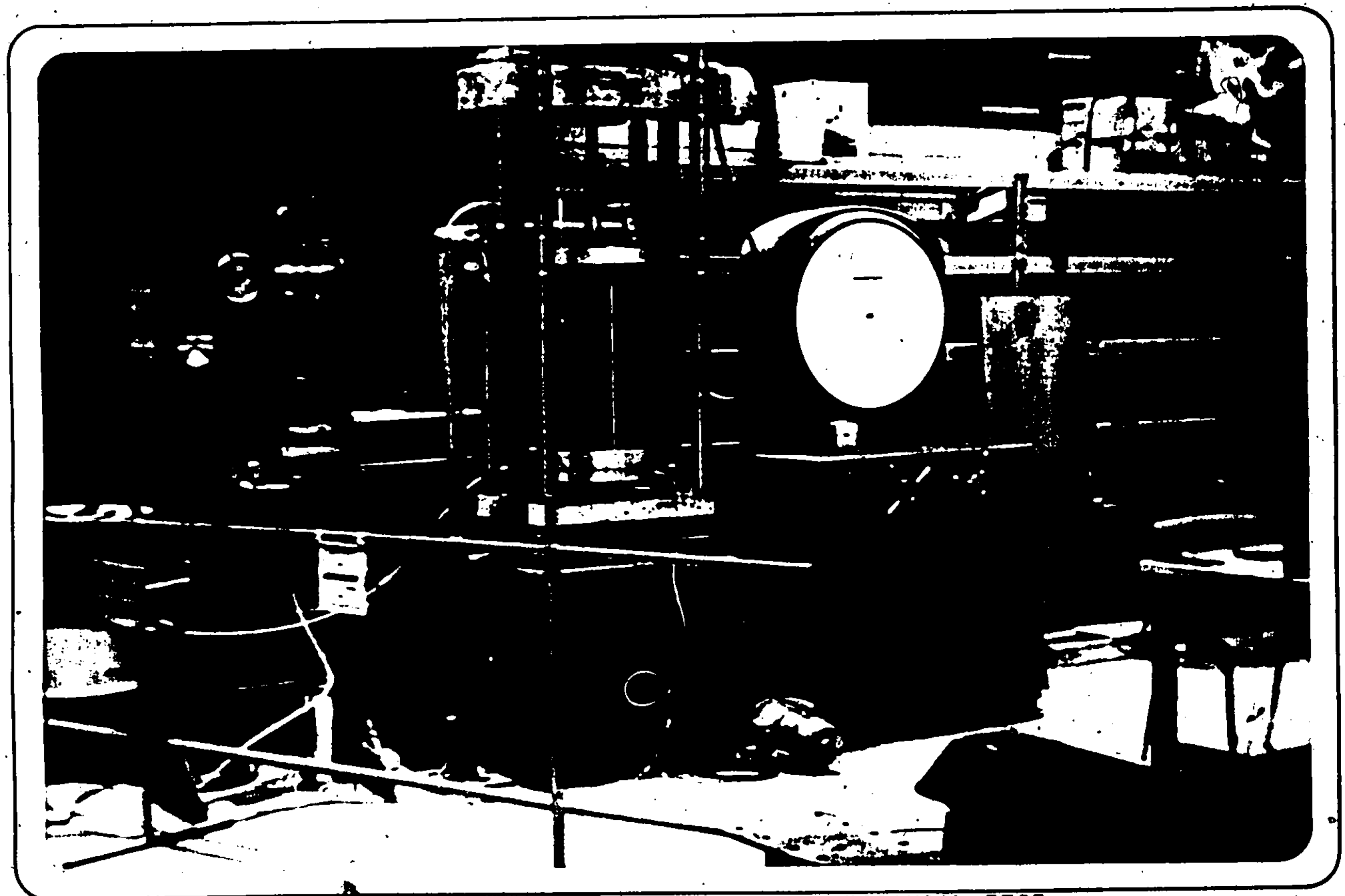

FIG. 3.4.5- PHOTOGRAPHIC VIEW OF TRIAXIAL TEST

3.5 PARAMETERS FOR REINFORCED EMBANKMENTS AND WALLS

The reinforced embankment tests were influenced by the following parameters:

1. spreading of the sand backfill (following the selected geometry of the embankment)
2. placement of the reinforcing mesh
3. strain gauging of the mesh (if applicable)
4. vertical loading of the hydraulic jacks
5. recording of the test data
   a) applied pressure by the central footing
   b) settlement of the central footing
   c) strain in reinforcing mesh (if applicable)

The reinforced wall tests were also influenced by the above parameters in addition to the following:

1. wall panel geometry and behaviour
2. attachment of reinforcing mesh to the wall panels
3. outward displacement of the wall panels under an applied pressure.

The design parameters for the large-scale models of reinforced embankments and walls have previously been described or are analysed in greater detail in chapter IV.

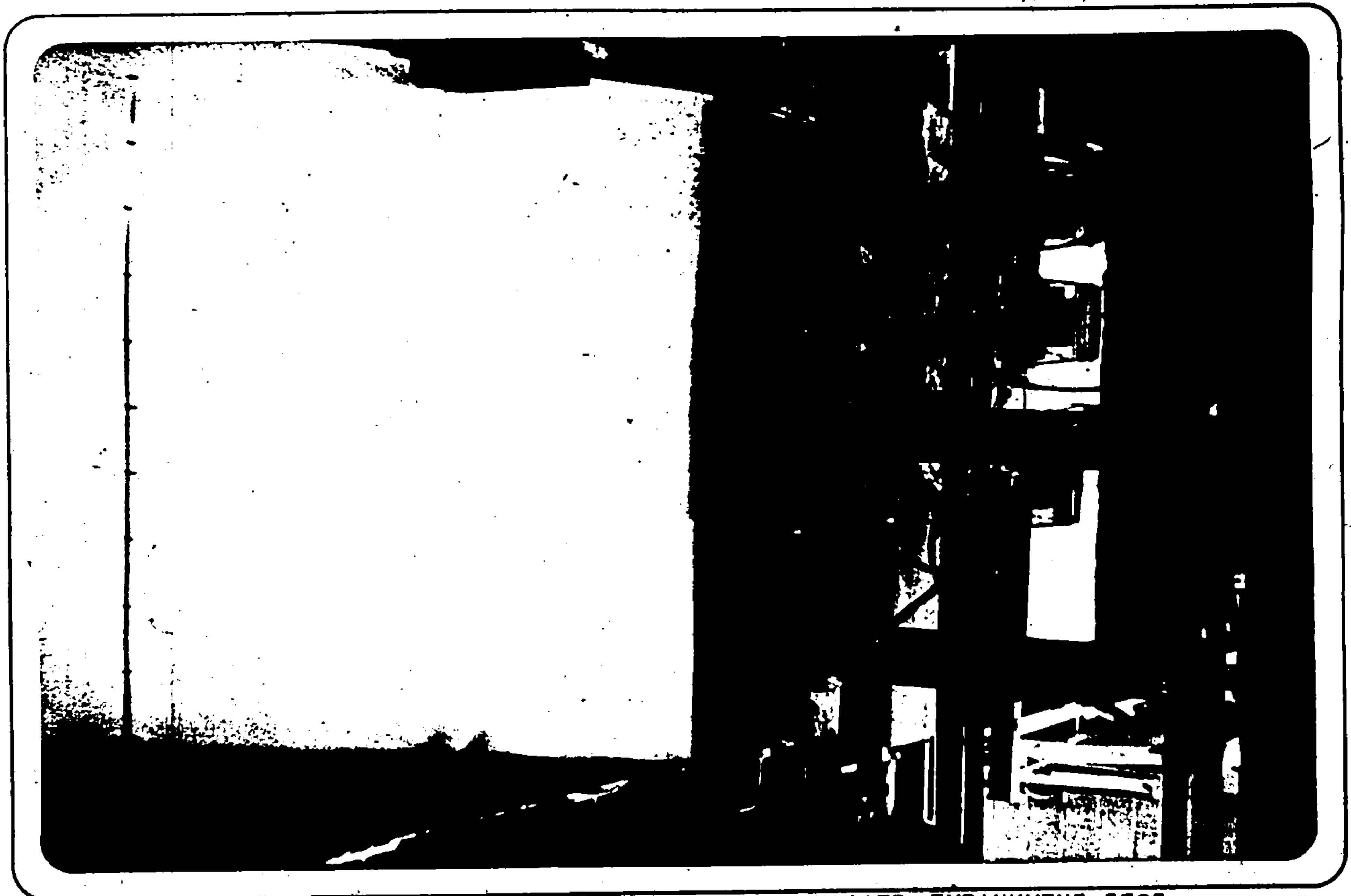

FIG. 3.4.6- PHOTOGRAPHIC VIEW OF A REINFORCED EMBANKMENT TEST

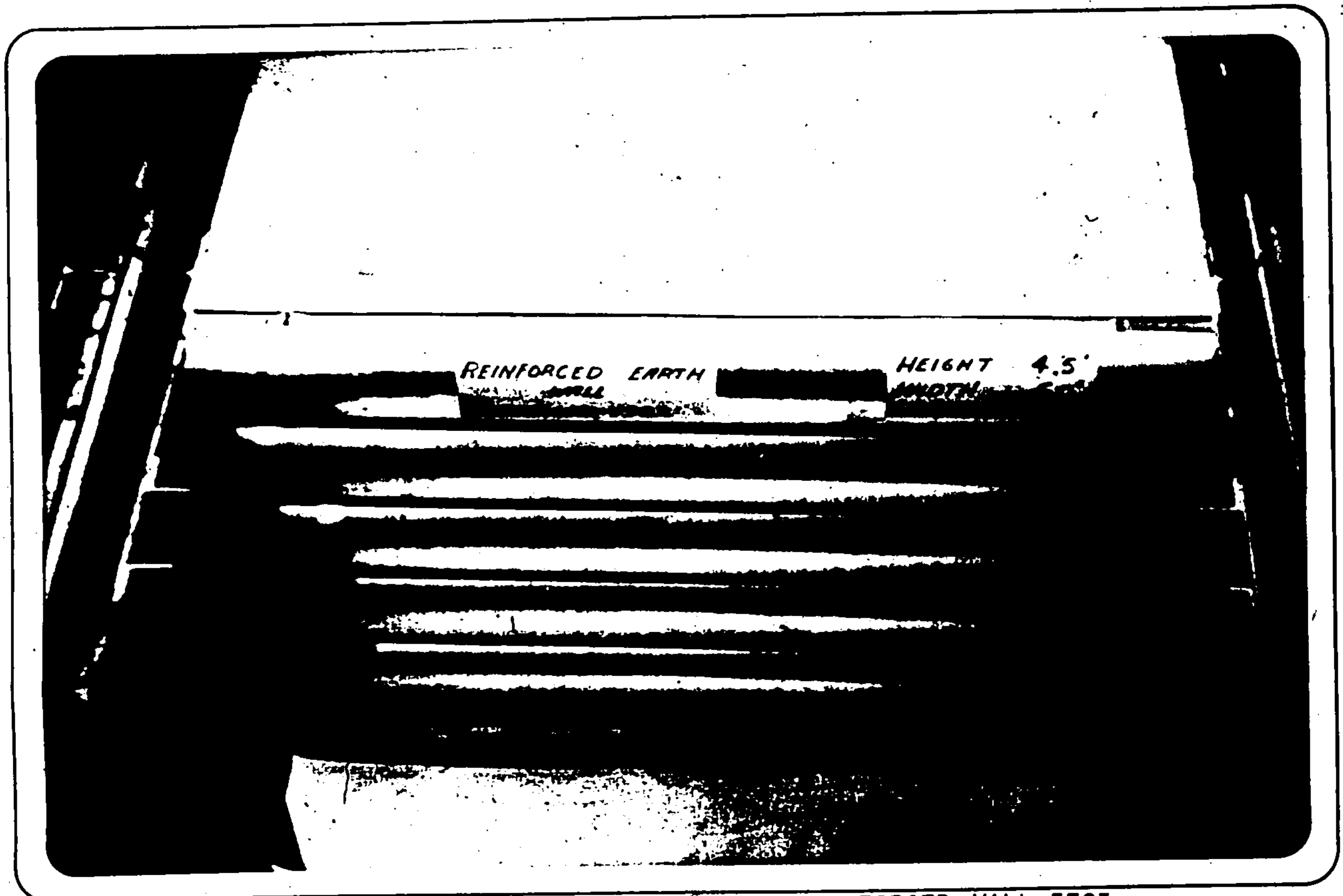

FIG. 3.4.7- PHOTOGRAPHIC VIEW OF A REINFORCED WALL TEST

Chapter IV

EXPERIMENTAL RESULTS

4.1 PULLOUT TESTS

The pullout resistance of different materials susceptible of being used for earthwork reinforcement was investigated in order to determine if the patented 'Reinforced Earth' concept is indeed the most efficient earth retaining system.

As was stated by Schlosser and Elias (1979), the pullout tests of individual reinforcements are idealizations and are not completely representative of the friction which is developed along the reinforcement. However, these tests yield valuable results, among them:

1. The apparent average coefficient of friction along the reinforcement, which is defined in chapter V, as well as the peak and residual values which can be observed from displacement curves.
2. The factors which influence the friction.
3. The tensile forces which are generated along the reinforcement following the application of a pullout load.

However, Romstad et al. (1979) demonstrated that results of pullout tests agree well with model test results and that pullout tests, not direct shear tests, should be used to determine the frictional behaviour of the soil-strip interaction.

In the following series of pullout tests, load-displacement curves and tensile forces at selected locations on the reinforcing material were generated for each type of reinforcement.

4.1.1 Testing program

A total of 33 pullout tests were performed involving three types of steel reinforcement.

1. cold rolled flat strips
   (38 mm wide, 4.7 mm thick, of varying length)
2. Reinforced Earth Company ribbed strips
   (40 mm wide, 5.0 mm thick, 3 metres in length)
3. wire mesh system (used as temperature reinforcement in reinforced concrete floor slabs); 4.8 mm diameter bars, 0.46 metre wide with varying crossbar spacing, and lengths.

   a) 76 mm x 152 mm crossbar spacing (3 in x 6 in)
   b) 152 mm x 152 mm crossbar spacing (6 in x 6 in)
   c) 305 mm x 152 mm crossbar spacing (12 in x 6 in)
   d) 457 mm x 152 mm crossbar spacing (18 in x 6 in)

The author acknowledges the fact that many of the pullout tests were performed by Mr. Guy Felio during his stay at the University of Ottawa as a research engineer from 1980 to 1981. The author performed the last six pullout tests involving the wire mesh system with a reduced length of 1.93 metres.

A schematic representation of the layout of the different reinforcement systems in the pullout box is presented in figures 4.1.1 and 4.1.2. Figure 4.1.3 demonstrates photographically a pullout test in progress.

4.1.2 Cold rolled flat strips

The cold rolled flat strips varied in length, from one to three metres, and most were strain gauged to measure the tensile forces along the reinforcing strips. The strips were tested at three levels of overburden pressure, or an equivalent height of sand of 0.46, 0.91 and 1.37 metres. The average unit weight of the crushed silica sand backfill was measured to be 16.1 kN/m³ (I_d=97.5%) for the flat strip tests.

The tests were performed on:

1. plain strips
2. gauged strips with connecting wires taped to the steel reinforcement
3. and gauged strips with wires loose

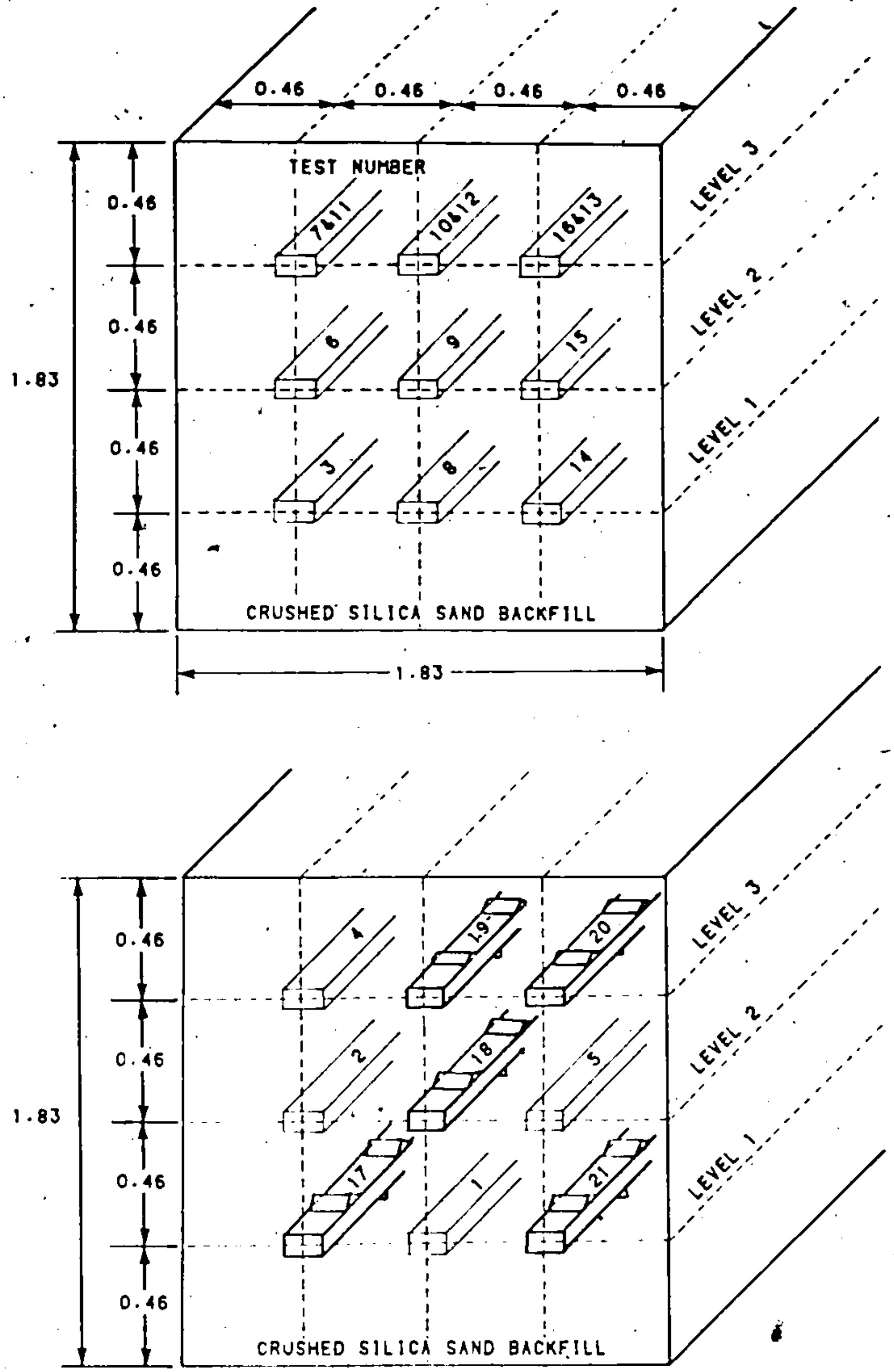

ALL DIMENSIONS IN METRES

FIG. 4.1.1- ELEVATION VIEW OF PULLOUT TEST SET-UP FOR FLAT AND RIBBED STEEL STRIPS

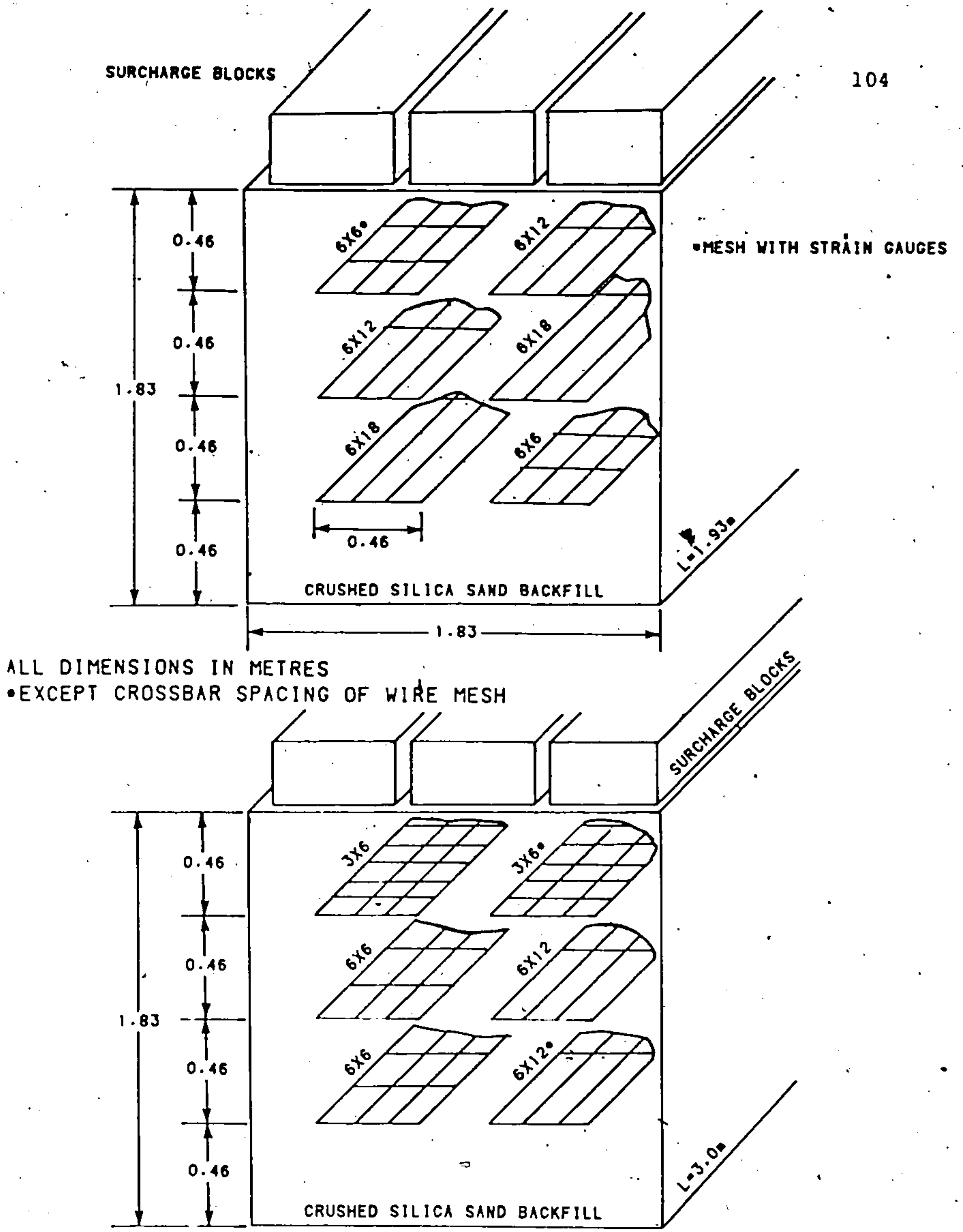

FIG. 4.1.2- ELEVATION VIEW OF PULLOUT TESTS FOR STEEL WIRE MESH

FIG. 4.1.3- PULLOUT TEST

The rate of pullout displacement was selected arbitrarily and kept constant at 0.30 mm/minute. Figure 4.1.4 illustrates the configuration of the different flat strips that were used in the tests and the positioning of the strain gauges.

The strain gauges, terminals and wires on the gauged flat strips generated an excessive passive resistance. Therefore, the tests performed on the ungauged strips must be regarded as giving a more realistic load-displacement relationship.

Table 2 summarizes the testing program on flat strips and clearly indicates the extreme influence of strain gauges on flat strips. The peak pullout resistance is quadrupled when gauges are added over a length of three metres. The lack of reliability of the gauged strips is demonstrated by tests 12 and 16, where a decrease in overburden pressure is accompanied by an increase in pullout load which is contrary to what would be expected.

In every case, as the test proceeded and the pullout load increased, some sudden relaxation or slip of the reinforcing strip would occur. This drop in the pullout load would be followed by an increase in load until slippage occurred again.

Another point worth mentioning is the fact that the peak pullout resistance occurs at a pullout strain which varies with the length of the sample,the overburden pressure, and whether or not strain gauges were installed.

Figures 4.1.5 to 4.1.7 show the load-displacement curves for flat smooth strips and figures 4.1.8 to 4.1.10 demonstrate the tensile force distribution along each strip that was gauged during pullout at specific pullout strain values. In most cases, the location of the maximum tension force is not where the load is applied but at a certain distance into the backfill material.

TABLE 2

Summary of pullout tests on flat strips

test#	length (m)	depth (m)	sur-charge	over-burden press. (kPa)	gauges	peak load (kN.)	displ. @ peak (mm)	peak stress (kPa)
1	3	1.37	no	22.1	no	1.04	1.0	5823
2	3	0.91	yes	21.7	no	0.97	5.0	5431
3	3	1.37	no	22.1	yes	4.50	70.0	2520
4	3	0.46	yes	21.3	yes	4.39	40.0	2458
5	3	0.91	yes	21.7	side	2.87	14.0	1607
6	3	0.91	no	14.7	yes	3.82	60.0	2139
7	3	0.46	no	7.4	yes	2.89	70.0	1618
8	2	1.37	no	22.1	yes	2.00	25.0	1120
9	2	0.91	no	14.7	yes	3.08	70.0	1725
10	2	0.46	no	7.4	yes	2.43	80.0	1361
11	1	0.46	yes	21.1	no	0.66	10.0	3695
12	1	0.46	yes	21.1	yes	1.18	50.0	6607
13	1	0.46	yes	21.1	yes	1.86	45.0	1041
14	1	1.37	no	22.1	yes	1.75	40.0	9798
15	1	0.91	no	14.7	yes	1.30	155.0	7279
16	1	0.46	no	7.4	yes	1.53	50.0	8567

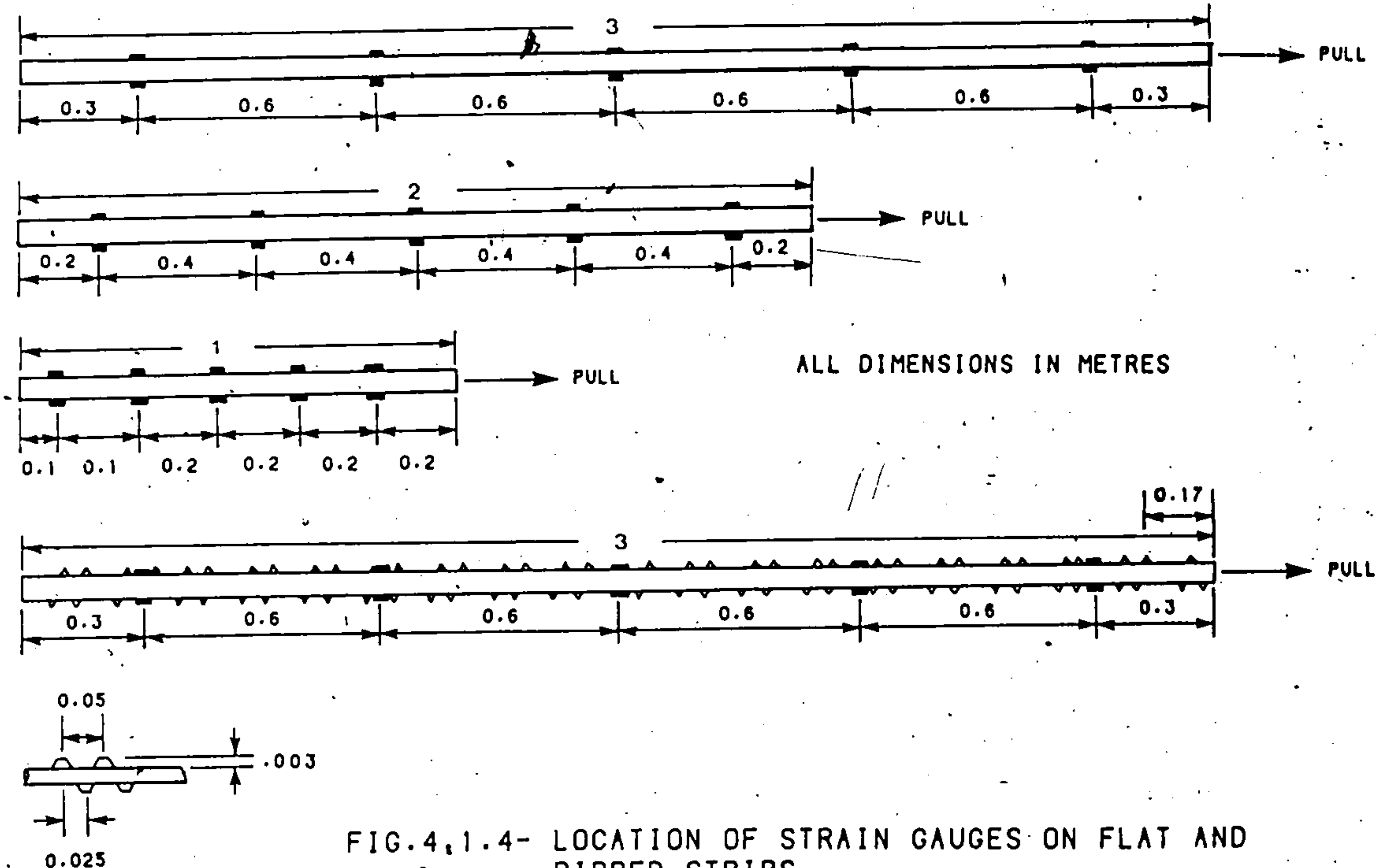

FIG.4.1.4- LOCATION OF STRAIN GAUGES ON FLAT AND RIBBED STRIPS

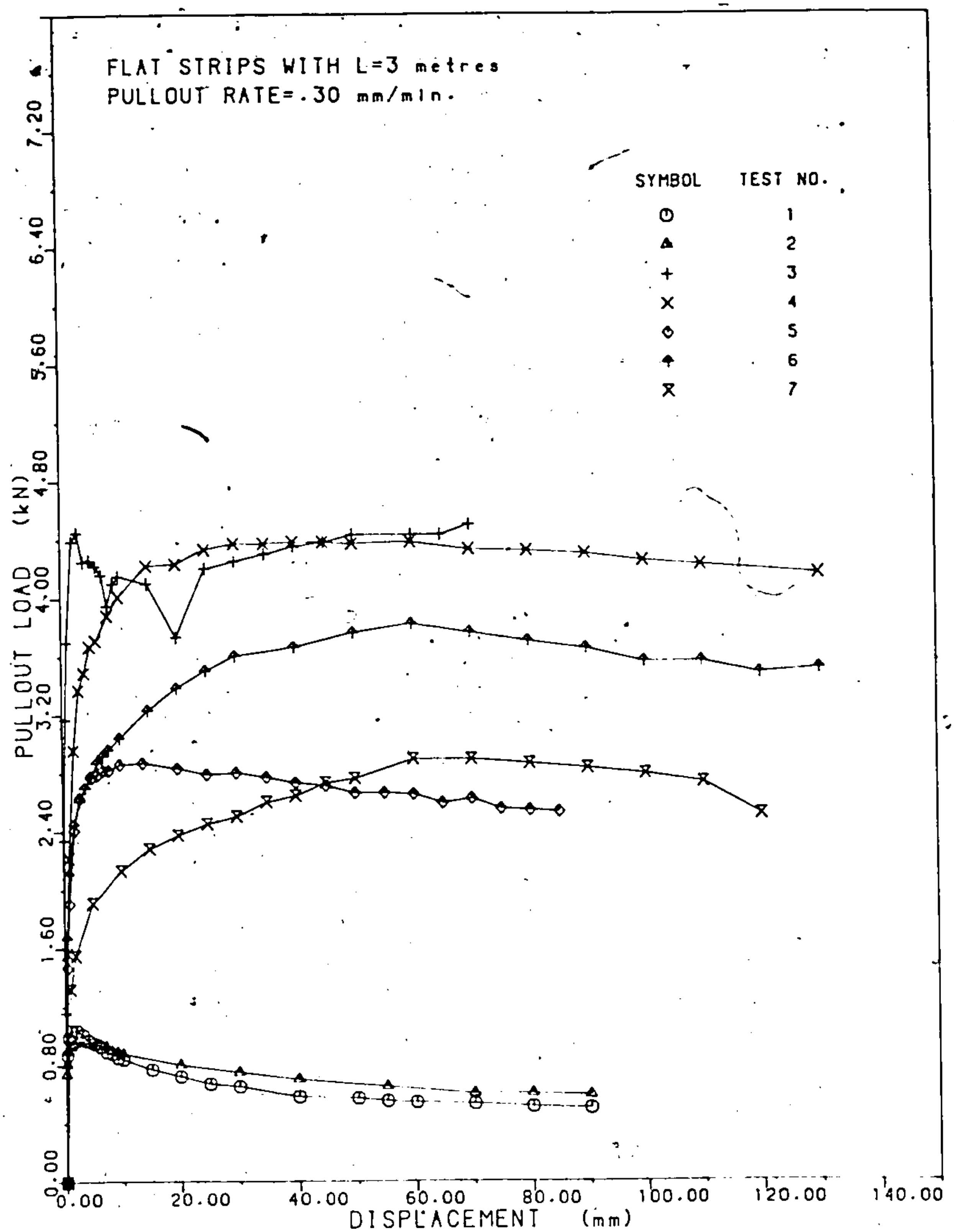

FIG. 4.1.5- PULLOUT LOAD VS. DISPLACEMENT FOR FLAT STRIPS, L= 3 metres

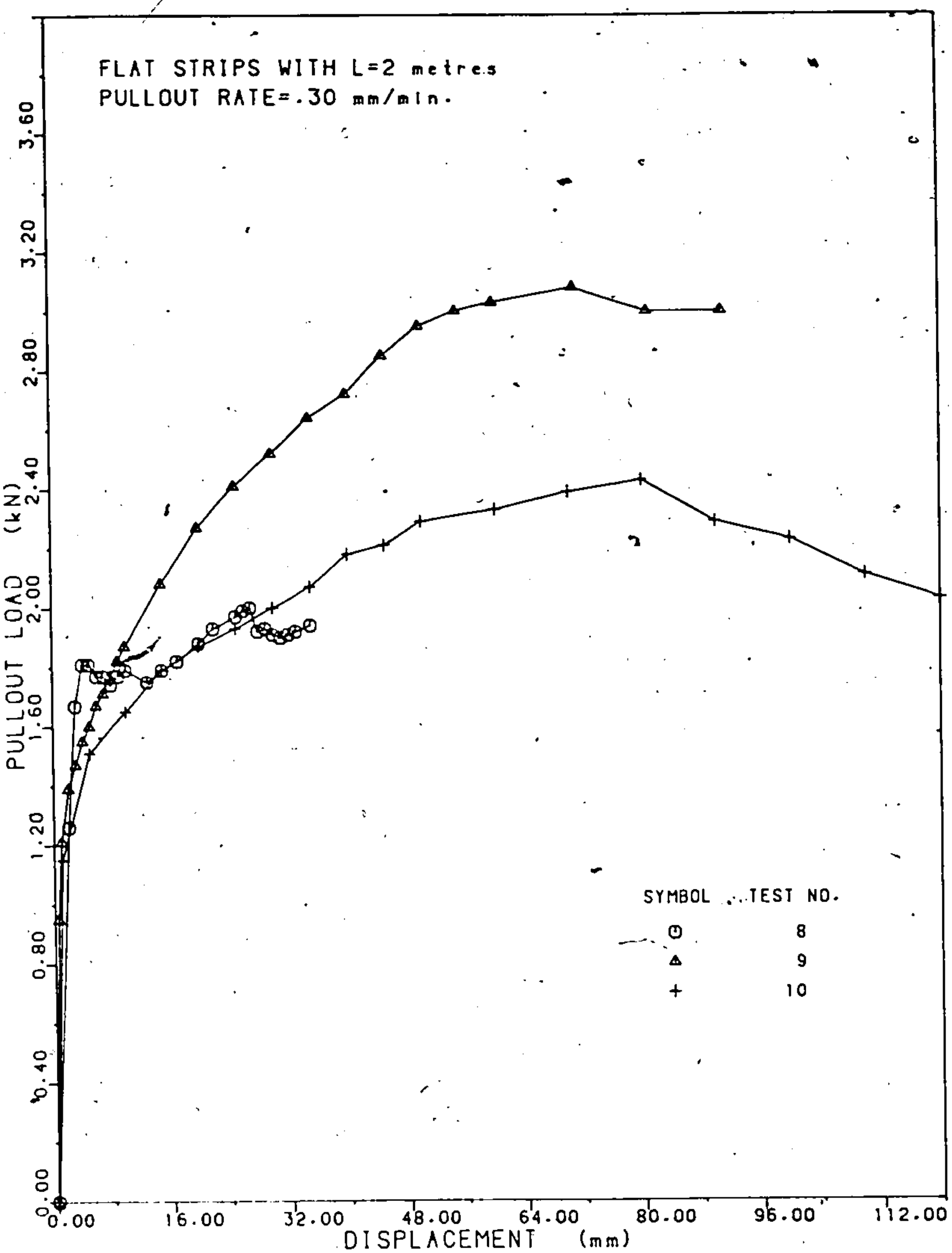

FIG. 4.1.6- PULLOUT LOAD VS. DISPLACEMENT FOR FLAT STRIPS, L= 2 metres

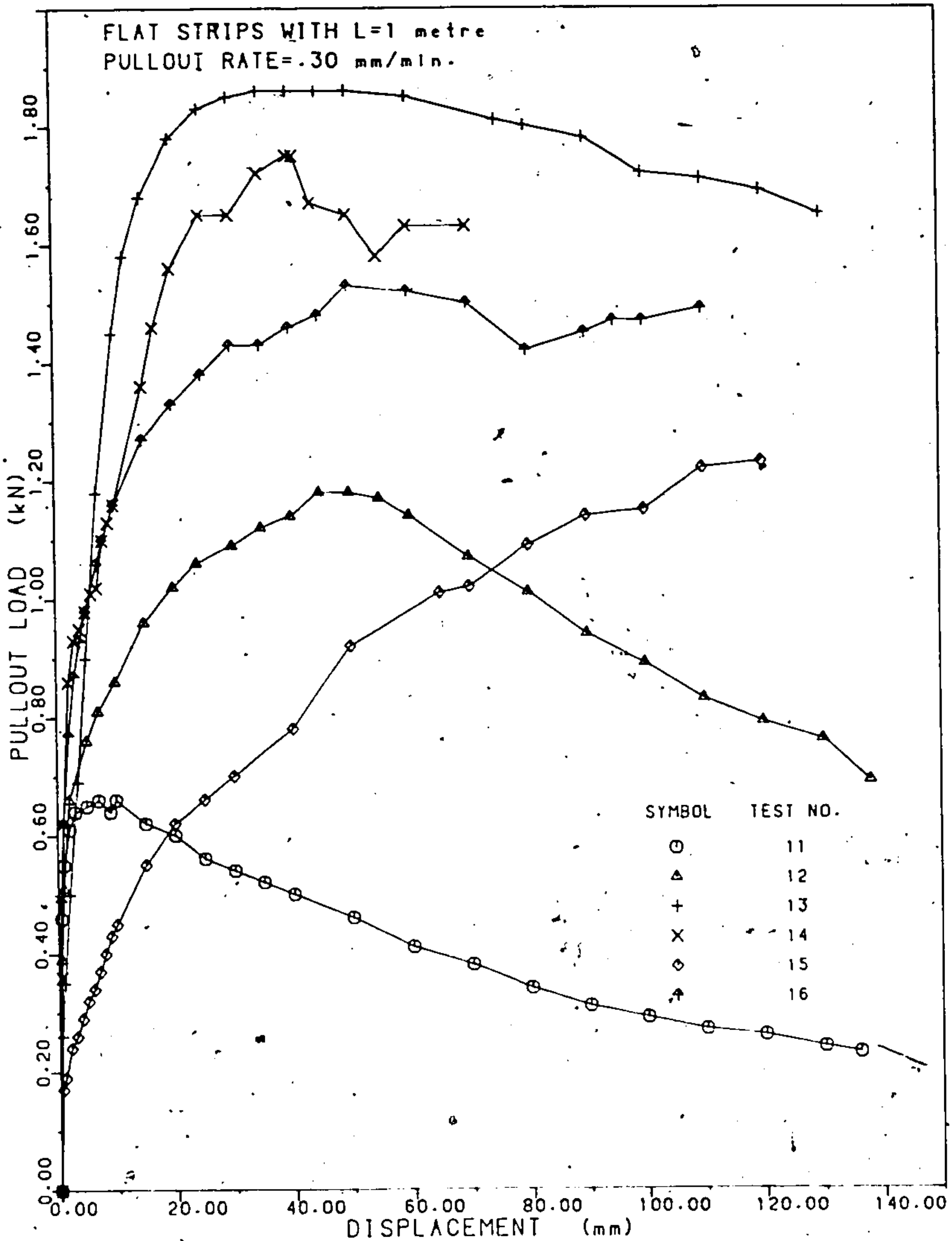

FIG. 4.1.7- PULLOUT LOAD VS. DISPLACEMENT FOR FLAT STRIPS, L= 1 metre

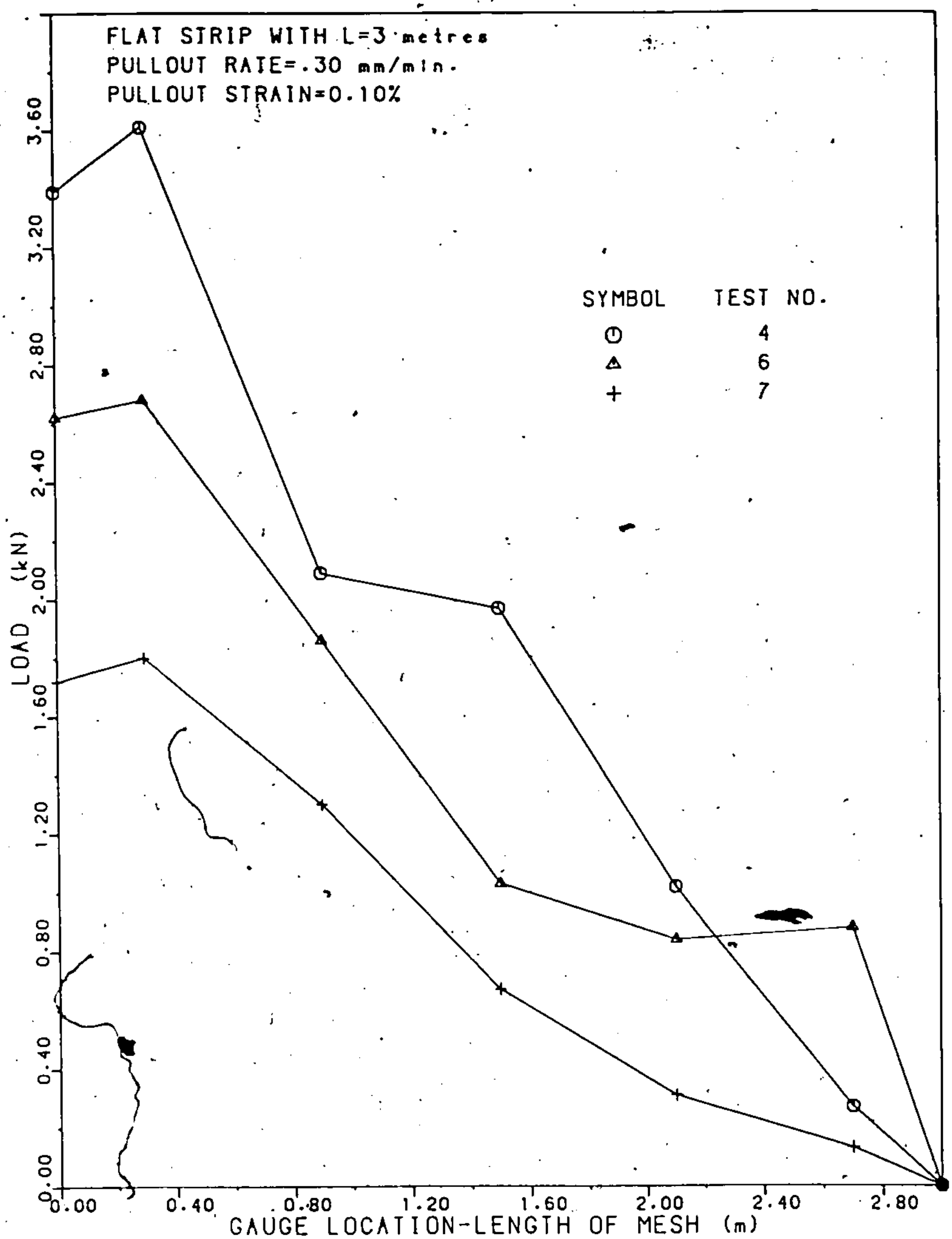

FIG. 4.1.8- TENSILE LOAD ON FLAT STRIPS
L= 3 metres

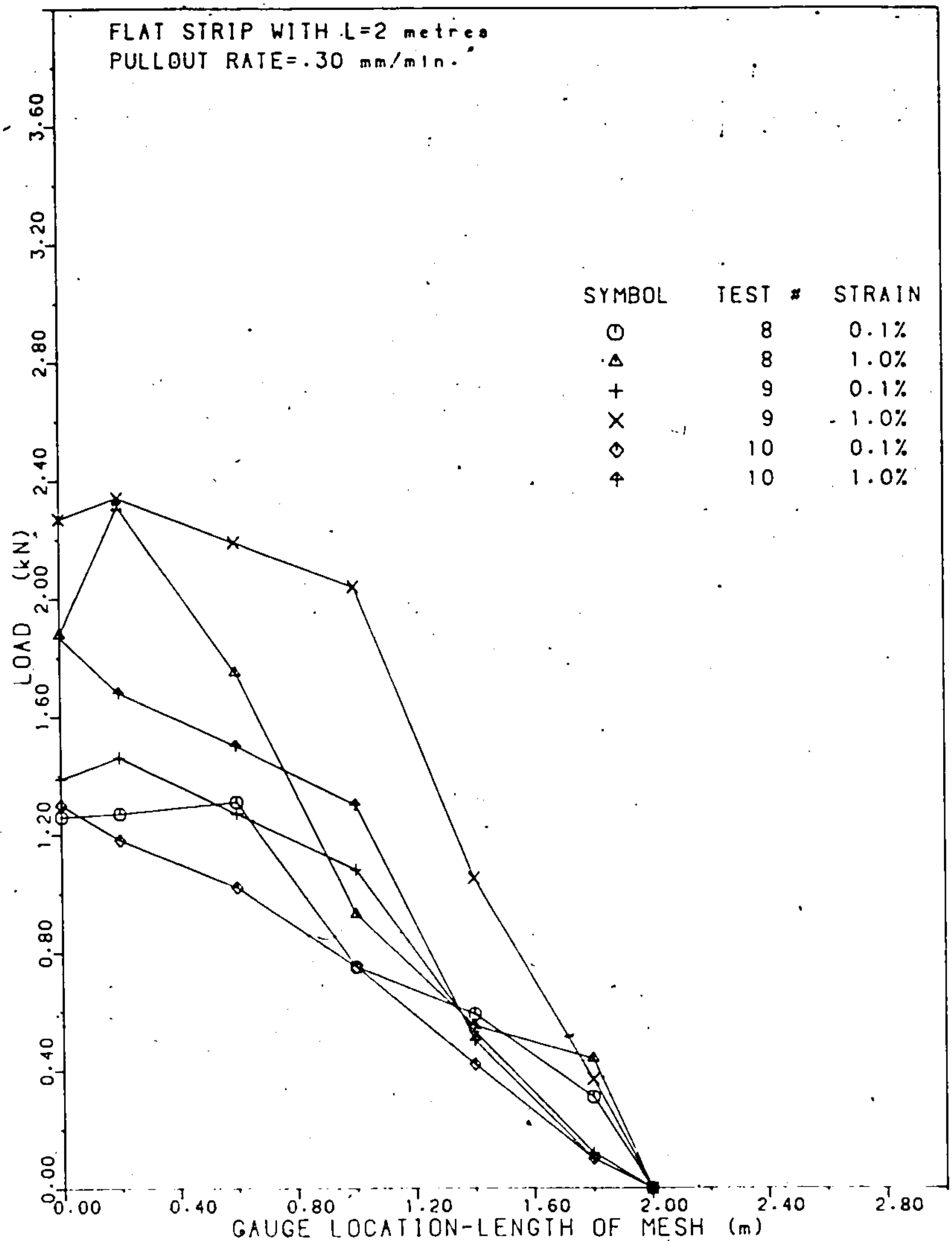

FIG. 4.1.9- TENSILE LOAD ON FLAT STRIPS
L= 2 metres

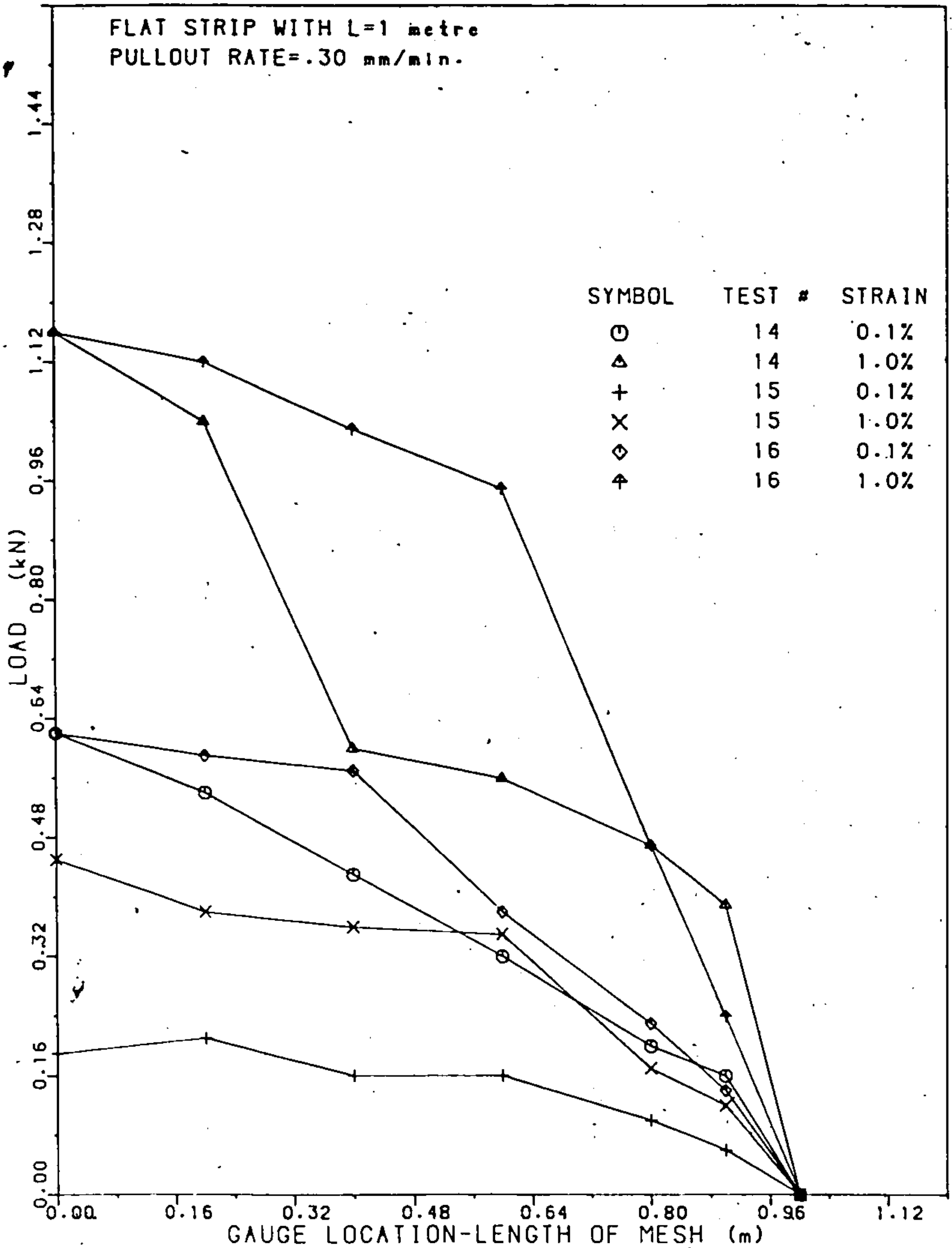

FIG. 4.1.10- TENSILE LOAD ON FLAT STRIPS
L= 1 metre

4.1.3 Reinforced Earth company ribbed strips

The Reinforced Earth Company strips were either galvanized or left untreated (test 19). All the strips were three metres in length and were tested at two levels of overburden pressure corresponding to heights of soil of 1.37 and 0.91 metres.

The rate of pullout was kept at 0.30 mm/minute and the unit weight of the crushed silica sand was measured, to be 16.1 kN/m³ (I_d=97.5%). The ribbed strips were tested on a tensile loading machine and the failure tensile load was found to be 90.3 kN.

Figure 4.1.4 shows a longitudinal cross-section of a Reinforced Earth ribbed strip. Table 3 summarizes the pullout testing program developed for the ribbed strips.

It becomes evident from the load-displacement curves (fig. 4.1.11) that the introduction of strain gauges in tests 20 and 21 did not influence the pullout resistance to the same extent as with the flat strips. This can be attributed to the presence of the ribbed sections which already increase substantially the friction and bearing resistance between the reinforcing strip and the sand backfill.

Once again, the same sudden relaxation of the pullout load was witnessed and was accompanied with a loud 'bang' occurring at regular intervals.

TABLE 3

Summary of pullout tests on ribbed strips

test#	length (m)	depth (m)	sur-charge	over-burden press. (kPa)	gauges	peak load (kN.)	displ. @ peak (mm)	peak stress (kPa)
17	3	1.37	no	22.1	no	9.37	25.0	46,850
18	3	0.91	yes	21.7	no	11.83	24.0	59,150
19	3	0.46	yes	21.3	no	10.93	40.0	54,650
20	3	0.46	yes	21.3	yes	9.56	38.0	47,800
21	3	1.37	no	22.1	yes	9.13	41.0	45,650

Comparing the ribbed strips to the flat strips, it is found:

1. The peak pullout capacity of the ribbed strips is approximately ten times greater than the flat strips capacity (10,150 N vs. 1,050 N); which demonstrates the efficiency (interlocking effect and passive resistance) of the ribs in the Reinforced Earth strips.

2. The peak pullout capacity is obtained at a displacement of about 3 mm for the ungauged flat strips of three metres in length, and approximately 35 mm for the ribbed strips.

3. The peak is very accentuated in the case of the flat strips (L= 3m), that leads to a residual value of the tensile force equal to approximately one-half of the peak value at a pullout strain of 2% (60 mm). In the case of the ribbed strips (L= 3m), the peak is flat and the residual value at a pullout strain of 2% is between 80 and 90% of the peak value.

4. The tensile forces developed in the ribbed strips (fig. 4.1.12) indicate that the maximum stress will occur at a certain distance inside the facing and not at the load application point. This duplicates the results of the flat strips.

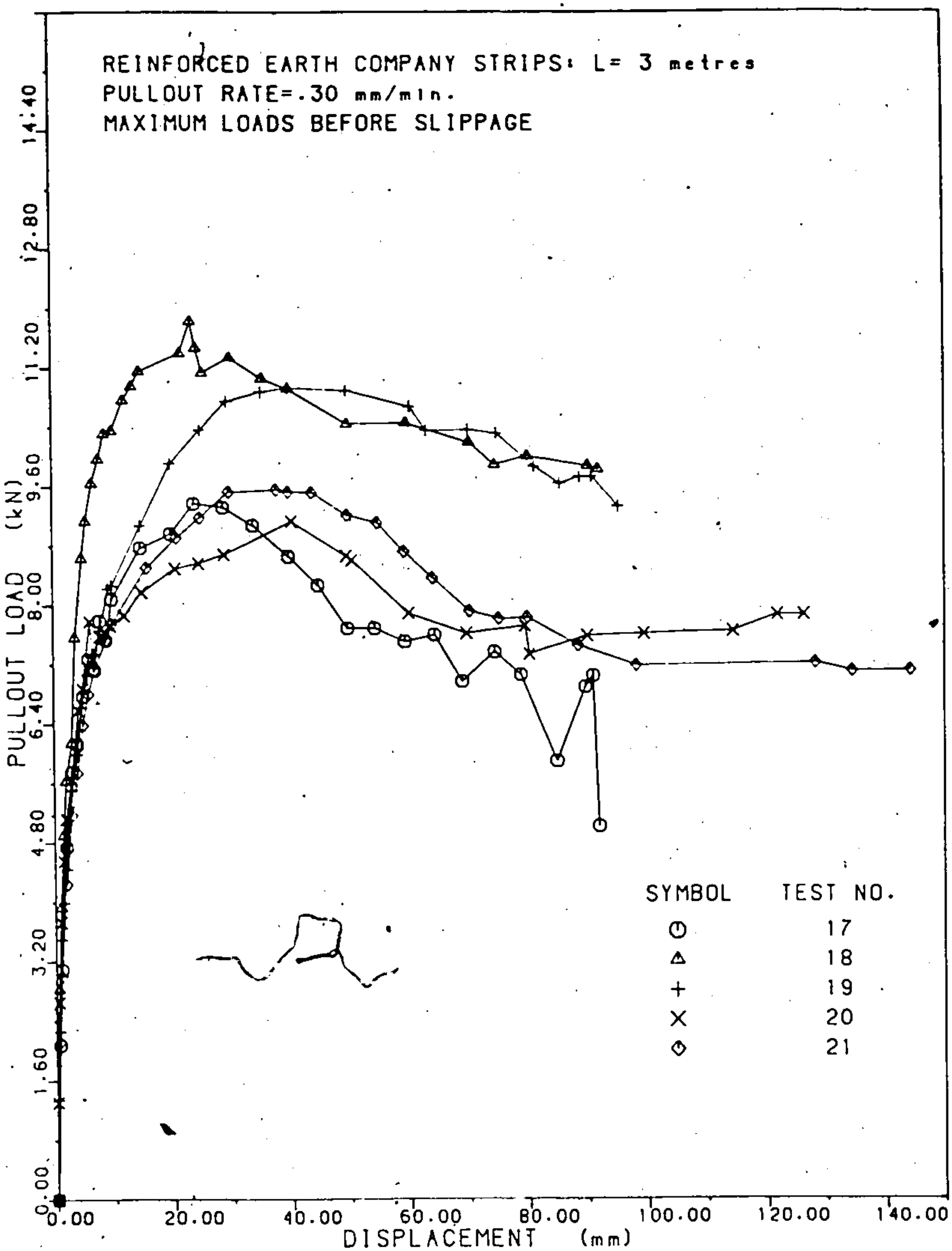

FIG. 4.1.11- PULLOUT LOAD VS. DISPLACEMENT FOR RIBBED STRIPS

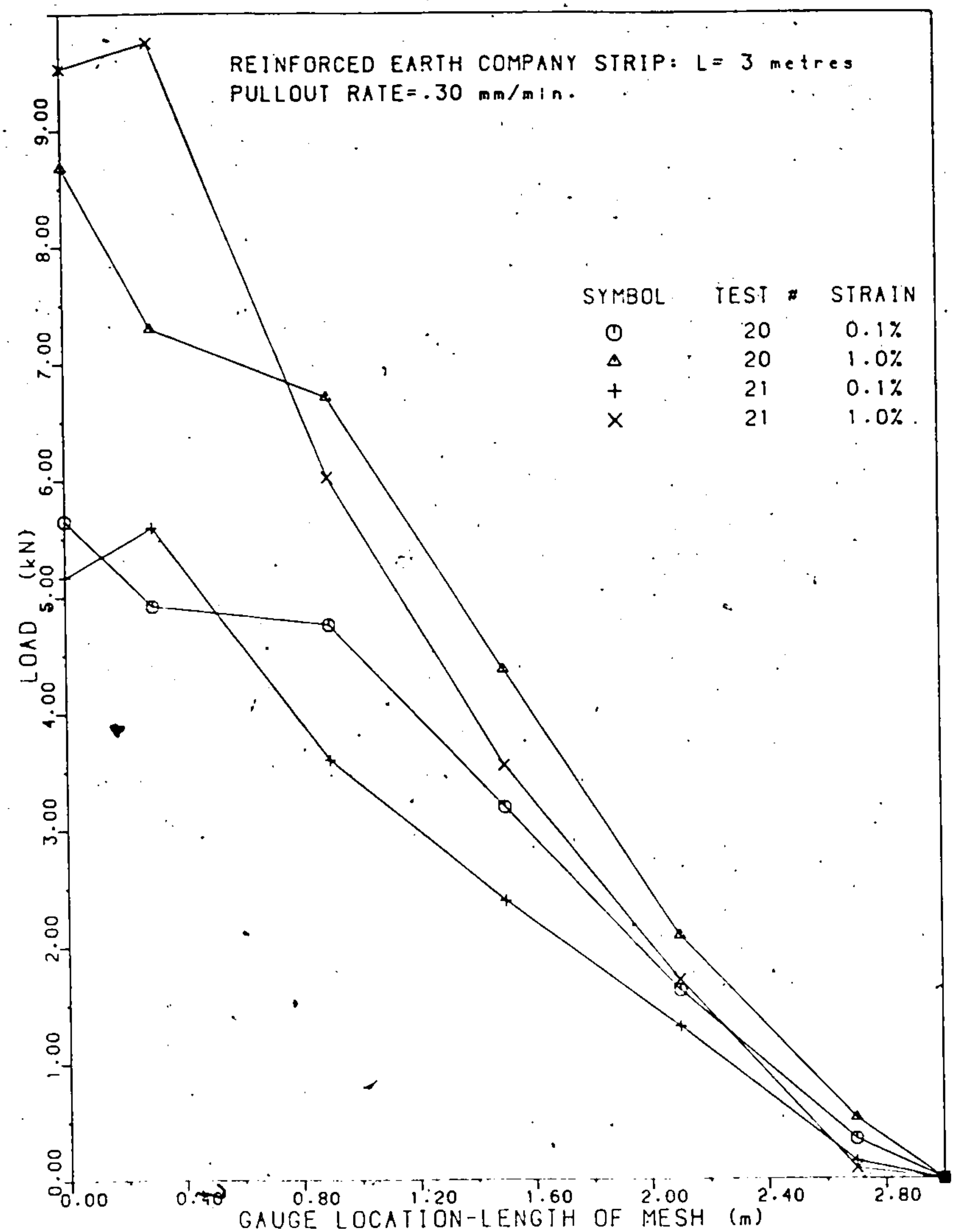

FIG. 4.1.12- TENSILE LOAD ON REINFORCED EARTH STRIPS

4.1.4 Wire mesh system

The steel wire mesh which is used as temperature reinforcement in concrete floor slabs is available commercially with a bar diameter of 4.8 mm (3/16 in.) and a crossbar spacing of 152 mm x 152 mm (6 in. x 6 in.).

To create a 12 in. x 6 in. section or an 18 in. x 6 in. section, crossbars were cut-off, and to create 3 in. x 6 in. sections, additional cross-bars were spot welded between the existing transverse members. The spot welded joint failure load was tested to be 10,200 N, and the bar resistance to failure was 12,250 N.

From this point on, the crossbar spacing of the wire mesh will only be referred to numerically (i.e. 6x6, 12x6 etc.) and in the imperial measurement in which they are available.

For reference purposes, the metric equivalent of the 3x6, 6x6, 12x6, and 18x6 sections is 76 mm x 152 mm, 152 x 152 mm, 305 mm x 152 mm, and 457 mm x 152 mm respectively.

Figures 4.1.13 to 4.1.16 show the configuration of the mesh sections employed and the location of the tensile strain gauges whenever applicable.

It was not possible to calibrate each wire mesh strip individually as in the previous pullout tests for tensile strain readings, however a sample bar consisting of a strain gauge mounted on a 4.8 mm diameter bar (taken from the mesh to be tested) was calibrated on a tensile loading machine.

The following value was obtained for the calibration of the test data on the strain reading units (see fig. 4.1.17):

1 strain reading division = 3.57 N

TABLE 4

Summary of pullout tests on wire mesh

test#	length (m)	cross bar spacing	sur-charge	over-burden press. (kPa)	gauges	peak load (kN)	displ. @ peak load (mm)
22	3	3x6	yes	21.9	yes	31.40	33.5
23	3	3x6	yes	14.6	no	29.52	28.5
24	3	6x6	no	21.9	yes	31.75	21.3
25	3	6x6	no	14.6	no	26.41	48.4
26	3	12x6	no	21.9	yes	33.20	77.7
27	3	12x6	no	14.6	no	19.96	47.8
28	1.93	6x6	no	22.1	no	31.57	79.3
29	1.93	6x6	yes	14.7	yes	29.15	95.5
30	1.93	12x6	yes	22.1	no	24.41	100.8
31	1.93	12x6	no	14.7	no	19.82	97.0
32	1.93	18x6	no	22.1	no	20.01	85.1
33	1.93	18x6	no	14.7	no	16.80	97.3

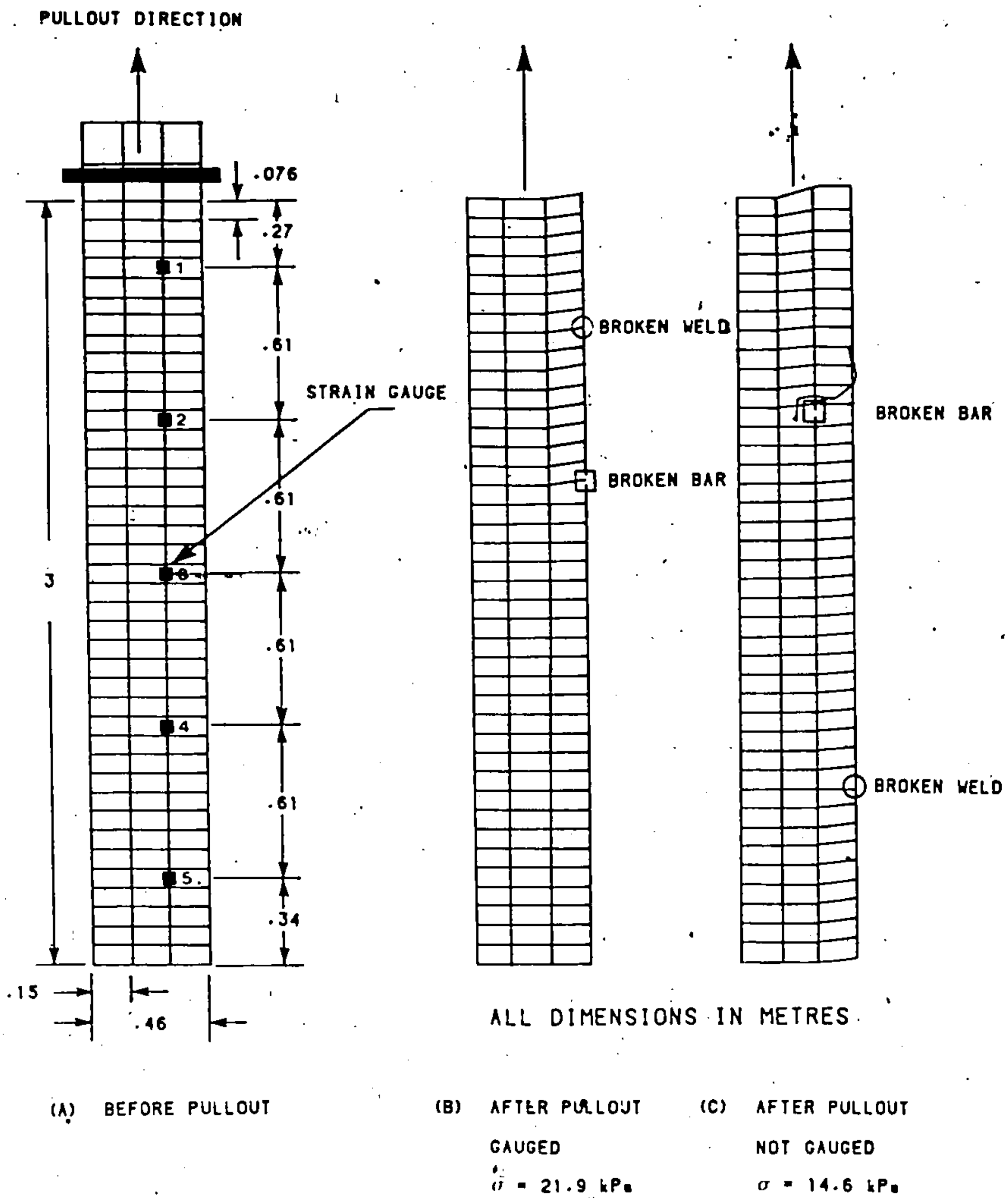

FIG. 4.1.13- PLAN VIEW OF 6x3 MESH BEFORE AND AFTER PULLOUT TEST

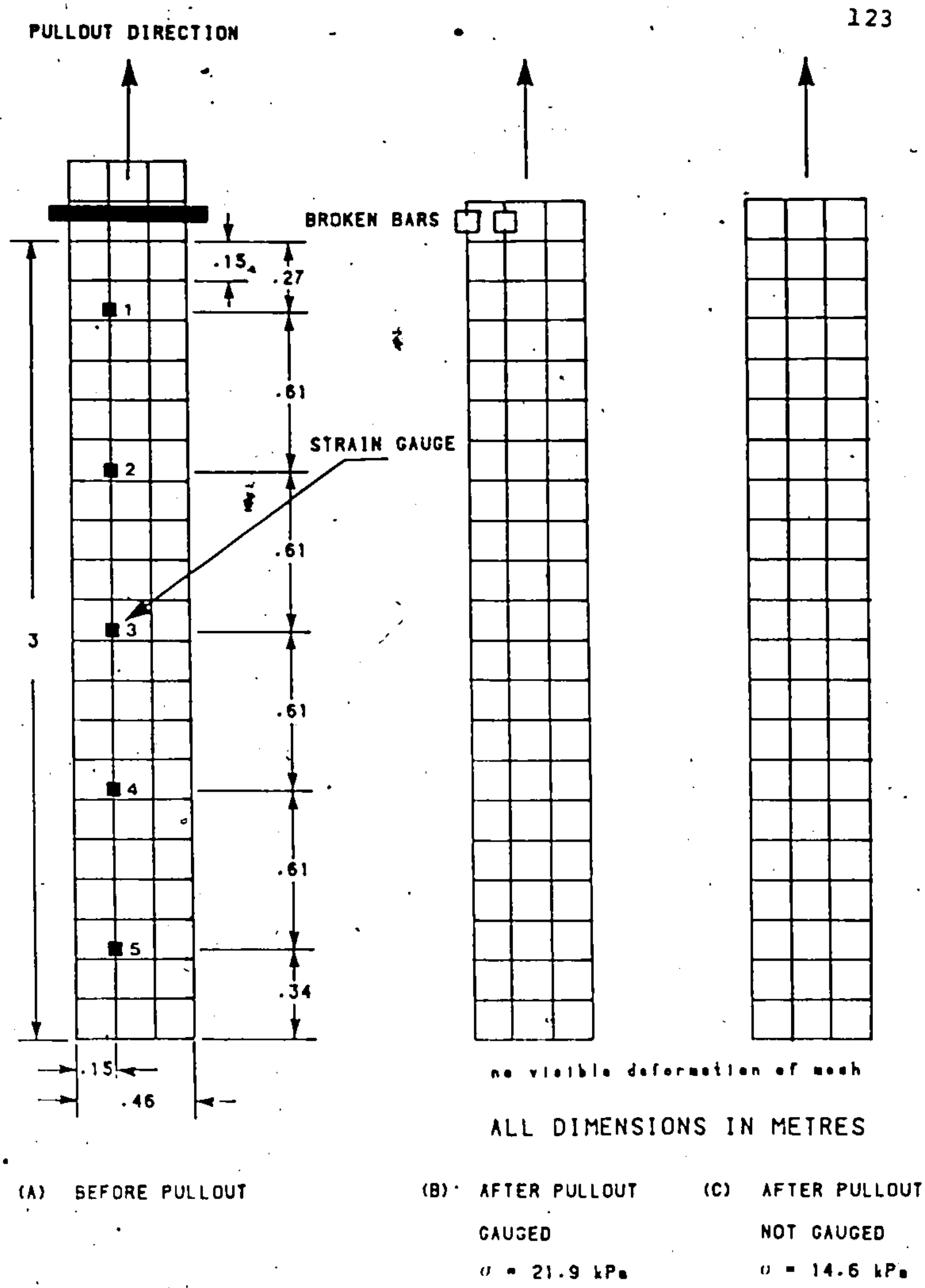

FIG. 4.1.14- PLAN VIEW OF 6x6 MESH BEFORE AND AFTER PULLOUT TEST

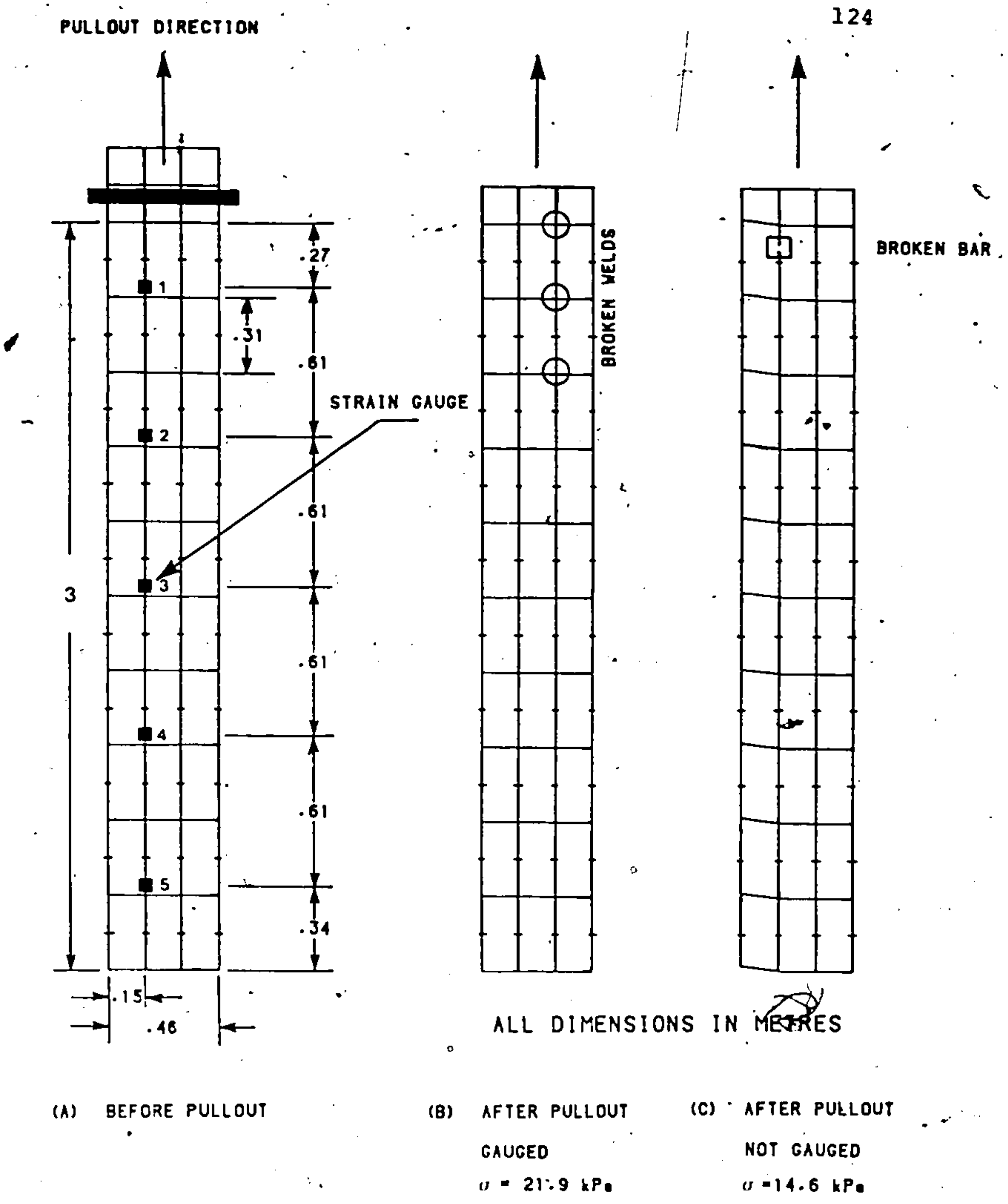

FIG. 4.1.15- PLAN VIEW OF 6x12 MESH BEFORE AND AFTER PULLOUT TEST

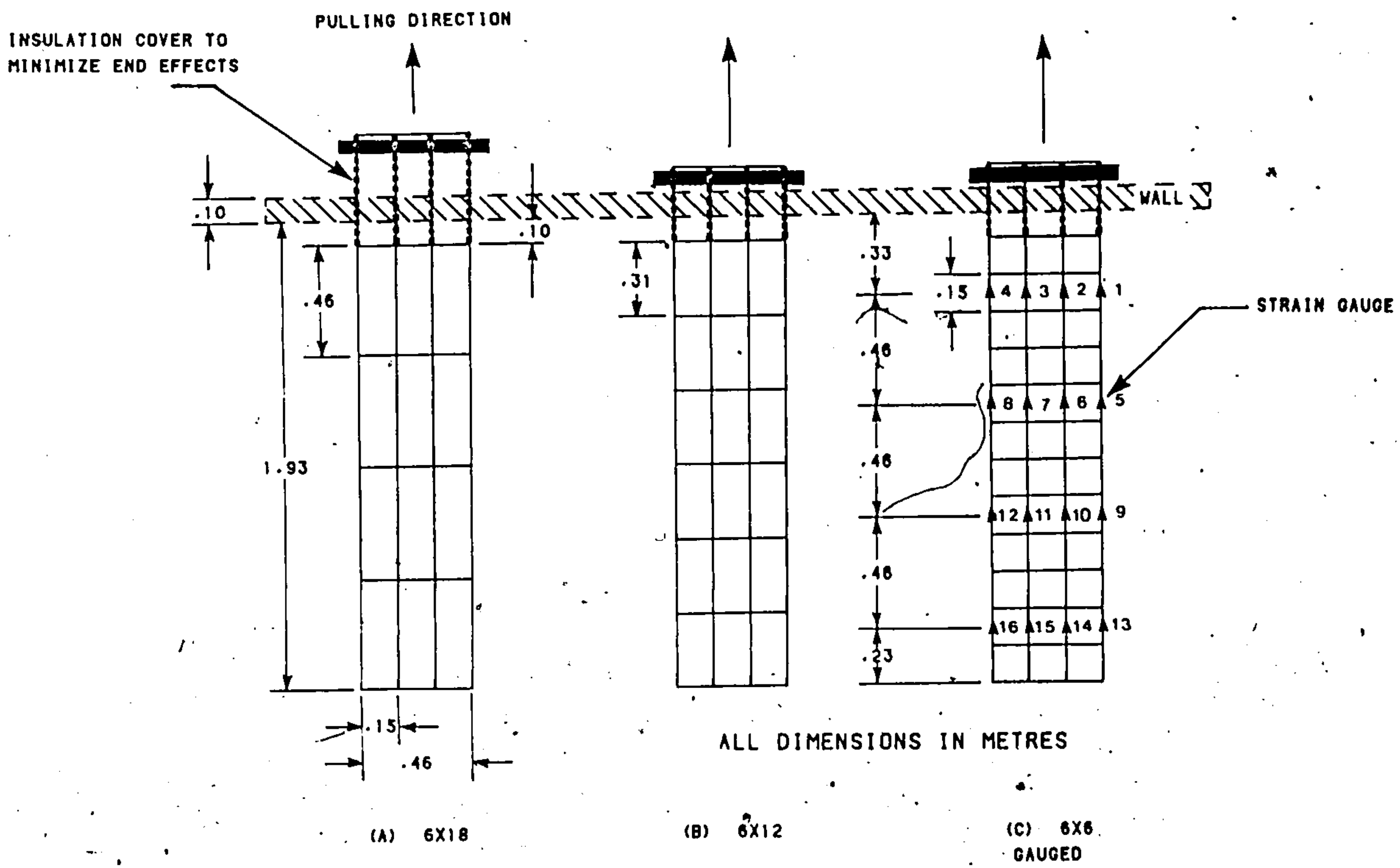

FIG. 4.1.16- PLAN VIEW OF WIRE MESH USED IN FINAL SERIES OF PULLOUT TESTS

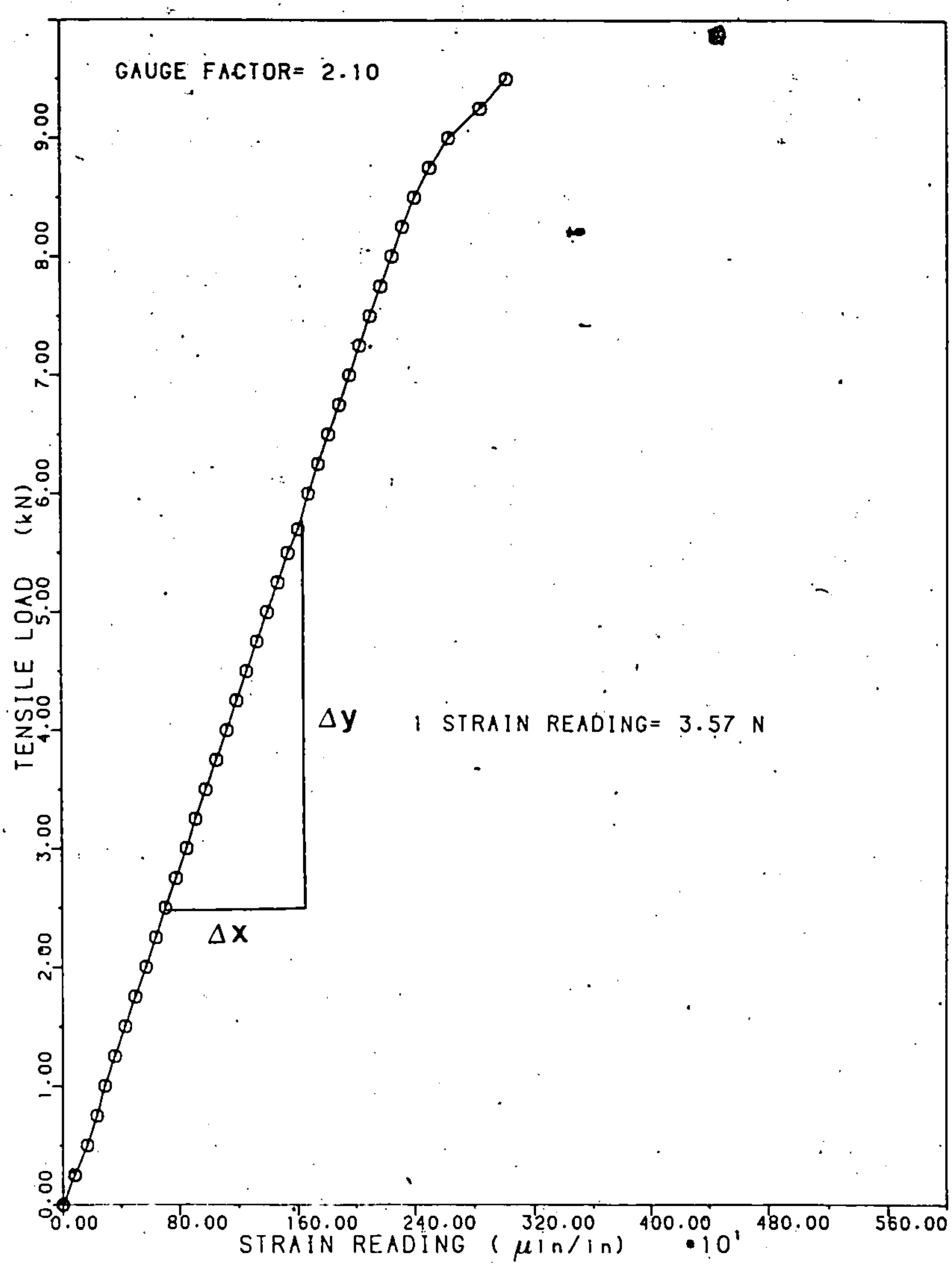

FIG. 4.1.17- STRAIN CALIBRATION OF MESH

The wire mesh pullout tests results are summarized in table 4 and illustrated on figures 4.1.18 to 4.1.26.

The rate of pullout was kept constant at 0.30 mm/minute with a density index of the backfill soil of 94.7% for the wire mesh of three metres length.

The rate of pullout was 0.23 mm/minute with a density index of 96.2% for the wire mesh of 1.93 metres length.

As can be seen in figures 4.1.18 and 4.1.19 (pullout load vs. displacement, with L= 3 metres), the actual pullout capacity of the three metres length mesh was not achieved due to material failure. Instead of testing the soil/reinforcement interaction pullout capacity, it was the yield strength of the steel wire mesh which was tested. The excessive length of mesh in effect, anchored the system.

Figure 4.1.13 (Plan view of 3x6 mesh with L=3 metres, before and after pullout) demonstrates what happens to the mesh during pullout. The load on the mesh increased until failure was achieved at a weak link in the wire mesh system. As the load continued to be applied, the section before the break was deformed towards the loading point, while the section after the break was not deformed. The load then increased until the failure capacity of the next weak link was reached.

As can be seen from the tensile stress curves of the three metres length mesh, the tensile load on the middle bars was at or near the failure load level.

To investigate further the soil/mesh behaviour, a shorter length of mesh (L= 1.93 metres) was tested. To avoid spot welding problems the crossbar spacings selected for testing were the 6x6, 12x6, and the 18x6 sections. The shorter length avoided the bar failure problem and permitted pullout tests which did not deform the mesh. Therefore, the pullout load values represent the bearing capacity resistance of the mesh against pullout at a predetermined overburden pressure.

Figures 4.1.23 and 4.1.24 illustrate the pullout test results of the 1.93 metres long mesh.

The tensile load graphs indicate the load distribution on the four longitudinal bars. The load on the middle bars is approximately two times the load on the outside bars. In other words, each inside bar carries 1/3 of the load and each outside bar carries 1/6 of the applied load.

The pullout load vs. displacement curves show that the load increases were not constant and cannot be described by a smooth curve relationship. A peak load was always followed by a sudden drop in load and a large deformation as the maximum bearing resistance was reached on the crossbars. This was then followed by a load pickup until the next relaxation. Table 4 shows that the peak pullout resistance is a function of not only the overburden pressure but also the crossbar spacing, and the mesh length.

This statement can be expanded to include the bar diameter, the yield strength of the steel, the configuration and the density of the backfill material.

One interesting res[illegible] of the wire mesh pullout tests is the relatively consta[illegible]eak pullout resistance of the 6X6 section which seems to be less sensitive to the overburden pressure or the length of the mesh. For this reason and for modelling purposes, the 6x6 sections were selected for further research into sloped reinforced embankments and reinforced walls.

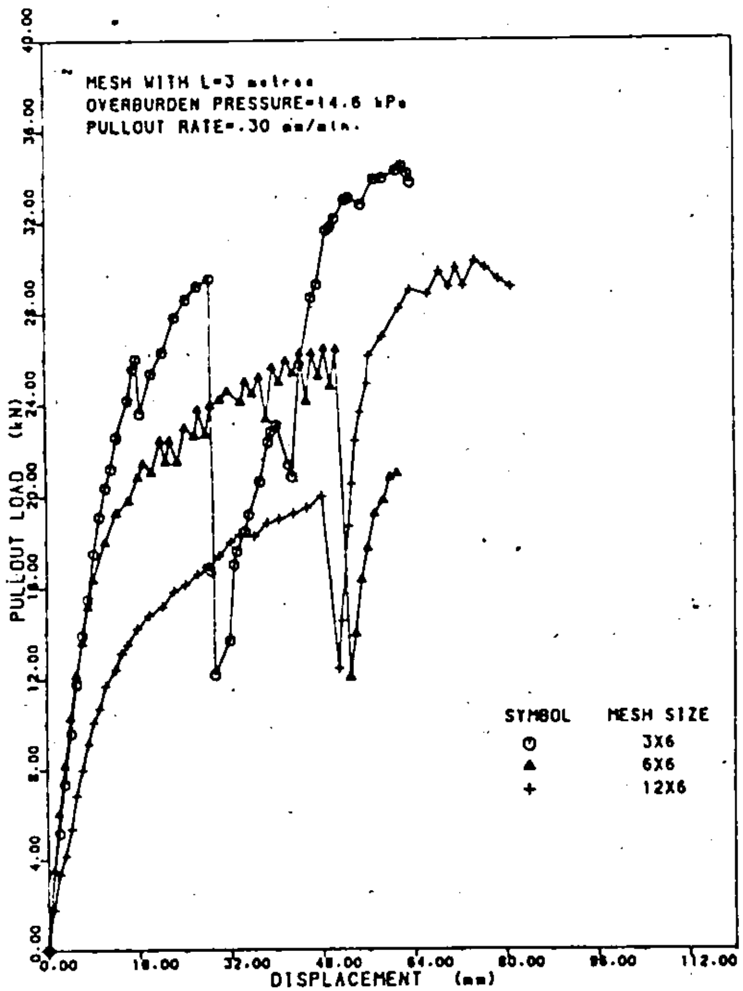

FIG. 4.1.18- PULLOUT LOAD VS. DISPLACEMENT FOR WIRE MESH OVERBURDEN PRESSURE= 14.6 kPa

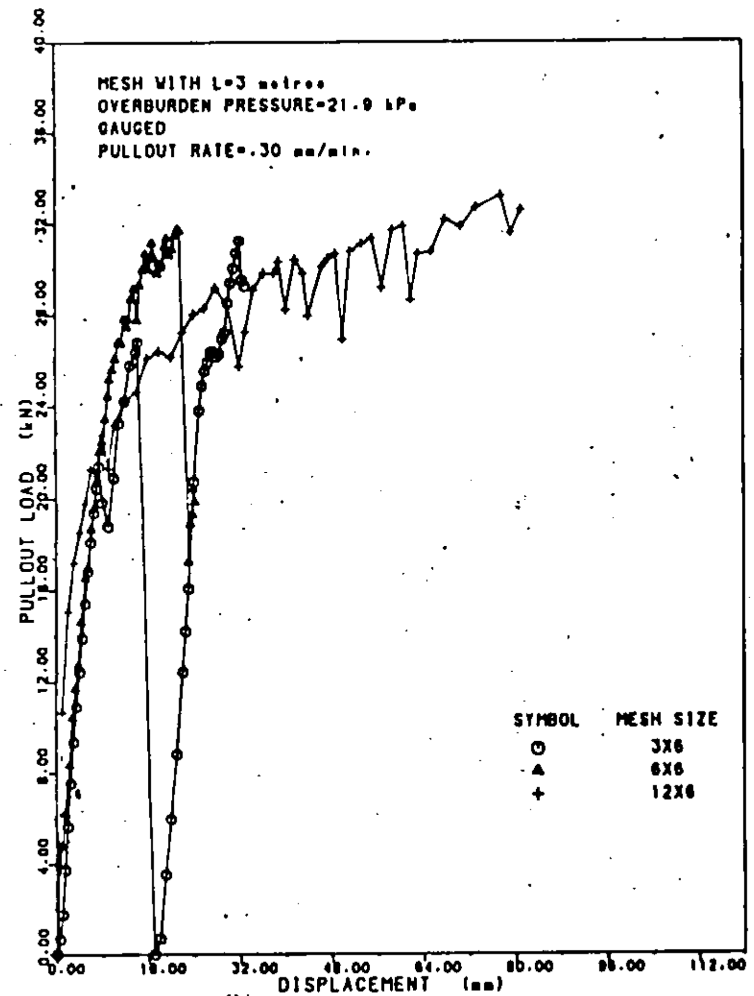

FIG. 4.1.19- PULLOUT LOAD VS. DISPLACEMENT FOR WIRE MESH OVERBURDEN PRESSURE= 21.9 kPa

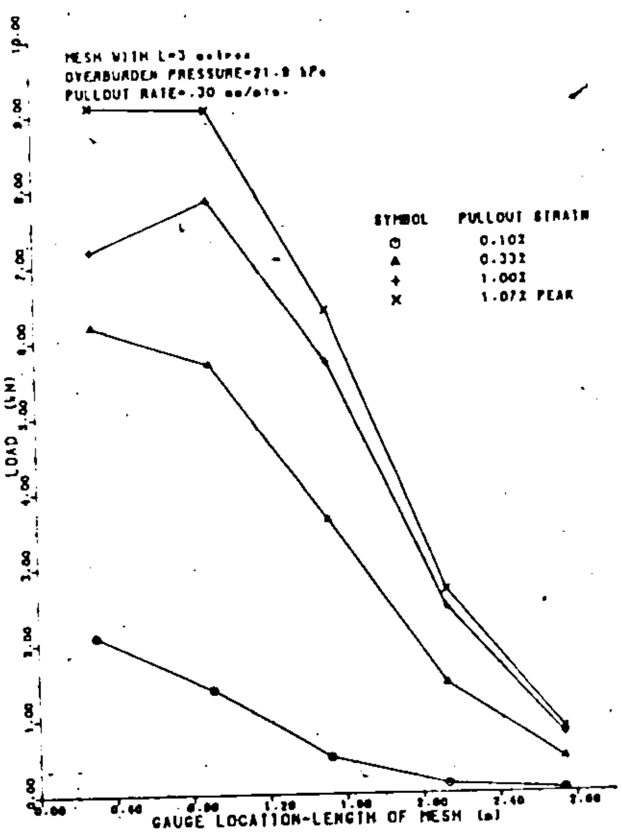

FIG. 4.1.20- TENSILE LOAD IN 3X6 MESH AT THE MIDDLE BAR

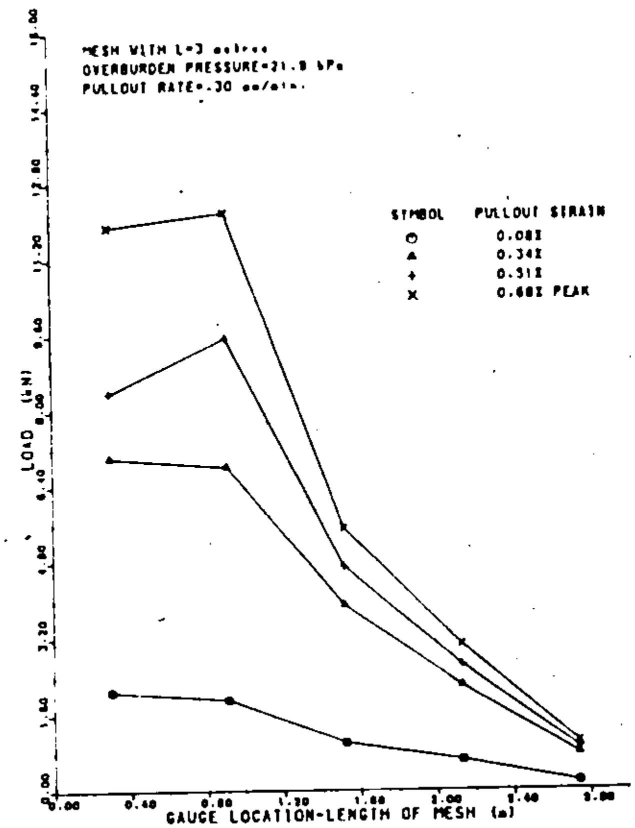

FIG. 4.1.21- TENSILE LOAD IN 6X6 MESH AT THE MIDDLE BAR

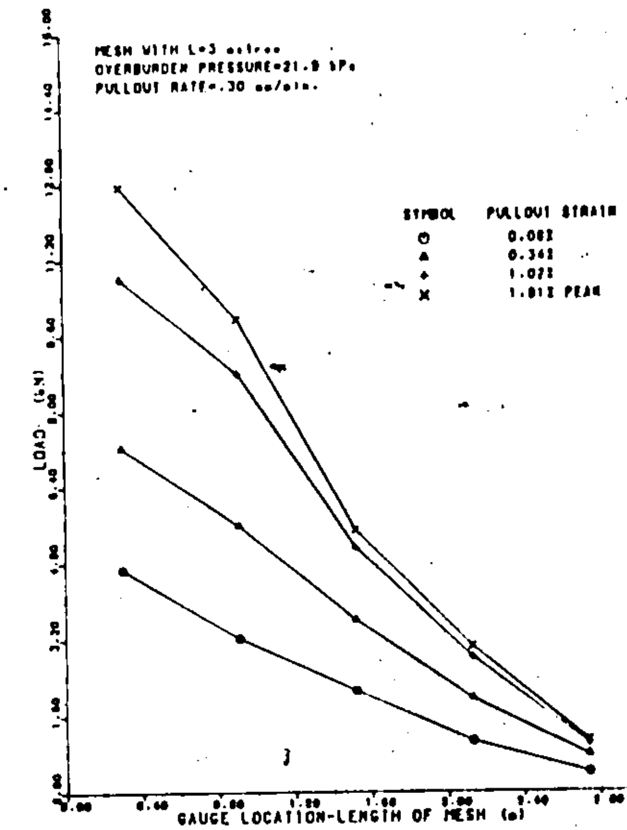

FIG. 4.1.22- TENSILE LOAD IN 12X6 MESH AT THE MIDDLE BAR

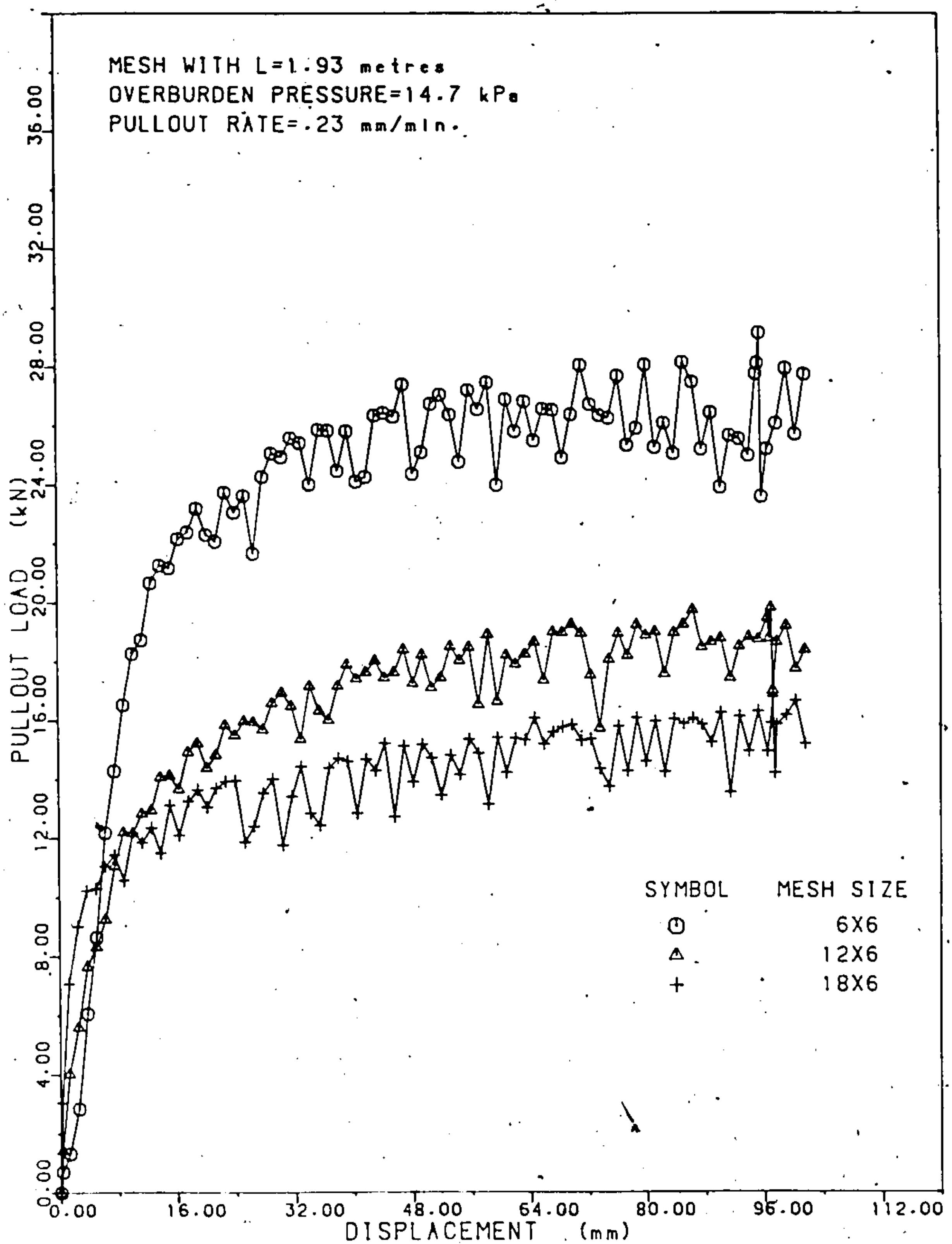

FIG. 4.1.23- PULLOUT LOAD VS. DISPLACEMENT FOR WIRE MESH

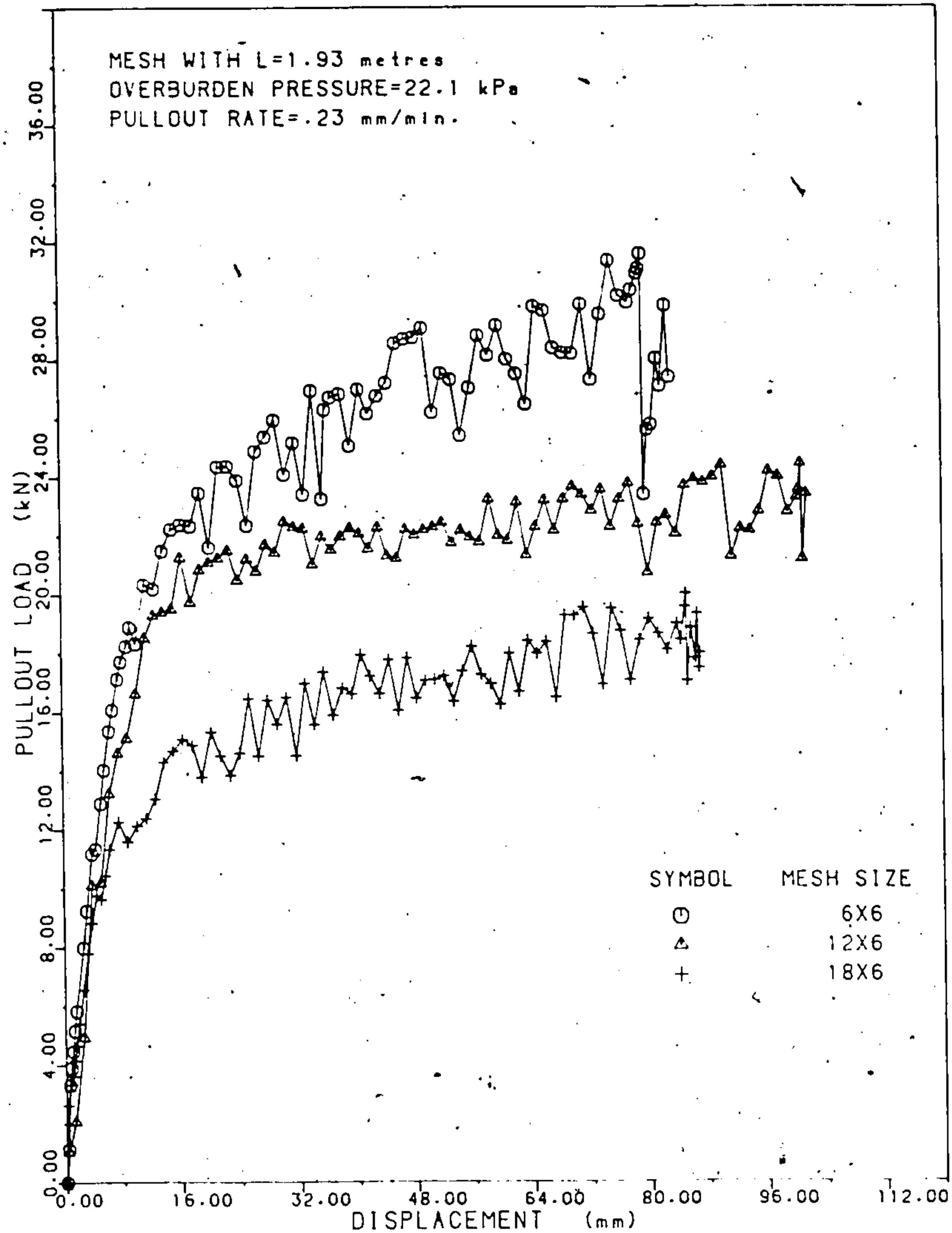

FIG. 4.1.24- PULLOUT LOAD VS. DISPLACEMENT FOR WIRE MESH

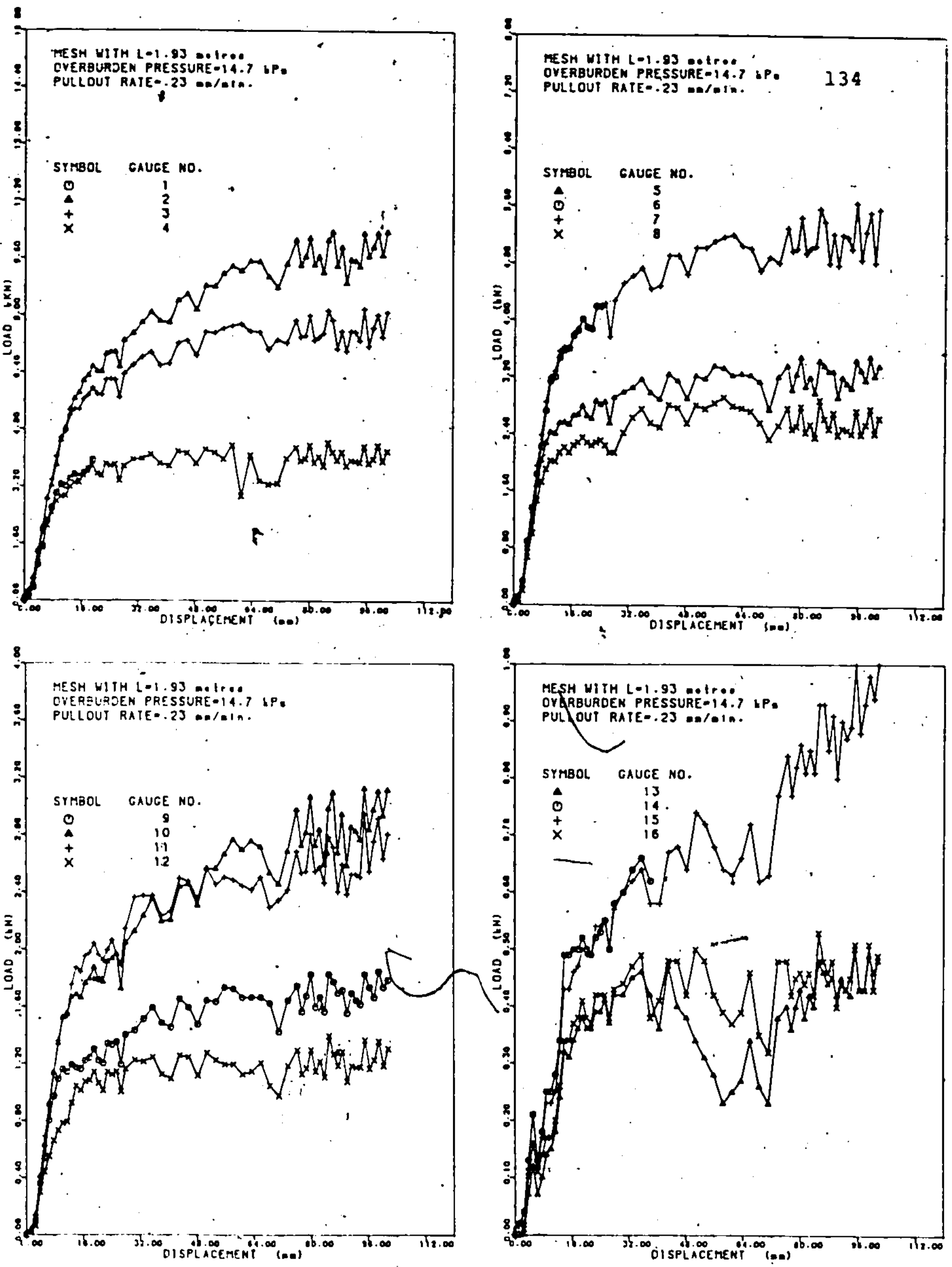

FIG. 4.1.25- TENSILE LOAD IN 6x6 MESH

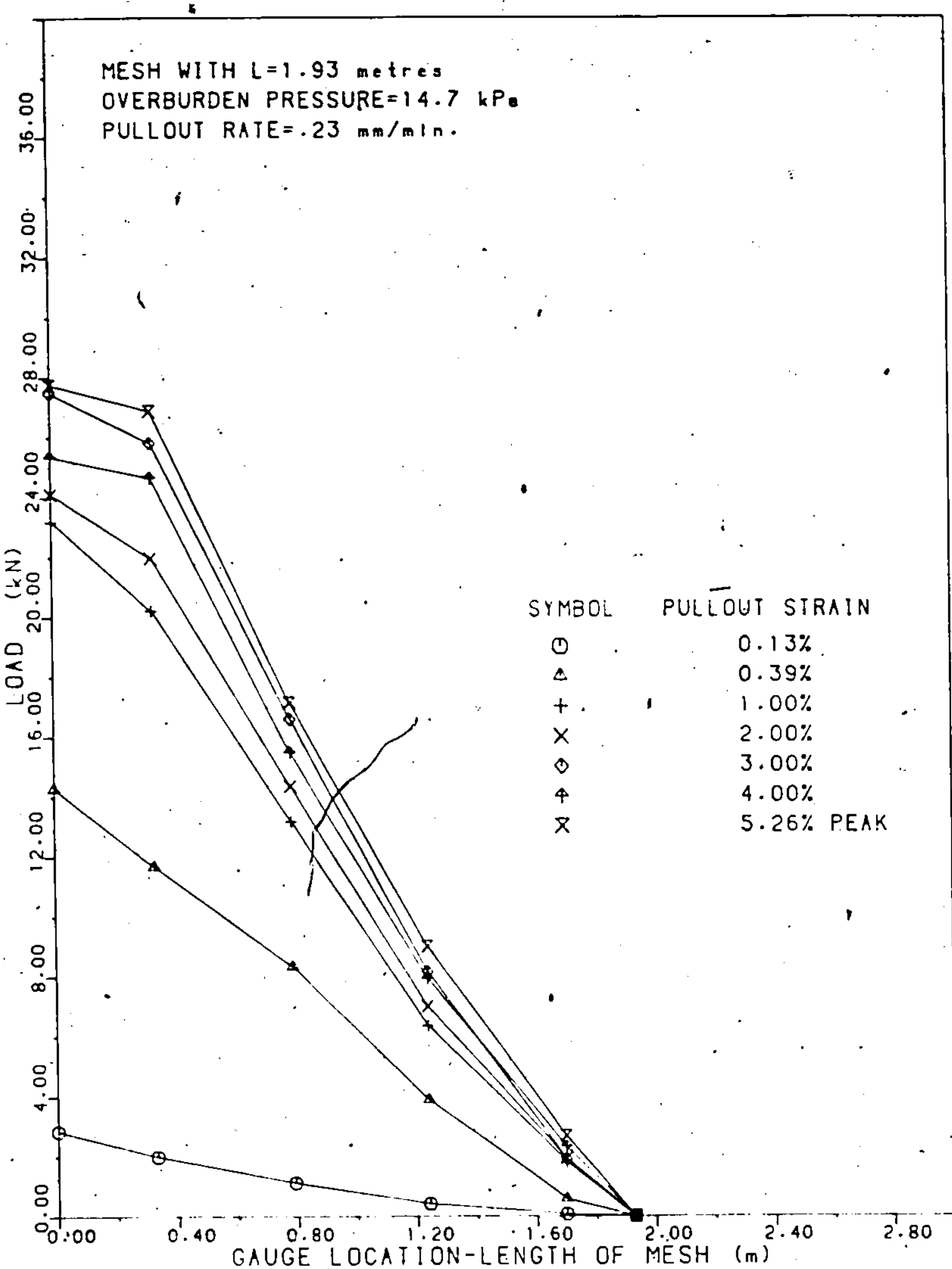

FIG. 4.1.26- TENSILE LOAD IN 6X6 MESH

4.1.5 Comparison of reinforcing systems

One way to compare the effectiveness of the different reinforcing systems is to establish the pulling resistance per surface area of steel for each system. Since the surface area of steel reinforcing is proportional to its weight, we can establish a ratio of peak pulling resistance per weight of steel.

TABLE 5

Comparison of pullout resistance ratios by weight

Reinforcing systems	Weight of steel (kg/m)	total wt. (kg)	steel ratio	peak pullout resistance (kN)	peak pullout resistance corrected for steel weight (kN)	pullout resistance ratio vs. ribbed strips
ribbed L= 3m	1.56	4.68	1	10.16	10.16	1
flat L= 3m	1.40	4.20	.9	1.04	1.16	0.11
wire mesh						
6x6	1.31	2.53	.54	31.57	58.46	5.7
12x6	1.08	2.08	.44	24.41	55.48	5.5
18x6	0.91	1.76	.38	20.01	52.66	5.2
L= 1.93m						

Table 5 shows that for the same surface area (weight of steel), the wire mesh has more than five times the pullout resistance of the ribbed strips.

4.1.6 Summary of pullout tests

Based on large scale laboratory pullout tests performed using different types of steel reinforcement, the following conclusions can be reached:

1. The load-deformation curves indicate a linear relationship until the yield limit of the steel is reached, then a non-linear shape is developed by the reinforcement/backfill combined behaviour.

2. Data obtained from the placement of strain gauges on the reinforcing elements indicates that the maximum tensile stress due to the pullout loads occurs just inside the reference wall, a short distance into the soil backfill. This statement holds true for all three types of steel reinforcement.

3. Tensile stresses dissipate very rapidly along the length of the reinforcing member, and stresses near the end of the embedded strip are minimal.

4. The pullout resistance of the reinforcing strip is a function of the overburden pressure exerted on the strip. The pullout load increases until the yield strength of the steel member is reached.

5. Installation of strain gauges on flat smooth strips increases the pullout resistance of the strips. The strain gauges behave in the same way as the ribbed

sections in the Reinforced Earth strips by increasing the passive resistance (anchor effect) between the backfill and the reinforcing element.

6. For the same surface area and weight, the standard wire mesh used as temperature reinforcement in concrete floor slabs exhibits a pullout resistance that is more than five times that of the ribbed strips.

7. A decrease in crossbar spacing in the wire mesh system results in a higher pullout resistance.

8. If the length of the reinforcing strip is of sufficient length so that the system is considered anchored, the controlling factor in a pullout test becomes, the structural strength of the reinforcing material.

Figure 4.1.27 compares typical load-displacement curves for all three systems investigated.

The wire mesh system of reinforcement will now be further investigated in the following sections with triaxial compression tests, reinforced embankment and reinforced wall tests in order to examine its behaviour under strip loading conditions.

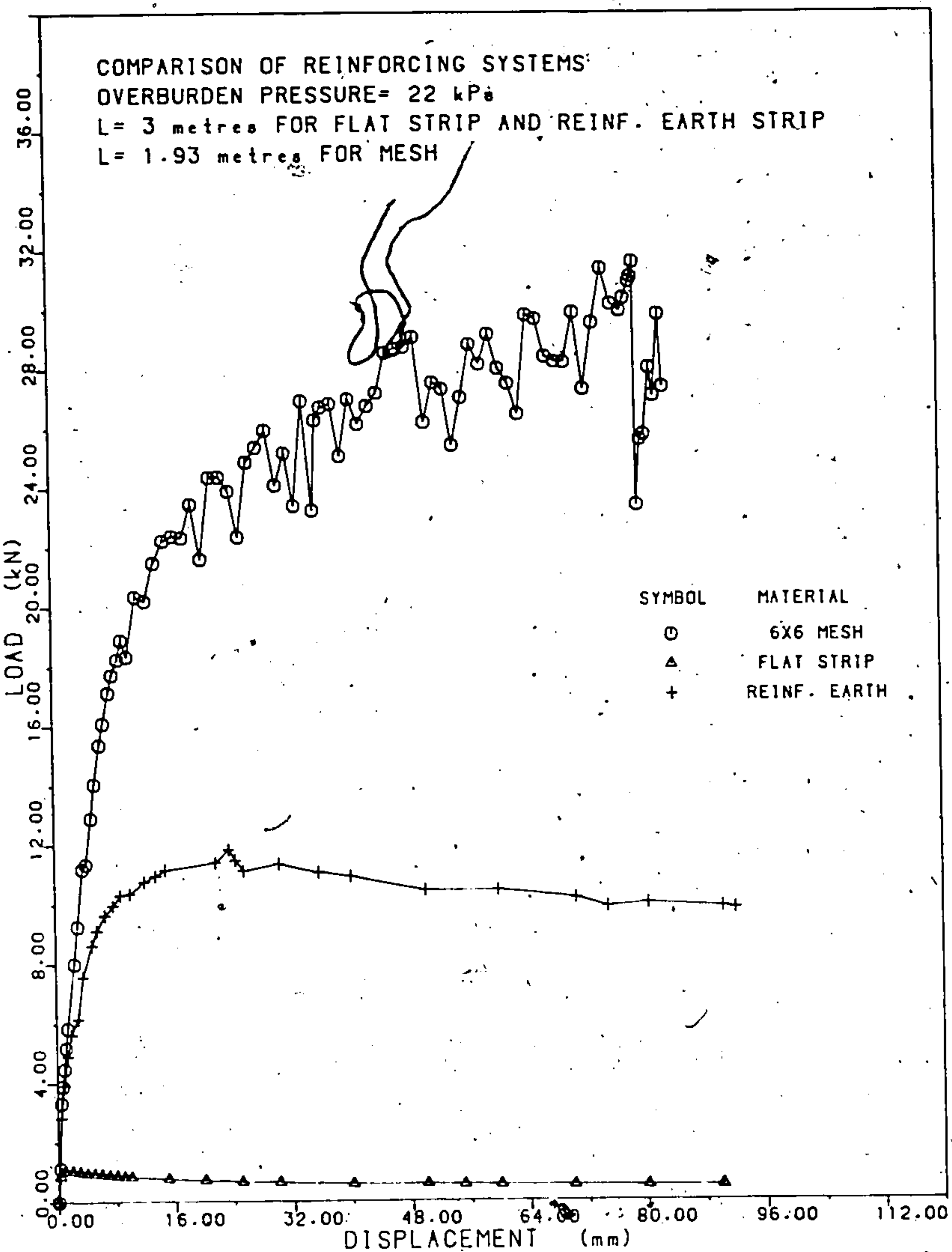

FIG. 4.1.27- COMPARISON OF REINFORCING SYSTEMS BY PULLOUT TESTS

4.2 TRIAXIAL TESTS

The shear strength characteristics of a sand can be determined from the results of either direct shear tests or drained triaxial tests.

To simulate the loading conditions in the sandbox model, dense dry sand samples (I_d = 95%) were loaded triaxially in order to compare the change in friction angle created by the introduction of reinforcing members.

With a dense sand there will be a considerable degree of interlocking between particles and before complete shear failure can take place this interlocking must be overcome in addition to the frictional resistance at the point of contact.

The friction angle is dependent on too many parameters to be accurately defined in this study, but by keeping the variables as constant as possible one can obtain an apparent angle of friction for a specific situation. The variables include the configuration of the reinforcing mesh (geometry, number of reinforcing layers, diameter of reinforcing bars, etc.), the void ratio in the sample, the influence of the end restraints, the duration of the test, changes in principal stress directions, and the usual experimental errors.

Having considered its drawbacks, the triaxial test is still used since there is basically no better way to analyse the internal friction angle of a soil sample.

4.2.1 Triaxial tests on crushed silica sand

A series of triaxial tests were performed on the backfill soil material utilized for the subsequent reinforced embankments and reinforced wall tests. A summary of the testing program is presented in table 6 . The triaxial testing procedure was described previously in section 3.4.

TABLE 6

Summary of triaxial tests on sand

test#	I_d (%)	confining pressure σ_3 (kPa)	initial area (m²)	corrected area @ max. σ (m²)	maximum deviator stress (kPa) σ	axial stress σ_1 (kPa)
11	96.3	34.5	.0435	.0474	160.7	194.1
4	97.0	172.2	.0430	.0474	600.4	771.1
1	96.5	344.5	.0430	.0490	1057.6	1400.2
2	96.5	344.5	.0425	.0473	1058.9	1401.7
3	96.9	551.2	.0434	.0489	1613.6	2162.9

The strength of a soil is usually defined in terms of the stresses developed at the peak of the stress-strain curve. Figure 4.2.1 illustrates the Mohr failure envelope for the crushed silica samples.

The Mohr envelope is curved for confining stresses under 170 kPa and linear for stresses above that level. This is explained by the fact that granular soils are frictional in nature but with a deviation from purely frictional behaviour because of the effect of confining stresses upon interlocking of the sand particles.

Since the subsequent embankment and wall tests are carried out at high confining stresses, the Mohr envelope is fitted by a straight line for normal stresses between 0 and 2000 kPa. The actual Mohr envelope for this soil passes through the origin of the Mohr diagram; the soil will not stand as a cylinder if the confining pressure is zero.

Thus, the strength of the crushed silica sample is expressed by the Mohr-Coulomb failure law:

$$\tau = c + \sigma \tan \phi$$

where:

c = cohesion intercept (kPa)

ϕ = friction angle (degrees)

τ = shear stress (kPa)

σ = normal stress (kPa)

Figure 4.2.1 gives us an angle of internal friction ϕ of 34.9°.

An alternate way to plot the results of a series of triaxial strength tests is the use of the s'-t' diagram or the effective stress path method. Table 7 gives the values of s' and t' corresponding to the peak points of the stress strain curves in terms of principal effective stresses.

TABLE 7

Summary of s'-t' values for sand

test#	confining pressure σ_3 (kPa)	maximum normal stress σ_1 (kPa)	$\frac{\sigma_1 + \sigma_3}{2}$ (kPa) s'	$\frac{\sigma_1 - \sigma_3}{2}$ (kPa) t'
11	34.5	194.5	114.3	79.8
4	172.2	771.1	471.7	299.5
1	344.5	1400.2	872.4	527.9
2	344.5	1401.7	873.1	528.6
3	551.2	2162.9	1357.1	805.9

The curve drawn through these points is called the Kf-line. The Kf-line may be fitted by a straight line over the stress range of interest. The straight line fit shown on figure 4.2.2 is inclined at an angle α = 29.8° and intercepts the vertical axis at: a = 27 kPa. The simple relationship that exists between α and ϕ is defined by:

$$\sin \phi = \tan \alpha$$

Therefore, the s'-t' diagram gives an internal angle of friction of 35.0°.

Since it is less subjective to fit a line through a series of data points, than to attempt to pass a line tangent to many circles, the apparent angle of friction obtained from the s'-t' diagram of 35.0° for the crushed silica sand was selected for the subsequent research program.

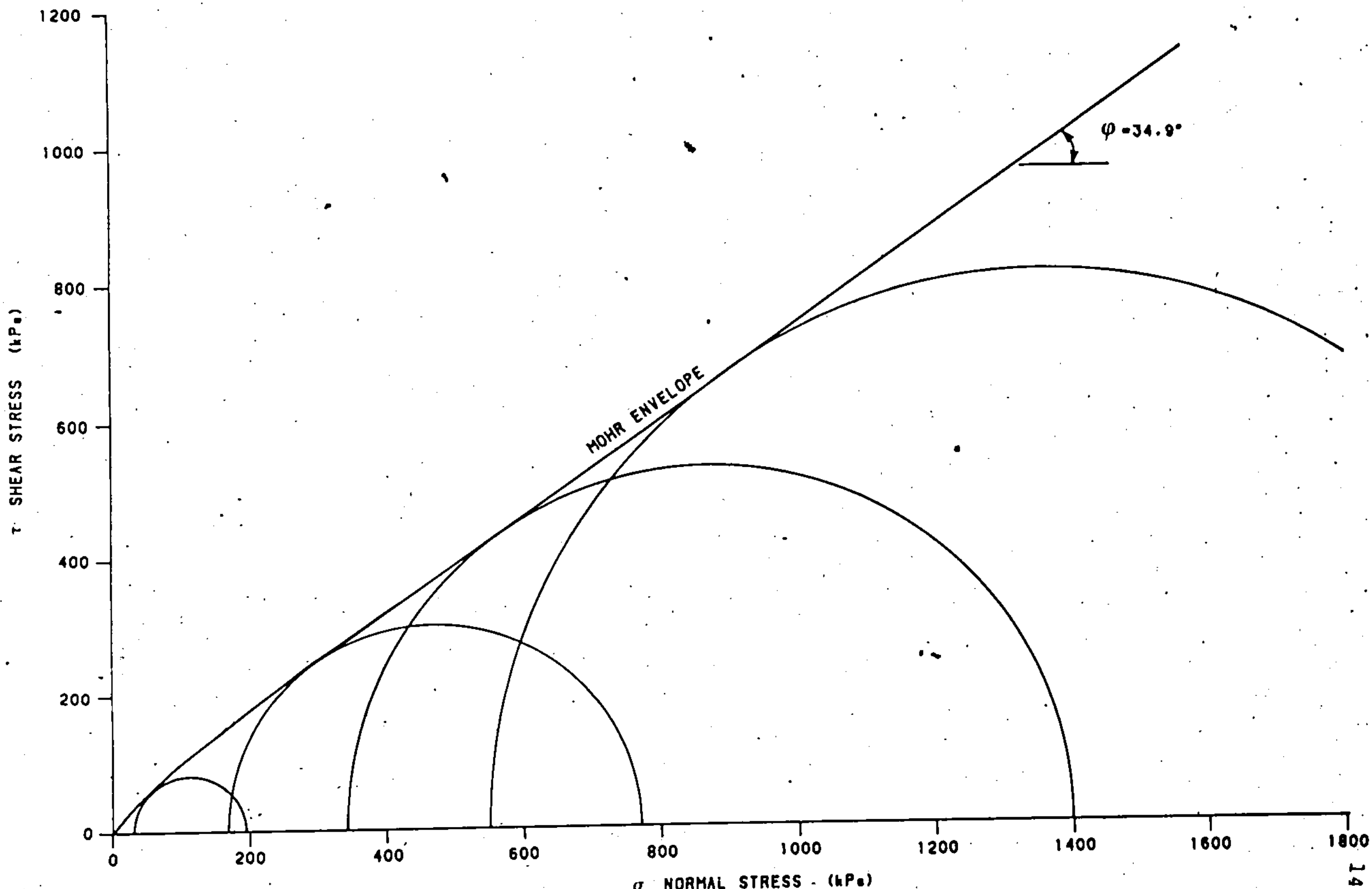

FIG. 4.2.1- MOHR FAILURE ENVELOPE FOR CRUSHED SILICA SAND

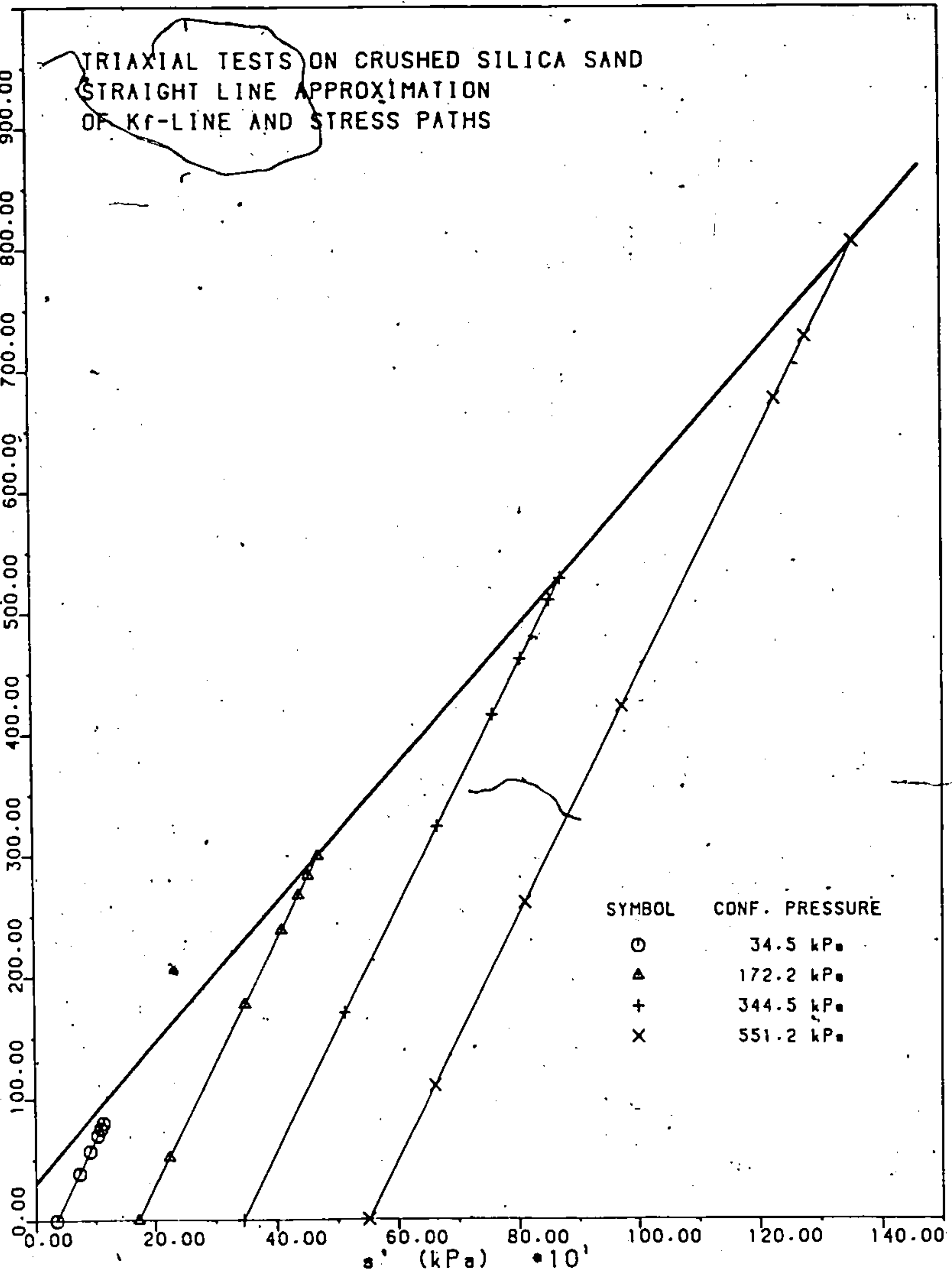

FIG. 4.2.2- s'-t' DIAGRAM AND EFFECTIVE STRESS PATHS FOR CRUSHED SILICA SAND

4.2.2 Triaxial tests on reinforced sand samples

A second series of triaxial tests was performed on the crushed silica sand, this time with layers of reinforcing wire mesh interspaced throughout the sample.

The size and geometry of the wire mesh was modelled on the reinforced wall tests discussed in subsequent sections.

Figure 4.2.3 presents an elevation view of the two configurations selected for triaxial testing and compares them to a typical reinforced wall test set-up. Figure 4.2.4 shows a plan view of a test sample.

The wire mesh utilized is an electrically welded fabric made from galvanized wire with a 16 gauge diameter (1.6 mm or 1/16 in.) and a crossbar spacing of 1x1 inch (25.4 mm x 25.4 mm).

To prevent piercing the sample membrane, a minimum 50 mm band was left unreinforced surrounding the mesh.

The modelling was performed by comparing percentages of steel to sand in surface area and volume for triaxial samples and reinforced wall tests.

Table 8 shows that the percentage of steel used in the triaxial tests was slightly greater than the typical amount of steel in the sandbox, but for practical and availability reasons, it was decided to pursue the testing with a 16 gauge diameter mesh.

A summary of the testing program is supplied in table 9. and figure 4.2.5 illustrates the Mohr failure envelope for the reinforced sample.

TABLE 8

Modelling percentages in triaxial tests

test	% steel to total surface area	% steel to total volume
triaxial tests	3.9	0.18
reinforced wall tests	2.5	0.075

TABLE 9

Summary of triaxial tests on reinforced sand

test#	I_d (%)	confining pressure σ_3 (kPa)	initial area (m²)	corrected area @ max.σ (m²)	maximum deviator stress σ (kPa)	axial stress σ_1 (kPa)
test set-up no. 2						
10	96.5	34.5	.0439	.0512	525.2	559.7
7	95.4	172.2	.0430	.0489	1089.0	1261.2
8	97.8	344.5	.0441	.0492	1736.1	2080.6
9	94.7	551.2	.0438	.0503	2417.4	2968.6
test set-up no. 1						
6	95.4	172.2	.0430	.0452	665.4	837.6

Using a straight line relationship for the confining stresses of interest and the Mohr-Coulomb failure law we obtain an apparent angle of friction for the composite sample of 39.9°. An apparent cohesion intercept of c= 90 kPa is recorded from figure 4.2.5. The positive intercept is due to the cohesive nature of the composite reinforced soil system.

The s'-t' values for the tests are listed in table 10 and the Kf-line is presented in figure 4.2.6 .

TABLE 10

Summary of s'-t' values for reinforced sand

test#	confining pressure σ_3 (kPa)	maximum normal stress σ_1 (kPa)	$\frac{\sigma_1 + \sigma_3}{2}$ (kPa) s'	$\frac{\sigma_1 - \sigma_3}{2}$ (kPa) t'
10	34.5	559.7	297.1	262.6
7	172.2	1261.2	716.7	544.5
8	344.5	2080.6	1212.6	868.1
9	551.2	2968.6	1759.9	1208.7

The straight line fit is inclined at an angle $\alpha = 32.4°$ and intercepts the vertical at: a= 90 kPa.

Therefore the s'-t' diagram gives an apparent internal angle of friction for the composite samples of 39.5° according to the Mohr-Coulomb law. This represents an increase of 4.5° from the natural unreinforced samples. Table 11 summarizes the friction angle results.

Figure 4.2.7 shows photographically the test samples before and after being loaded triaxially and figure 4.2.8 illustrates a wire mesh reinforcing layer after being tested. The deformation of the mesh is quite evident and

TABLE 11

Summary of apparent friction angle results

type of test	apparent angle of friction by Mohr failure envelope (degrees)	apparent angle of friction by s'-t' diagram (degrees)
crushed silica sand	34.9	35.0
wire mesh reinforced sand	39.9	39.5

substantiates the theory that the load transfer is accomplished by the bearing resistance action of the crossbars which then transfer the load to the longitudinal bars, therefore placing them in tension.

The top layer of reinforcement in test #9, (fig. 4.2.8), with a confining pressure of 551.2 kPa was the only mesh which suffered broken wires (in three locations). The wire mesh was tested to failure in a tensile loading machine and the failure load was reached at 1000 N.

Test no. 6, with 172.2 kPa confining pressure was tested using set-up no. 1. This configuration left a zone of unreinforced sand at the base of the test sample allowing the reinforced section to behave as a block and to penetrate into the unreinforced zone. Since this loading behaviour did not permit the maximization of the peak stresses in the sample, set-up no. 1 was abandoned in favor of set-up no. 2 (fig. 4.2.3).

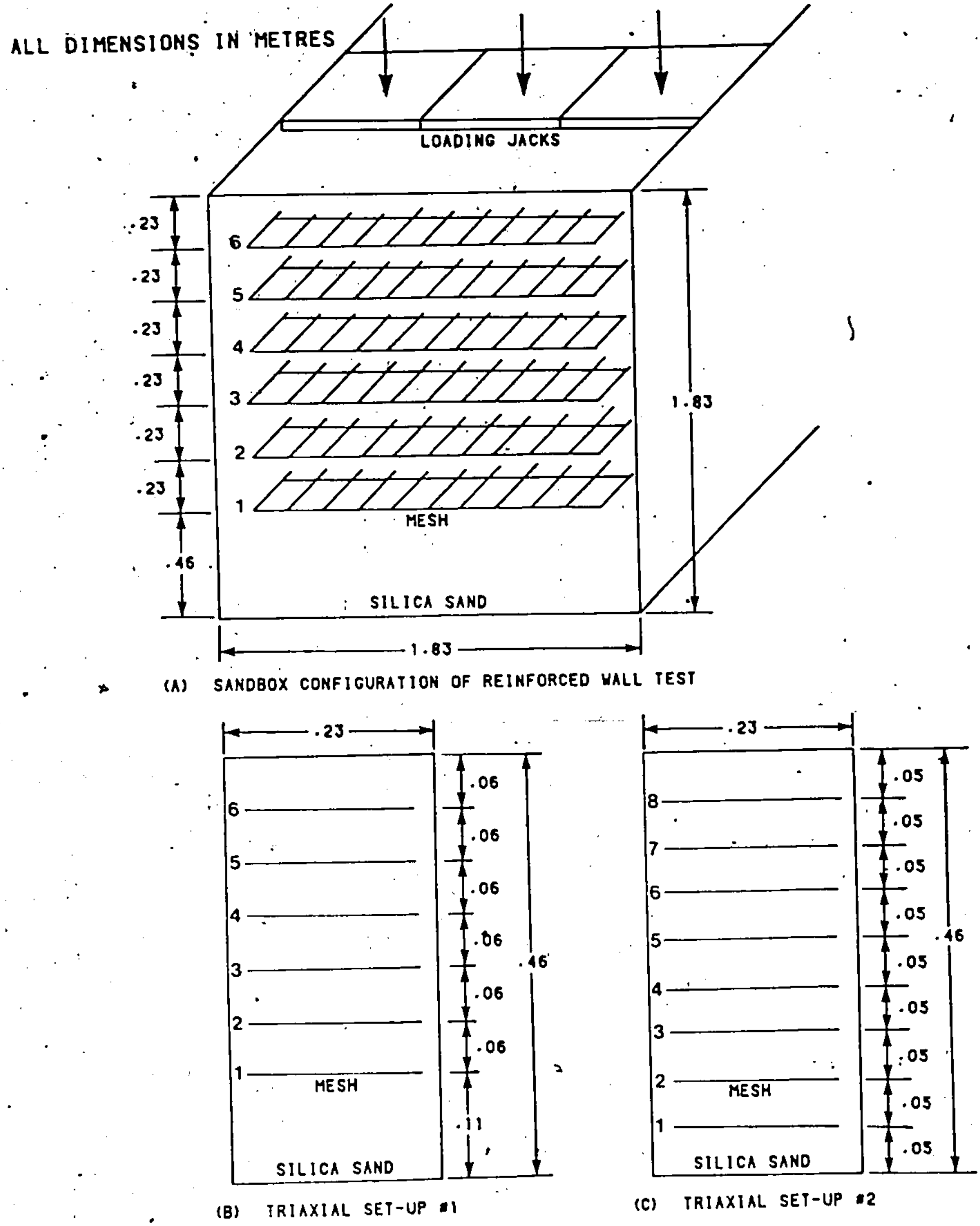

FIG. 4.2.3- ELEVATION VIEW OF A REINFORCED WALL TEST AND TRIAXIAL SET-UPS

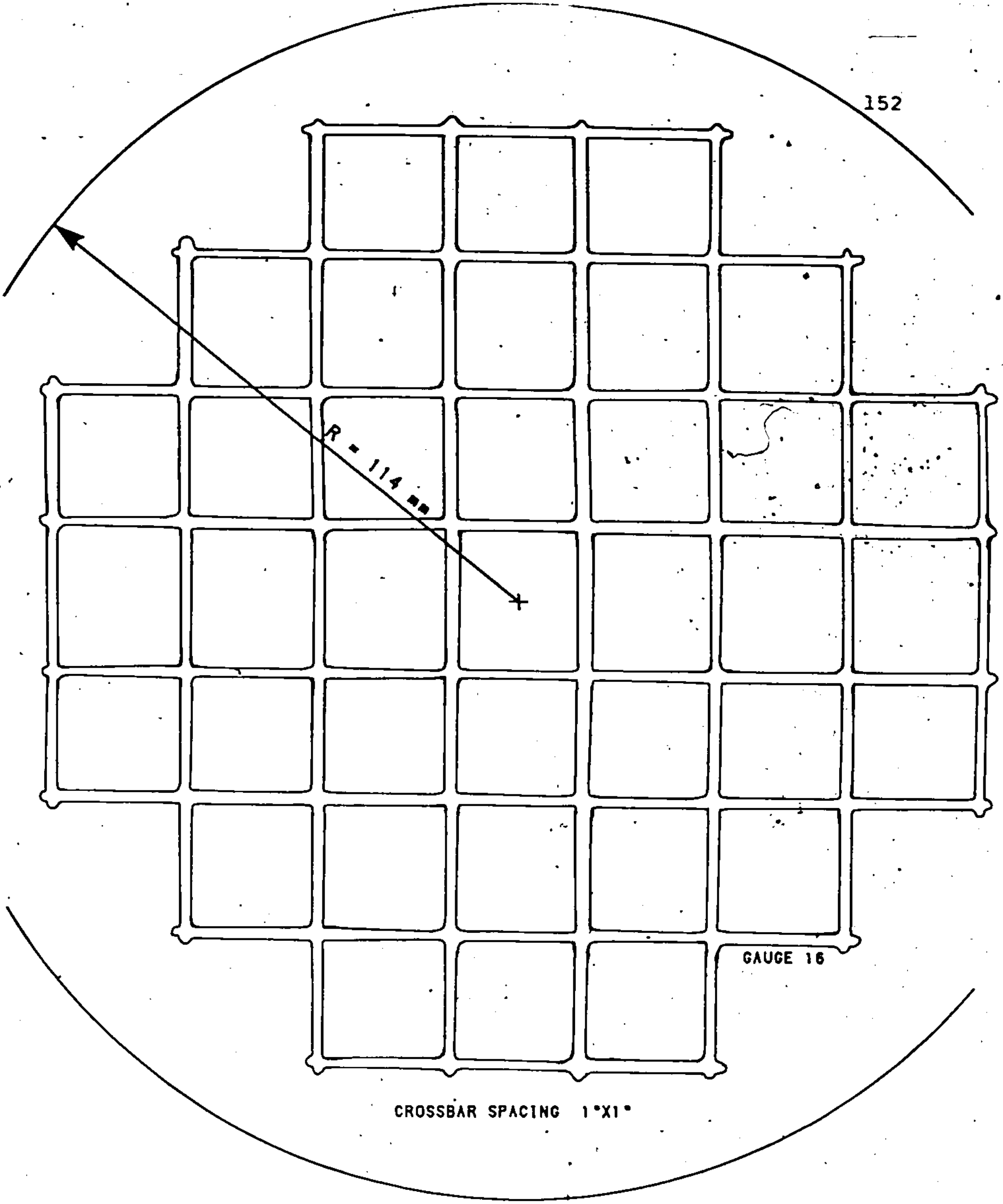

FIG. 4.2.4- PLAN VIEW OF REINFORCED TRIAXIAL TEST SAMPLE (FULL SCALE)

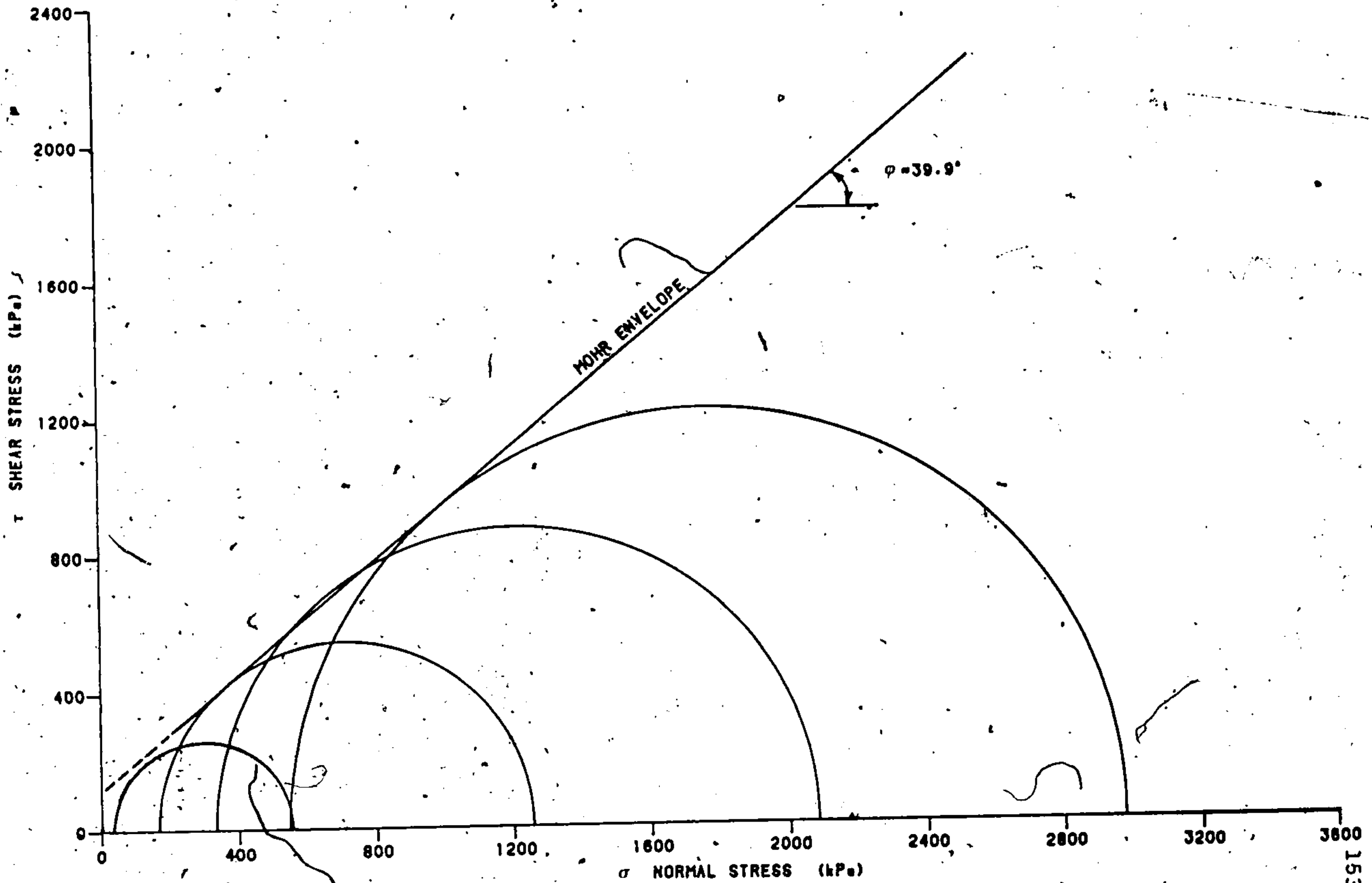

FIG. 4.2.5 MOHR FAILURE ENVELOPE OF WIRE MESH REINFORCED SAMPLES

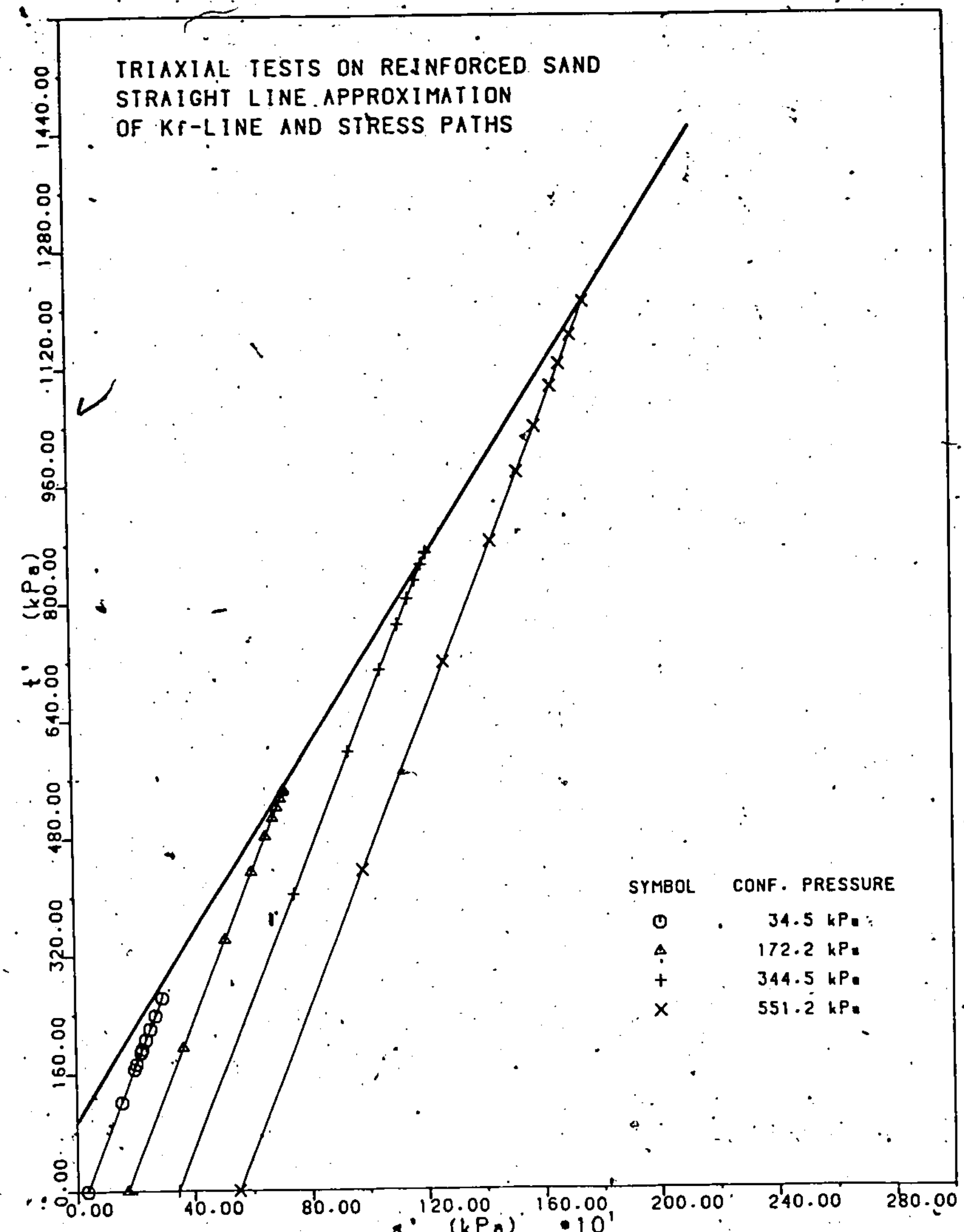

FIG. 4.2.6- s'-t' DIAGRAM AND EFFECTIVE STRESS PATHS FOR MESH REINFORCED SAMPLES

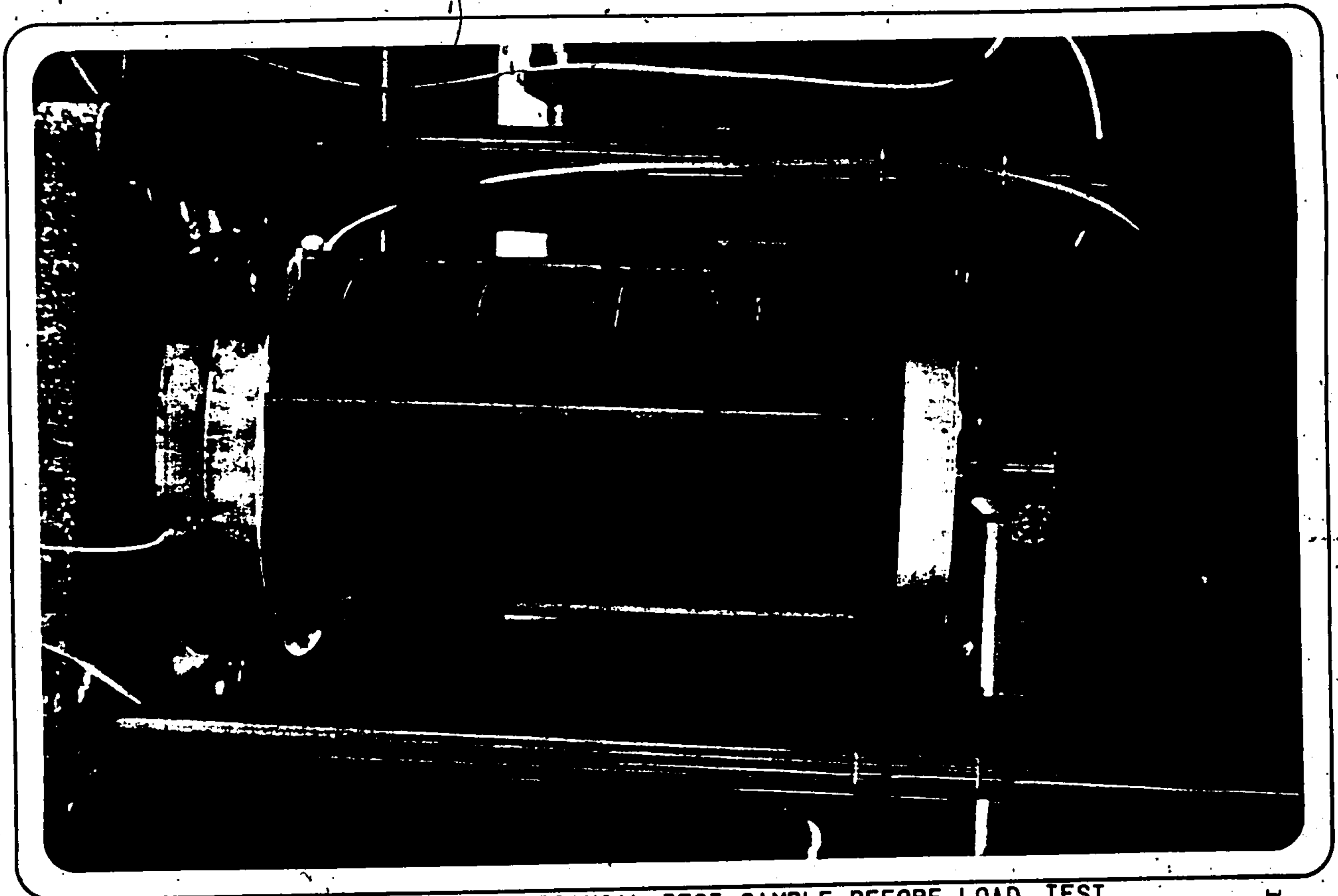

FIG. 4.2.7 (a) - TRIAXIAL TEST SAMPLE BEFORE LOAD TEST

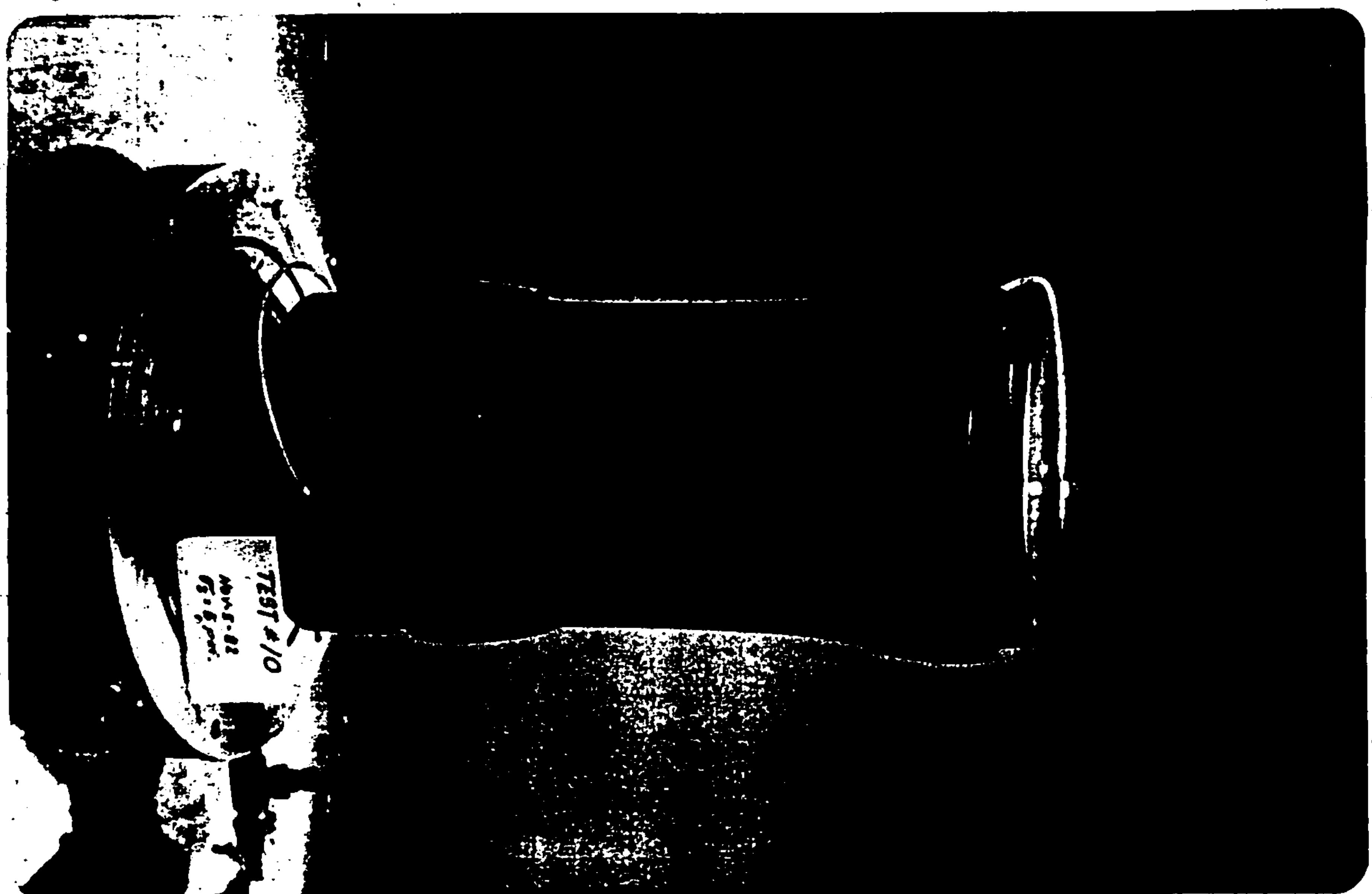

FIG. 4:2.7 (b)- TRIAXIAL TEST SAMPLE AFTER LOAD TEST

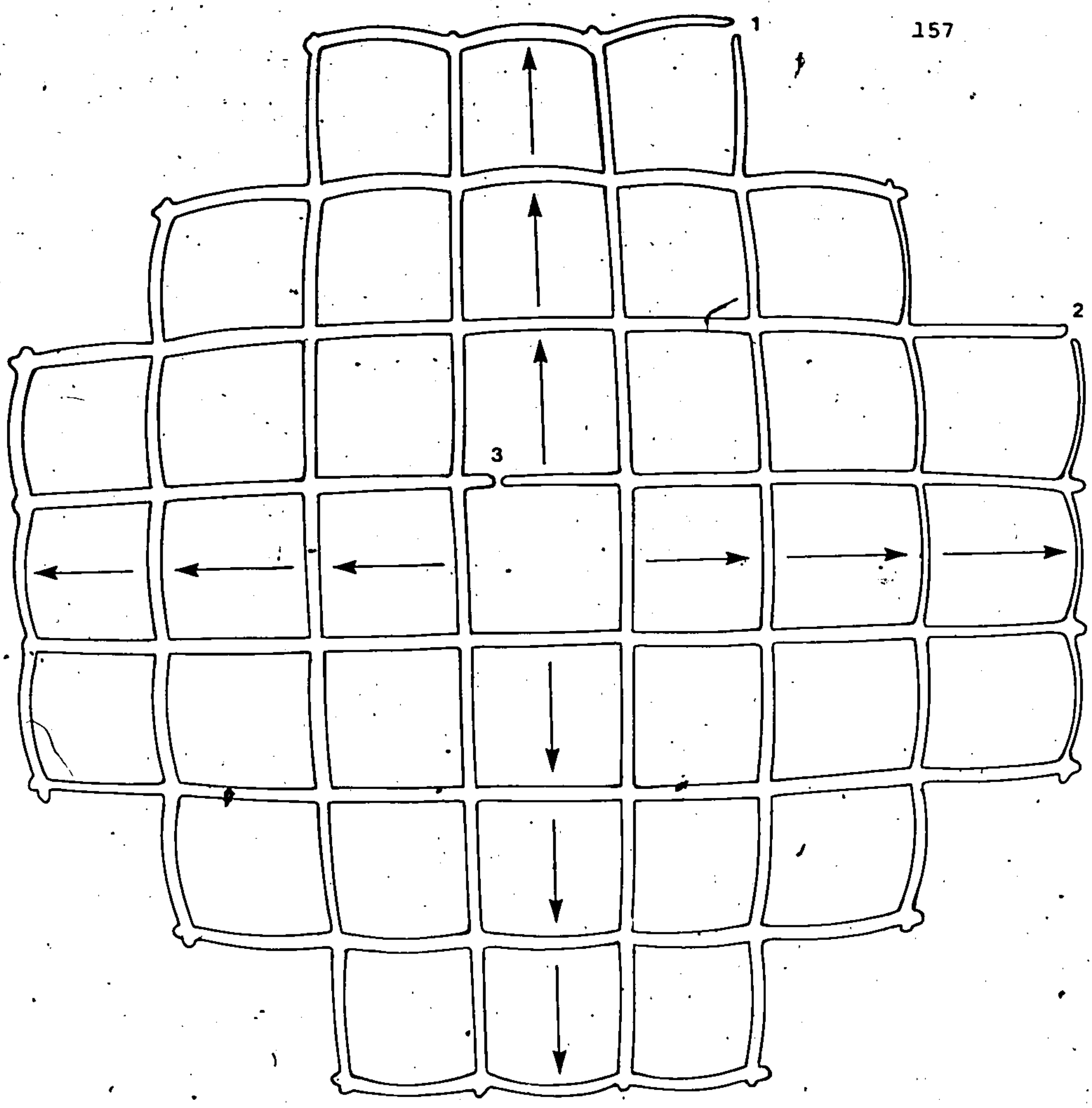

FIG. 4.2.8- PLAN VIEW OF REINFORCING MESH AFTER
TRIAXIAL TEST (FULL SCALE), σ_3 =551.2 kPa

4.2.3 Summary of triaxial tests

The surface area of each test sample during triaxial loading was corrected for axial strain, volumetric strain and membrane resistance.

The membrane correction, which was due to the restraint imposed on the sample by the rubber membrane enclosing it,was in the order of 1 to 2 kPa for both reinforced and non-reinforced samples.

This correction was obtained using the method described by Bishop and Henkel (1962) and is clearly very small when compared to the deviator stresses and can be neglected in this particular case.

Figures 4.2.9 to 4.2.12 compare the behaviour of the reinforced samples to the unreinforced samples for each specific confining pressure.Table 12 highlights the findings.

TABLE 12

Comparison of reinf. and natural samples

confining pressure (kPa) σ_3	axial strain ratio @ peak stresses (reinf/sand)	volumetric strain ratio @ peak stresses of sand samples (reinf/sand)	$(\sigma_1 - \sigma_3)$ ratio @ peak stresses (reinf/sand)
34.5	1.96	0.77	3.28
172.2	1.41	0.68	1.81
344.5	1.11	0.55	1.64
551.2	1.30	0.13	1.50

As can be seen from table 12 and figures 4.2.9 to 4.2.12, the reinforcing mesh has a profound effect on the peak deviator stress applied to the sample and on the volumetric strain. In other words, the load capacity of the structure is increased significantly (1.5 to 3.3 times greater load capacity) and the volume change due to the load is reduced greatly (1.3 to 7.7 times less volume change).

What is apparent also is that these increases in structural strength are a function of the confining pressure.The deviator stress increase is not as great for higher confining pressures but the decrease in volumetric change is proportional to the confining pressure.

The subsequent reinforced embankments and walls were tested under plain strain conditions in order to eliminate friction effects from the side walls. Brinch Hansen (1970) recommended a 10% increase in the angle of internal friction obtained from triaxial tests for plain strain conditions.

$$\phi_{\text{plain strain}} = 1.1\ \phi_{\text{triaxial}}$$

This would indicate that the direct shear test yields a more accurate analysis of the friction angle. However, Rahman (1980) investigated the variation in internal angle of friction for the crushed silica sand used in this analysis, using both the triaxial and the direct shear method, and found no significant difference between the two methods.

Therefore, a friction angle of 35° for the crushed silica sand and 39° for the reinforced backfill is selected as a lower limit for subsequent research into reinforced embankments and reinforced walls. This value is obviously only applicable to backfill material similar to the one tested (crushed silica sand) and to a wire mesh reinforcement.

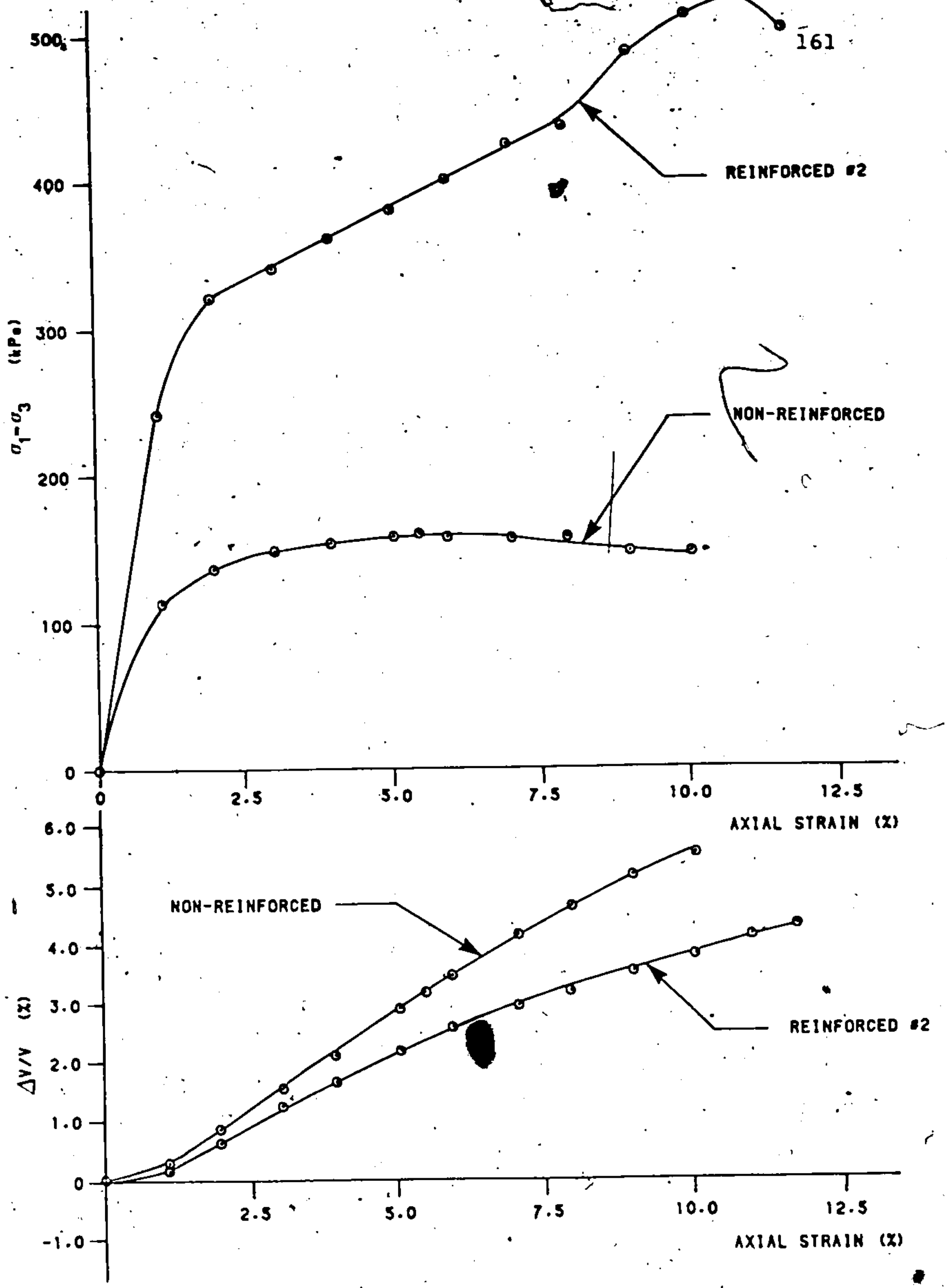

FIG. 4.2.8- COMPARISON OF DEVIATOR STRESS AND CHANGE IN VOLUME FOR REINFORCED AND NON-REINFORCED SAMPLES, σ_3 = 34.5 kPa

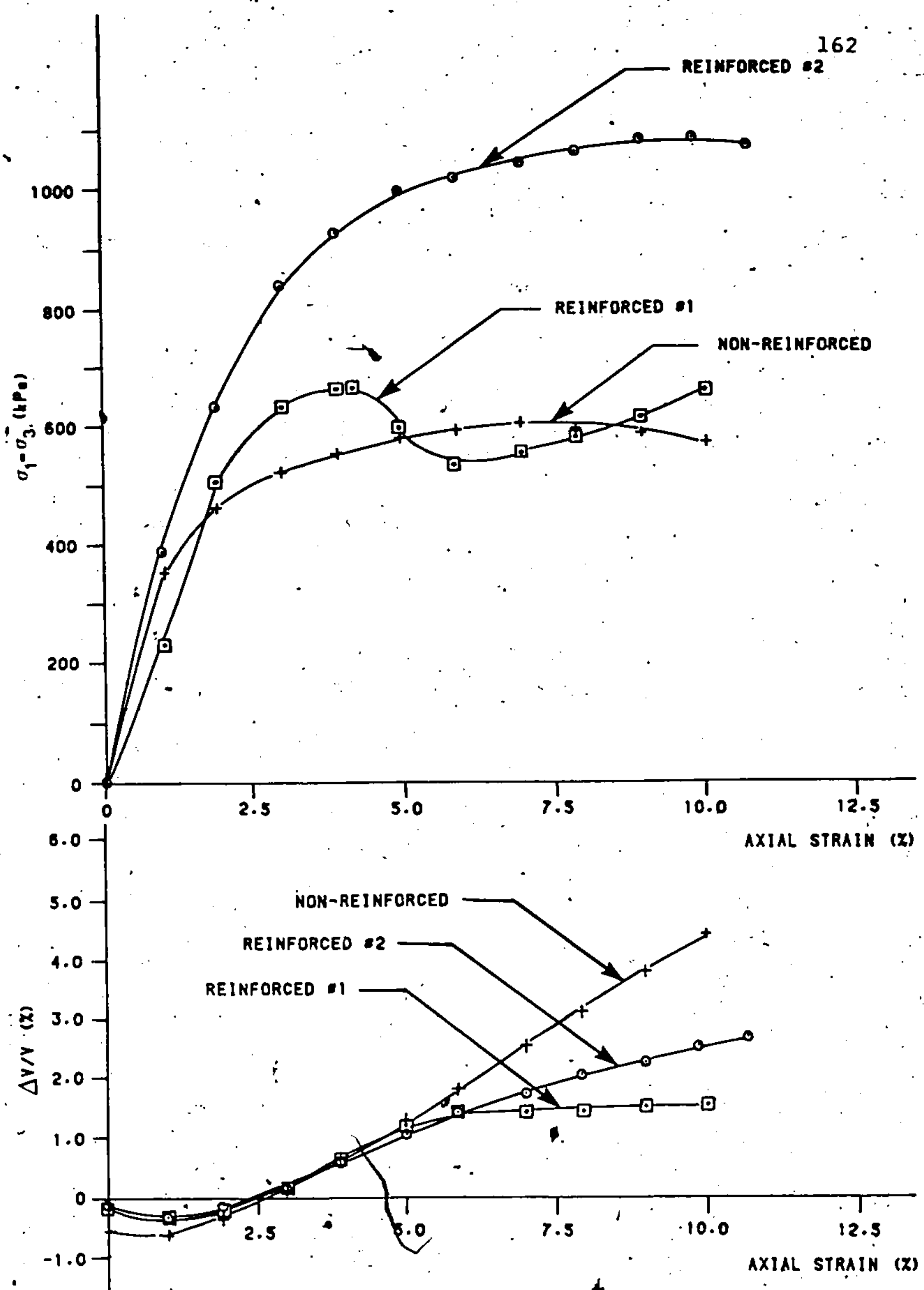

FIG. 4.2.10- COMPARISON OF DEVIATOR STRESS AND CHANGE IN VOLUME FOR REINFORCED AND NON-REINFORCED SAMPLES, σ_3 = 172.2 kPa

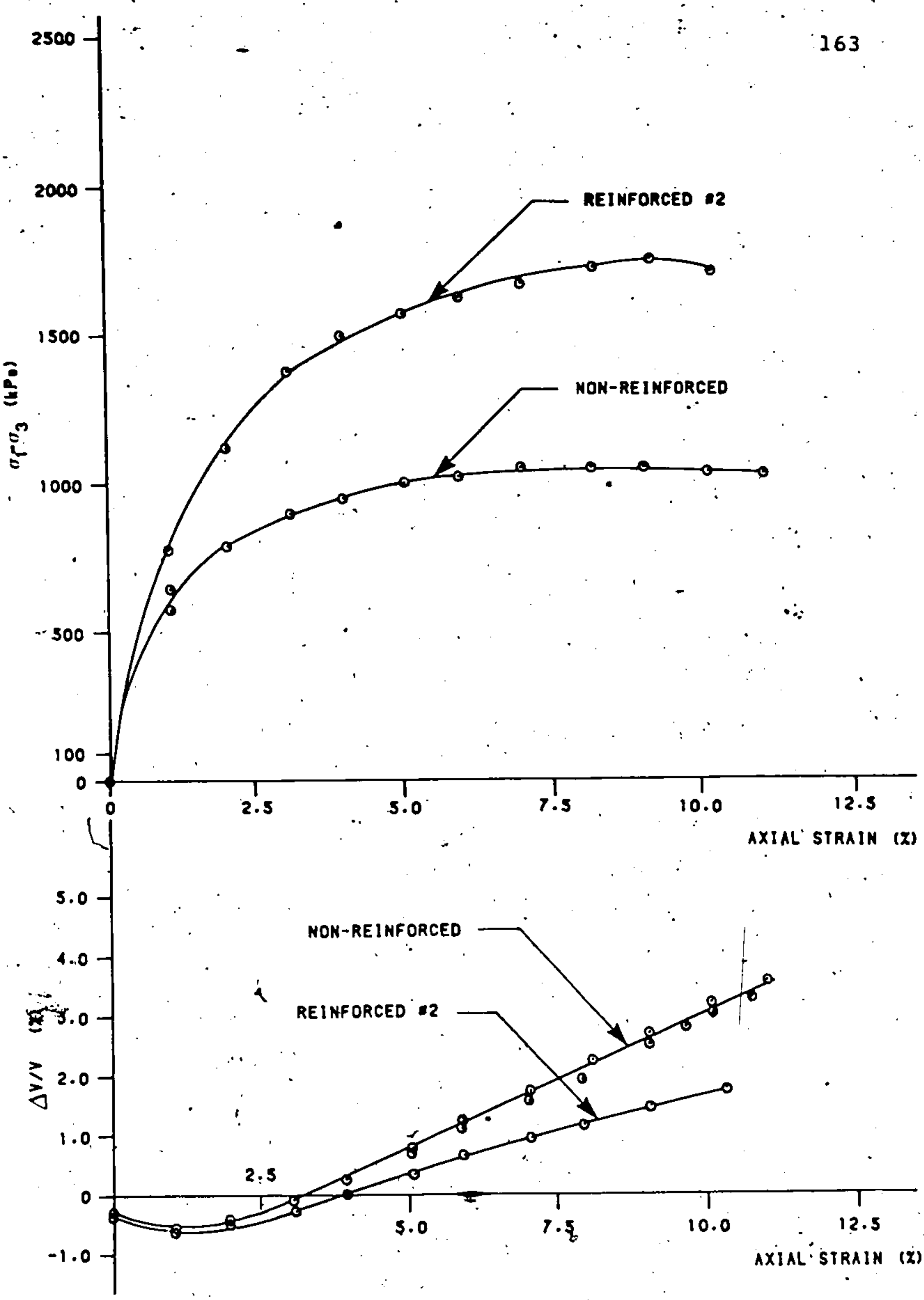

FIG. 4.2.11- COMPARISON OF DEVIATOR STRESS AND CHANGE IN VOLUME FOR REINFORCED AND NON-REINFORCED SAMPLES, σ_3 =344.5 kPa

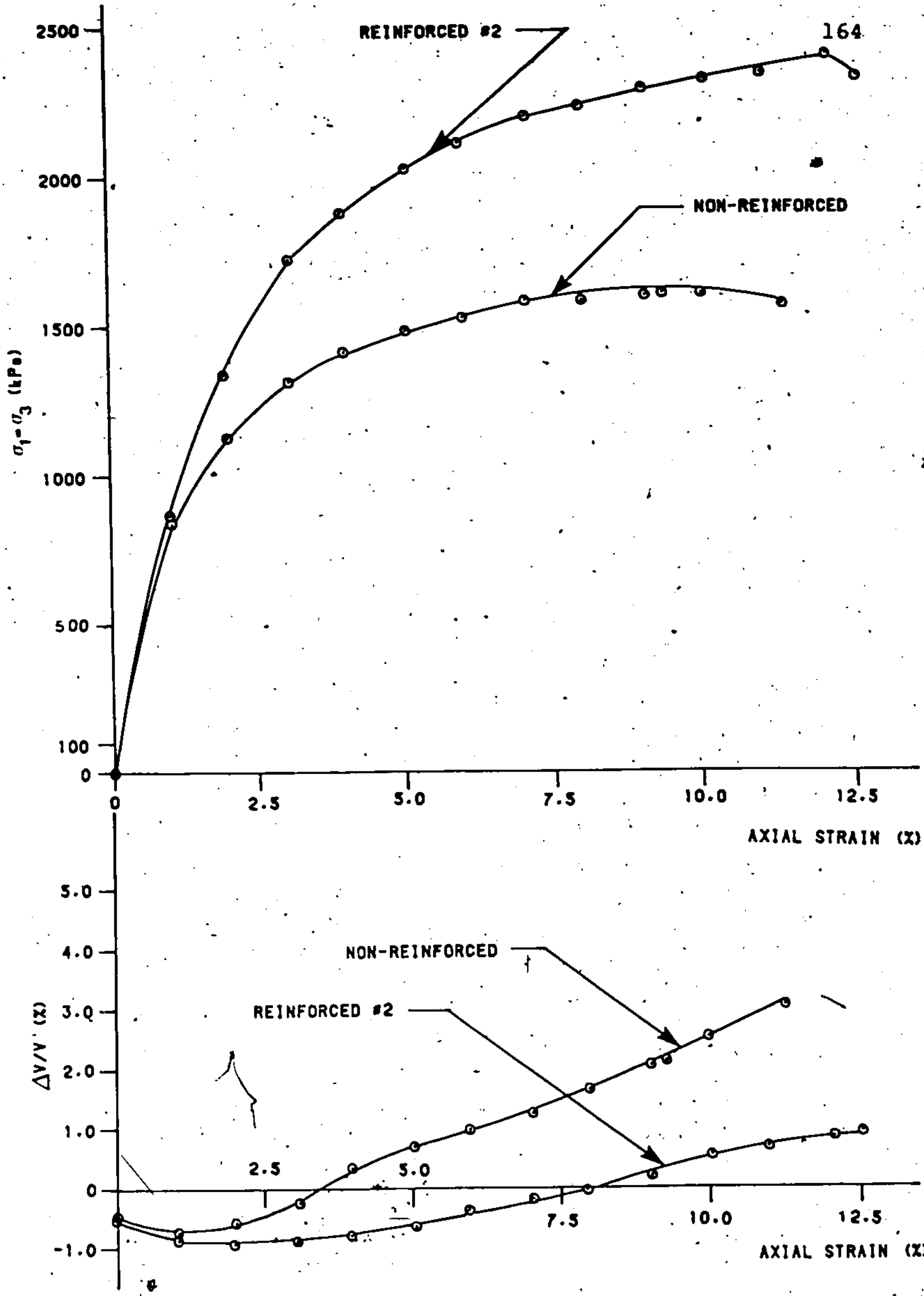

FIG. 4.2.12- COMPARISON OF DEVIATOR STRESS AND CHANGE IN VOLUME FOR REINFORCED AND NON-REINFORCED SAMPLES, σ_3 = 551.2 kPa

4.3 BEARING CAPACITY OF FOOTINGS ON REINFORCED EMBANKMENTS

Snaith, Bell, and Dubois (1979) stated that in order to keep construction costs of an embankment to a minimum it would be beneficial to be able to do the following with the aid of soil inclusions:

1. use low-grade fill from adjacent cuttings to form the embankment.
2. construct the embankment on poor foundation soils without the use of expensive measures such as piles.
3. steepen the embankment side slopes to minimize land acquisition.

It is with the latter point in mind that three large scale reinforced embankments were constructed and loaded to failure in order to investigate the change in bearing capacity provided by the inclusion of layers of steel mesh reinforcement.

As described by Snaith et al. (1979), the classical mode of failure due to surcharge of an embankment side slope is due to a rotational shear and an obvious way to combat this is to lay reinforcing elements across the potential surface of failure to act in a similar way as shear reinforcing bars in a concrete structure.

The reinforcing elements must be of sufficient strength to resist rupture, but must also be anchored to the soil adjacent to the zone of failure.

4.3.1 Reinforced embankment with natural slope

The slope of the first embankment was constructed by stopping the sand spreader at the predetermined position of the crest of the slope and letting the sand tumble down the slope. The geometry of the embankment is illustrated in figures 4.3.1 to 4.3.3.

This method permitted the observation of the angle of repose created by the introduction of the reinforcing members. The slope angle was measured to be 34° after completion of the embankment.

Whenever a granular material is dumped, it generally finds itself in a loose state. For the loose state, ϕ essentially equals ϕ_{cv} (critical friction angle). Thus the angle of repose for dumped sand or gravel is about equal to the angle of internal friction for the loose state, ϕ_{cv}.

In 1974, Hasnain determined that the internal angle of friction of the backfill sand utilized in the embankment tests was between 30 and 35 degrees for a loose state. Since the actual friction angle may deviate by ±3 degrees or more from the value given by the triaxial tests, it can be stated that the reinforcing mesh did not have a noticeable effect on the angle of repose of the slope.

The four reinforcing layers were steel wire mesh (as described in previous sections) with a 12x6 crossbar spacing (0.3m x 0.15m), a length of 2.13 metres and a width of 1.52 metres.

A schematic diagram of a mesh layer is presented in figure 4.3.1 along with the location of the strain gauges which were calibrated to a value of 11.34 N/reading unit.

A strip footing load was applied at the crest of the slope with the strain in the mesh, the settlement of the footing jacks, and the load applied being the parameters measured during the test.

Figure 4.3.4 illustrates the axial tensile load generated in the reinforcing bars of the mesh by the applied stress.

Subsequent probing of the slope indicated some changes in density of the soil in the vicinity of the mesh layers after failure was attained. This shows that some of the failure planes were situated along or near the reinforcing layers.

Figure 4.3.5 illustrates the local planes of weakness obtained by probing the embankment along with the tensile or compressive loads registered in the mesh layers at maximum bearing pressure. Utilizing these two indicators, a probable failure surface through the embankment is drawn.

The actual failure load was determined to occur at 61 kN per footing or more accurately; the bearing stress at failure was 163 kPa. Failure was determined to be when a loading stress could not be sustained without producing continuous settlement of the footings.

The presence of the rigid base was deemed not to have influenced the bearing capacity of the embankment since the thickness of the soil layer between the footing and the rigid base was thicker than twice the width of the footing (2B). Also, the presence of the dummy footings on each side of the central jack nullified the wall friction effects on the central footing where the measurements were taken and created a plain strain condition.

A slope analysis of the same embankment without reinforcing layers, using the Bishop slip circle method, yields a maximum failure stress of 150 kPa. Therefore, the induced bearing capacity improvement is in the order of 10%.

This minimal improvement in bearing capacity can be explained by the method of construction of the embankment which created an area of loose sand deposit in the slope itself, while the rest of the embankment had a density index of 94.2%. The looseness of the sand did not permit permit the anchorage of the reinforcing layers and the full use of the reinforcing system.

In fact it can be said that the mesh was relatively ineffectual and was an integral part of the outward sliding mass.

This test demonstrated the crucial importance of anchoring the reinforcing layers of mesh in the embankment.

To properly study the reinforced embankment problem, further tests were performed and are discussed in the following sections. These tests did not allow the presence of loose sand deposits and insured the anchorage of the reinforcing mesh layers.

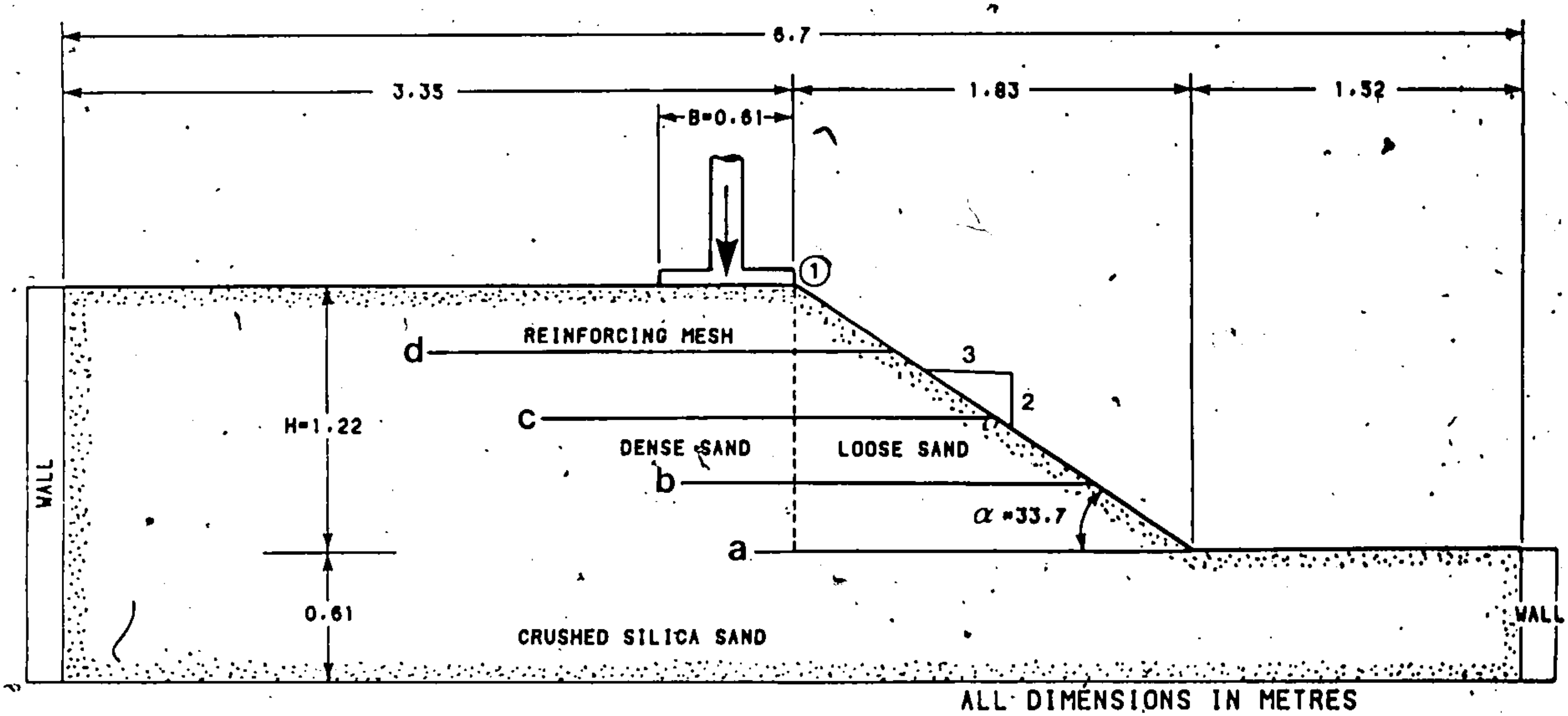

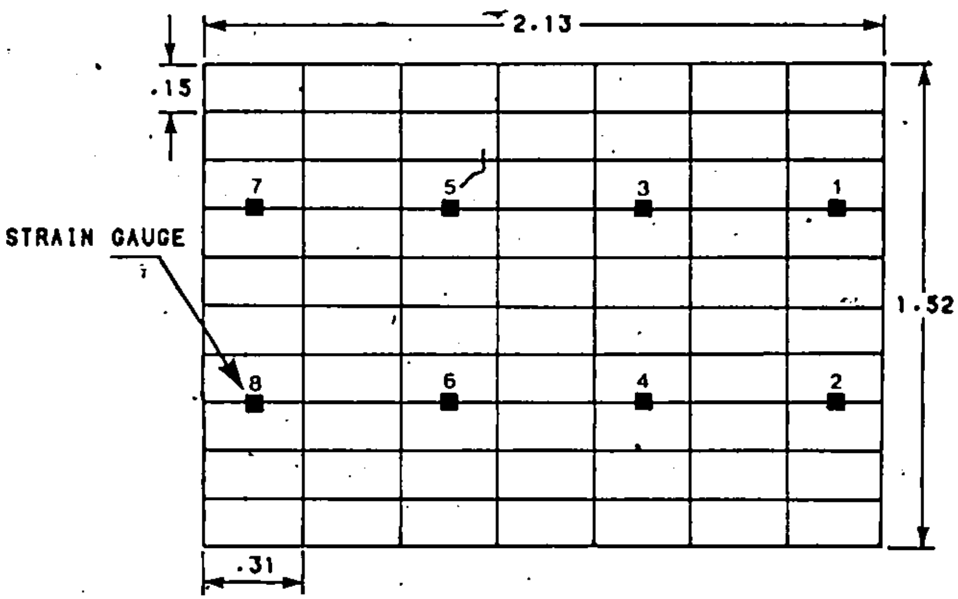

FIG. 4.3.1- PROFILE VIEW OF REINFORCED EMBANKMENT (SET-UP #1) WITH STRAIN GAUGE LOCATIONS ON REINFORCING MESH

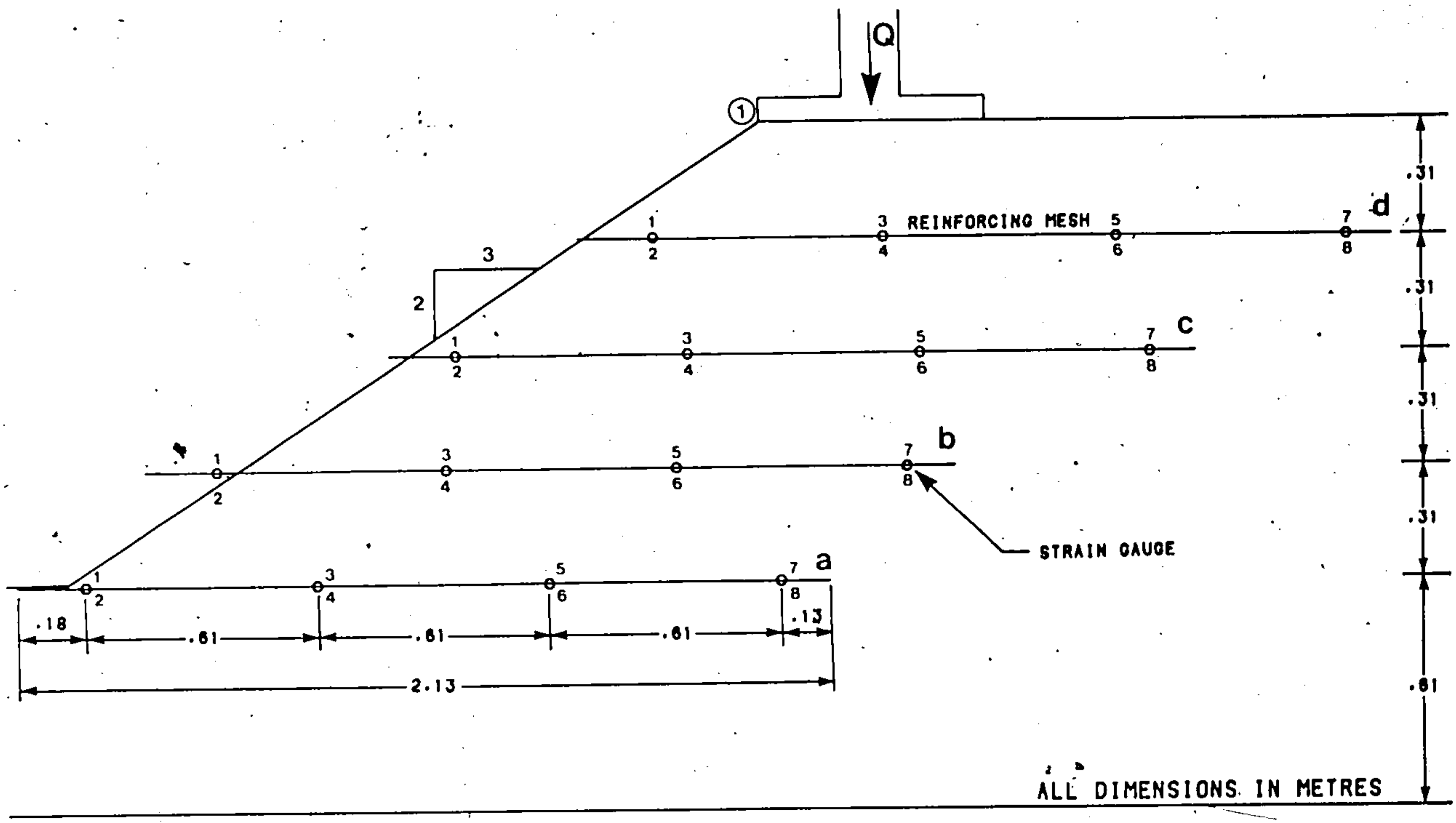

FIG. 4.3.2- PROFILE VIEW OF REINFORCED EMBANKMENT (SET-UP #1) WITH STRAIN GAUGE POSITIONS

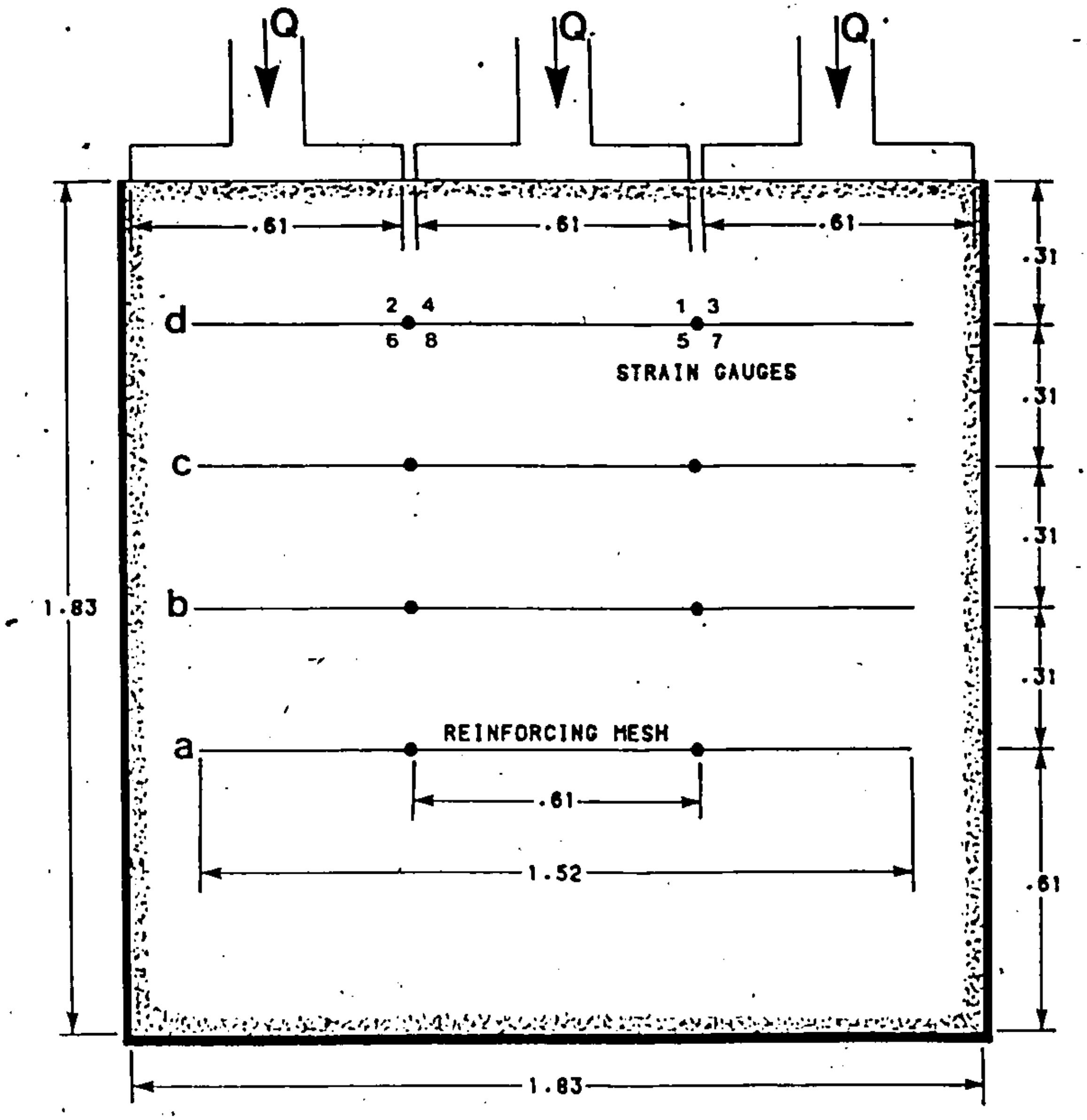

ALL DIMENSIONS IN METRES

FIG. 4.3.3- FRONT VIEW OF REINFORCED EMBANKMENT

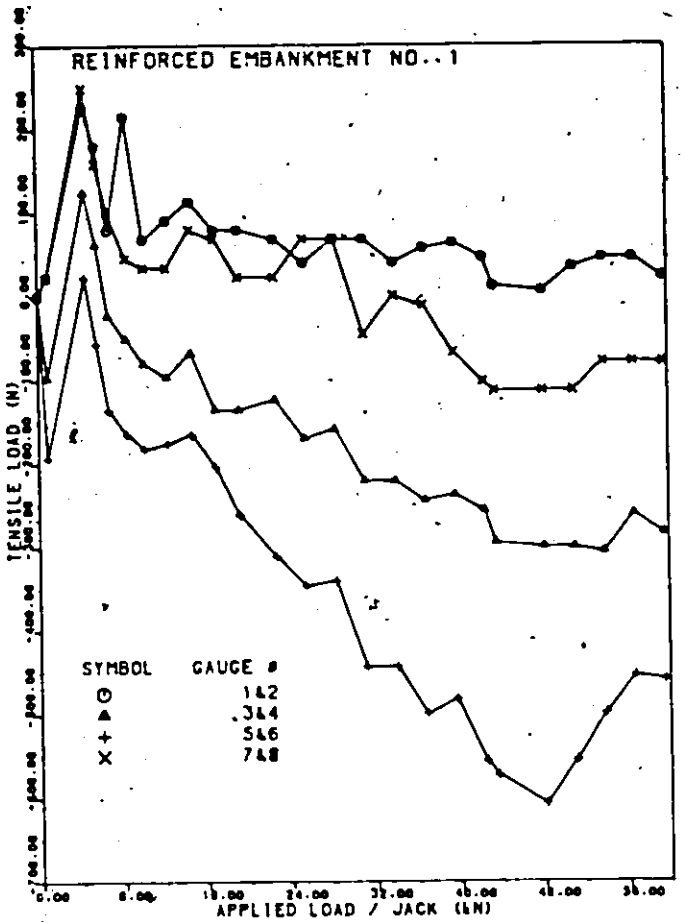

FIG. 4.3.4a- TENSILE LOAD ON REINFORCING MESH "A" FOR EMBANKMENT #1

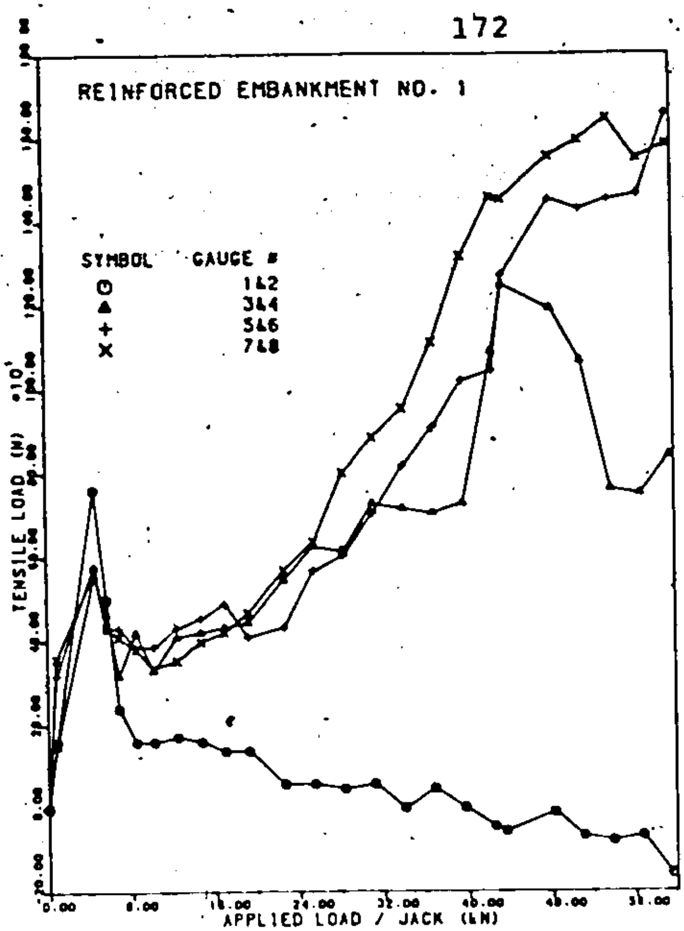

FIG. 4.3.4b- TENSILE LOAD ON REINFORCING MESH "B" FOR EMBANKMENT #1

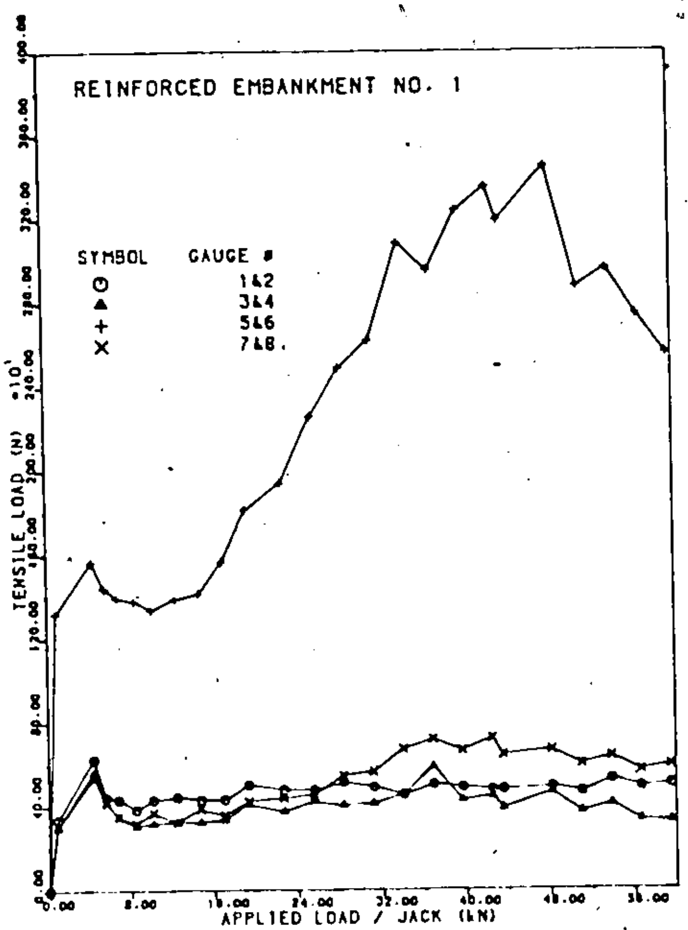

FIG. 4.3.4c- TENSILE LOAD ON REINFORCING MESH "C" FOR EMBANKMENT #1

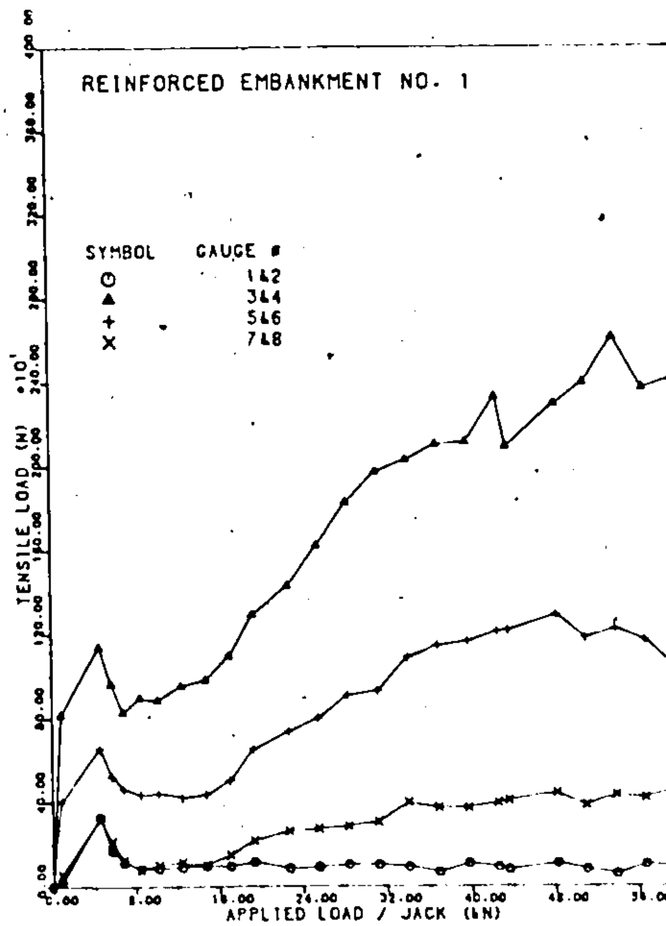

FIG. 4.3.4d- TENSILE LOAD ON REINFORCING MESH "D" FOR EMBANKMENT #1

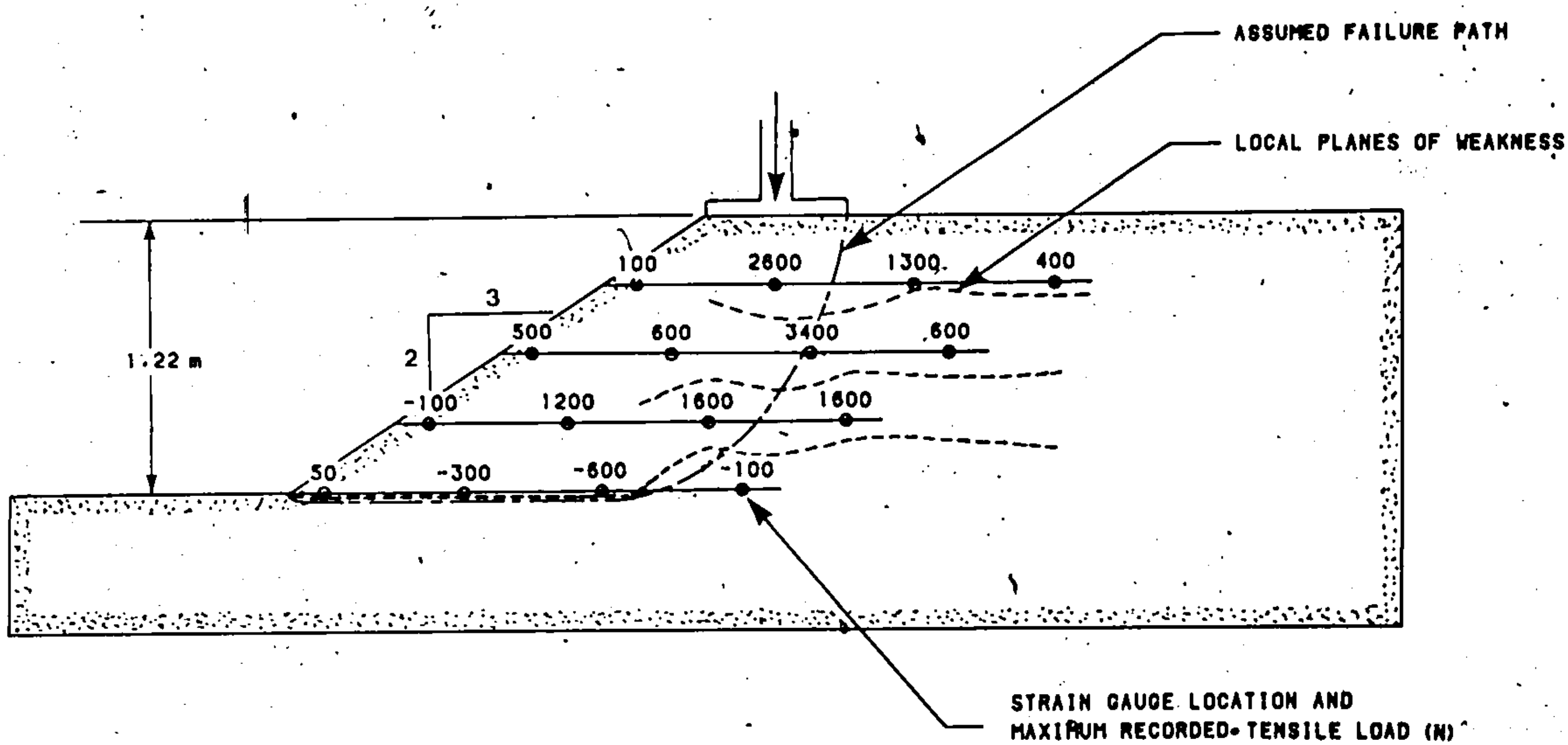

FIG. 4.3.5- ASSUMED FAILURE SURFACE OF REINFORCED EMBANKMENT #1

4.3.2 Reinforced embankments with 2:1 slopes

Deschênes (1978) investigated a series of large scale model embankments in order to determine the bearing capacity of footings beneath or adjacent to a slope of crushed silica sand (simulating granular material). The present study utilized the same facilities and equipment that were used for those earlier tests. The results of the embankment tests were expressed in terms of bearing capacity factors ($N_{\gamma q}$).

With all other design parameters remaining constant, two reinforced embankments were constructed and tested to determine the effect of the reinforcing mesh on the bearing capacity of the footings placed at the crest of the embankments.

In 1957, Meyerhof suggested that the bearing capacity can be given by the bearing capacity factor ($N_{\gamma q}$). The bearing equation takes on the form:

$$q = 1/2 \ \rho \ g \ B \ N_{\gamma q}$$

where

q = ultimate footing stress

ρ = the density of the soil

g = the acceleration due to gravity

B = the footing width

Therefore, the bearing capacity factor $N_{\gamma q}$ can be determined from the above equation, since all other quantities are known.

Table 13 describes the characteristics of each embankment tested and figures 4.3.6 and 4.3.7 illustrate the geometry of the reinforced embankments.

TABLE 13

Summary of embankment tests

Vertical loading- 0.61 m footings- 2:1 embankment slope

test	footing location	unit wt. kg/m³	ultimate bearing pressure kPa	settlement @ 210 kPa (mm)	% inc. in bearing capacity	% decr. in settlement	bearing capacity factor $N_{\gamma q}$
1	crest	1607	210	32	-	-	44
R-2	crest	1615	251	16.5	20	48	52
R-3	crest	1625	538	12.3	156	62	111

test 1: unreinforced embankment - crushed silica sand
test R-2: reinf. embankment #2- crossbar spacing 6x12- Y=.3m
test R-3: reinf. embankment #3- crossbar spacing 6x6- Y=.15m

The load-settlement relationships are shown graphically in figure 4.3.8.

The method of determining the ultimate bearing capacity of footings is based on suggestions made by Vesic (1973). According to Vesic, the ultimate load is the point at which the slope of the load-settlement curve first reaches zero or a steady, minimum value.

The first reinforced embankment was strain gauged as indicated in figure 4.3.6 and the tensile loads measured in the mesh as the applied stress was increased are shown in figure 4.3.9.

These measurements, along with the local planes of weakness obtained by probing the embankments permitted the localization of probable failure surfaces in the reinforced embankments (see figures 4.3.10 and 4.3.11).

The location of the local planes of weakness was determined by pushing a 3 mm diameter probe vertically into the soil mass as indicated in section 3.2.1.

It is worthwhile to note that the mesh inclusions seemed to participate in the formation of shear surfaces, most notably at the base of the embankments.

Table 13 shows that the introduction of reinforcing mesh increases the ultimate bearing capacity of the footings on the embankments by as much as 156% and reduces the settlement of the footings by as much as 62%.

By introducing a relationship between the ultimate bearing capacity and the settlement versus the amount of reinforcing steel mesh in the embankment, we obtain the exponential curves presented in figure 4.3.12.

These curves illustrate the efficiency and attractiveness of utilizing reinforcing mesh in embankments as a means of increasing the bearing capacity of footings and decreasing settlement. In other words a typical road embankment with reinforcing mesh can be constructed at a steeper side slope angle, therefore minimizing land requirements.

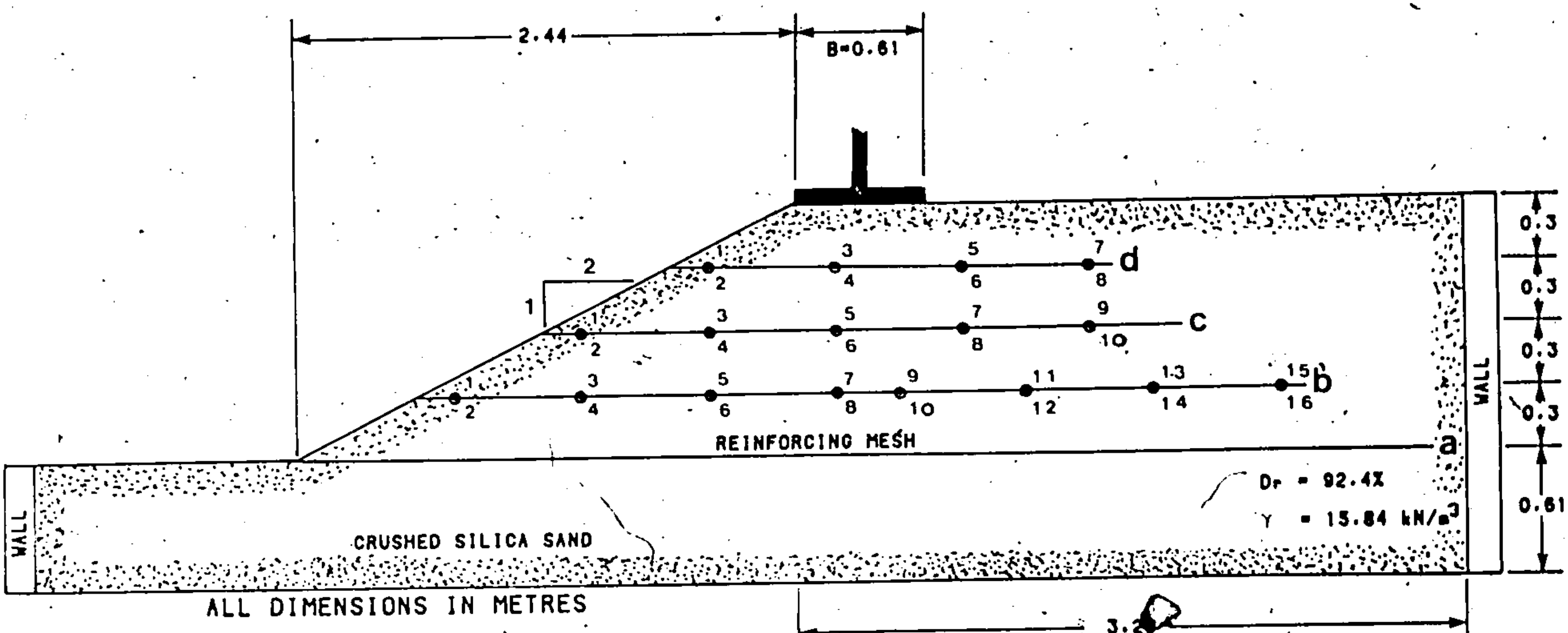

FIG. 4.3.6- PROFILE VIEW OF REINFORCED EMBANKMENT #2 WITH STRAIN GAUGE LOCATIONS ON REINFORCING MESH

MESH #	CHARACTERISTICS			
	LENGTH (m)	WIDTH (m)	CROSSBAR SECTIONS (IN)	GAUGED
A	5.49	1.52	6X12	NO
B	4.27	1.52	6X12	YES
C	3.05	1.52	6X12	YES
D	2.13	1.52	6X12	YES

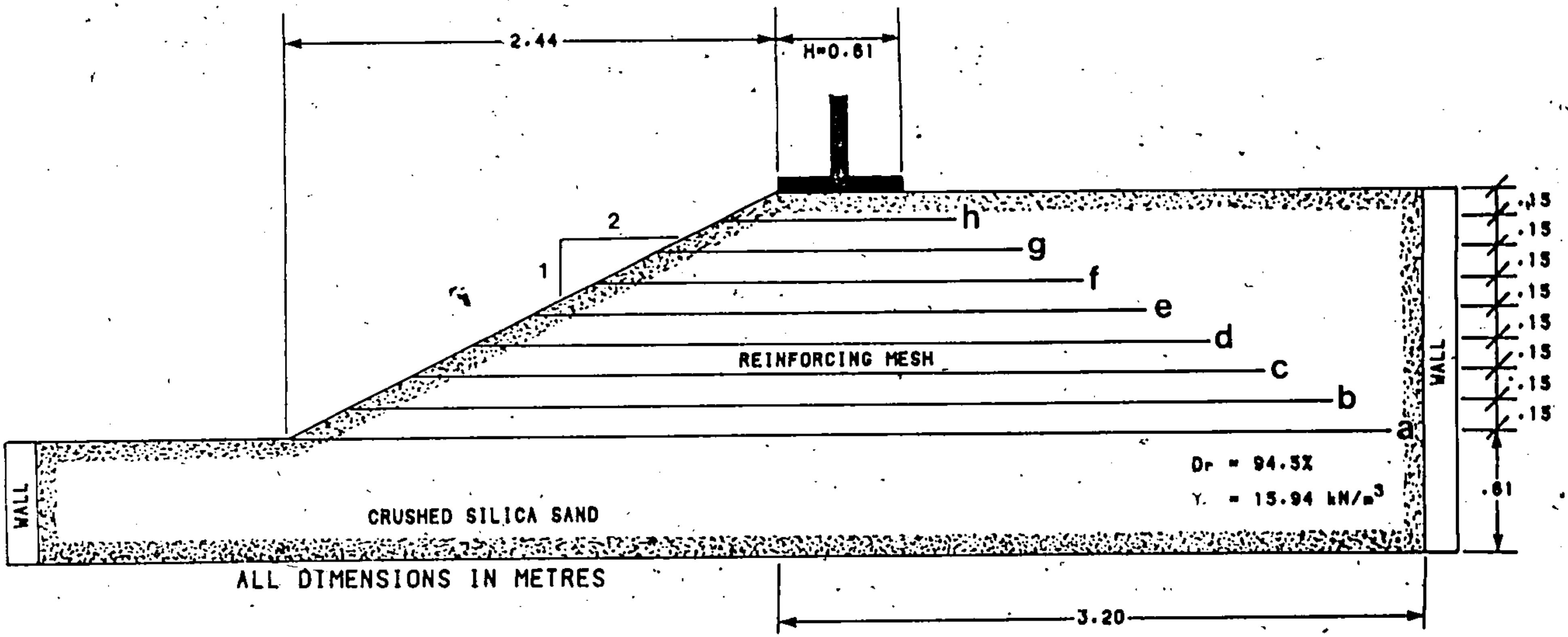

FIG. 4.3.7- PROFILE VIEW OF REINFORCED EMBANKMENT#3

MESH #	CHARACTERISTICS			
	LENGTH (m)	WIDTH (m)	CROSSBAR SPACING (in)	GAUGED
a	5.49	1.52	6X6	NO
b	4.88	1.52	6X6	NO
c	4.27	1.52	6X6	NO
d	3.66	1.52	6X6	NO
e	3.05	1.52	6X6	NO
f	2.44	1.52	6X6	NO
g	1.83	1.52	6X6	NO
h	1.22	1.52	6X6	NO

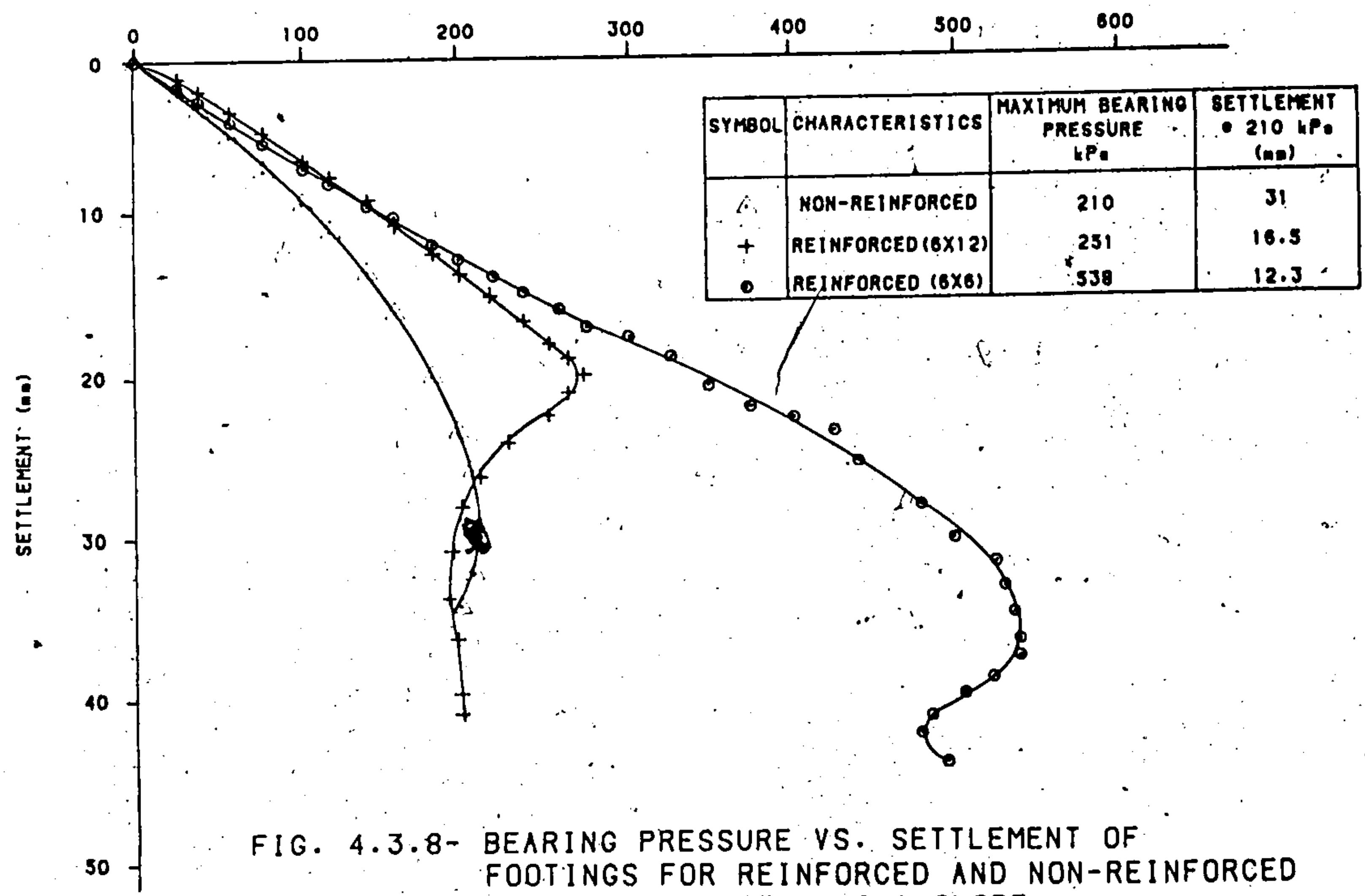

SYMBOL	CHARACTERISTICS	MAXIMUM BEARING PRESSURE kPa	SETTLEMENT @ 210 kPa (mm)
△	NON-REINFORCED	210	31
+	REINFORCED (6X12)	251	16.5
⊙	REINFORCED (6X6)	538	12.3

FIG. 4.3.8- BEARING PRESSURE VS. SETTLEMENT OF FOOTINGS FOR REINFORCED AND NON-REINFORCED EMBANKMENTS WITH A 2:1 SLOPE

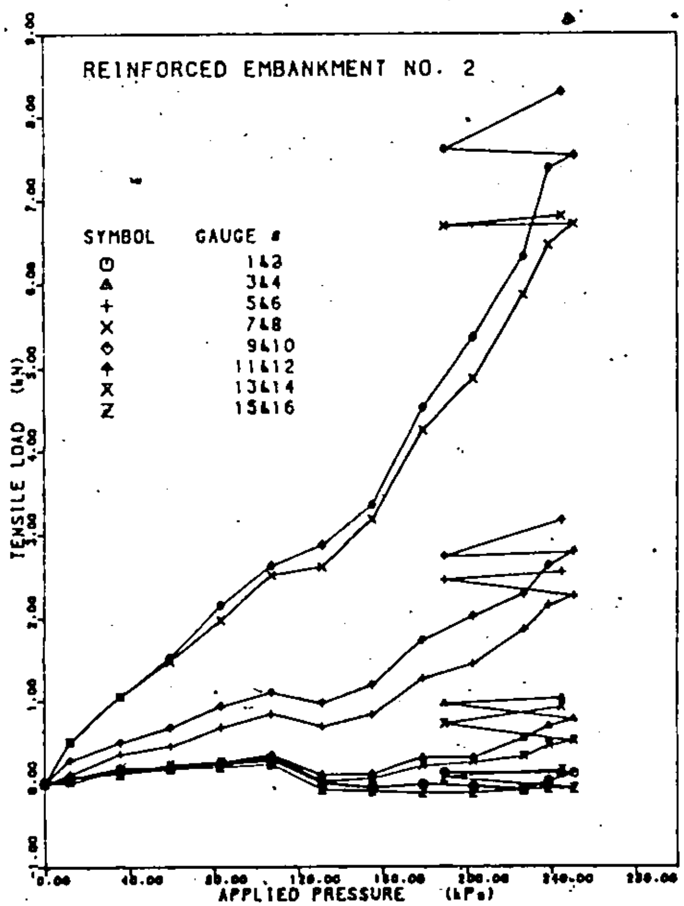

FIG. 4.3.9a- TENSILE LOAD ON REINFORCING MESH "B" FOR EMBANKMENT #2

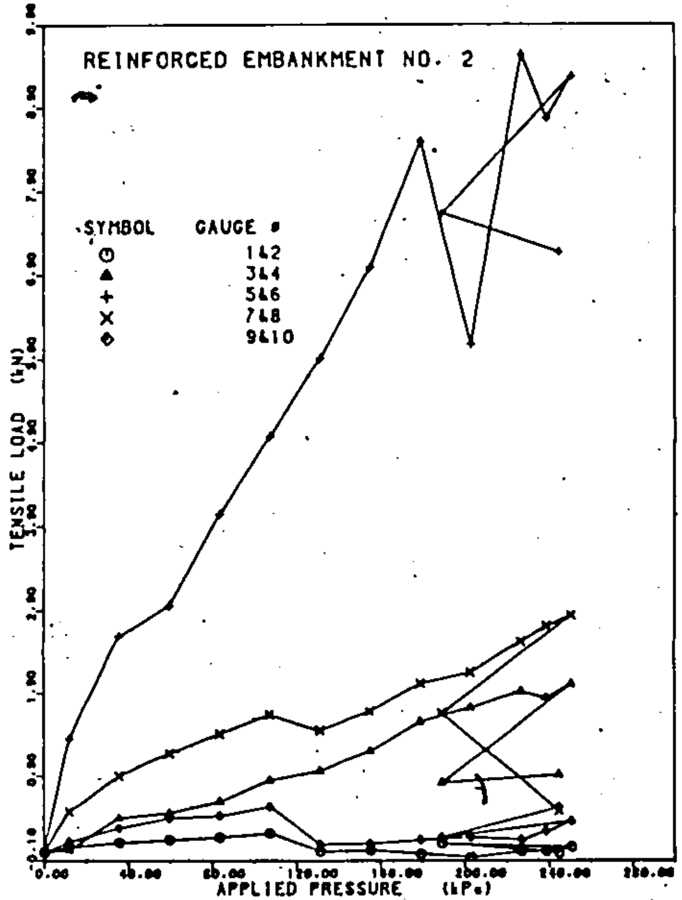

FIG. 4.3.9b- TENSILE LOAD ON REINFORCING MESH "C" FOR EMBANKMENT #2

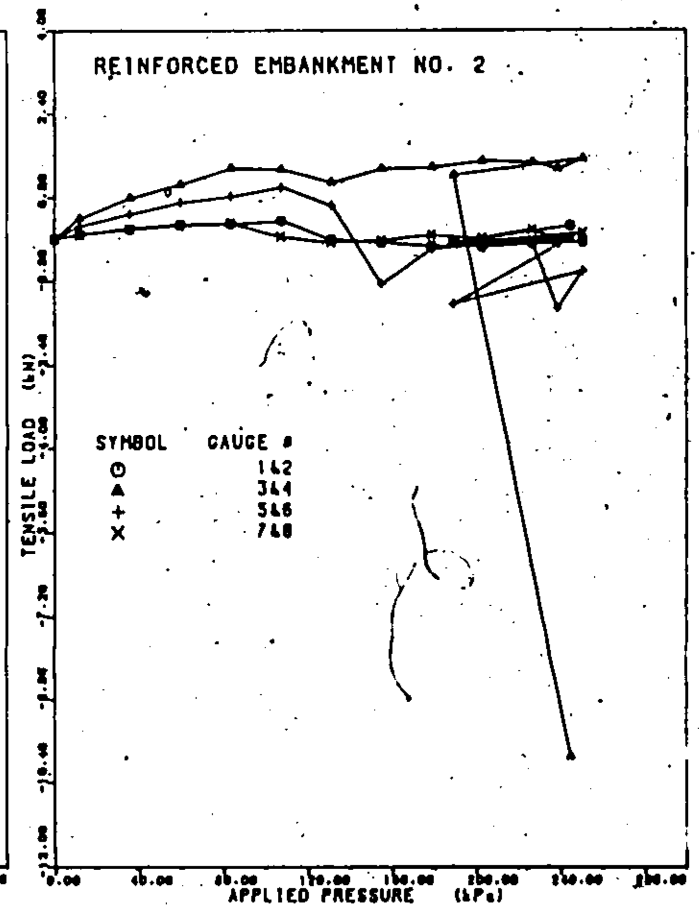

FIG. 4.3.9c- TENSILE LOAD ON REINFORCING MESH "D" FOR EMBANKMENT #2

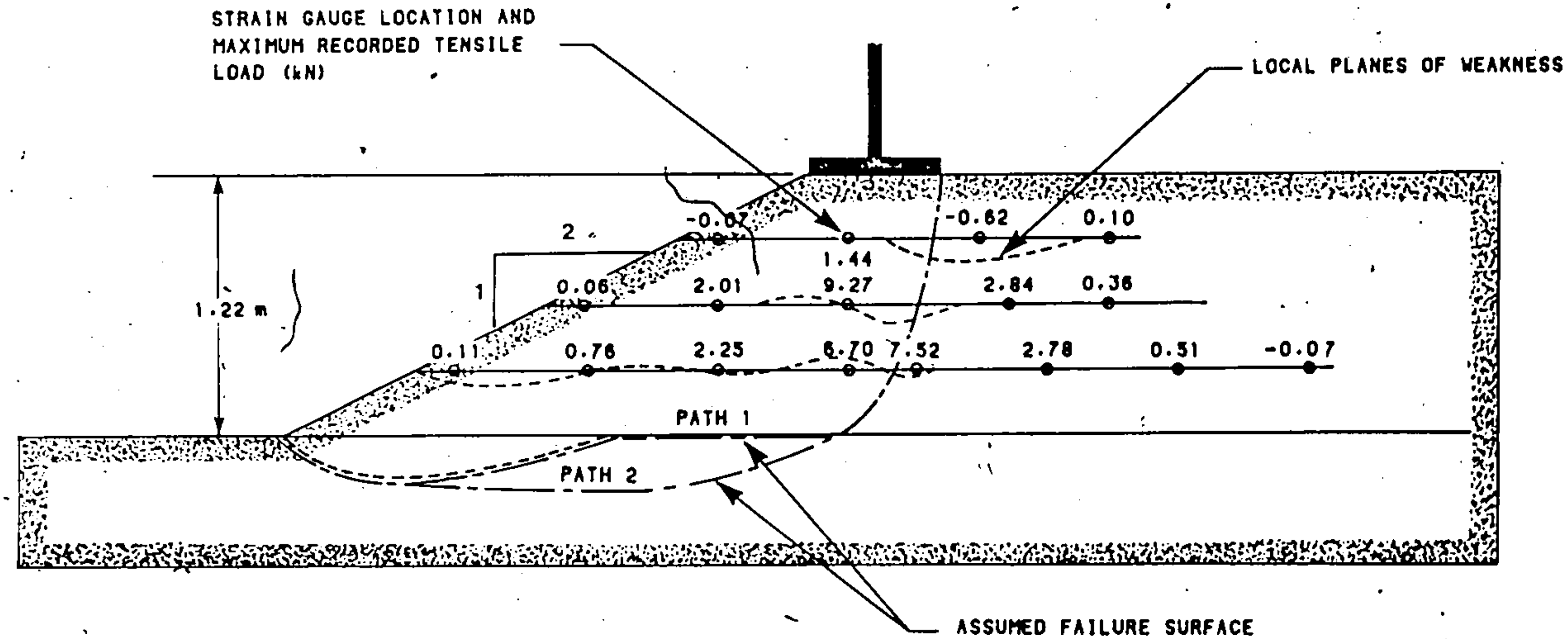

FIG. 4.3.10- ASSUMED FAILURE SURFACE OF EMBANKMENT #2

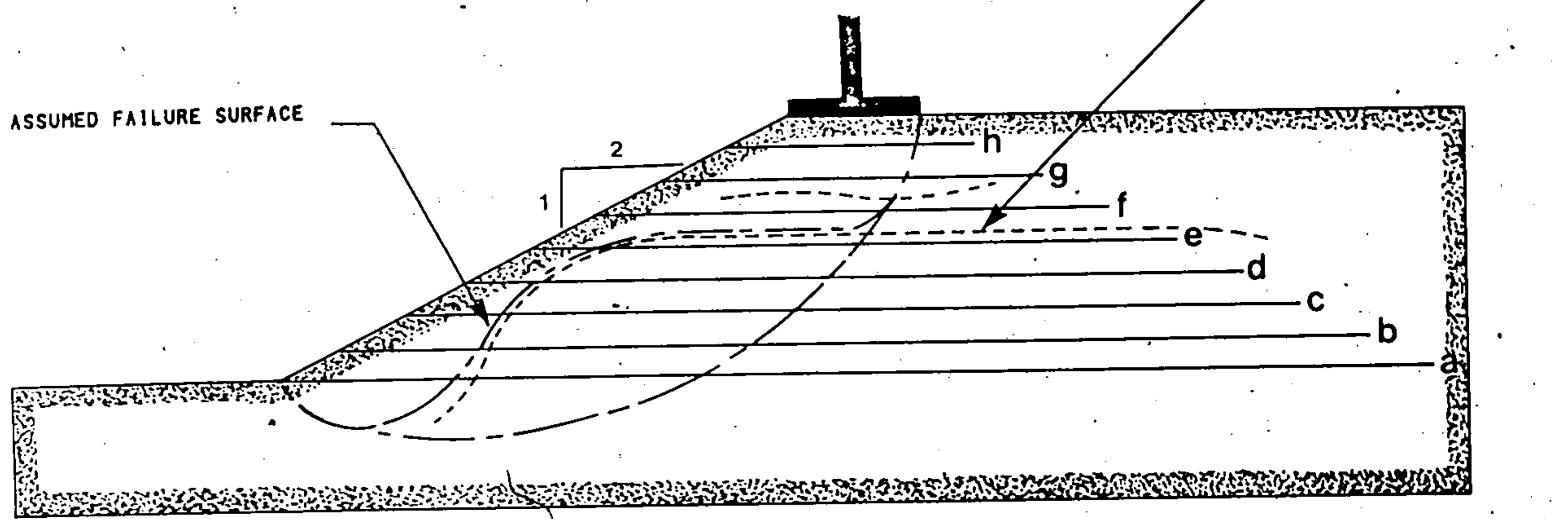

FIG. 4.3.11- ASSUMED FAILURE SURFACE FOR EMBANKMENT #3

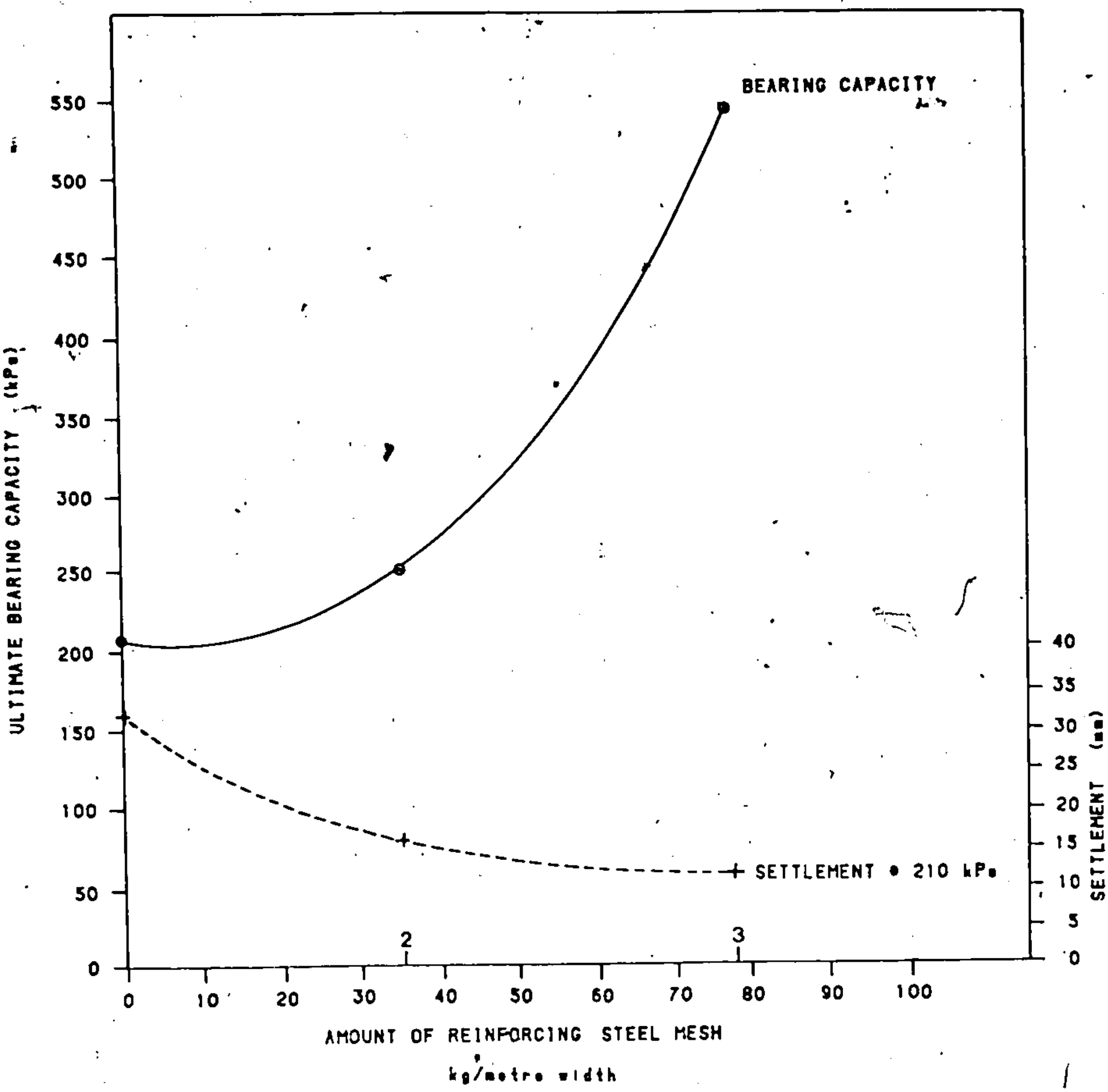

FIG. 4.3.12- RELATIONSHIP BETWEEN BEARING CAPACITY AND SETTLEMENT VS. AMOUNT OF REINFORCING STEEL IN REINFORCED EMBANKMENTS

4.4 BEARING CAPACITY OF FOOTINGS ON REINFORCED WALLS

A final series of large-scale model tests was conducted on four reinforced earth walls. These structures consisted of horizontal layers of reinforcing steel mesh of varying length (having the same characteristics as in the pullout and embankment tests, with a 6x6 crossbar spacing, .15m x .15m) interspaced at constant vertical intervals within a crushed silica sand backfill, the mesh being attached to aluminum wall panels of semi-elliptical shape.

The wall panels were 1.83 metres wide, 0.23 metre high and had a skin thickness of 1.6 millimetres. The panels were manufactured to permit a vertical linkage between the panels and therefore allow the construction of the wall structure to proceed in stages.

The construction stages were identical for all four tests:

1. placement of layer of reinforcing mesh at the desired height level
2. bolting of the mesh to the wall panel using 'U' bolt connections
3. spreading of the sand backfill at the desired density up to the next level of reinforcement
4. repetition of the process until the wall has attained the final height of 1.37 metres.

The width to height ratio of the test apparatus should not be less than 1.0 to 1.25 in order to keep the error due to side wall arching (wall friction effect) below 10 percent (Hausmann 1978). In the following series of tests, the ratio was kept at a constant value of 1.34, theoretically limiting wall friction effects to less than 10 percent.

Figure 4.4.1 illustrates a typical wall test and figure 4.4.2 highlights the wall panels and the 'U' bolt connection.

The wall panels do not insure the overall stability of the structure but act only as a means of preventing the backfill soil from flowing out. As a means of testing the previous statement, the erection of a non-reinforced wall structure was attempted, but immediate wall overturning verified the stated assumption.

All four tests were subjected to a surcharge strip load to determine the maximum bearing capacity of the footings on a reinforced soil structure. The wall panel deflections were measured along with the applied pressure and settlement of the footings.

In model test W-3, strain gauges were installed along the reinforcement mesh in order to measure the resulting tensile forces supplied at each level of reinforcement by the applied pressure.

Model test W-2 differed from the other three tests by not having the reinforcing mesh bolted to the wall panels. This was accomplished in order to investigate whether or not a significant decline in bearing capacity would occur with non-bolted reinforcing members.

As in the previous pullout and embankment experiments, slippage of the applied pressure on the earth structure occurred at regular intervals. This slippage can be physically described as a loud stress relieving 'bang'. Axial stress increases on the crossbar members until a maximum tensile load is achieved which is then followed by a sudden drop in axial stress and consequently a drop in bearing pressure.

Table 14 summarizes the reinforced earth walls testing programme and figure 4.4.3 illustrates the applied pressure-settlement relationships of the different configurations of reinforcement. The following sections will examine each test in detail.

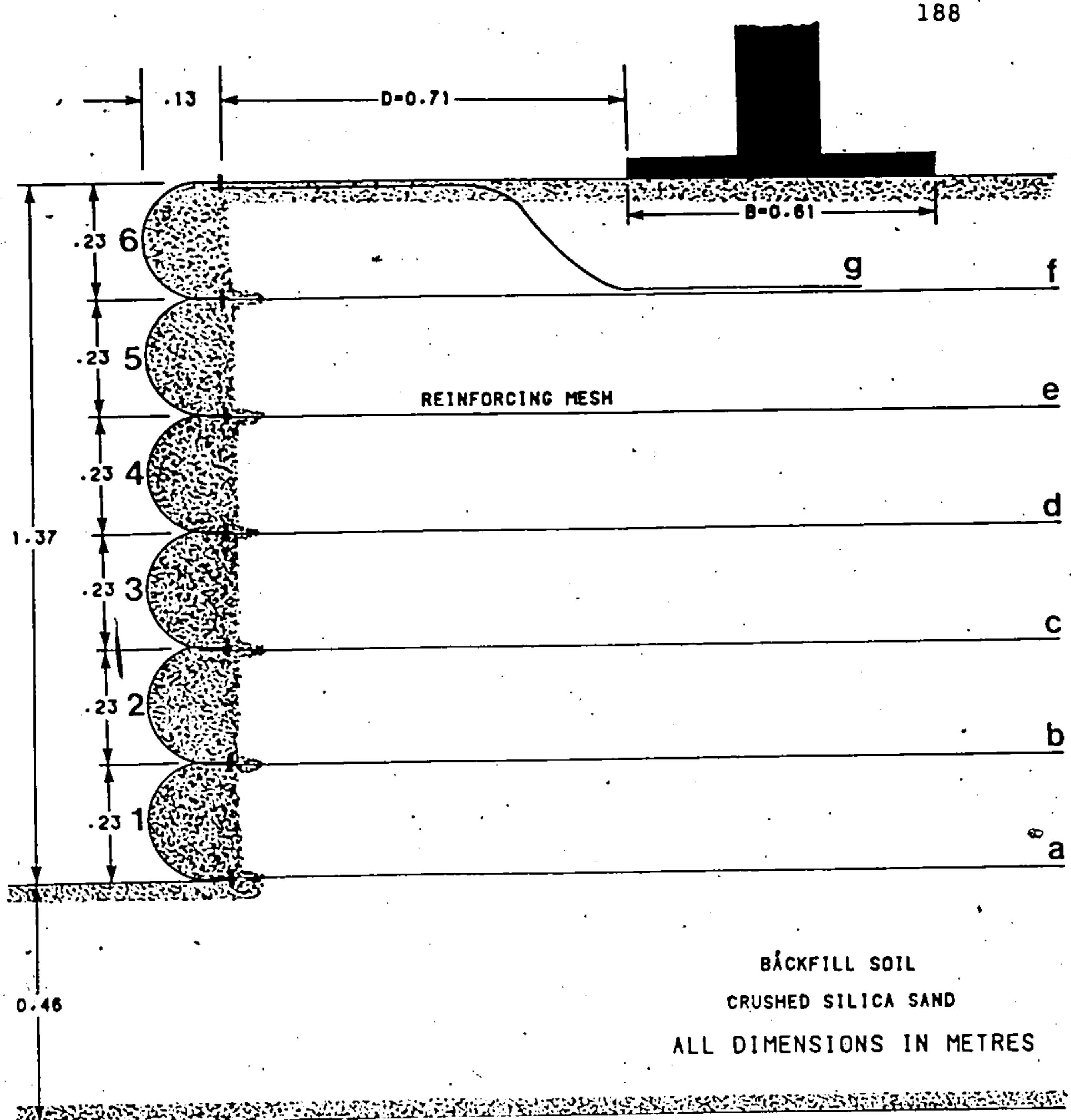

MESH CHARACTERISTICS: CROSSBAR SPACING: 6X6 (.15m X .15m)
WIDTH: 5' (1.52m)
LENGTH: VARYING LENGTH
BAR DIAMETER: 3/16" (4.8 mm)

WALL PANELS: 1/16" (1.6 mm) THICK ALUMINUM PANELS
6' (1.83 m) WIDE

FIG. 4.4.1- TYPICAL REINFORCED WALL CONFIGURATION

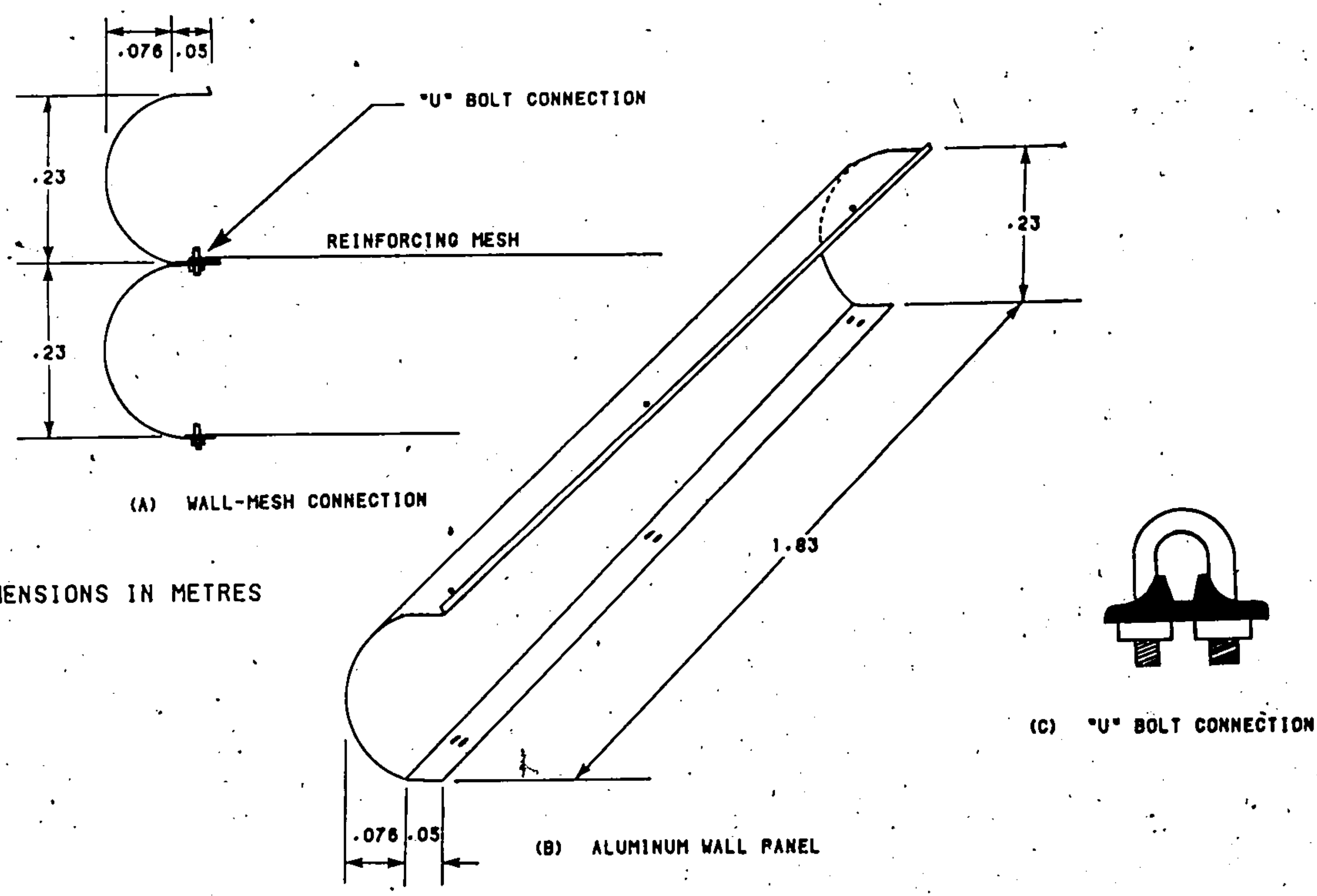

ALL DIMENSIONS IN METRES

FIG. 4.4.2- WALL-MESH COMPONENTS

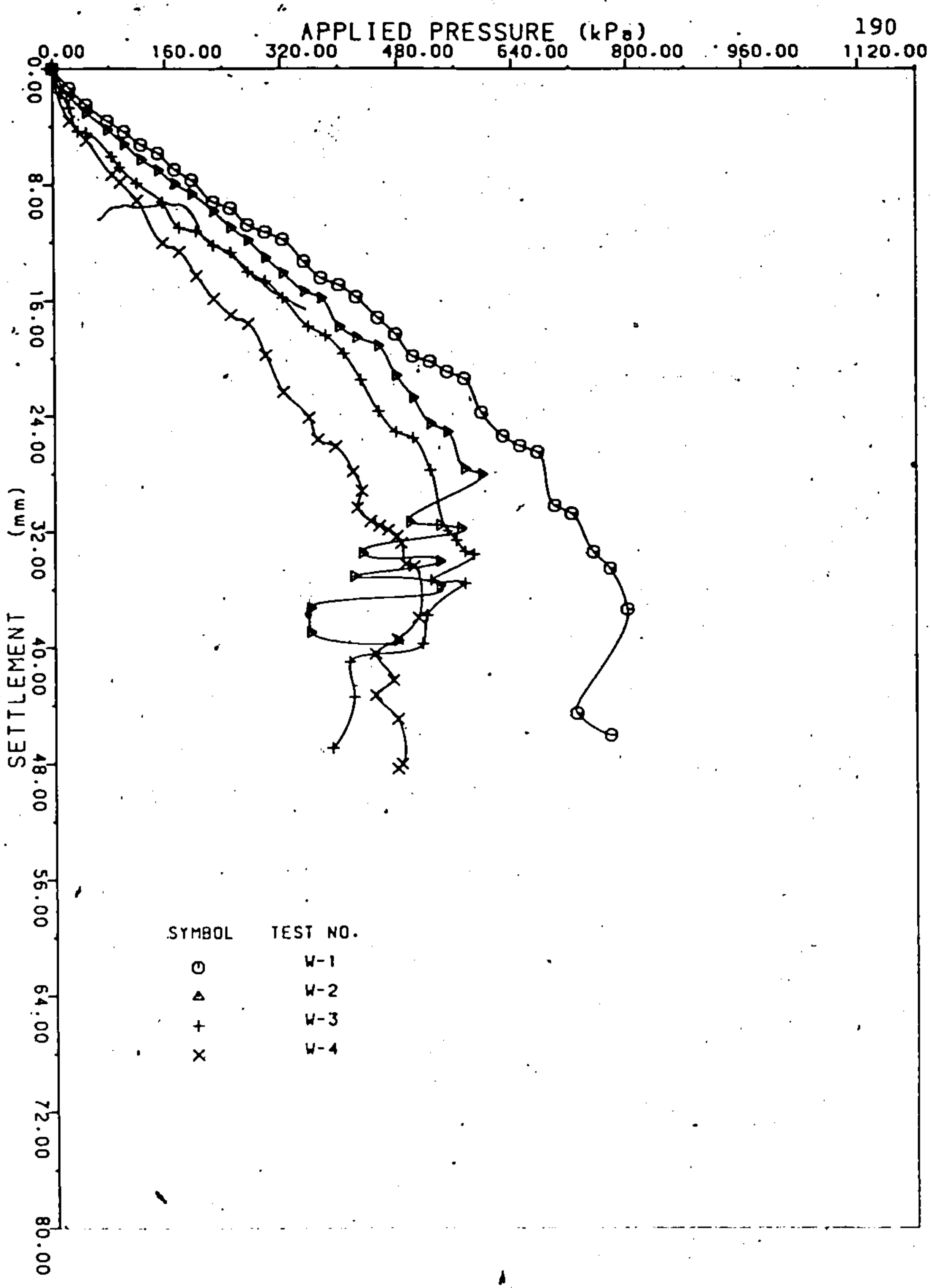

FIG. 4.4.3- APPLIED PRESSURE VS. FOOTING SETTLEMENT FOR REINFORCED WALL TESTS

TABLE 14

Summary of reinforced wall tests

test#	unit weigth of back-fill soil kN/m³	footing location D (m)	bolted to wall panel	gauged	length of mesh (m)	settl. of central footing (mm)	ultimate bearing capacity of structure (kPa)
W-1	15.91	0.71	yes	no	4.27	37.3	800
W-2	15.94	0.71	no	no	4.27	28.0	597
W-3	16.02	0.23	yes	yes	2.74	33.5	585
W-4	15.86	0.71	yes	no	1.37	37.9	508

4.4.1 Reinforced wall tests W-1 and W-2

Reinforced wall test W-1 consisted of six mesh layers of 4.27 metres in length (three times the height of the wall) with a vertical spacing of 0.23 metre, all bolted to the aluminum wall panels.

A seventh layer of mesh of 1.22 metres was connected to the top section of the upper panel to minimize overturning of the top panel. Figure 4.4.4 shows graphically the test layout.

As indicated in table 14, the ultimate bearing capacity of the structure was measured to be 800 kPa, this ultimate bearing capacity was defined at the point at which the slope of the load settlement curve first reaches zero or a steady,minimum value.

Figure 4.4.5 illustrates the configuration of the reinforcing mesh layers after the load test was executed. Only the upper three layers had any noticeable deformation of the crossbar members, and mesh E sustained the most important deflections including weld and bar failures. This indicates that at a height of H/3 from the upper surface (H being the total height of the wall) the tensile forces supplied to the mesh layers have attained a level greater than 12.2 kN (bar failure load) beneath the footing.

Utilizing figure 4.4.5 and by probing the soil structure, the points of maximum tensile stress in the soil stratum can be determined and therefore a probable failure plane through the structure is identified. This failure plane is shown on figure 4.4.6.

Figure 4.4.7 demonstrates the outward wall panel displacement as the bearing pressure applied to the wall is increased. Once again, the maximum tensile stresses can be located at mesh E or at H/3 of the total height of the wall.

The objective of wall test W-2 was the examination of the influence of bolting the mesh to the wall panels on the bearing capacity of the structure. Figure 4.4.8 illustrates the layout of the test.

The earth structure consisted of six layers of mesh of 4.27 metres in length, identical to the previous test but not bolted to the wall panels. Each reinforcement layer was placed horizontally at the mid-point of the panels, and to prevent the wall from overturning during erection six layers of mesh 0.61 and 0.76 metres in length were bolted to the wall panels between each layer of mesh of 4.27 metres. These additional layers of reinforcement undoubtebly influenced the bearing capacity measurements however, their small length prevents any anchorage effect to take place and one can neglect their presence.

The ultimate bearing capacity of this structure was measured at 597 kPa, or a 25% drop of capacity from the bolted system. Furthermore, at an applied pressure of 500 kPa, the settlement of the footings increases from 19.8 mm in test W-1 to 22.7 mm for test W-2, or an increase of 14.6% in settlement (figure 4.4.9).

In examining the deformation of the mesh reinforcement after the load test (figure 4.4.10) and the presence of a ridge of displaced sand 0.6 metre behind the footings, probable failure zones can be assumed through the earth structure. These zones differ substantially from test W-1 and are presented in figure 4.4.11.

Figure 4.4.12 shows the outward wall panel displacement as the bearing pressure applied is increased. At 500 kPa, the displacement of the wall panels was subjected to a substantial increase in the upper three panels for the non-bolted test compared to the bolted test. This increase varies from approximately 170% in the upper panels to 75% in panel three to approximately 30% in the lower three panels.

Once again, it becomes clear that mesh E sustained the greatest tensile load transfer from the applied pressure. In other words, if the total height of the wall is considered to be H, the point of maximum tensile stress is located this time at H/4 from the upper soil surface.

Summarizing these two tests, it becomes evident that the bolting of the anchored reinforcing layers increases the bearing capacity of the strip footings, reduces the footing settlements and minimizes the wall panel outward deflections. The reason for this improvement is that the wall facing distributes the confining effect of the reinforcement more uniformly over the soil stratum.

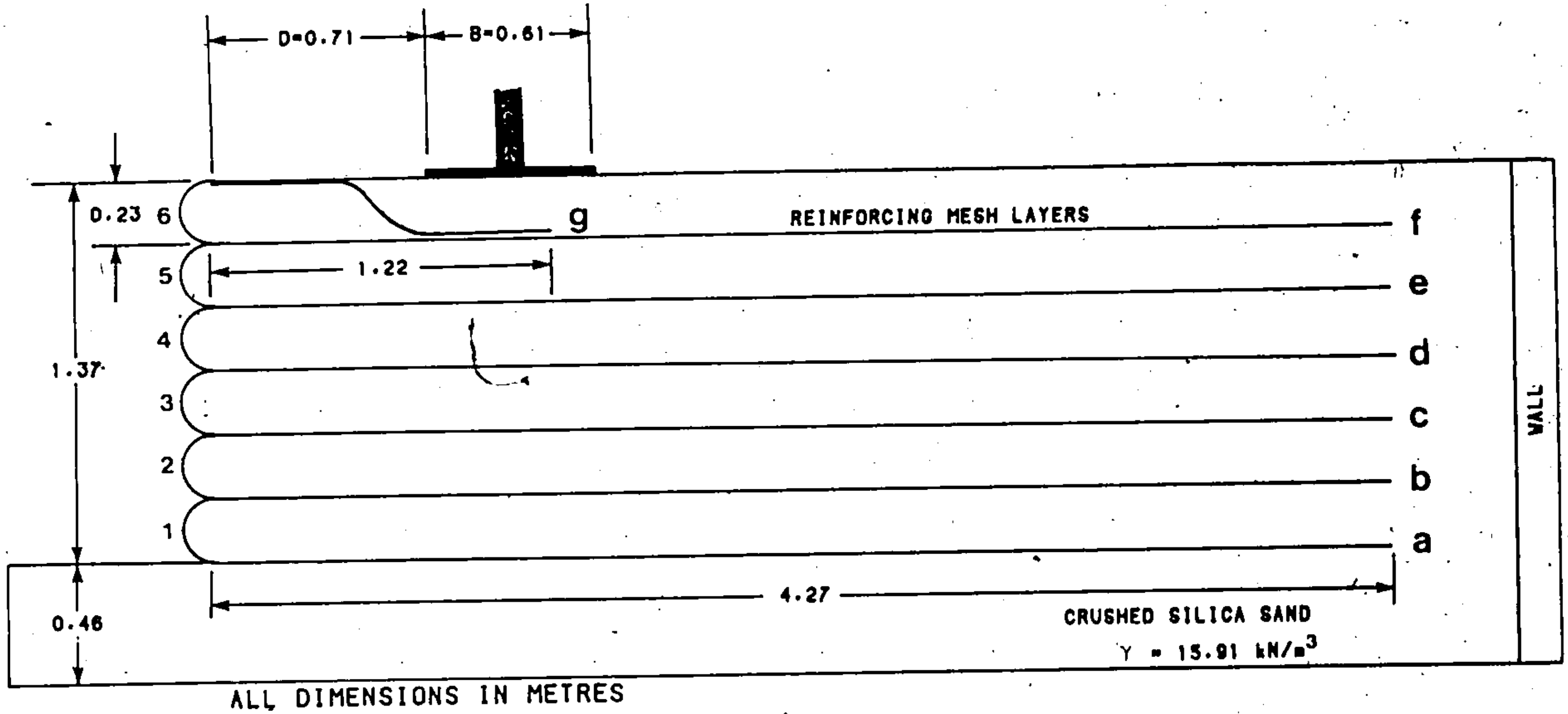

FIG. 4.4.4- SCHEMATIC REPRESENTATION OF REINFORCED WALL TEST W-1

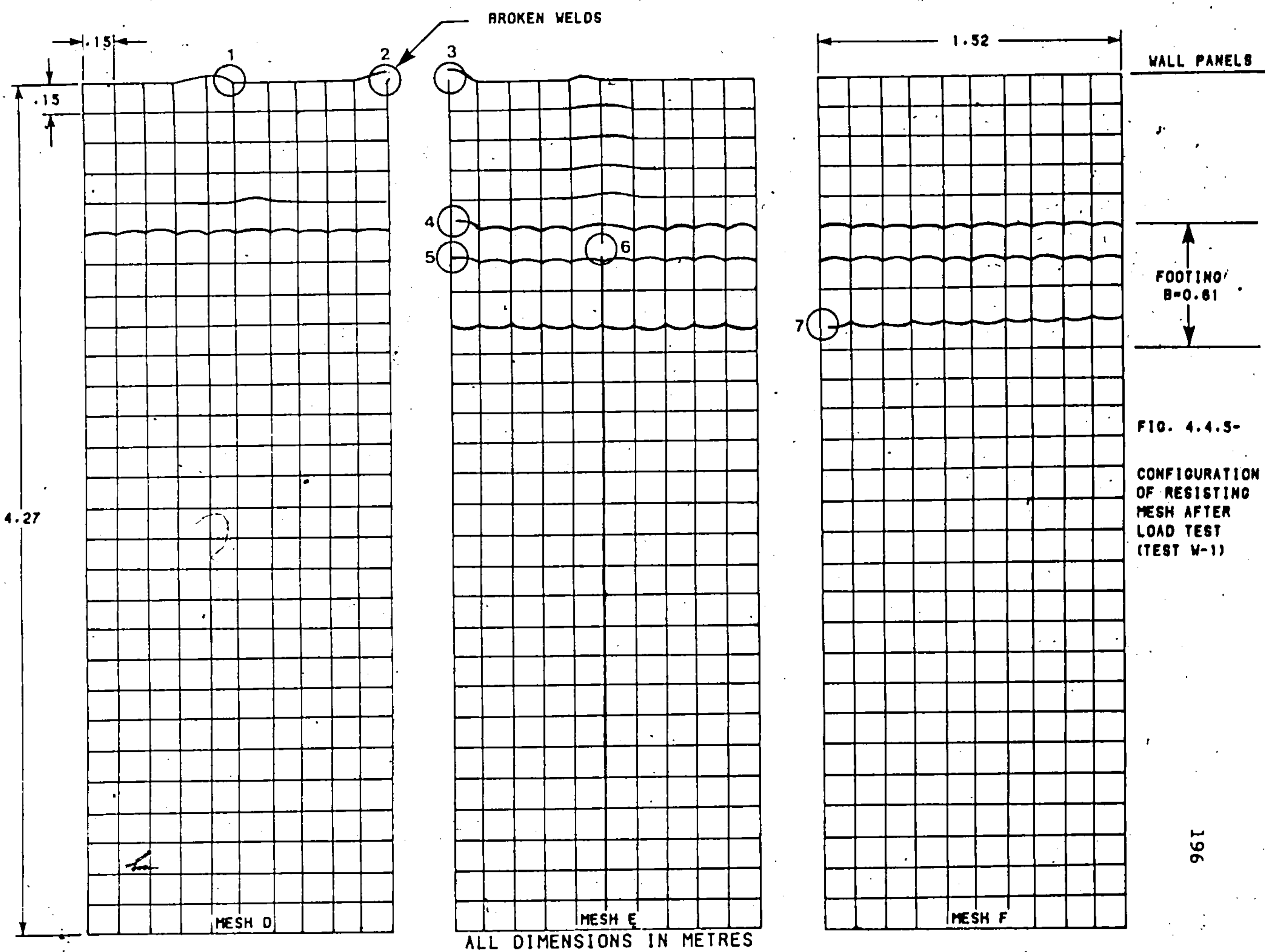

FIG. 4.4.5- CONFIGURATION OF RESISTING MESH AFTER LOAD TEST (TEST W-1)

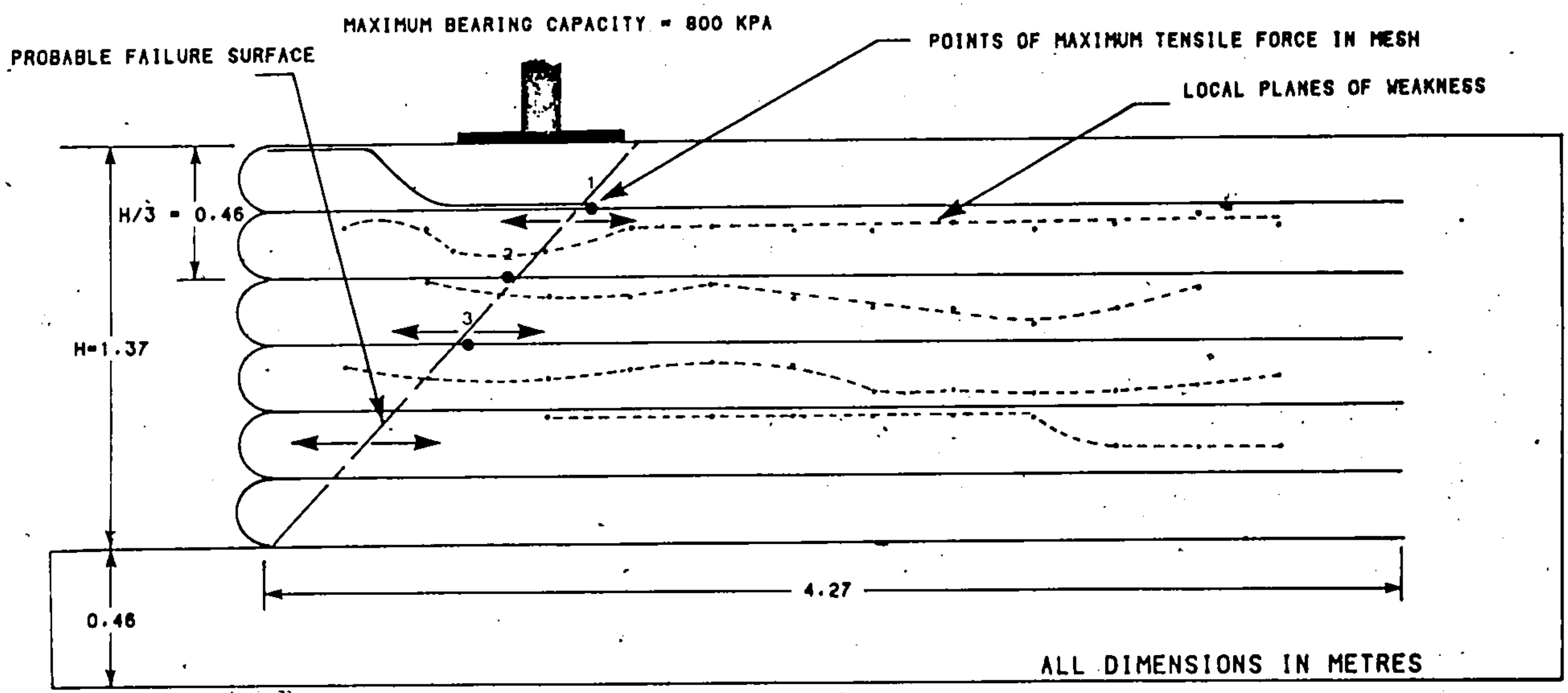

FIG. 4.4.6- FAILURE SURFACE OF REINFORCED WALL STRUCTURE W-1

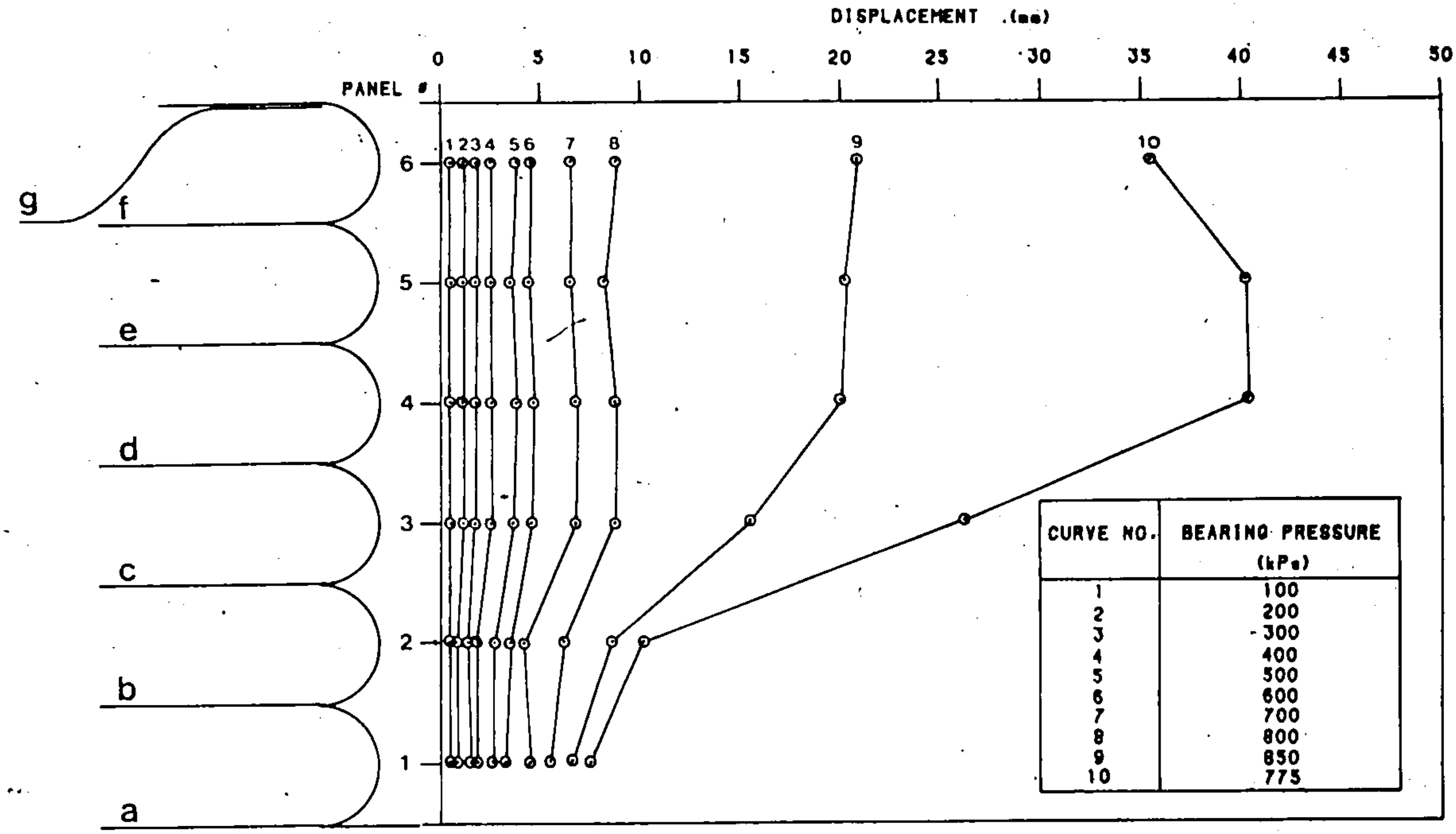

FIG. 4.4.7- WALL PANEL DISPLACEMENT WITH INCREASING BEARING PRESSURE FOR TEST W-1

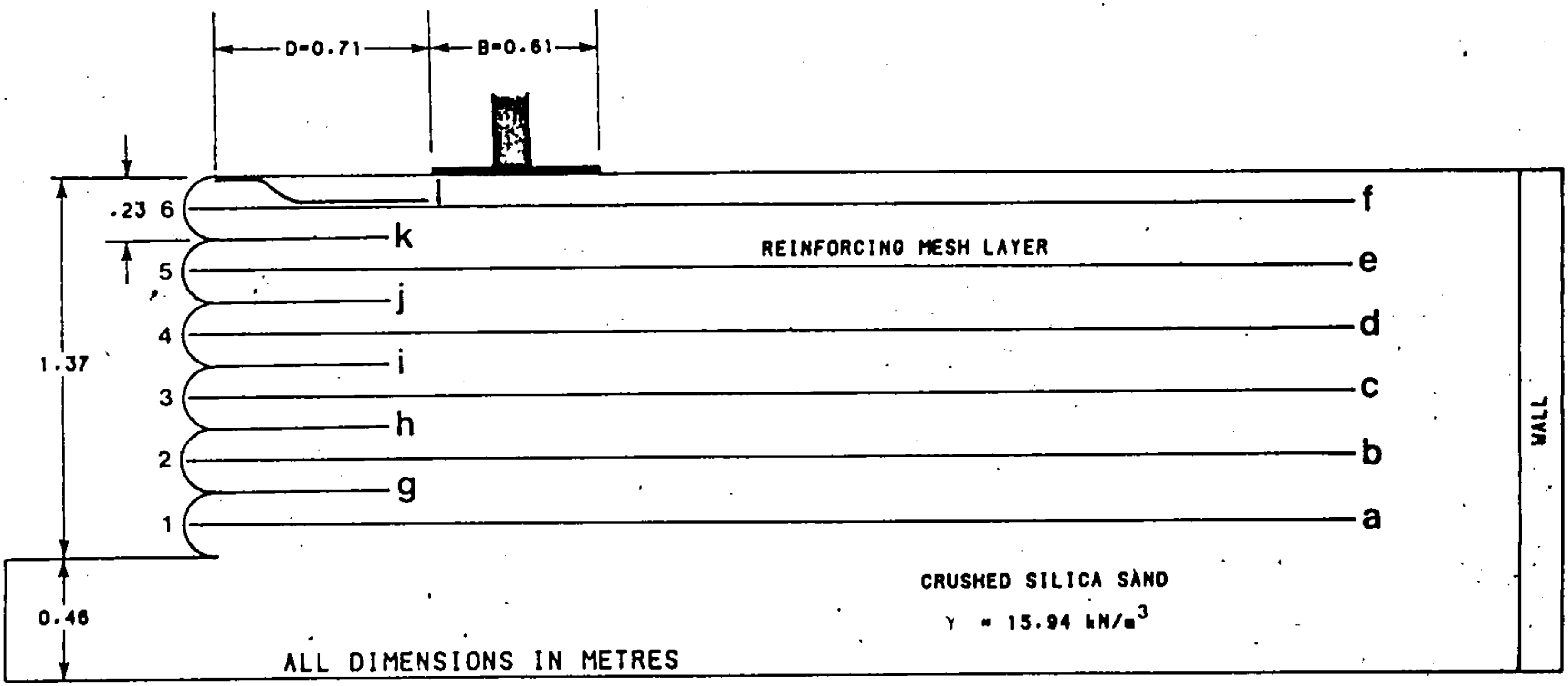

MESH	LENGTH (m)
a-f	4.27
g-k	0.61
l	0.76

FIG. 4.4.8- SCHEMATIC REPRESENTATION OF REINFORCED WALL TEST W-2

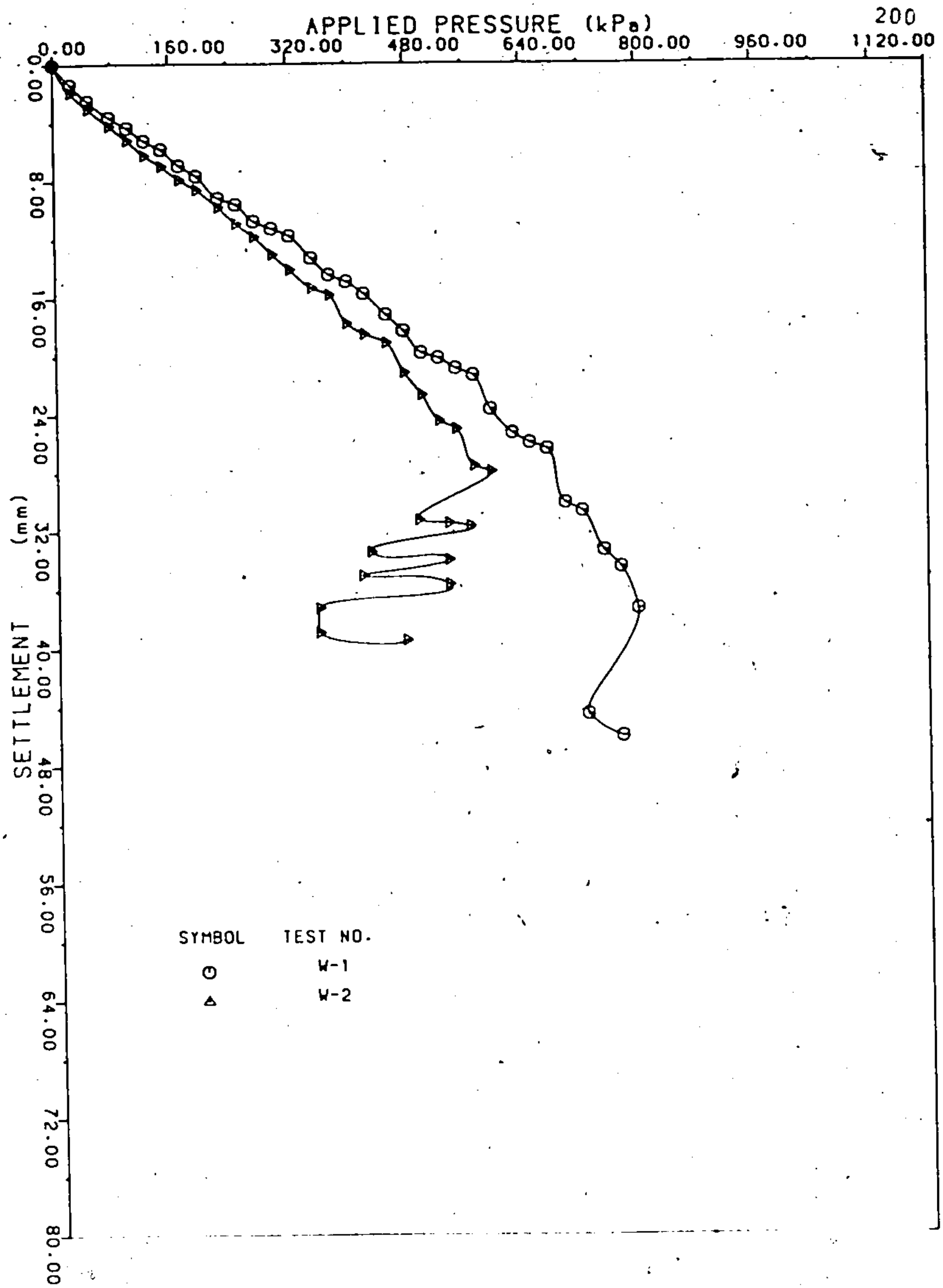

FIG. 4.4.9- APPLIED PRESSURE VS. FOOTING SETTLEMENT FOR REINFORCED WALL TESTS W-1 AND W-2

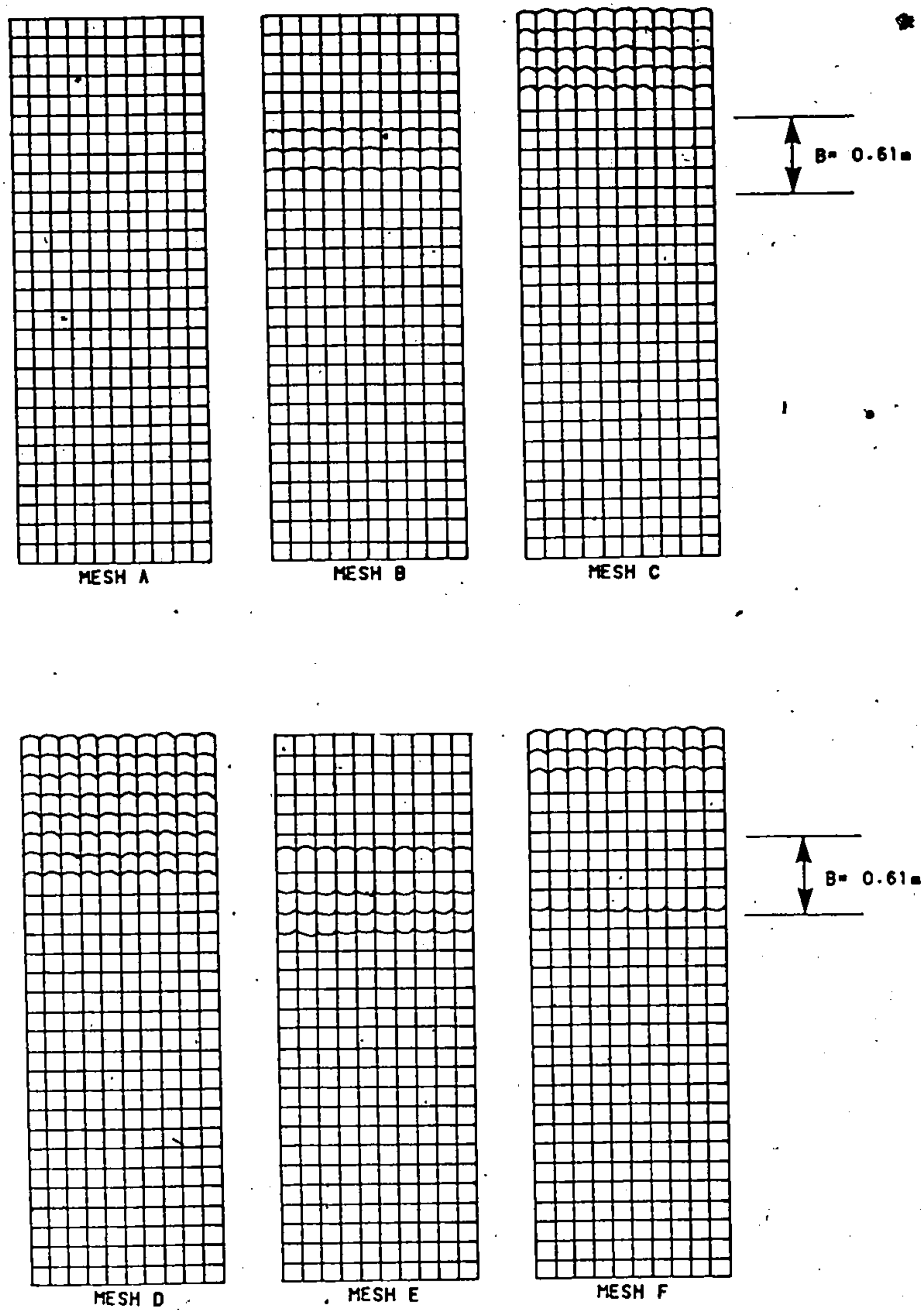

FIG. 4.4.10- DEFORMATION OF RESISTING MESH AFTER LOAD TEST (REINFORCED WALL W-2)

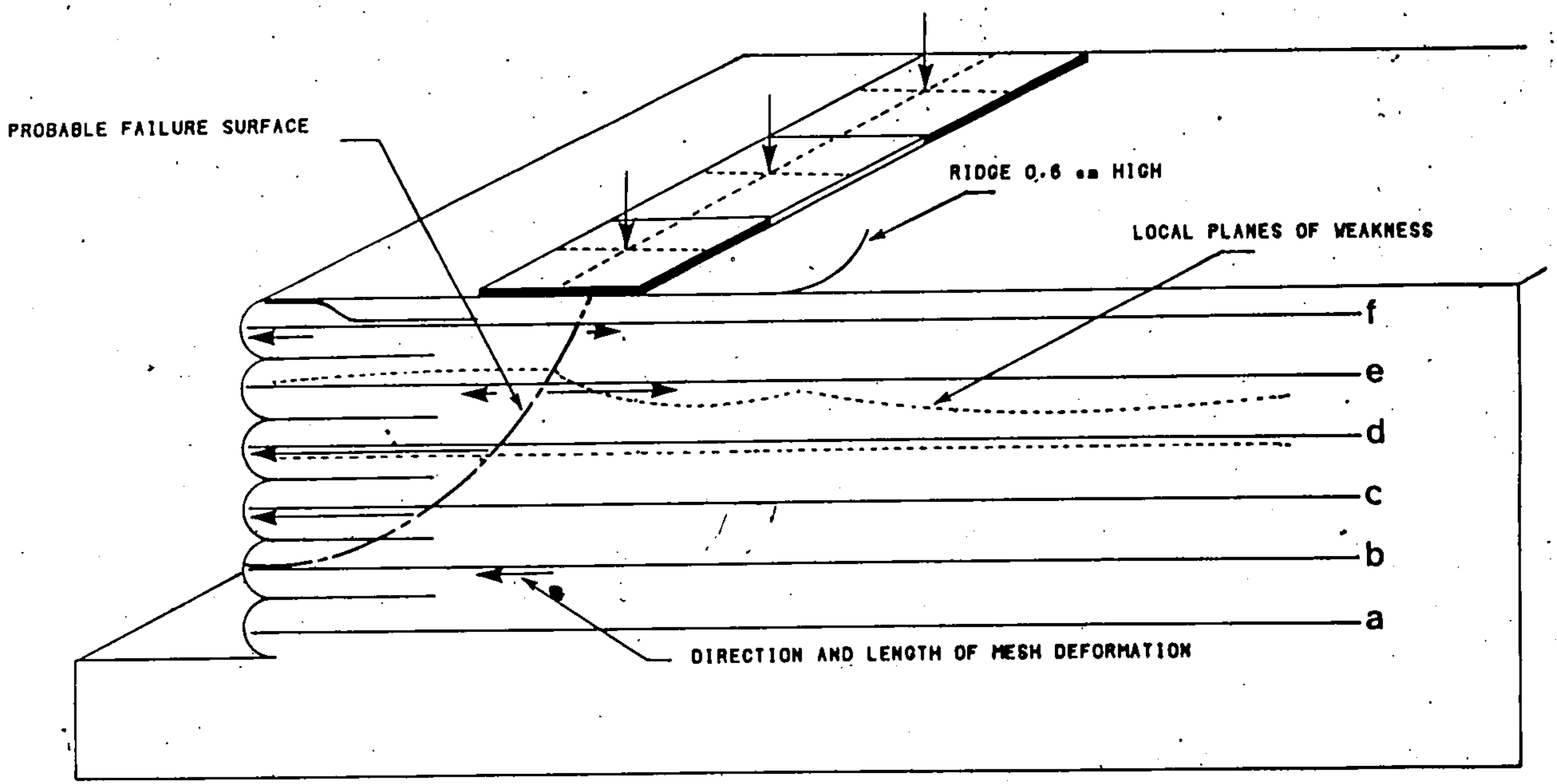

FIG. 4.4.11- FAILURE SURFACE IN REINFORCED WALL STRUCTURE W-2

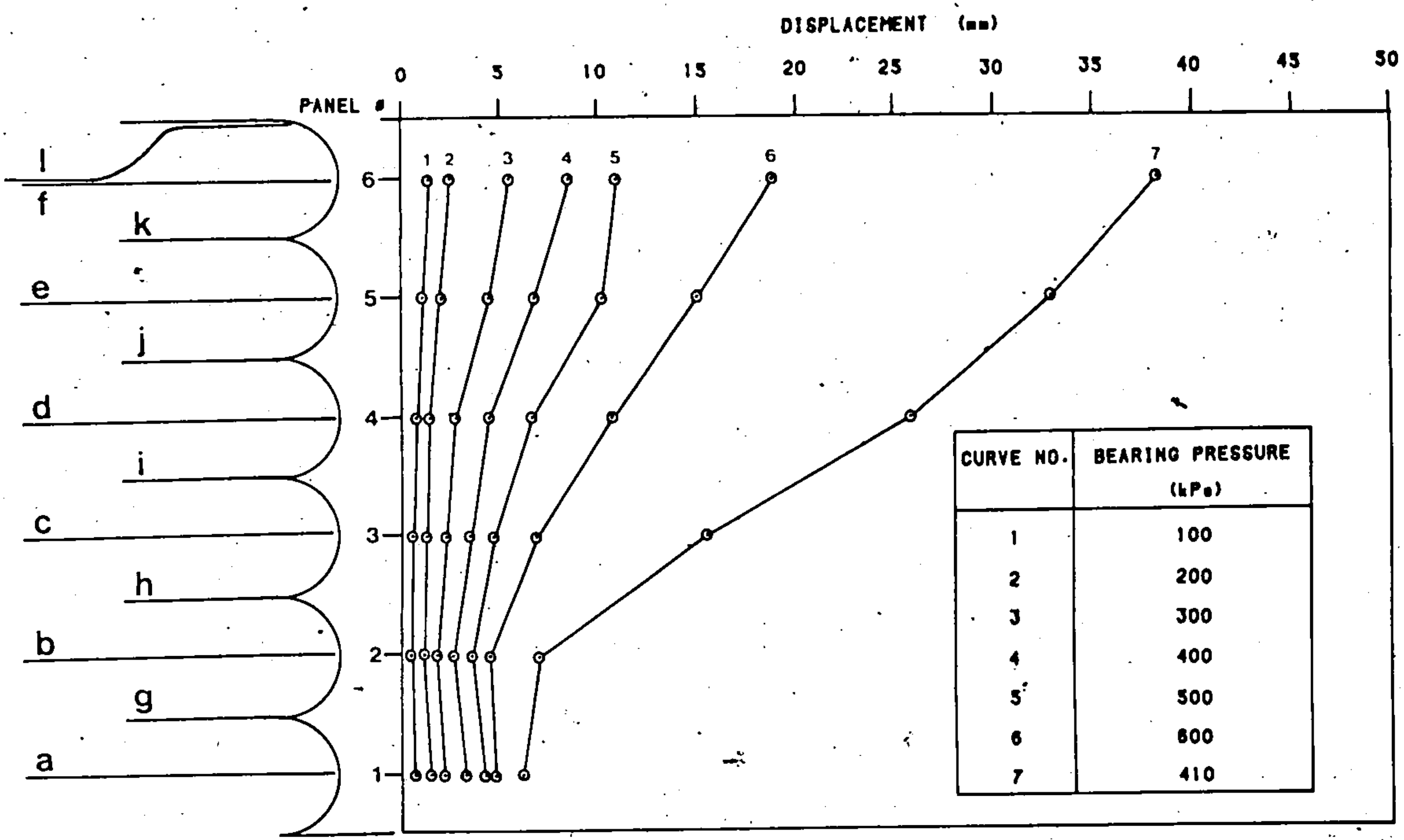

FIG. 4.4.12- WALL PANEL DISPLACEMENT WITH INCREASING BEARING PRESSURE FOR TEST W-2 (UNBOLTED)

4.4.2 <u>Reinforced wall test W-3</u>

Wall test W-3 was similar to wall test W-1 except for two important parameters, the length of the reinforcing mesh was reduced to 2.74 metres (twice the height of the wall) and the footings were moved to within 0.23 metre of the wall panels, as illustrated on figure 4.4.13.

Another important variation from test W-1 is the inclusion of strain gauges in the reinforcing mesh which permitted the measurement of the tensile forces applied to the reinforcing members by the strip footings. The layout of a typical mesh layer is shown on figure 4.4.14.

Figure 4.4.15 compares the bearing pressure versus settlement relationships of tests W-1 and W-3. A drop in bearing capacity of 27% is observed (800 vs. 585 kPa) and an increase in settlement of the footings at 500 kPa of 28% is measured (19.8 vs. 22.5 mm).

Figure 4.4.16 shows the deformation of the mesh layers after the load test and figures 4.4.17 and 4.4.18 illustrate the distribution of the tensile forces in the reinforcing mesh at 300 kPa and at maximum bearing pressure obtained from the strain gauges. From the deformation of the mesh, and the maximum tensile forces a probable failure plane can be determined and is shown on figure 4.4.19.

The wall panel deflections are shown on figure 4.4.20 and the increase in deflection from test W-1 ranges from 225% in the uppermost panel to 100% in the lowermost panel.

After describing the test results it is of interest to determine which of the parameter changes had the greatest influence on the behaviour of the wall structure:

1. the shortening of the mesh; or
2. the smaller distance between the wall panels and the footings.

Going back to the pullout tests, it was observed that a mesh of three metres in length was considered to be anchored and that only the yield stress of the steel was being tested, while a mesh of 1.93 metres in length was pulled out without deformation of the crossbar members.

However the peak pullout load for a 6x6 (.15m x .15m) crossbar spacing for both lengths at high overburden pressure is considered to be identical (as shown in table 4). Therefore it can be concluded that the 2.74 metres mesh in wall test W-3 was anchored to the same degree as test W-1 for a strip footing test, and that the significant parameter which influenced the behaviour of test W-3 was the distance (D) between the wall panels and the footing, which was reduced by a factor of three if we take the curvature of the wall panels in consideration.

In summary, by moving the footing location from 1.36B to 0.59B (B= footing width), the bearing capacity of the structure is reduced by 27%, the settlement of the footings is increased by 28% while the outward displacement of the wall panels is increased substantially.

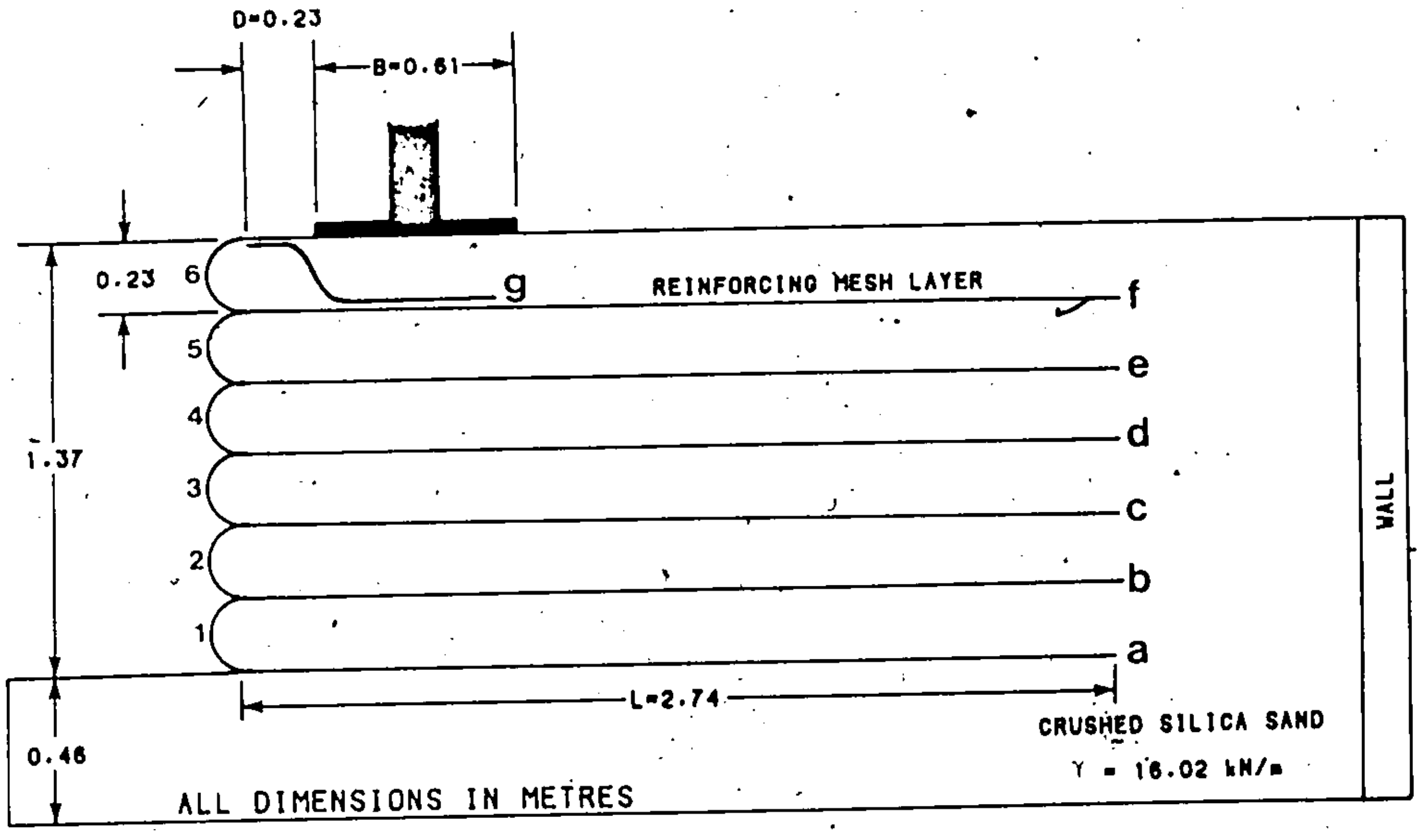

FIG. 4.4.13- SCHEMATIC REPRESENTATION OF REINFORCED WALL TEST W-3

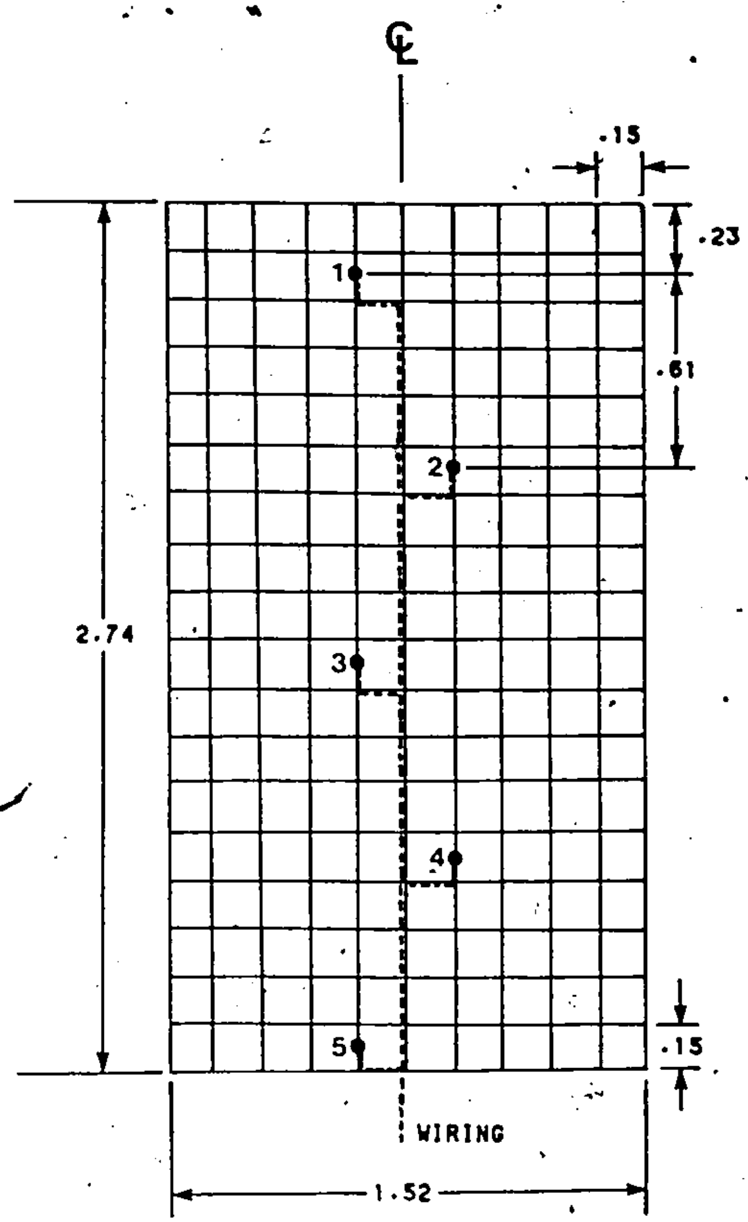

ALL DIMENSIONS IN METRES

FIG. 4.4.14- TYPICAL MESH LAYOUT AND POSITION OF STRAIN GAUGES FOR TEST W-3

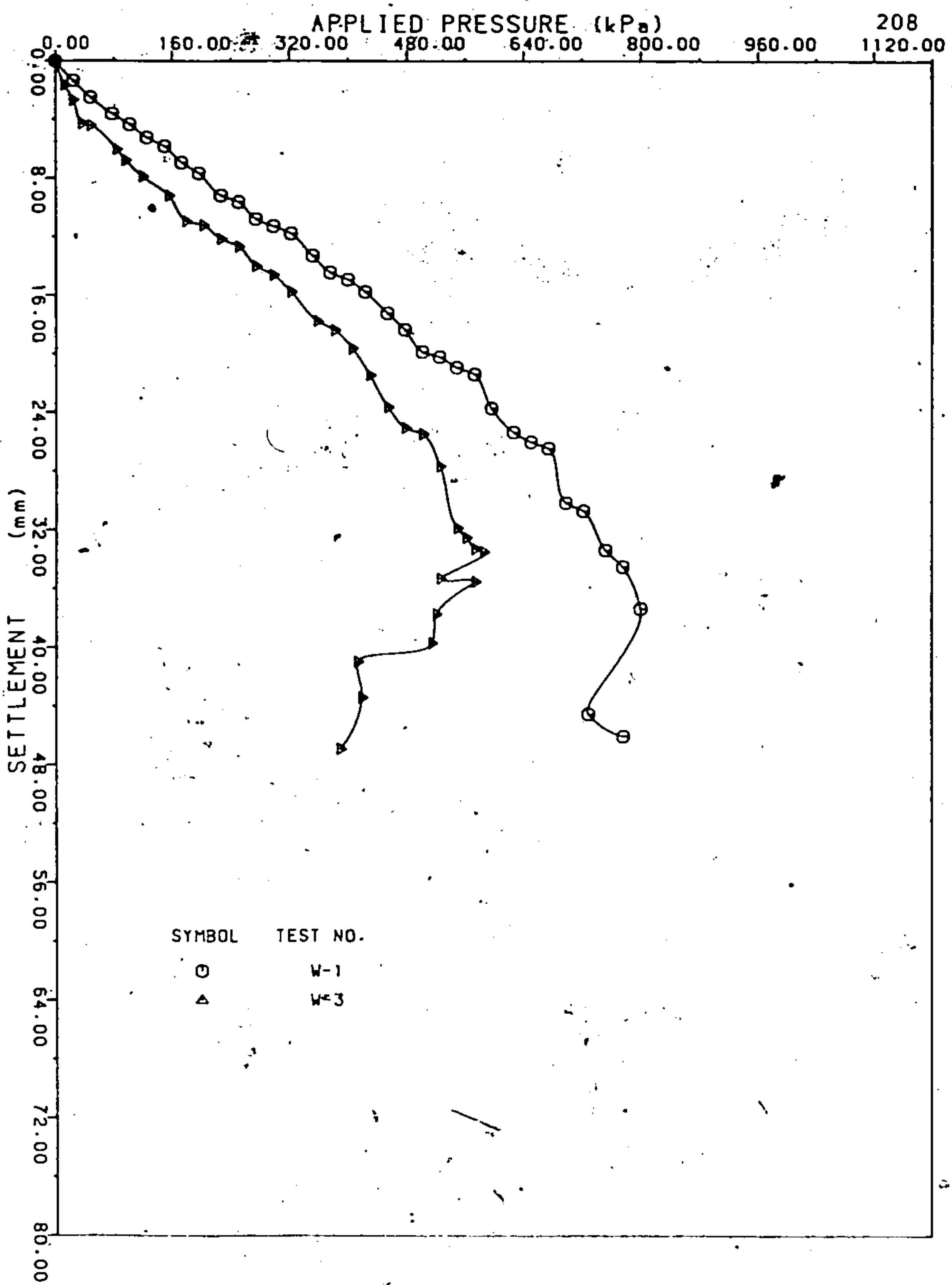

FIG. 4.4.15- APPLIED PRESSURE VS. FOOTING SETTLEMENT FOR REINFORCED WALLS W-1 AND W-3

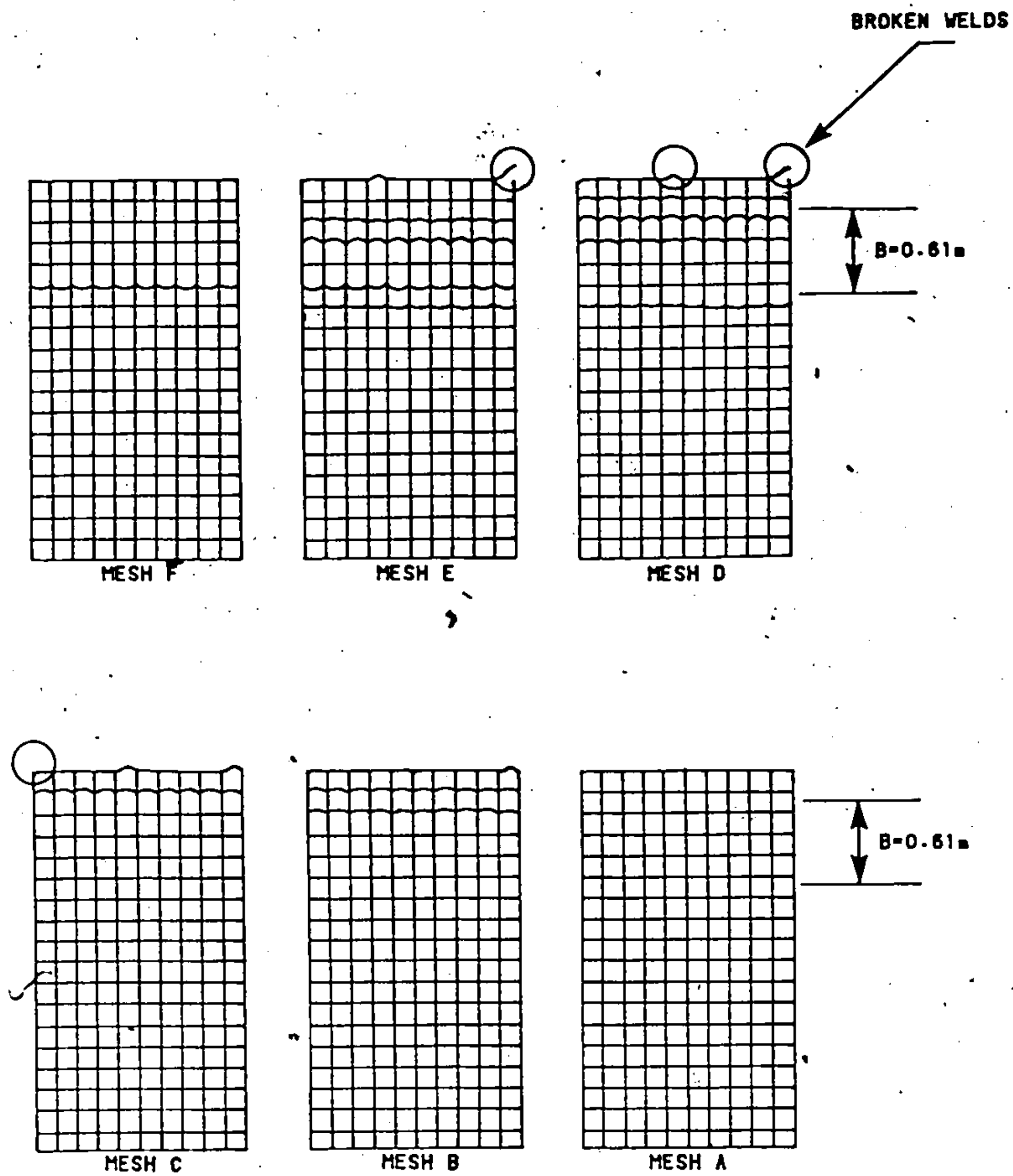

FIG. 4.4.16- DEFORMATION OF REINFORCING MESH AFTER LOAD TEST (REINFORCED WALL W-3)

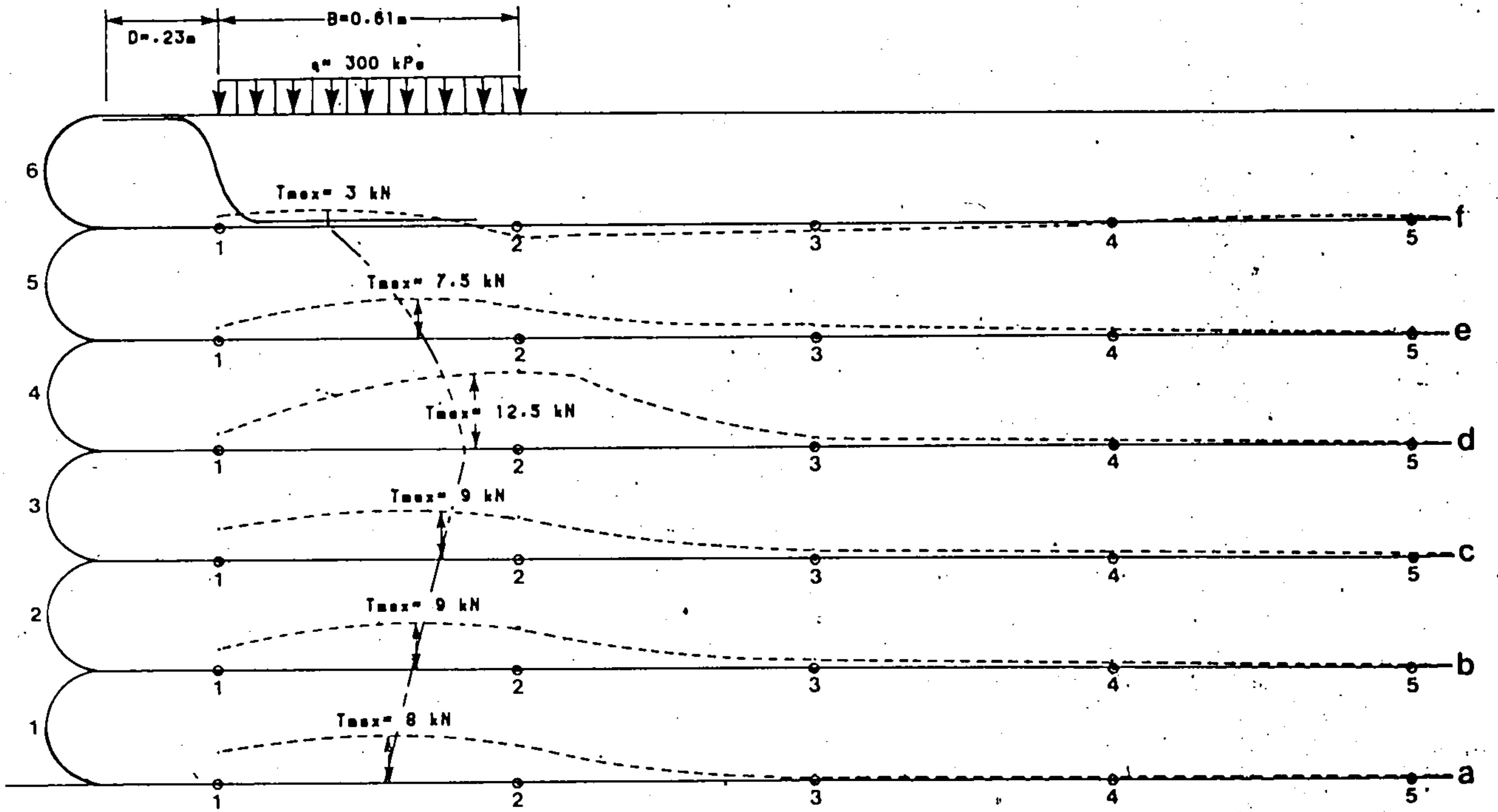

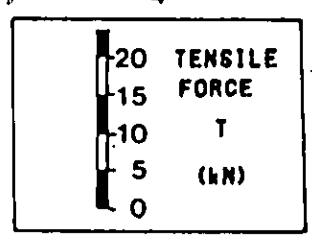

FIG 4.4.17- DISTRIBUTION OF TENSILE FORCES IN REINFORCING MESH FOR TEST W-3 AT A BEARING PRESSURE OF 300 kPa

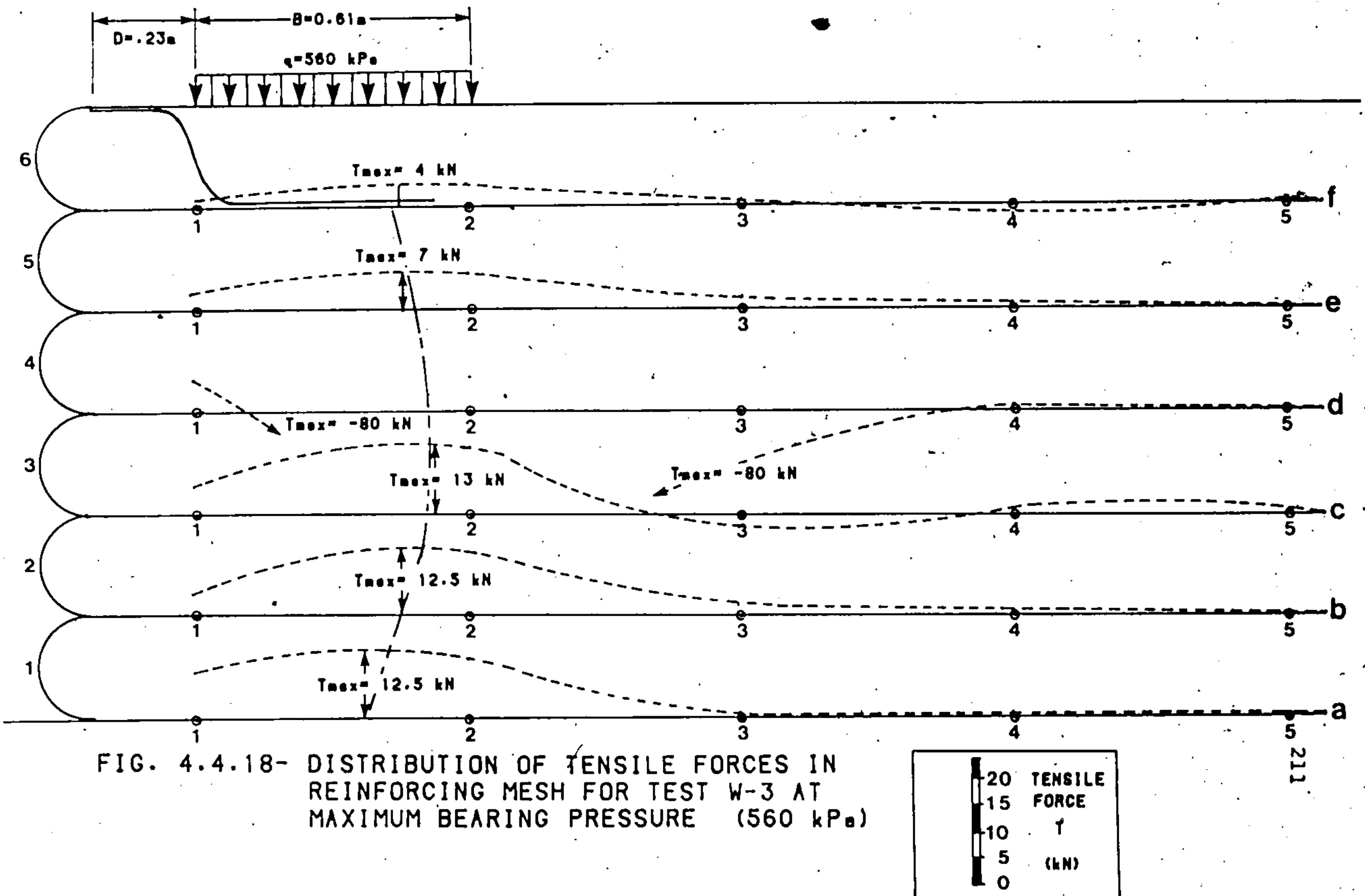

FIG. 4.4.18- DISTRIBUTION OF TENSILE FORCES IN REINFORCING MESH FOR TEST W-3 AT MAXIMUM BEARING PRESSURE (560 kPa)

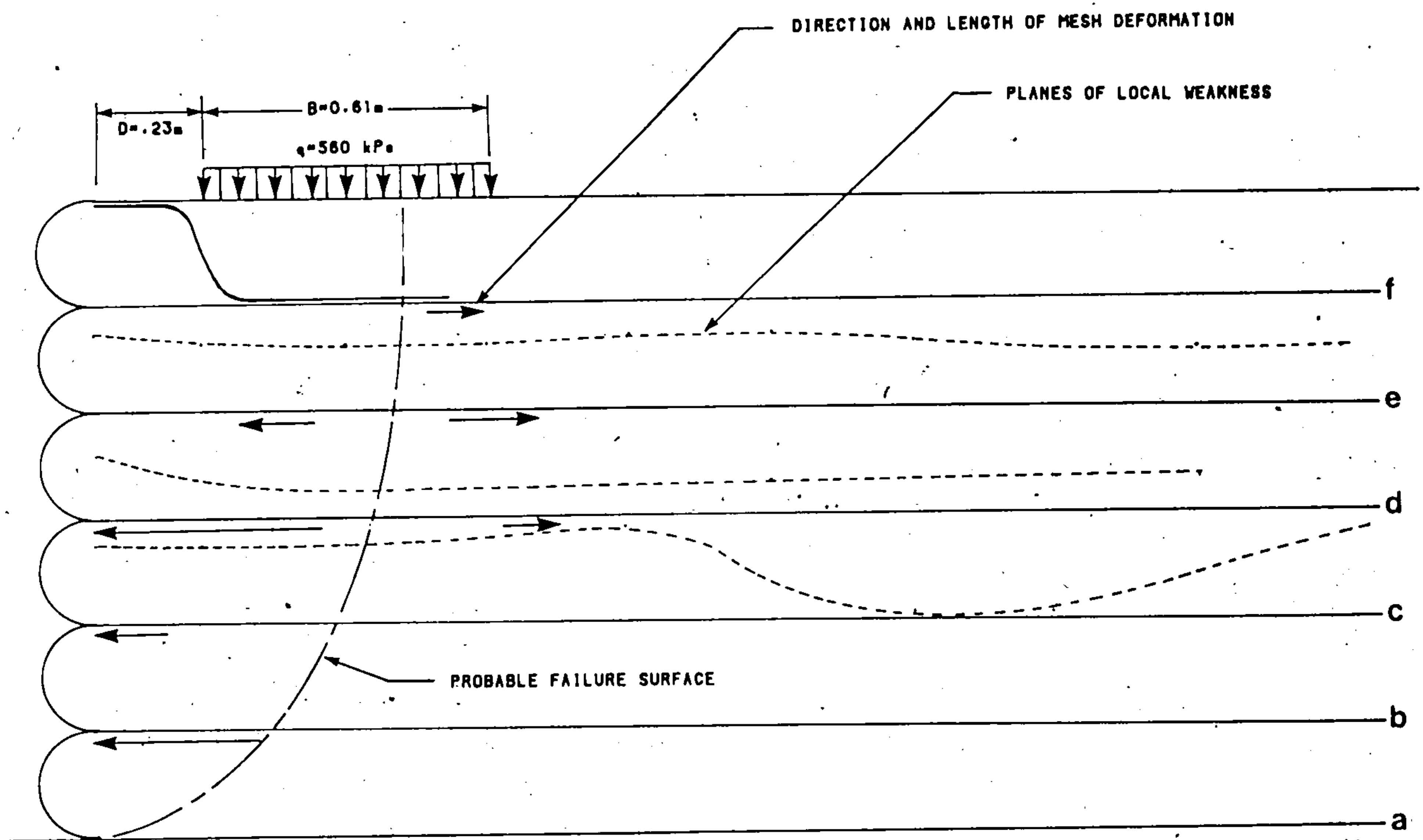

FIG. 4.4.19- FAILURE SURFACE (LOGARITHMIC SPIRAL)
FOR REINFORCED WALL STRUCTURE W-3

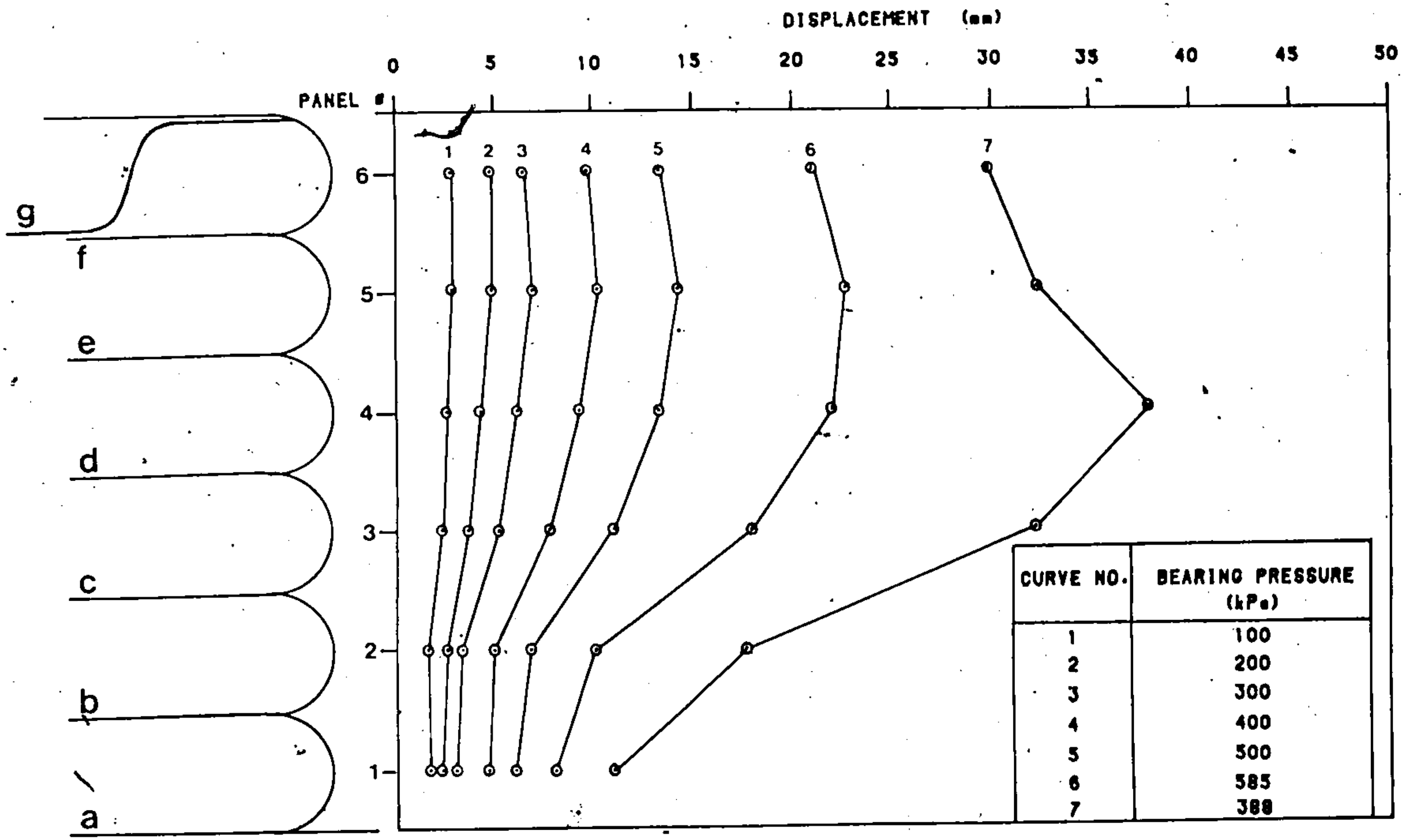

FIG. 4.4.20- WALL PANEL DISPLACEMENT WITH INCREASING BEARING PRESSURE FOR TEST W-3

4.4.3 Reinforced wall test W-4

Wall test W-4 was similar to wall test W-1 with only one parameter change,, the length of the reinforcing mesh, which was reduced to 1.37 metres.

Figure 4.4.21 illustrates schematically the test layout and figure 4.4.22 compares the loading behaviour of wall W-4 to walls W-1 and W-3.

Figure 4.4.23 shows the deformation of the upper two mesh layers after the loading test and figure 4.4.24 illustrates a probable failure mechanism. The wall panel displacements are shown on figure 4.4.25.

This last wall test demonstrates that by reducing the length of the reinforcement to 1.37 metres (100% of the total height of the wall) or by a factor of three compared to the initial test W-1, the bearing capacity of the wall structure is reduced by 37% (508 vs. 800 kPa), the footing settlement is increased by 73% at a bearing pressure of 500 kPa (34.3 mm vs. 19.8 mm) while the wall panel deflections remain compatible to those of test W-1, with the exception of panel 5 which is actually pulled in by the applied pressure.

The failure planes illustrated on figure 4.4.24 are substantiated by the deflection of the crossbar members in the upper mesh layers and by the behaviour of panel 5.

The pulling-in of the wall panels occurred because the mesh layers are not sufficient in length to be anchored in the soil stratum. Eventhough the bearing capacity is adequate when compared to tests W-2 and W-3, the excessive settlement of the footings and the unusual reaction to the applied load does not permit long term acceptance of an earth structure of similar configuration and parameters.

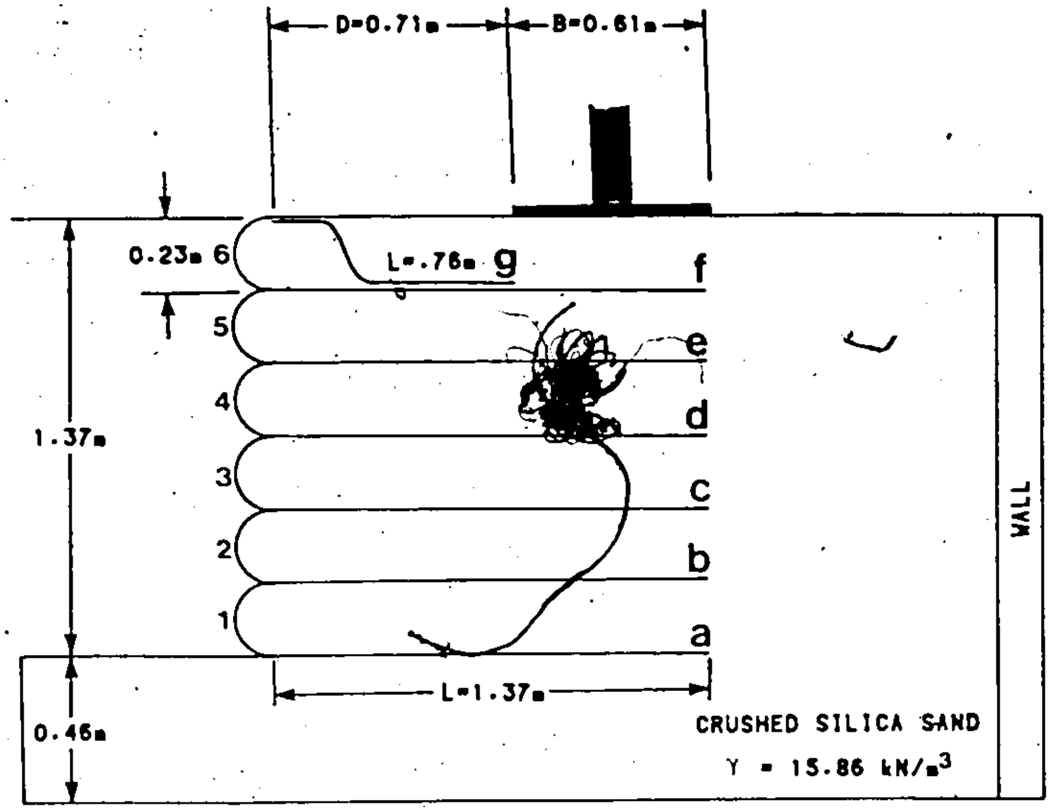

FIG. 4.4.21- SCHEMATIC REPRESENTATION OF REINFORCED WALL TEST W-4

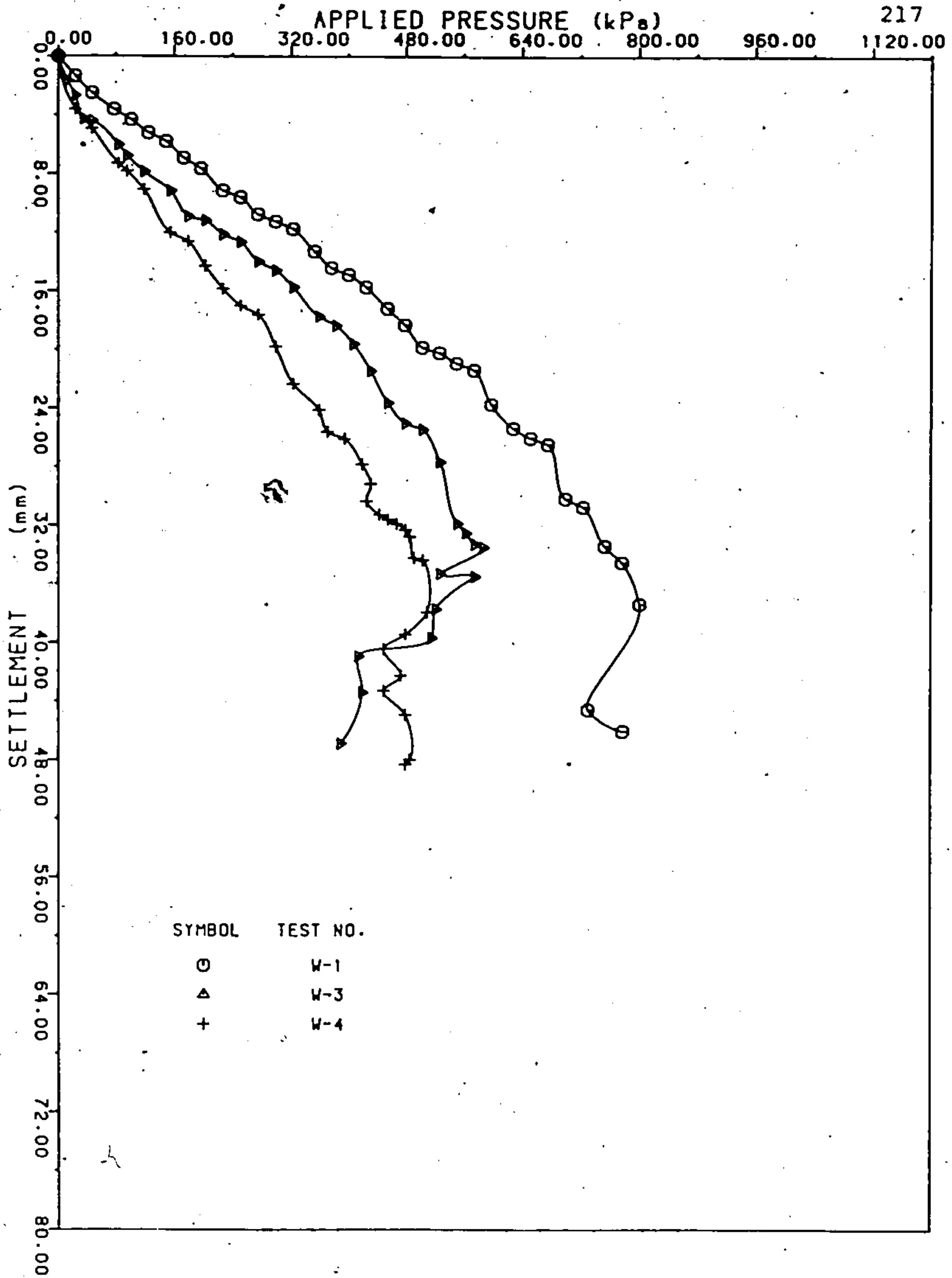

FIG. 4.4.22- APPLIED PRESSURE VS. FOOTING SETTLEMENT FOR WALL TESTS W-1, W-3 AND W-4

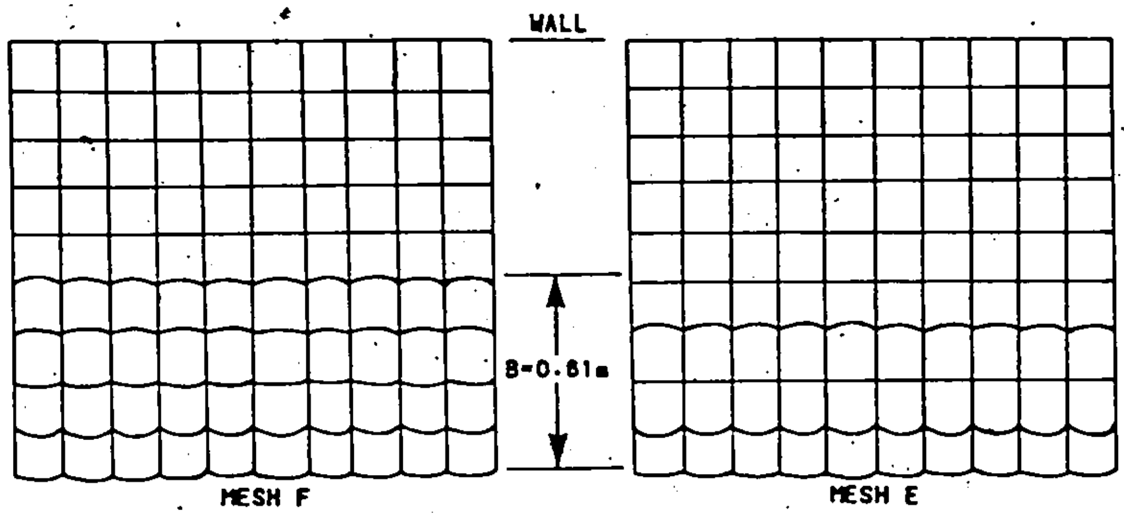

FIG. 4.4.23- DEFORMATION OF UPPER REINFORCING MESH LAYERS AFTER LOAD TEST (REINFORCED WALL W-4)

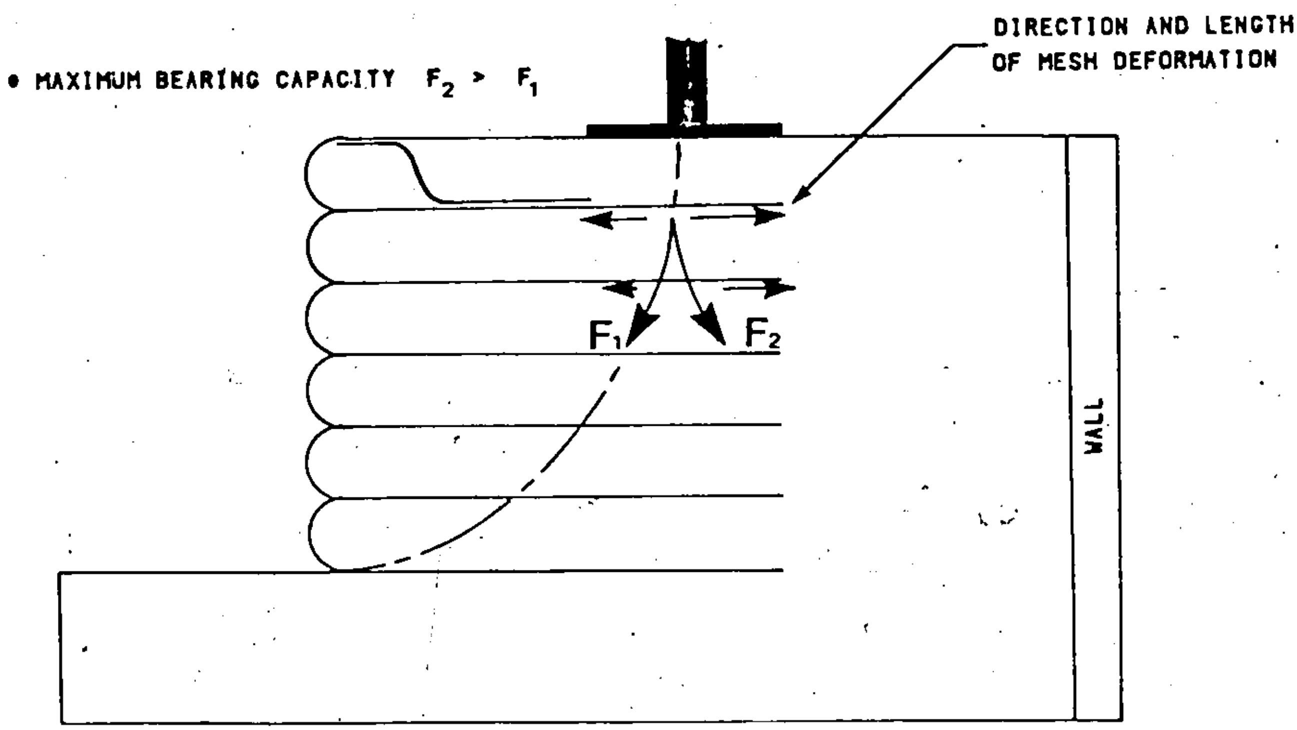

FIG. 4.4.24- FAILURE SURFACE FOR REINFORCED WALL W-4

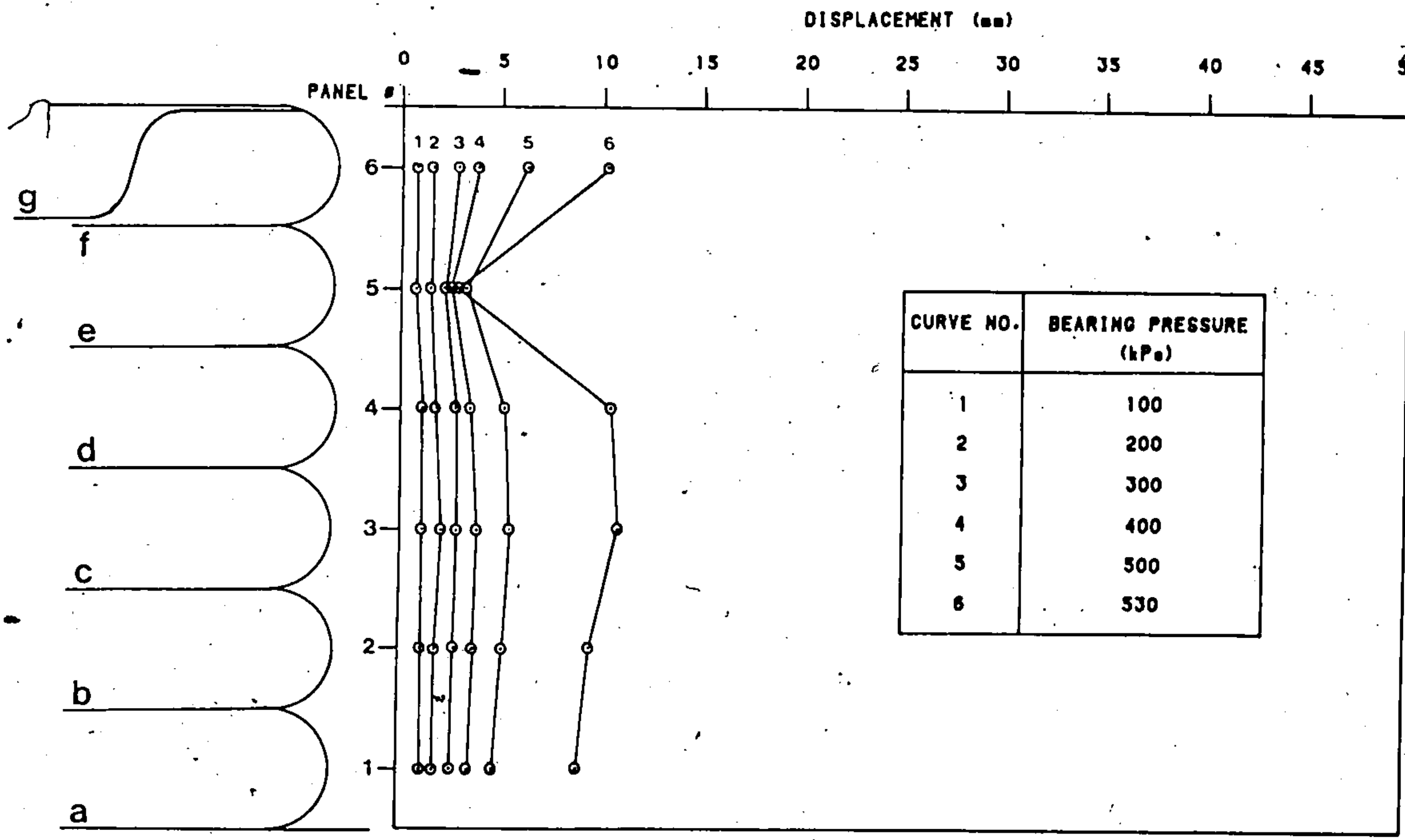

FIG. 4.4.25- WALL PANEL DISPLACEMENT WITH INCREASING BEARING PRESSURE FOR TEST W-4

Chapter V

APPLICATION OF THEORETICAL CONCEPTS TO EXPERIMENTAL RESULTS

The theoretical developments and formulae described in chapter II deal mostly with the Reinforced Earth Company's method of earth reinforcement. The formulae were developed for the long thin reinforcing strips which accomplish the stress transfer from earth, to tensile reinforcement through friction.

The research program described in this thesis, investigated the behaviour of earth structures reinforced with steel wire mesh. This system of reinforcement accomplishes the stress transfer by using the bearing pressure developed against the crossbars which then transmit the force from the soil mass to the longitudinal bars, hence developing tensile forces in these bars.

Therefore, only theoretical developments which analyse systems of reinforcement using wire mesh (VSL Retained Earth 1981) or synthetic grids (Iwasaki and Watanabe 1978, and Tensar grids 1982) bear a direct relationship to the research program.

5.1 PULLOUT TESTS

Since the peak load represents the maximum mobilized friction grip or bearing resistance against pullout, a factor of safety can be evaluated using the peak loads as failure loads and the design tensile loads can be calculated using the following equation (Chang et al., 1976):

$$FS = FS_{slippage} = \frac{P}{Ka\ \gamma\ H\ X\ Y}$$

P being the peak failure pulling load.

The application of this formula is rather restrictive since it uses the factor of safety as a means of evaluating the effectiveness of a reinforcing system. A factor of safety of four is not twice as safe as another system with a factor of safety of two. The relationship is not linearly proportional.

A more sensible way to evaluate the effectiveness of the different reinforcing systems is to compare the skin friction force introduced into the system. The skin friction force can be evaluated by the following equation (Chang et al., 1976):

$$\text{Skin friction force} = 2F = 2\ \gamma\ H\ b\ L\ \tan\delta$$

where:

F = friction force on one face of the reinforcement in kN

b = width of reinforcing strip in metres

L = length of reinforcing strip in metres

δ = skin friction angle between soil and reinforcement

H = height of fill in metres above the reinforcement

γ = unit weight of soil in kN/m³

Therefore, the apparent friction angle between soil and flat or ribbed steel reinforcement can be found.

$$\tan \delta = \frac{2F}{2 \gamma H w L}$$

Table 15 summarizes herein these calculations.

Since the presence of strain gauges on flat strips influences greatly their pullout resistance (four fold increase), only the flat strips with no gauges are examined.

Table 15 shows that the ribs on the Reinforced Earth strips increase the apparent skin friction angle between soil and steel and increase the peak pullout load by a factor of ten.

TABLE 15

Skin friction angle for flat and ribbed strips

test#	Reinf. systems	peak pullout load (kN)	width b (m)	length L (m)	over-burden pressure (kPa)	tan δ apparent coef. of friction	δ apparent skin friction angle (deg.)
1	flat	1.04	.038	3	22.1	.206	11.7
2	flat	0.97	.038	3	21.7	.196	11.1
11	flat	0.66	.038	1	21.1	.411	22.4
avg.	ribbed	10.16	.040	3	21.7	1.95	62.9

However, since the stress transfer mechanism of the steel wire mesh is fundamentally different from the flat or ribbed strips, an alternative way to evaluate the coefficient of friction between the reinforcing element and the soil mass is to calculate the anchorage factor, A_c.

The anchorage factor is measured by the following equation (Al-Yassin 1980):

$$A_c = \frac{P_{max}}{\sigma_v \, b \, d \, N}$$

where

P_{max} = maximum pullout load

σ_v = normal pressure

b = width of cross bars

d = diameter of cross bars

N = number of cross bars

Table 16 summarizes the anchorage factor calculations for the steel wire mesh reinforcing system, and figure 5.1.1 shows the relationship between the normal pressure and the anchorage factor for different cross bar widths.

An extrapolation of the curves in figure 5.1.1 towards the higher normal pressures that are encountered in actual earth structures indicates that the anchorage factor stabilizes itself at an approximate value of 45 for the 6x6 sections and a value of 65 for 12x6 and 18x6 sections.

Hence, the anchorage factor A_c, can be employed as a design parameter for wire mesh reinforced structures such as embankments and walls.

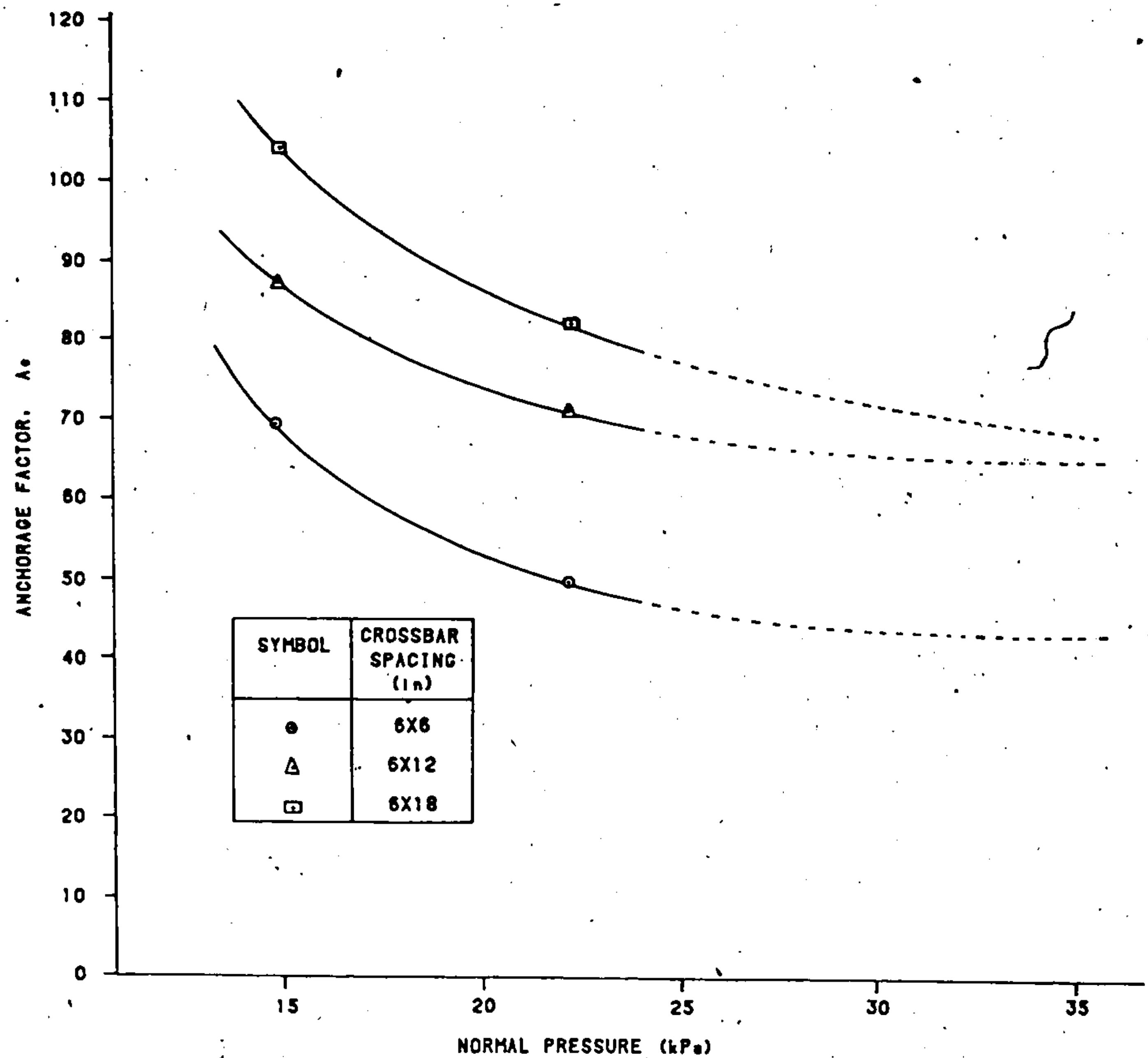

FIG. 5.1.1- RELATIONSHIP BETWEEN NORMAL PRESSURE AND ANCHORAGE FACTOR FOR VARYING CROSSBAR WIDTHS

TABLE 16

Anchorage factor for wire mesh elements

test#	cross bar spacing (in)	peak pullout load (kN)	width b (m)	length L (m)	over-burden pres-sure (kPa)	number of cross bars N	anchorage factor A_c
28	6x6	31.57	.457	1.93	22.1	13	50.1
29	6x6	29.15	.457	1.93	14.7	13	69.5
30	12x6	24.41	.457	1.93	22.1	7	71.9
31	12x6	19.82	.457	1.93	14.7	7	87.8
32	18x6	20.01	.457	1.93	22.1	5	82.6
33	18x6	16.80	.457	1.93	14.7	5	104.2

5.1.1 Comparison of reinforcing systems at the same stress level

A valid criticism of pullout tests which try to demonstrate that one reinforcing system is superior to another is that each system is stressed to different levels; i.e. at pullout, the applied stress in the wire mesh is much greater than in the ribbed strips.

Tables 17 and 18 present a comparison between the ribbed strips and the wire mesh when an identical working stress is applied to the reinforcing elements. A comparison can be made by calculating the volume of steel reinforcement necessary to resist a given load at a given stress level.

Table 17 shows the wire mesh members reaching and even exceeding the working stress under peak pullout loads while the ribbed strips reach only 1/6 of working stress.

However, by establishing a common stress level at which comparisons are made, table 18 shows that the wire mesh system requires less than 15% of the volume of steel necessary for the ribbed strips to resist the working stress. This demonstrates not only the efficiency but also the economy of the wire mesh system.

TABLE 17

Working stress analysis of reinforcing systems

reinf. system	load at rupture (kN)	cross-sectional area (mm²)	stress at rupture (MPa)	peak pullout resistance (kN)	assumed working stress (MPa)	tensile load at working stress (kN)
ribbed L=3m	90	200	450	10.2	300	60
	number of longitudinal bars					
	(1 bar)	(1 bar)	(1 bar)	(4 bars)	(4 bars)	(4 bars)
wire mesh L=1.93m						
6x6	12.3	18.1	680	31.6	300	21.6
6x12	12.3	18.1	680	24.4	300	21.6
6x18	12.3	18.1	680	20.0	300	21.6

TABLE 18

Comparison of reinforcing systems at working stress

reinf. system	volume of steel @ peak pullout load (m^3)	required volume of steel @ working stress (m^3)	required volume of steel for 60 kN tensile load (m^3)	weight of steel (kg)	steel ratio by weight
ribbed L=3m	.0006	.0035	.0035	27.3	1:1
wire mesh L=1.93m					
6x6	.00025	.00017	.00047	3.7	7.4:1
6x12	.00020	.00018	.00050	3.9	7.0:1
6x18	.00018	.00019	.00053	4.1	6.6:1

5.2 VARIATION OF FRICTION ANGLE WITH STRAIN

A major constraining factor for most engineering situations is the level of settlement which may be permitted without endangering the serviceability of the structure. In addition, the settlement (axial strain) determines the internal angle of friction of the loaded soil. As the axial strain (or lateral strain) is increased, the angle of internal friction of the soil will increase until the ultimate friction angle is reached.

Therefore, in order to use the appropriate angle of friction in the subsequent design procedures, the ϕ-strain relationship must be investigated.

Figures 4.2.9 to 4.2.12 compared the axial strain imposed on the triaxial tests with the deviator stress and the volumetric strain at varying confining pressures for reinforced and non-reinforced silica sand samples.

The lateral strain may be evaluated using Poisson's ratio which is the ratio of the lateral strain to axial strain during a compression test with axial loading. However, Poisson's ratio is unknown for the crushed silica sand and the following relationship is utilized for the evaluation of the lateral strain, assuming the sample deforms as a rigid cylinder.

$$\frac{dV}{V} = \frac{-\delta L}{L} + 2\,\frac{\delta D}{D}$$

$$\text{or}\quad \frac{\delta D}{D} = \tfrac{1}{2}\left(\frac{dV}{V} + \frac{\delta L}{L}\right)$$

dV/V being the volumetric strain, $\delta L/L$ the axial strain and $\delta D/D$ the lateral strain.

A summary of the stress-strain relationships obtained from figures 4.2.9 to 4.2.12 for the crushed silica sand is shown in table 19 . From table 19 ,Mohr circles are drawn at varying levels of strain (axial and lateral).

Figures 5.2.1 and 5.2.2 illustrate the Mohr envelopes and the corresponding internal angle of friction of the silica sand for varying levels of axial and lateral strain respectively..

A relationship between the strain and internal angle of friction, ϕ , is established and presented in figure 5.2.3 for axial strain and figure 5.2.4 for lateral strain. Since Ka, the coefficient of active earth pressure is a function of ϕ, the ordinates for ϕ in figures 5.2.3 and 5.2.4 can be duplicated with ordinates for Ka.

It becomes possible to determine Ka for the crushed silica sand from the strain values. Figures 5.2.3 and 5.2.4 can be used as a design tool in the determination of factors of safety and bearing capacities for reinforced embankment and wall models.

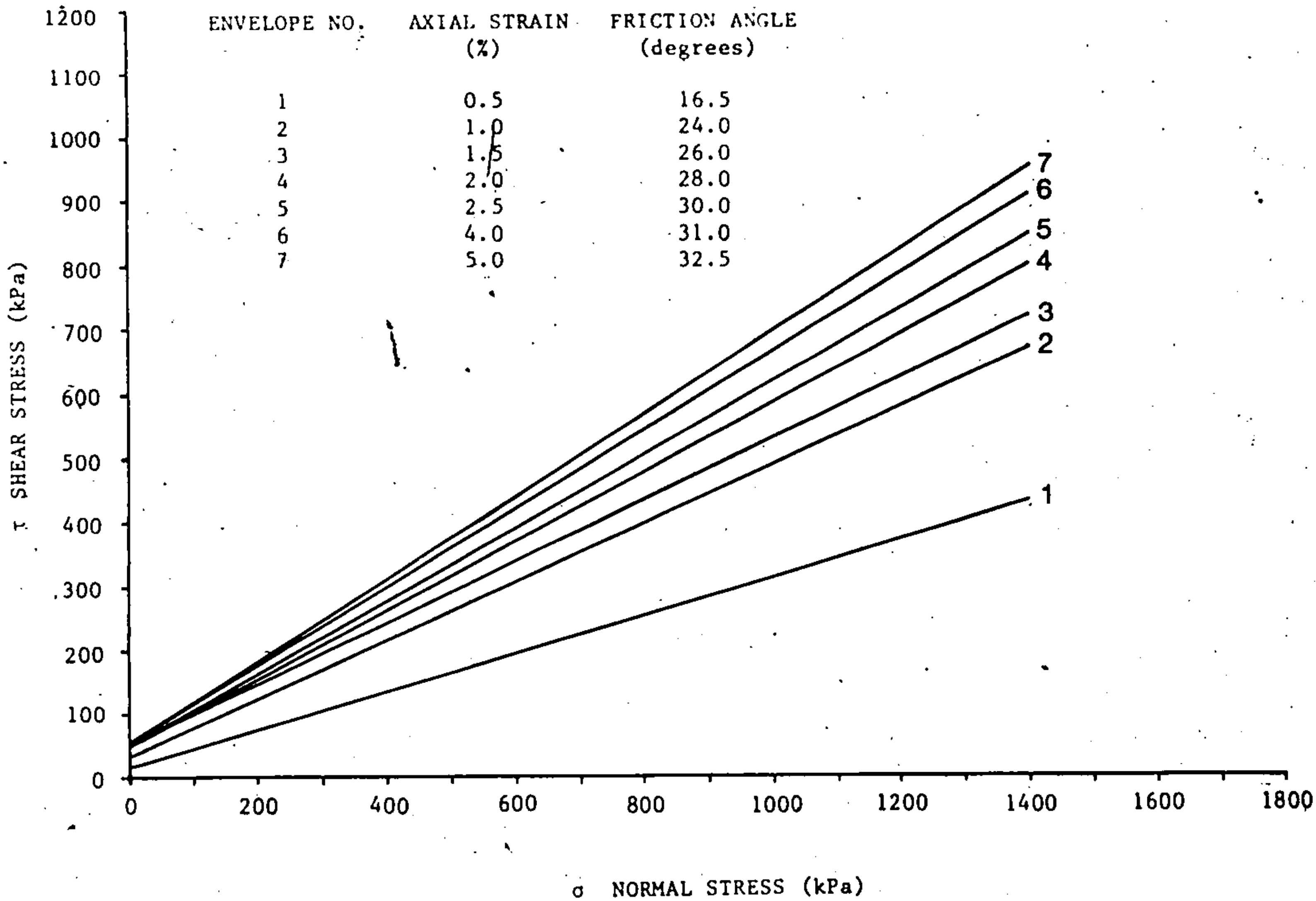

FIG. 5.2.1- MOHR FAILURE ENVELOPES FOR VARYING AXIAL STRAIN

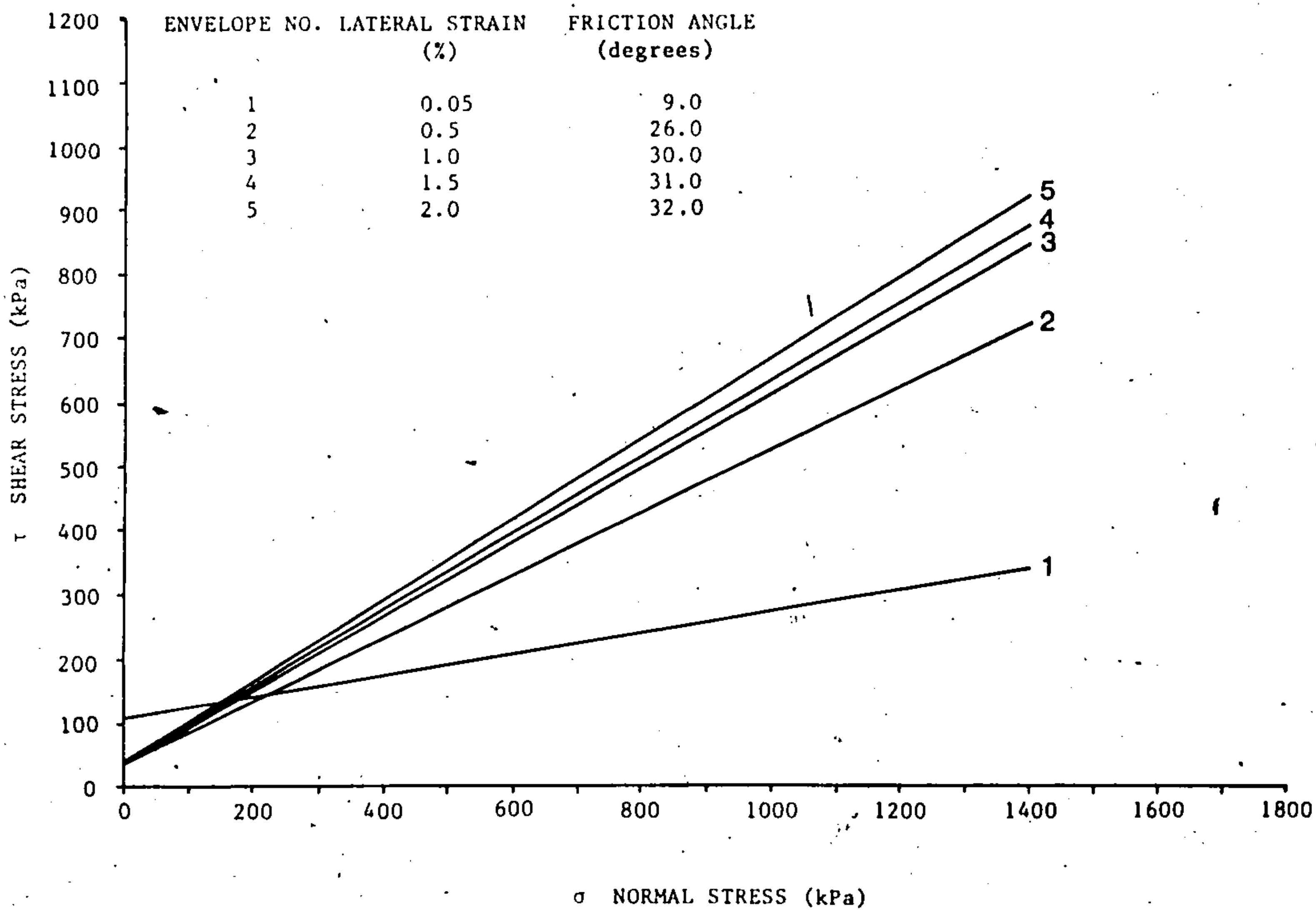

FIG. 5.2.2- MOHR FAILURE ENVELOPES FOR VARYING LATERAL STRAIN

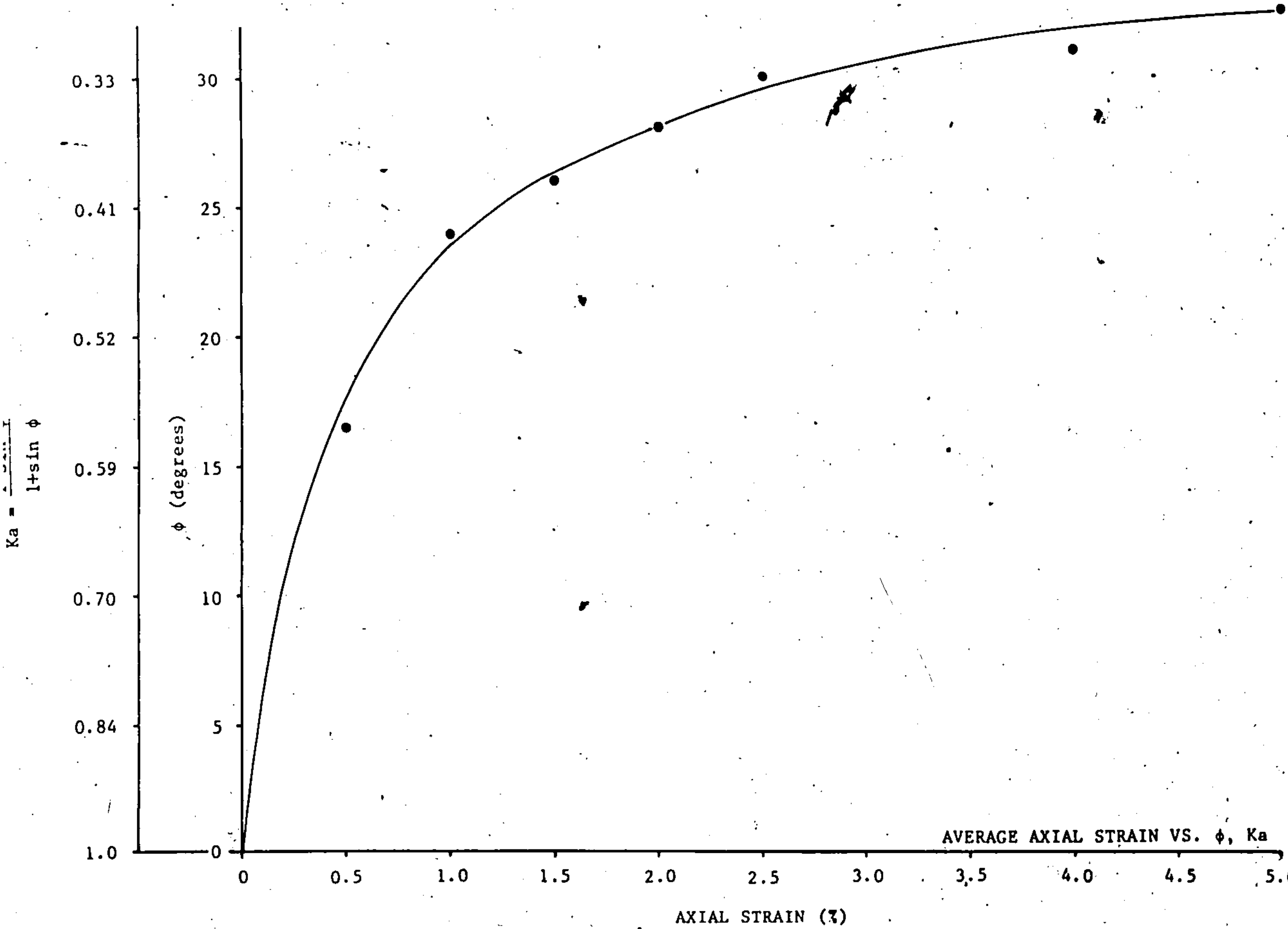

FIG. 5.2.3- VARIATION OF ANGLE OF FRICTION WITH AXIAL STRAIN

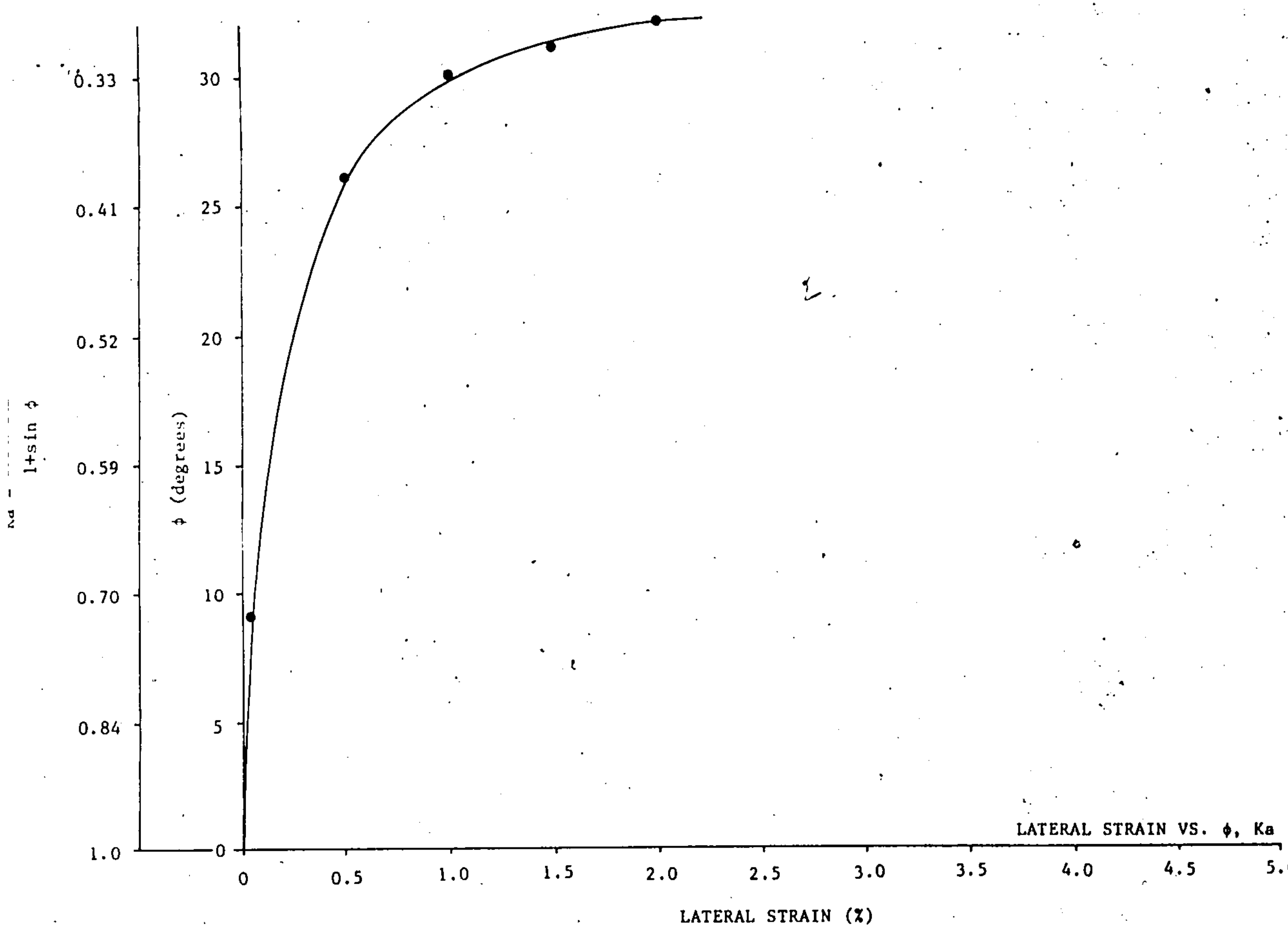

FIG. 5.2.4- VARIATION OF ANGLE OF FRICTION WITH LATERAL STRAIN

TABLE 19

Summary of stress-strain relationships for silica sand

confining stress σ_3 (kPa)	axial stress σ_1 (kPa)	axial strain $\delta L/L$ (%)	volumetric strain dV/V (%)	lateral strain $\delta D/D$ (%)
35	35	0	0	0
35	102	0.5	0.14	0.32
35	140	1.0	0.32	0.66
35	159	1.5	0.55	1.03
35	171	2.0	0.91	1.46
35	179	2.5	1.23	1.87
35	184	3.0	1.59	2.30
35	190	4.0	2.23	3.12
35	195	5.0	2.86	3.93
172	172	0	-0.48	-0.24
172	355	0.5	-0.62	-0.06
172	520	1.0	-0.62	0.19
172	591	1.5	-0.43	0.54
172	648	2.0	-0.24	0.88
172	672	2.5	0	1.25
172	696	3.0	0.24	1.62
172	729	4.0	0.76	2.38
172	753	5.0	1.19	3.10
345	345	0	-0.26	-0.13
345	738	0.5	-0.39	0.06
345	925	1.0	-0.46	0.27
345	1050	1.5	-0.46	0.52
345	1131	2.0	-0.39	0.81
345	1175	2.5	-0.26	1.12
345	1220	3.0	-0.09	1.46
345	1291	4.0	0.35	2.18
345	1345	5.0	0.78	2.89
551	551	0	-0.43	-0.22
551	1033	0.5	-0.61	-0.06
551	1431	1.0	-0.65	0.18
551	1551	1.5	-0.65	0.43
551	1694	2.0	-0.57	0.72
551	1774	2.5	-0.43	1.04
551	1846	3.0	-0.26	1.37
551	1953	4.0	0.26	2.13
551	2024	5.0	0.65	2.83

5.3 REINFORCED EMBANKMENT TESTS

The stability analysis of an embankment can be investigated by various methods and design procedures. Two methods of analysis which have been applied previously to wire mesh reinforced embankments are investigated and compared to the experimental results in the following section.

These methods are:

1. sliding block analysis
   a) Iwasaki and Watanabe (1978)
2. circular failure surface analysis
   a) Tobutt (1981)
   b) Tensar grids (1982)

5.3.1 Sliding block analysis

Using the analysis method described by Iwasaki and Watanabe (1978), a comparative study of the factors of safety for the experimental embankments can be performed.

The safety factor for the reinforced embankment becomes:

$$FS = \frac{R_s + R_n}{P}$$

where R_s is the resistance of the soil against the earth pressure P, and R_n is the resistance of the reinforcement against sliding.

As in section 2.5, R_n becomes:

$$R_n = 2 f \ [(W_L/B) + 1/2 \ \gamma H] \ L_1 + 1/4 \ \gamma \ H \ L_2$$

Table 20 summarizes the experimental results for embankments with a 2:1 slope. Using the average axial strain values obtained at the maximum bearing pressure, the corresponding internal angle of friction for each embankment test is determined from figure 5.2.3.

TABLE 20

Characteristics of reinforced embankment tests

test characteristics	maximum bearing pressure (kPa)	settlement of footings @ max. bearing pressure (mm)	axial strain @ max. bearing press. (average) (%)	internal angle of friction (degrees)	Ka
non-reinforced 2:1 slope	210	31	1.69	27	.376
mesh: 6x12 2:1 slope Y=.30m	251	20	1.09	24	.410
mesh: 6x6 2:1 slope Y=.15m	538	37	2.02	28	.360

TABLE 21

Analysis of embankments by sliding block method

test	factor of safety by sliding block analysis with $\phi=35°$ no surcharge	factor of safety by sliding block analysis with $\phi=35°$ @ max. bearing pressure	internal angle of friction by strain (degrees)	factor of safety by sliding block analysis with ϕ from strain no surcharge	factor of safety by sliding block analysis with ϕ from strain @ max. bearing pressure
non-reinforced	5.2	0.25	27	2.8	0.12
reinforced no. 2	19.2	0.71	24	11.4	0.42
reinforced no. 3	28.7	0.51	28	20.9	0.37

It becomes apparent that the introduction of the reinforcing mesh in the embankments produces a significant increase in the factor of safety (table 21) when no surcharge is applied to the embankment. However, the sliding block method of analysis is overly conservative in estimating the factors of safety when a surcharge is applied to the crest of the embankment. The design procedure leads to an unacceptable underestimation of the bearing capacity of footings on embankments.

5.3.2 Circular failure surface analysis

Tobutt (1981) and Tensar (1982) utilized a slightly modified Bishop method of slices which includes a resistance moment of the reinforcement about the slip circle centre which is added by superposition to the existing resistance moment of the unreinforced embankment.

Using the slope stability computer program for Bishop's method of analysis (Lam and Trak, 1982), a second comparative study of factors of safety for the embankment tests is ~~produced~~. Figure 5.3.1 illustrates the critical slip circles which were obtained for a non-reinforced embankment with varying levels of surcharge. These critical failure surfaces, determined by computer analysis, correspond more or less to the actual slip surfaces in the reinforced embankments and are therefore selected for the stability analysis of the reinforced embankments.

For a non-reinforced embankment, the factor of safety is determined by the following equation:

$$FS = \frac{S\ L\ R}{(Wx) + (qe')}$$

where S is the shear strength of the soil, L, the length of the slip plane, R, the radius from the centre of rotation of the slip plane, W, the weight of the earth segment, x, the lever arm of the earth segment to the centre of rotation, q, the surcharge and e', the eccentricity of the surcharge to the centre of rotation.

For a reinforced embankment, the resistance moment of the reinforcement is superimposed onto the above equation.

$$FS = \frac{S\ L\ R + Ty}{(Wx) + (qe)}$$

T being the permissible tensile load on the reinforcement. and y, the lever arm from the centre of gravity of the tension zone to the centre of rotation of the slip plane.

From the pullout tests, the permissible tensile load T on the wire mesh reinforcement was set at:

T = 35.8 kN per metre length per metre width
for the wire mesh with a 6x6 crossbar spacing

T = 27.7 kN per metre length per metre width
for the wire mesh with a 6x12 crossbar spacing

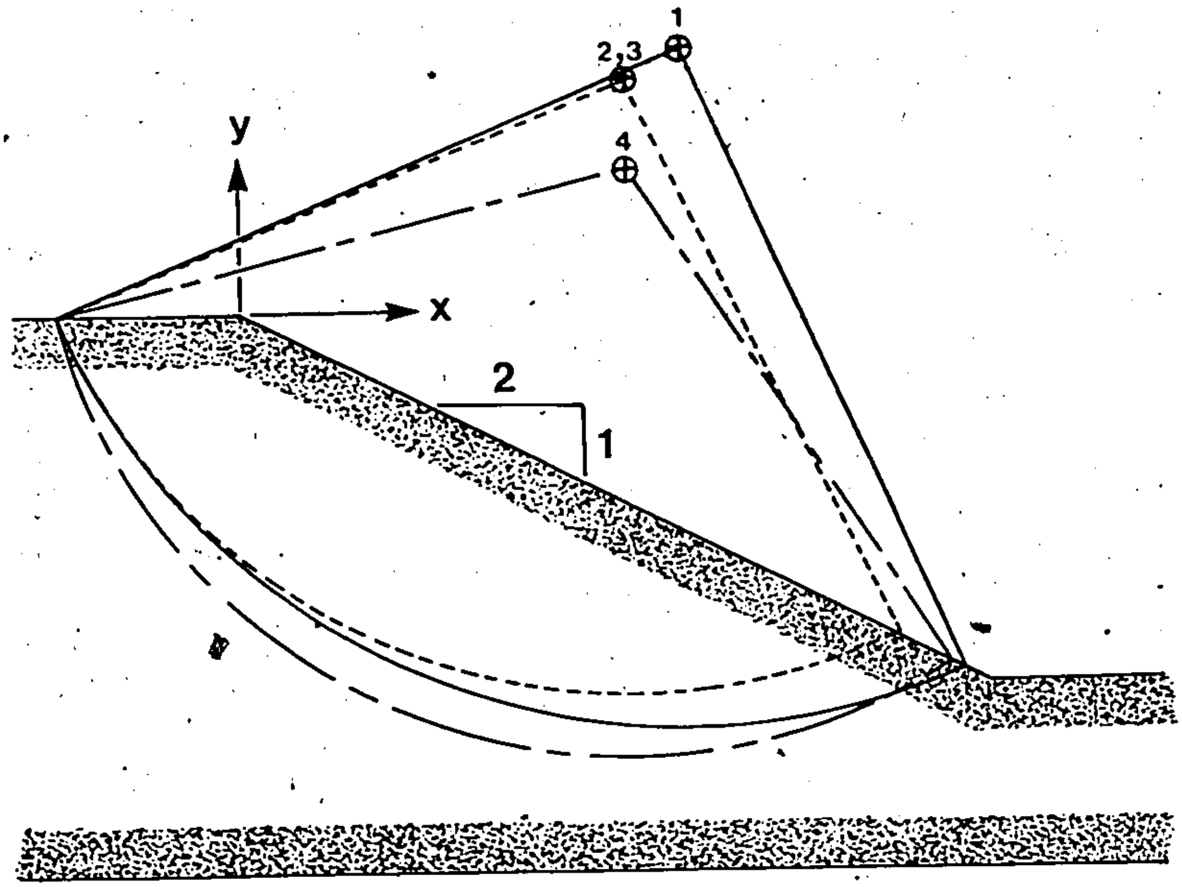

SLIP CIRCLE	DISTANCE FROM CREST x (m)	DISTANCE FROM CREST y (m)	SURCHARGE LOAD (kPa)	CALCULATED FACTOR OF SAFETY*
1	1.47	0.86	0.0	1.62
2	1.27	0.76	210.0	0.58
3	1.27	0.76	251.0	0.483
4	1.27	0.46	538.0	0.004

* USED IN LATER CALCULATIONS

FIG. 5.3.1- CRITICAL SLIP CIRCLES FOR NON-REINFORCED EMBANKMENTS WITH VARYING LEVELS OF SURCHARGE (BISHOP'S ANALYSIS)

The pullout tests also demonstrated that the optimum adherence length was approximately two metres for the wire mesh reinforcement. No significant increase in permissible tensile load occurs for wire mesh layers longer than two metres and an adherence length of three metres results in the mesh failing in tension.

Therefore, using the critical slip surfaces determined by Bishop's analysis for a non-reinforced embankment and superimposing the resistance moment of the reinforcement (maximum adherence length of two metres), the factors of safety for the reinforced embankments are determined and summarized in table 22 .

Once again, the introduction of the wire mesh reinforcement in the embankments increased the initial factor of safety significantly when no surcharge is applied (from 1.6 for a non-reinforced embankment to 26.5 for reinforced embankment no. 3). However, no clear trend is apparent when the factors of safety of the reinforced embankments at maximum bearing pressure are compared to the experimental value (FS= 1.0). The variation is due to the many parameters which affect not only the experimental models but also the design formulae.

Owing to the limited number of reinforced embankment tests that were performed, an extensive analysis and determination of factors of safety for reinforced embankments is beyond the scope of this thesis.

TABLE 22

Analysis of embankments by the Bishop method

test characteristics	maximum bearing pressure (kPa)	internal angle of friction by axial strain (degrees)	factor of safety by Bishop's method of analysis: no surcharge, $\phi=35°$	no surcharge, ϕ from axial strain*	@ maximum bearing pressure, $\phi=35°$	@ maximum bearing pressure, ϕ from axial strain*
non-reinforced	210	27	2.2	1.6	0.8	0.6
reinforced embankment no. 2	251	24	13.6	13.0	1.7	1.4
reinforced embankment no. 3	538	28	27.1	26.5	1.4	0.73

* average value, assuming strain = (total displacement)/(total depth)

However, it can be said that the design methods utilized in the analysis of wire mesh reinforced embankments cannot determine accurately bearing capacities of large scale model embankments and must therefore be employed with caution. The caution is especially due when the maximum friction angle of the soil is used, as the safety factor becomes unconservative.

5.4 REINFORCED WALL TESTS

In analysing theoretically the reinforced wall models, two design procedures which utilize wire mesh or polymer grids are suitable for the reinforcing material employed in the models.

The Tensar method (1982), described in section 2.13.2, puts forward the notion that the factor of safety against pullout of the reinforcing elements in a wall structure will be equal to:

$$FS = \frac{T_1}{Ka\ (\gamma h + q)\ d}$$

where Ka is the active earth pressure coefficient and equals $(1-\sin\phi)/(1+\sin\phi)$, T_1 is the permissible tensile strength of the reinforcing layer, d is the distance between reinforcing layers, and $\gamma h+q$ is the normal pressure applied to the layers.

The VSL Retained Earth method (1981), described in section 2.12, assumes that the factor of safety against pullout for the reinforced wall structures, after some mathematical manipulation, is equal to:

$$FS = \frac{d\ b\ \gamma\ h_i\ A_c\ ((L_b/a)+1)}{T_{max}}$$

where d is the diameter of the reinforcing bars, b is the width of the reinforcing mesh, A_c is the anchorage factor, L_b, the length over which bearing is considered, a is the spacing of the crossbars and finally T_{max} is the maximum force developed in the reinforcing elements.

Only the wall structures with the reinforcing mesh attached to the wall panels were investigated. As in the reinforced embankment analysis, the optimum length of adherence of the reinforcing mesh layers is set at two metres. Lengths greater than two metres do not increase substantially the pullout resistance of the mesh layers.

The factor of safety against pullout is measured for the mesh which sustained the greatest tensile load, therefore being most likely pulled out. In all cases where the mesh was attached to the wall panels, mesh E sustained the greatest tensile load.

As demonstrated in section 5.2, the internal angle of friction of the silica sand varies with both axial and lateral strains. Table 23 shows the strain values for each wall test and the corresponding friction angles. The lateral strain was obtained by measuring the outward deflection of the wall panels (figures 4.4.17,4.4.20 and 4.4.25) at maximum bearing pressure.

Hence, the factor of safety of the reinforced wall structures is calculated using both the axial and the lateral strains as a basis for Ka, the coefficient of active

TABLE 23

Characteristics of reinforced wall tests

test#	length of mesh (m)	ultimate bearing capacity q_{max} (kPa)	settlement (mm)	axial strain @ q_{max} (%)	wall panel displ. (mm)	maximum lateral strain @ q_{max} (%)	angle of friction for axial strain (degrees)	angle of friction for lateral strain (degrees)
W-1	4.27	800	37.3	2.04	20	0.47	28	26
W-3	2.74	585	37.9	2.07	23	0.84	28	29
W-4	1.37	508	33.5	1.83	10	0.73	27.5	28

earth pressure. Since these strain measurements are not available in practice for design purposes, the factors of safety are also calculated using 35° as the angle of friction.

Using the Tensar method of analysis, the factors of safety against pullout (none of the walls tested actually failed by pullout) for the reinforced walls are calculated and presented in table 24 . Discounting the special case of structure W-4, where the reinforcing mesh was not long enough to be anchored, the Tensar design method simulates closely the behaviour of the reinforced wall models, especially test W-1.

TABLE 24

Factor of Safety against pullout by the Tensar method

test no.	T kN/m per metre width	L adhe-rence length (m)	d (m)	$\gamma h+q$ (kPa)	factor of safety* $\phi=35°$	factor of safety* with ϕ from axial strain	factor of safety* with ϕ from lateral strain
W-1	35.8	2.0	.23	807	1.4	1.07	0.99
W-3	35.8	2.0	.23	592	1.9	1.42	1.46
W-4	35.8	0.8	.23	515	.45	.68	.68

* experimental wall models did not fail in pullout mode

Furthermore, since test W-3 was strain gauged, the actual tension in the longitudianl bars of the wire mesh is known and can be applied to the design formula. Also, as the lateral strain of each reinforcing layer varied with depth, the internal angle of friction at each respective depth can be established. Table 25 illustrates the analysis for wall test W-3.

The factors of safety calculated using the Tensar method of analysis for reinforced walls are for the most part close to the experimental values (FS=1.0).

The VSL Retained Earth method of analysis for wire mesh reinforced walls was also used to investigate the factors of safety for the models. The analysis is presented in table 26

TABLE 25

Factors of safety for test W-3 using the Tensar method

mesh no.	depth (m)	tensile load @ max. bearing pressure (kN)	lateral strain (%)	Ka from lateral strain	factor of safety
f	.23	4	.80	.35	using lateral strain FS= 1.14
e	.46	7	.82	.35	
d	.69	13	.73	.36	using axial strain FS= 1.23
c	.92	13	.51	.39	
b	1.15	12.5	.33	.45	
a	1.37	12.5	.26	.48	

The VSL analysis shows a definite overestimation of the bearing capacity of footings on reinforced wall models. The analysis appears not to be applicable when a surcharge (strip footing) is added to the self-weight of the structure. Also, the VSL method determines the factor of safety for pullout failure; since no pullout of the mesh layers occurred, a factor of safety higher than reality is calculated.

TABLE 26

Factor of safety against pullout by the VSL method

test no.	length of mesh (m)	ultimate bearing capacity (kPa)	d (mm)	b (m)	A_c *	a (m)	T_{max} (kN)	L_b (m)	γh_i (kPa)	factor of safety'
W-1	4.27	800	4.8	1.5	45	.15	13	2.0	7.4	2.7
W-3	2.74	585	4.8	1.5	45	.15	13	2.0	7.4	2.7
W-4	1.37	508	4.8	1.5	45	.15	13	0.8	7.4	1.2

* conservative value of anchorage factor
' experimental wall models did not fail in pullout mode

5.4.1 Analysis by circular arc method

Using the modified Bishop analysis proposed in section 5.3.2 for embankments and adapting the method for reinforced wall structures, an overall factor of safety can be determined.

Figure 5.4.1 illustrates the failure surfaces for all three bolted wall models. The failure surfaces are circular approximations of the failure surfaces which were proposed in chapter four. Three different assumptions of stress distributions due to the surcharge load are investigated (figure 5.4.2).

These assumptions will influence the development of the shear strength of the backfill soil and the ensuing factor of safety for the reinforced wall models. The assumptions are:

1. 1:1 diffusion
2. 2:1 diffusion
3. vertical diffusion (extreme case)

An overall factor of safety for the wall structures is produced for each stress diffusion. A subsequent analysis taking only the reinforcing mesh into account and discounting the contribution from the shear strength of the backfill soil is also undertaken and yields a very conservative factor of safety for the wall models. The analysis results are presented in table 27 .

Test W-2 was previously omitted from the analysis since the reinforcing mesh was not bolted to the wall panels as with the rest of the wall models. The analysis of test W-4 indicates some anomalies which cast doubt on the test results. As shown in figure 4.4.25, the second wall panel from the top, was actually being pulled in by the surcharge load in test W-4. This demonstrates that the reinforcing mesh was not anchored in the backfill, therefore, caution must be exercised with regards to the results of test W-4. Hence, only tests W-1 and W-3 can be analysed with confidence. However, there are two variables between tests

TABLE 27

Factor of Safety against pullout by circular arc method

test no.	length of slip circle L (m)	radius of slip circle R (m)	FACTOR OF SAFETY			
			vertical diffusion	2:1 diffusion	1:1. diffusion	reinforcement only
W-1	2.0	2.7	2.25	3.35	3.63	0.78
W-3	1.6	2.1	2.06	2.63	2.63	0.64
W-4	1.8	2.2	1.12	2.18	2.45	0.33

W-1 and W-3, varying length of mesh and varying distance of footings from the wall panels, which makes a direct comparison between the tests difficult.

The limited number of models does not permit an extensive analysis of the factors of safety for different wall structures when the length of reinforcing mesh is reduced or when the footings are moved closer to the wall panels. Therefore, the present study can only be regarded as an initial step in the analysis of wire mesh reinforced wall structures.

SLIP CIRCLE	TEST	LENGTH OF MESH (m)	BEARING CAPACITY (kPa)	DISTANCE FROM CREST x (m)	DISTANCE FROM CREST y (m)	RADIUS OF SLIP CIRCLE (m)
1	W-1	4.27	800	1.00	1.13	2.68
2	W-3	2.74	585	1.25	0.25	2.10
3	W-4	1.37	508	1.00	0.55	2.20

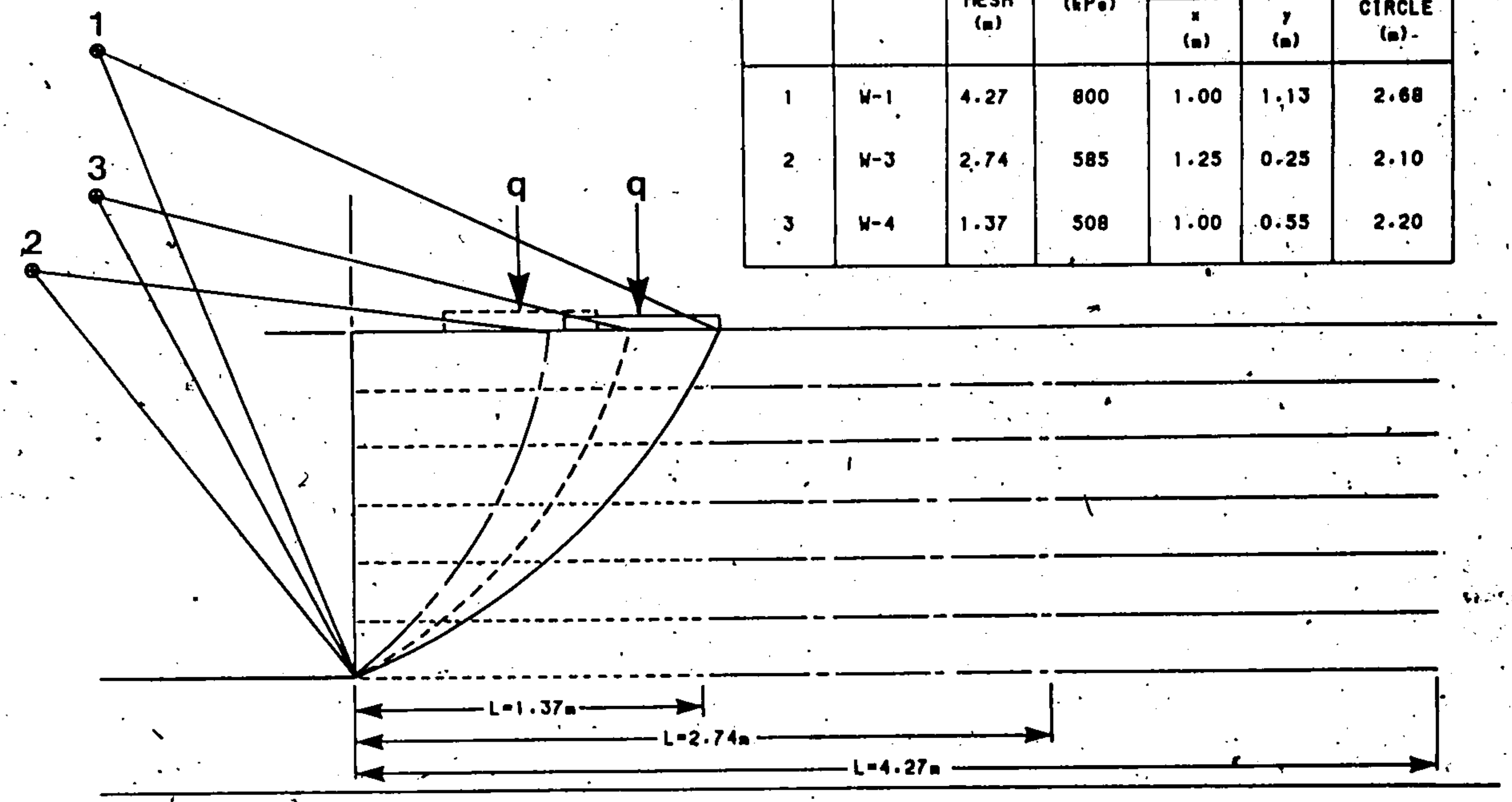

FIG. 5.4.1- CIRCULAR APPROXIMATION OF SLIP SURFACES FOR REINFORCED WALL TESTS

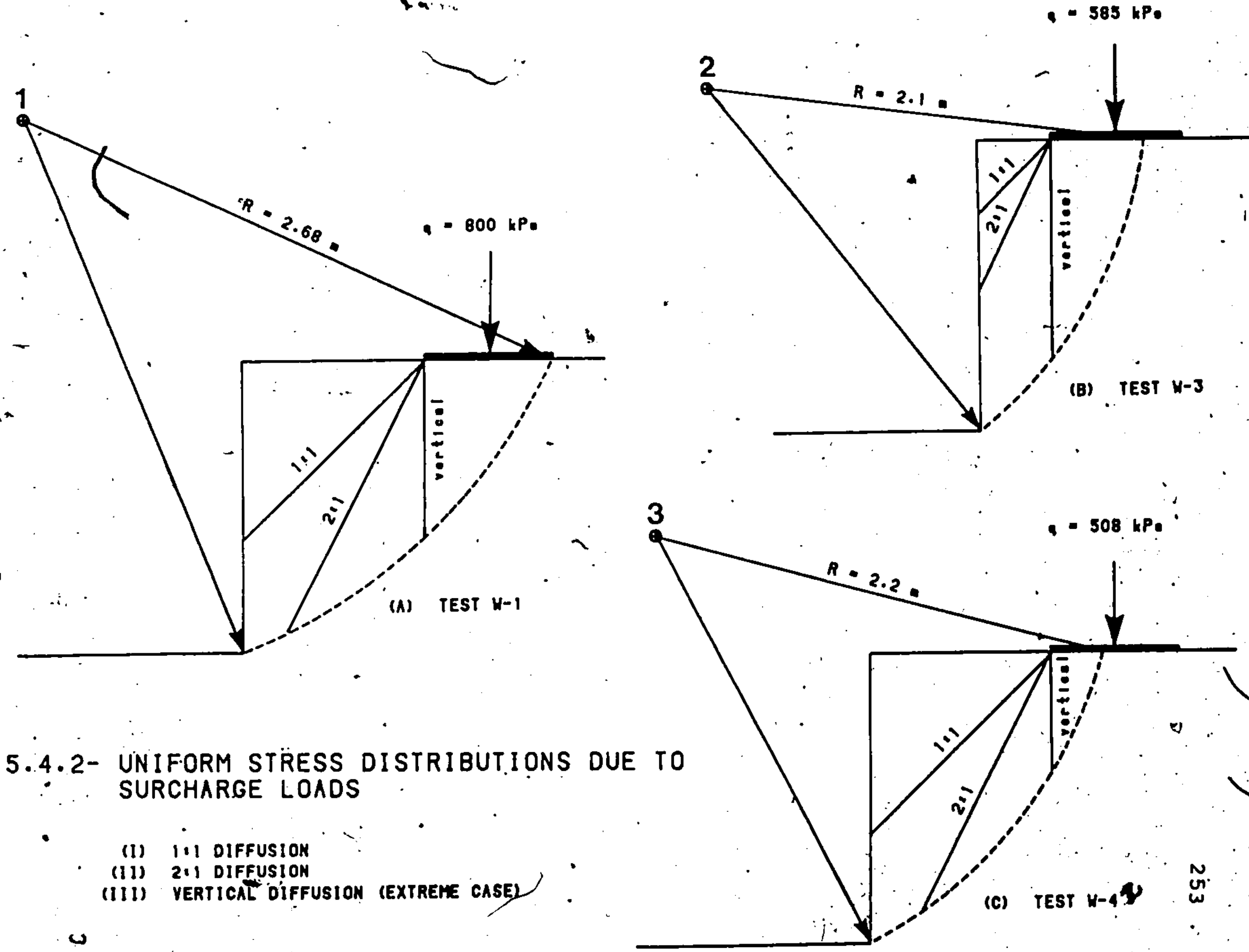

FIG. 5.4.2- UNIFORM STRESS DISTRIBUTIONS DUE TO SURCHARGE LOADS

(I) 1:1 DIFFUSION
(II) 2:1 DIFFUSION
(III) VERTICAL DIFFUSION (EXTREME CASE)

Chapter VI

CONCLUSIONS AND RECOMMENDATIONS

The experimental testing program previously described in this study permitted the analysis of earth structures with horizontal layers of steel wire mesh. The programme was composed of four distinct model tests and from these tests the following conclusions can be drawn:

1. Pullout tests

   a) For an identical working stress and weight, the standard wire mesh used as a temperature reinforcement in concrete floor slabs exhibits a pullout resistance that is more than five times that of the Reinforced Earth ribbed strips.

   b) If the length of the reinforcing strip is great enough that the system is considered anchored, the controlling factor becomes the structural strength of the reinforcing material.

   c) The anchorage factors determined from figure 5.1.1 were obtained by passing an empirical curve through the experimental data points and must be viewed with caution. It should be noted that linking the data points linearly would be unreasonable but would reduce the safety factors calculated in table 26.

2. Triaxial tests

   a) The introduction of wire mesh reinforcement in triaxial tests increases the load capacity of the structure (1.5 to 3.3 times greater) and reduces the volume change in the test samples (1.3 to 7.7 times smaller).

   b) The apparent angle of friction is increased from 35 degrees for the silica sand samples to 39.5 degrees for the composite samples (wire mesh-sand).

3. Embankment model tests

   a) Reinforcing mesh in embankments must be anchored beyond the probable failure path as to avoid becoming part of the outward sliding mass.

   b) The introduction of reinforcing mesh in embankments increases the ultimate bearing capacity of the embankment by as much as 156 percent and reduces the settlement of the footings by as much as 62 percent.

   c) No well defined failure paths were observed at maximum bearing pressures, however the reinforcing mesh layers assisted in the formation of shear surfaces.

   d) Design methods utilized in the analysis of wire mesh reinforced embankments do not determine accurately bearing capacities of large scale model embankments.

4. Wall model tests

   a) Tensile forces supplied to the mesh layers in reinforced wall structures reach a maximum at a height of H/3 from the top of the structure.

   b) Attaching the mesh to the wall panels distributes the confining effect of the reinforcement more uniformly over the soil stratum, therefore increasing the bearing capacity of the structure, decreasing the settlement of the footings and preventing failure by overturning.

   c) The position of the point load in a reinforced wall structure is of greater significance than the length of embedment when the mesh is anchored into the backfill.

   d) No well defined failure paths were observed at failure, however when the embedment length is sufficient to provide anchorage of the mesh layers, the critical failure path appears to assume a logarithmic spiral shape which is orthogonal to the surface and passes through the toe of the wall panels.

   e) In calculating the safety factors, all reinforcing mesh layers were assumed to be at maximum pullout load. Pullout of the mesh layers did not occur at failure loads, however rupture of reinforcing bars due to stress concentrations was observed.

Therefore it can be stated that maximum stress levels in the reinforcing elements were not reached simultaneously throughout the structure, stress concentrations appear to be transferred from layer to layer when bar rupture takes place in reinforcing elements. This phenomenon will reduce the calculated factors of safety substantially.

f) Design formulae, with the exception of the Tensar method, do not simulate accurately the behaviour of the reinforced wall models.

Due to the limited number of models that were constructed, the present study remains incomplete. Therefore, in order to complement this thesis, the author recommends the following series of tests:

1. Pullout tests under greater overburden pressures.
2. Reinforced enbankment tests with varying lengths of embedment of mesh and varying geometry.
3. Reinforced wall tests with varying lengths of embedment of mesh.
4. Reinforced wall tests under uniform load conditions.
5. Investigation of polymer plastic grids as reinforcing elements.

REFERENCES

1. Akinmusum, J.O., and Akinbolade, J.A., "Stability of loaded footings on reinforced soil", ASCE Journal of the Geotechnical Engineering Division, vol. 107, no. 6, pp. 819-827, June 1981.

2. Al-Hussaini, M.M., and Johnson, L.D., "Numerical analysis of a reinforced earth wall", ASCE Symposium on Earth Reinforcement, pp. 98-126, Pittsburgh, 1978.

3. Al-Hussaini, M.M., and Perry, E.B., "Field experiment of reinforced earth wall", ASCE Symposium on Earth Reinforcement, pp. 127-156, Pittsburgh, 1978.

4. Al-Yassin, Z.A., "Analysis of reinforced earth walls", Ph.D. Thesis, Dept. of Civil Engineering, University of California, Davis, 1979.

5. Al-Yassin, Z.A., "Laboratory pullout test results on VSL retained earth", VSL Corporation, Nov. 1980.

6. Bacot, J., Iltis, M., Lareal, P., Paumier, T., and Sanglerat, G., "Study of the soil reinforcement friction coefficient", ASCE Symposium on Earth Reinforcement, pp. 157-185, Pittsburgh, 1978.

7. Bacot, J., and Lareal, P., "Calculation of the critical height of failure for reinforced earth walls based on model studies", French text, Colloque International sur le Renforcement des Sols: Terre armeé et autres techniques, pp. 17-22, Paris, 1979.

8. Baguelin, F., "Construction and instrumentation of reinforced earth walls in French highway administration", ASCE Symposium on Earth Reinforcement, pp. 186-201, Pittsburgh, 1978.

9. Banerjee, P.K., "Principles of analysis and design of reinforced earth retaining walls", Journal of the Institution of Highway Engineers, pp. 13-18, Jan. 1975.

10. Bassett, R.H., and Last, N.C., "Reinforcing earth below footings and embankments", ASCE Symposium on Earth Reinforcement, pp. 202-231, Pittsburgh, 1978.

11. Bauer, G.E.A., and Gardner, N.J., "Investigation of reinforced earth structures- research proposal", University of Ottawa, Dec. 1980.

12. Bauer, G.E.A., Shields, D.H., and Scott, J.D., "The bearing capacity of footings on compacted approach fills", Ontario Joint Transportation and Communications Research Program- Final Report, University of Ottawa, 1978.

13. Binquet, J., "Analysis of failure of reinforced earth walls", ASCE Symposium on Earth Reinforcement, pp. 232-251, Pittsburgh, 1978.

14. Bishop, A.W., and Henkel, D.J., The measurement of soil properties in the triaxial tests. 2nd edition, Edward Arnold Ltd., 1962.

15. Bolton, M.D., Choudhury, S.P., and Pang, P.L.R., "Modelling reinforced earth", Ground Eng., vol. 11, no. 6, Sep. 1978.

16. Bolton, M.D., Choudhury, S.P., and Pang, P.L.R., "Reinforced earth walls: a centrifugal model study", ASCE Symposium on Earth Reinforcement, pp. 252-281, Pittsburgh, 1978.

17. Bowles, J.E., Engineering properties of soils and their measurements. McGraw-Hill Book Co., 1970.

18. Brinch Hansen, J., "A revised and extended formula for bearing capacity", bulletin no. 28, Danish Geotechnical Institute, pp. 5-11, Copenhagen, 1970.

19. Chang, J.C., Hannon, J.B., and Forsyth, R.A., "Interaction of earthwork reinforcement and soil", ASCE Journal of the Geotechnical Engineering Division, vol. no. GT, 1976.

20. Chang, J.C., Hannon, J.B., and Forsyth, R.A., "Pull resistance and interaction of earthwork reinforcement and soil- Multiple aspects of soil mechanics", Transportation research record 640, pp. 1-7, 1976.

21. Chapuis, R.P., "Stabilité interne des murs en Terre Armée", French text, Can. Geotech. J., vol. 14, pp. 389-398, 1977.

22. Chapuis, R.P., "La compression triaxiale des sols armés", French text, Can. Geotech. J., vol. 17, no. 2, pp. 153-164, May 1980.

23. Craig, R.F., Soil mechanics. Van Nostrand Reinhold Co., 1974.

24. Deschênes, J.-H., "Bearing capacity of footings close to slopes of cohesionless soil", Ph.D. Thesis, Dept. of Civil Engineering, University of Ottawa, 1978.

25. Elias, V., "Friction in reinforced earth utilizing fine grained backfills", Colloque International sur le Renforcement des Sols: Terre Armée et autre Techniques, pp. 435-438, Paris, 1979.

26. Felio, G.Y., "Reinforced earth- research project", Unpublished report, University of Ottawa, March 1981.

27. Felio, G.Y., "General maintenance of the sandbox facilities", Unpublished report, University of Ottawa, March 1981.

28. Forsyth, R.A., "Alternative earth reinforcements", ASCE Symposium on Earth Reinforcement, pp. 358-370, Pittsburgh, 1978.

29. Hasnain, M., "Shear strength characteristics of a crushed sand", M.A.Sc. Thesis, Dept. of Civil Engineering, University of Ottawa, 1974.

30. Herrmann, L.R., and Al-Yassin, Z.A., "Numerical analysis of reinforced soil systems", ASCE Symposium on Earth Reinforcement, pp. 428-457, Pittsburgh, 1978.

31. Holtz, R.D., "Special applications- state of the art and general report", ASCE Symposium on Earth Reinforcement, pp. 77-97, Pittsburgh, 1978.

32. Hoshiya, M., "Strength of reinforced earth retaining walls", ASCE Symposium on Earth Reinforcement, pp. 458-472, Pittsburgh, 1978.

33. Houle, C.A., "Analysis of reinforced earth structures using physical models", M. Eng. Thesis, Dept. of Civil Engineering, Carleton University, 1982.

34. Ingold, T.S., "Reinforced earth- theory and design", Highw. Eng., vol. 28, no. 7, pp. 2-14, July 1981.

35. Iwasaki, K., and Watanabe, S., "Reinforcement of railway embankments in Japan", ASCE Symposium on Earth Reinforcement, pp. 473-500, Pittsburgh, 1978.

36. Jones, C.J.F.P., "Practical design considerations", Symposium on Reinforced Earth and other Composite Soil Techniques, Transport and Road Research Laboratory, Supplementary report 457, pp. 39-54, Edinburgh, 1977.

37. Jones, C.J.F.P., "York method of reinforced earth construction", ASCE Symposium on Earth Reinforcement, pp. 501-527, Pittsburgh, 1978.

38. Jones, C.J.F.P., "Lateral earth pressures acting on the facing units of reinforced earth structures", Colloque International sur le Renforcement des sols: Terre Armée et autres Techniques, pp. 77-82, Paris, 1979.

39. Juran, I., and Schlosser, F., "Theoretical analysis of failure in reinforced earth structures", ASCE Symposium on Earth Reinforcement, pp. 528-555, Pittsburgh, 1978.

40. Juran, I., and Schlosser, F., "Theoretical study of traction forces in slabs of reinforced earth structures", French text, Colloque International sur le Renforcement des Sols: Terre Armée et autres Techniques, pp. 77-82, Paris, 1979.

41. Juran, I., Schlosser, F., Long, N.T., and Legeay, G., "Full scale experiment on a reinforced earth wall supporting vertical loads at the upper surface", French text, Colloque International sur le Renforcement des Sols: Terre Armée et autres Techniques, pp. 557-562, Paris, 1979.

42. Kennedy, J., Laba, J.T., and Mossaad, M.A., "Reinforced earth retaining walls under strip load", Can. Geotech. J., vol. 17, no. 3, pp. 382-394, Aug. 1980.

43. Lam, T.M., and Trak, B., "STAB: Slope stability computer program for Bishop's and Fellenius' methods of analysis- User's manual", Dept. of Civil Engineering, University of Ottawa, 1982.

44. Lambe, T.W., and Whitman, R.V., Soil mechanics, SI version. John Wiley and Sons, 1979.

45. Lee, K.L., Adams, B.D., and Vagneron, J.-M.J., "Reinforced earth retaining walls", ASCE Journal of the Soil Mechanics and Foundations Division, pp. 745-764, Oct. 1973.

46. Lee, K.L., "Mechanisms, analysis and design of reinforced earth- state-of-the-art report", ASCE Symposium on earth reinforcement, pp. 62-76, Pittsburgh, 1978.

47. Madani, C., Long, N.T., and Legeay, G., "Behaviour of reinforced earth in repeated triaxial compressive loading", Colloque International sur le Renforcement des Sols: Terre Armée et autres Techniques, pp. 83-88, Paris, 1979.

48. McGown, A., "The strength of sloped reinforced earth embankments", Highw. Eng., vol. 29, no. 2, pp. 19-21, Feb. 1982.

49. Mckittrick, D.P., and Gedney, D.S., "Reinforced earth: a new alternative for earth-retention structures", ASCE Civil Engineering, vol. 45, no. 10, pp. 58-61, Oct. 1975.

50. Mckittrick, D.P., "Reinforced earth: application of theory and research to practice", Symposium on Soil Reinforcing and Stabilising Techniques in Engineering Practice, Sydney, Australia, Oct. 1978.

51. Meyerhof, G.G., "The ultimate bearing capacity of foundations on slopes", Proceedings of the 4th Int. Conf. S.M.F.E., vol. 3, pp. 384-386, London, 1957.

52. Moore, R.J., "Large scale triaxial testing on granular 'A' and crushed quartz sand", Unpublished report, University of Ottawa, 1978.

53. Murray, R.T., "Research at the transport and road research laboratory to develop design criteria for reinforced earth", Symposium on Reinforced Earth and other Composite Soil Techniques, Transport and Road Research Laboratory, Supplementary Report 457, pp. 55-87, Edinburgh, 1977.

54. Naylor, D.J., "Study of reinforced earth walls allowing strip slip", ASCE Symposium on Earth Reinforcement, pp. 618-643, Pittsburgh, 1978.

55. Netlon Ltd., "Designing with Tensar- techniques and design philosophy for utilising Tensar grids in the reinforcing of soil structures", Netlon Civil Engineering Department, 1982.

56. Nicholls, R.L., "Comparison of fabric sheet-reinforced earth design methods", Can. Geotech. J., 18, pp. 585-592, 1981.

57. Osman, M.A., Finlay, T.W., and Sutherland, H.B., "The internal stability of reinforced earth walls", Colloque International sur le Renforcement des Sols: Terre Armée et autres Techniques, pp. 107-112, Paris, 1979.

58. Phan, T.L., Segrestin, P., Schlosser, F., and Long, N.T., "Stability analysis of reinforced earth walls by two slip circle methods", French text, Colloque International sur le Renforcement des Sols: Terre Armée et autres Techniques, pp. 119-123, Paris, 1979.

59. Popescu, E.M., "Some considerations on the design methods of reinforced earth retaining walls", Colloque International sur le Renforcement des Sols: Terre Armée et autres Techniques, pp. 131-137, Paris, 1979.

60. Rahman, M.G., "Bearing capacity and settlement of circular footings on sand", M.A.Sc. Thesis, Dept. of Civil Engineering, University of Ottawa, 1980.

61. Reinforced Earth Company, "Reinforced earth", Literature and Promotional Pamphlets,

62. Romstad, K.M., Al-Yassin, Z.A., Hermann, L.R., and Shen, C.K., "Stability analysis of reinforced earth retaining structures", ASCE Symposium on Earth Reinforcement, pp. 686-713, Pittsburgh, 1978.

63. Schlosser, F., and Vidal, H., "Reinforced earth", Translation of article "La terre armée" published in Le Bulletin de Liaison des Laboratoires RoutiersPonts et chaussées, no. 41, Nov. 1969.

64. Schlosser, F., and Elias, V., "Friction in reinforced earth", ASCE Symposium on Earth Reinforcement, pp. 735-763, Pittsburgh, 1978.

65. Schlosser, F., and Guilloux, A., "Friction between soil and strips in reinforced earth structures", Colloque International sur le Renforcement des Sols: Terre Armée et autres Techniques, pp. 151-156, Paris, 1979.

66. Schlosser, F., and Segrestin, P., "Local stability analysis method of design of reinforced earth structures", French text, Colloque International sur le Renforcement des Sols: Terre Armée et autres Techniques, pp. 157-162, Paris, 1979.

67. Segrestin, P., "Design of reinforced earth structures assuming failure wedges", French text, Colloque International sur le Renforcement des Sols: Terre Armée et autres techniques, pp. 163-168, Paris, 1979.

68. Shen, C.K., Mitchell, J.F., DeNatale, J.S., and Romstad, K.M., "Laboratory testing and model studies of friction in reinforced earth", Colloque International sur le Renforcement des Sols: Terre Armée et autres Techniques, pp. 169-174, Paris, 1979.

69. Shields, D.H., Scott, J.D., Bauer, G.E., Deschênes, J.-H., and Barsvary, A.K., "Bearing capacity of foundations near slopes", 9th Int. Conf. Soil Mech. and Found. Eng., pp. 715-720, Tokyo, 1977.

70. Smith, A.K.C., and Bransby, P.L., "The failure of reinforced earth walls by overturning", Géotechnique, 26, 376-381, 1976.

71. Smith, A.K.C., and Wroth, C.P., "The failure of model reinforced earth walls", Symposium on Reinforced Earth and other Composite Soil Techniques, Transport and Road Research Laboratory, Supplementary report 457, pp. 109-131, Edinburgh, 1977.

72. Smith, A.K.C., and Wroth, C.P., "The failure of model reinforced earth walls", ASCE Symposium on Earth Reinforcement, pp. 794-855, Pittsburgh, 1978.

73. Smith, A.K.C., and Wroth, C.P., "Failure mechanisms in model reinforced earth walls", Ground Eng., vol. 11, no. 6, pp. 43-45, Sep. 1978.

74. Smith, G.N., "Principles of reinforced earth design", Symposium on Reinforced Earth and other Composite Soil Techniques, Transport and Road Research Laboratory, Supplementary report 457, pp. 2-21, Edinburgh, 1977.

75. Snaith, M.S., Bell, A.L., and Dubois, D.D., "Embankment construction from marginal material", Colloque International sur le Renforcement des Sols: Terre Armée et autres Techniques, pp. 175-180, Paris, 1979.

76. Soydemir, C., and Espinosa, A., "Model behavior of reinforced earth walls", Colloque International sur le Renforcement des Sols: Terre Armée et autres Techniques, pp. 181-184, Paris, 1979.

77. Tobutt, D.C., "The strength of sloped reinforced earth embankments", Highw. Eng., vol. 28, no. 8-9, pp. 22-25, Aug.-Sep. 1981.

78. Vidal, H., "Reinforced earth", Annales de l'Institue Technique du Batiment et des Travaux Publics, Supplément au no. 299, Nov. 1972.

79. Vidal, H., "The development and future of reinforced earth- Keynote address", ASCE Symposium on Earth Reinforcement, pp. 1-61, Pittsburgh, 1978.

80. VSL Corporation "Rock and soil stabilization systems", Literature and Promotional Pamphlets, 1981.

81. Walkinshaw, J.L., "Reinforced earth construction", Dept. of Transportation, Federal Highway Administration (FHWA) U.S., Report no. FHWA-DP-18, 1975.